

# **For Reference**

---

**NOT TO BE TAKEN FROM THIS ROOM**



Ex LIBRIS  
UNIVERSITATIS  
ALBERTAENSIS



## REQUEST FOR DUPLICATION

entitled 1) subsurface flow.

[illegible]

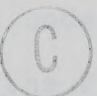




THE UNIVERSITY OF ALBERTA

SUBFEM: A SUBSURFACE FLOW MODEL FOR A FOREST ENVIRONMENT

by

 GRAHAM R. HILLMAN

A THESIS

SUBMITTED TO THE FACULTY OF GRADUATE STUDIES AND RESEARCH

IN PARTIAL FULFILMENT OF THE REQUIREMENTS FOR THE DEGREE

OF DOCTOR OF PHILOSOPHY

IN


WATER RESOURCES

DEPARTMENT OF CIVIL ENGINEERING

UNIVERSITY OF ALBERTA

SPRING 1983





Digitized by the Internet Archive  
in 2022 with funding from  
University of Alberta Library

<https://archive.org/details/Hillman1983>



## ABSTRACT

Land managers frequently need to assess the effects of forest cover removal on water yield, water regime, and water quality. They may also want to know what happens when forest cover is deliberately removed, in a prescribed manner, for the purpose of enhancing water supplies.

One way of approaching these problems is to first develop simulation models and then compare model results with those obtained in the field. Once the validity of a model has been established it may be used to predict the impact of a particular forest harvesting pattern on soil water and streamflow, or to predict practical watershed management prescriptions to improve water yielding characteristics of specified river basins.

Several physically based watershed simulation models have been developed for these purposes. Although they adequately simulate many hydrological processes, treatment of the subsurface flow component is usually less than satisfactory.

This study is an attempt to rectify the situation through development of a physically based, distributed, subsurface flow finite element model (SUBFEM), in which forest vegetation appears as an integral part. The model simulates the effects of different vegetation patterns on soil water distribution and streamflow. Water withdrawal by trees is simulated by means of sinks located at appropriate near-surface nodes within the finite element mesh.







Initial tests on the model, for one- and two-dimensional infiltration into originally unsaturated soil, produced results that compare favourably with those of other investigators.

Simulations showed that a smaller volume of soil is affected by evaporation than by transpiration for a fixed evaporation or transpiration demand. Potential gradients are greater during evaporation.

In another set of simulations evapotranspiration from sloping profiles was examined. Trees were assumed to occupy different positions on the slope: lower slope only, upper slope only, completely forested, clearcut (no trees), and patchcut.

Quite distinct patterns for both total potential and volumetric water content were obtained. They reflected the differential drain on soil water by trees and by evaporation.

Time step size, mesh coarseness, and two model parameters (initial conditions and saturated hydraulic conductivity) were subjected to sensitivity analyses. The conclusions drawn from these analyses are outlined below.

Time step size, under certain conditions, is critical, and will determine whether convergence to a solution is possible. Mesh coarseness can influence the time at which outflow from an originally unsaturated system begins.

Both the time at which outflow commences, and the volume of flow from an originally unsaturated system, are





affected by changes in initial conditions. The wetter the initial conditions, the earlier outflow begins. SUBFEM is very responsive to changes in saturated hydraulic conductivity.

It is felt that the primary usefulness of SUBFEM rests in its capability to simulate the processes of infiltration, transpiration, and interflow, It can best be used to study hydrologic processes on vegetated or partially vegetated hillslopes. An example of this kind of application is the simulation of a plot study on Fernow Experimental Forest, West Virginia. Data from the field study showed that, for an input of 7.75 cm of rain over 12 hr, the plot produced about 0.4 cm of outflow. The simulation data indicated that the entire volume of rain falling on the plot was absorbed by the soil.

Suggestions for improving and applying the model are presented.





## ACKNOWLEDGEMENTS

I am much indebted to my employer, the Canadian Forestry Service (Northern Forest Research Centre), Environment Canada for providing me with the opportunity to undertake this study. The financial support and development leave granted by Environment Canada are gratefully acknowledged.

The advice, support, and encouragement of my advisor, Dr. Jac. Verschuren, are greatly appreciated. His guidance was particularly invaluable when the going was difficult.

Drs. Stan. Cabay (Computing Science) and Dave Murray (Civil Engineering) deserve special mention for their many efforts to enlighten me on the mysteries of the finite element method. Ray Howells and Al. Dunbar, both of the Civil Engineering Department, provided much valuable assistance and advice regarding computer use, particularly use of the integrated graphics routine. To them, my heartfelt thanks.

A special thank you is extended to Donna Ball, Bruce Robson (Northern Forest Research Centre), and Ryan Shannon for doing an excellent job of drafting the figures. The skillful assistance of Phil. Debnam (Northern Forest Research Centre), who provided essential photographic services, is also gratefully acknowledged.

I am much obliged to Dr. C. A. Troendle of the Rocky Mountain Forest and Range Experiment Station, Colorado, for providing me with data from his subsurface flow plot, located in the Fernow Experimental Forest, West Virginia.





Finally, to my wife, Velma, and family I owe a debt of gratitude for their patience and understanding during the protracted course of this study.





## TABLE OF CONTENTS

Chapter	Page
I. INTRODUCTION .....	1
II. LITERATURE REVIEW .....	5
A. History Of Forest Hydrology And Watershed Management Research .....	5
B. Development Of Forest Hydrology And Watershed Management In Alberta .....	29
C. The Watershed System .....	37
D. Watershed And Hydrologic Modelling .....	52
E. Development Of Subsurface Flow Equations And Methods For Obtaining Their Solutions .....	79
Saturated flow .....	79
Unsaturated flow .....	82
Saturated and unsaturated flow in an integrated subsurface flow system .....	91
III. STRATEGY FOR MODEL DESIGN .....	94
IV. MATHEMATICAL DEVELOPMENT OF SUBSURFACE FLOW MODEL .....	106
A. Governing Equations .....	106
B. Finite Element Simulation .....	107
C. Application Of Finite Difference Approximations To Time Domain .....	115
D. Treatment Of Boundary Conditions, Sinks, And Seepage Faces .....	119
V. SIMULATIONS: RESULTS AND DISCUSSION .....	121
A. Unsaturated Flow .....	121
Model validation .....	121
Evaporation and transpiration from a large box of soil .....	137
B. Combined Saturated-Unsaturated Flow .....	166





Rainfall simulation .....	166
Changing boundary conditions .....	177
Sensitivity analyses .....	186
C. Model Versus Prototype .....	200
VI. SUMMARY AND CONCLUSIONS .....	205
A. Summary .....	205
B. Conclusions .....	207
C. Suggestions For Further Research .....	210
VII. LITERATURE CITED .....	212
VIII. APPENDICES .....	226
A. Appendix A. Development Of Coordinate Functions Using Area Coordinates For Triangular Elements And Integration Of Resulting Expressions .....	227
B. Appendix B. Program SUBFEM - User's Manual ...	232
C. Appendix C. Program SUBFEM - Computer Code ...	245
D. Appendix D. Example Of Input Data Set Required To Run SUBFEM .....	272





## LIST OF TABLES

Table	Page
1. Increases in water yield following forest cutting, by forest type, geographic location and type of cutting (Adapted from Anderson <u>et al.</u> , 1976; and Hibbert, 1967).	11
2. Effects of reforestation and afforestation on water yield (Adapted from Anderson <u>et al.</u> , 1976; and Hibbert, 1967).	14
3. Effects of reforestation on peak flows from selected experimental watersheds (Adapted from Anderson <u>et al.</u> , 1976).	15
4. Estimated potentials for increased water yields from forest and range lands in the United States through programs of vegetative management (Adapted from Sopper, 1971).	28
5. Impact of timber removal on simulated snow distribution, evapotranspiration, and water available for runoff on the Fool Creek Watershed (Adapted from Betters, 1975).	74
6. Water budget components for an average water-year on the Chicken Creek Watershed at different stages of succession (Adapted from Jaynes, 1978).	75



## LIST OF FIGURES

Figure		Page
1.	Hydrographs for Wagon Wheel Gap watershed, Colorado (Adapted from Bates and Henry, 1928).	17
2.	Hydrographs for Fool Creek watershed, Fraser, Colorado (Adapted from Leaf, 1975).	20
3.	Relation of mean annual streamflow to forest cover adjusted for effect of latitude. Upper Volga Basin. (After Rakhmanov, 1970b).	26
4.	Map showing Rocky Mountains Forest Reserve (Adapted from maps published by the Alberta Government).	31
5.	Stanford Watershed Model IV flowchart (After Crawford and Linsley, 1966).	57
6.	Block-centred nodal grid for subsurface flow model (After Freeze, 1971).	60
7.	Schematic of PROSPER (After Huff <u>et al.</u> , 1977).	65
8.	Wall-and-step forest - a cutting pattern for improved water yield from snow zone forests (After Anderson, 1960).	70
9.	Conceptual hydrologic model.	95
10.	Two-dimensional hillslope profile for simulating subsurface flow.	96
11.	Uniform valley formed by escarpments.	97
12.	a) Finite element discretization for one-dimensional infiltration into Yolo Light Clay (After Beven, 1975). b) Comparison of SUBFEM solution with those obtained by Philip (1957) and Beven (1975).	124
13.	One-dimensional, vertical infiltration - total potential (a) and volumetric water content (b) after 10,000 sec.	126
14.	One-dimensional, vertical infiltration - advancing wetting front and infiltration capacity.	128





15.	One-dimensional evaporation - total potential (a) and water content (b) after 10,000 sec.	130
16.	Finite element discretization for two-dimensional horizontal infiltration into a block of Yolo Light Clay (After Beven, 1975).	132
17.	Two-dimensional, horizontal infiltration - total potential after 6 hr.	133
18.	Two-dimensional, horizontal infiltration - water content [a) and b)] and total potential [c)] fields after 6 hr.	134
19.	Two-dimensional, horizontal infiltration - advancing wetting front and infiltration capacity.	136
20.	Finite element discretization for evaporation, transpiration, and evapotranspiration from a flat section of Yolo Light Clay.	138
21.	Evaporation from a flat profile - pressure potential (a), total potential (b), and water content (c), after 240 hr.	140
22.	Transpiration from a flat profile - total potential (a) and water content (b) after 240 hr.	143
23.	Evapotranspiration from a flat profile - total potential (a) and water content (b) after 240 hr.	146
24.	Evapotranspiration from a sloping profile - total potential (a) and water content (b) after 240 hr.	148
25.	Evapotranspiration from a sloping profile - total potential (a) and water content (b) after 480 hr.	150
26.	Trees on lower slope - total potential (a) and water content (b) after 240 hr.	152
27.	Trees on lower slope - total potential (a) and water content (b) after 480 hr.	154
28.	Trees on upper slope - total potential (a) and water content (b) after 240 hr.	155





29.	Trees on upper slope - total potential (a) and water content (b) after 480 hr.	157
30.	Clearcut simulation - total potential (a) and water content (b) after 240 hr.	159
31.	Clearcut simulation - total potential (a) and water content (b) after 480 hr.	160
32.	Patchcut simulation (two cut strips and three forested strips) - total potential (a) and water content (b) after 240 hr.	163
33.	Patchcut simulation (three cut strips and two forested strips) - total potential (a) and water content (b) after 240 hr.	165
34.	Rainfall on a flat profile - total potential (a) and water content (b) after 240 hr.	168
35.	Rainfall on a sloping profile - total potential (a) and water content (b) after 240 hr.	170
36.	Hydrographs for a 10-day rainfall (10 mm/day), for two mesh sizes, and different initial conditions.	171
37.	Rainfall on a sloping profile - total potential (a) and volumetric water content (b) after 240 hr. Obtained using a 217-node, 360-element mesh.	173
38.	Rainfall on a sloping profile with $\psi_i = -10, -50, \text{ and } -100$ cm - total potential (a) and volumetric water content (b) after 240 hr. Fine mesh simulation.	176
39.	Recession curves - obtained when rainfall rate is changed from 10 to 2 mm/day, and time step sizes are 0.1 and 0.01 hr.	179
40.	Recession curves - obtained when rainfall rate is changed from 10 to 2 mm/day, and time step sizes are 6, 3, and 1 hr.	180
41.	Recession curves - obtained when rainfall rate is changed from 10 to 0 mm/day, and time step sizes are 0.1 and 0.01 hr.	182
42.	Recession curves - obtained when rainfall rate is changed from 10 to 0 mm/day, and time step sizes are 6, 3, and 1 hr.	183



43.	Total potential at end of first time step following cessation of 10 cm rainfall.	184
44.	Hydrographs obtained for different time step sizes using a 64-node, 90-element mesh.	187
45.	Hydrographs produced by meshes of different coarseness, and a time step size of 24 hr.	191
46.	Hydrographs produced by meshes of different coarseness, and a time step size of 3 hr.	192
47.	Hydrographs obtained using a 114-node mesh and different initial conditions.	194
48.	Variation of discharge over time for different values of saturated hydraulic conductivity ( $K_s$ ).	196
49.	Water content in Yolo Light Clay after 10 days of rainfall, for two values of saturated hydraulic conductivity ( $K_s$ ).	197





## I. INTRODUCTION

The eastern slopes of the Rocky Mountains in Alberta form the headwaters of the Athabasca and Saskatchewan River systems. The Saskatchewan River, which drains mountains, foothills and plains, is the primary source of water for the Canadian Prairies, and is therefore extremely important to the economy of that area. A far greater proportion of the Saskatchewan River's total annual flow is derived from the heavily forested mountains and foothills than from the plains. Consequently, water production is considered by some to be the prime use of the East Slopes region. In the past, management of the East Slopes watersheds has been essentially protective in nature. However, as population pressures increase, the demands for good quality water also increase and ways must be found to meet these demands. One way of increasing the water supply is to remove, in a prescribed manner, some of the forest cover from the high water-yielding portions of the watershed.

Industrial activity such as forestry, coal, oil, and gas exploration is increasing on the East Slopes as the search for, and the exploitation of, additional natural resources intensifies. It is important that land managers be able to assess the effects of such activity on water yield, water regime, and water quality since there is convincing evidence that removing forest cover for wood production or other industrial uses can result in an increase in stream



discharge from the cutover areas. A reduction in water quality can also result if due consideration is not given to proper design of roads and water course crossings.

One way of approaching the kind of problems outlined above is to first develop watershed simulation models and then compare model results with those obtained in the field. Once the validity of a model has been established it may be used to predict the impact of a particular forest harvesting pattern on streamflow. Alternatively, it can be used to predict practical watershed management prescriptions to improve water yielding characteristics of specified river basins.

The type of conceptual model envisaged here is one in which the individual components or hydrologic processes are related to various forest stand parameters such as species composition, age, stand density (stems per hectare), basal area ( $\text{m}^2$  per hectare), and areal distribution. When all trees are removed from an area, such as occurs during clearcutting, all the stand parameters for that area become equal to zero.

For many hydrologic processes, models based on these kind of relationships and which produce satisfactory results are available. They are well documented in the literature. For example, several models have been developed which simulate the effects of the forest and forest harvesting on snow accumulation, redistribution, and melt. Other processes as related to forest stand parameters have not been so well





defined. Subsurface flow is perhaps the most complex of these.

Ideally, the preferred forest vegetation manipulation watershed model is one which is completely physically based and which is capable of predicting with a fair degree of accuracy: a) the cutting pattern and amount of forest to be removed in order to obtain a hydrograph with specified characteristics, b) how a variety of land uses will change the hydrographs of affected streams, and c) the changes in water quality produced by forestry and other industrial operations on the watershed. The model must be simple enough that it can be applied by forest, land, and water managers to areas for which data is not extensive. A watershed model possessing all these characteristics does not exist.

Although many watershed models are available, few are designed to solve forest watershed problems, and fewer still contain a physically based subsurface flow component. Often, this component is simulated, if at all, in a somewhat arbitrary manner.

The purpose of this project is to progress toward the idealized model described above, by developing a physically based subsurface flow model which provides for simulation of forest stands. The subsurface model will: a) identify the main flow paths taken by water through the porous media to the stream channel after it passes through the air-soil interface, and b) quantify the outflow from the seepage face at the stream channel, so that streamflow response to



watershed treatment and precipitation can be determined.

It is felt that this purpose can be best achieved by pursuing the following objectives:

1. to develop from Darcy's Law and the continuity equation a mathematical model of two-dimensional transient unsaturated and saturated flow through porous media, applicable under natural conditions;
2. to incorporate the mathematical model as part of a physically based synthesis of the hydrologic cycle;
3. to use the synthesized model to simulate behaviour of hillslopes following treatment, and to check simulation results against field data from treated hillslopes.



## II. LITERATURE REVIEW

### A. History Of Forest Hydrology And Watershed Management Research

The interrelationships between forests and water have long been recognized. As early as 1215, Louis VI of France issued "The decree of water and forests." In 1342, a community in Switzerland reserved the first protection forest as a safeguard against avalanches (Kittredge, 1948). Since that time many countries have taken similar and additional measures such as reforestation and construction of check dams to curtail erosion or to prevent damage to life and property by torrents and avalanches. However, most of the significant scientific and legal developments related to forest-water interactions have occurred over the past 150 years.

During this period the United States emerged as a leader in the field of forest-water relations research and many reports were published on the effects, deleterious or otherwise, of forest cover removal on climate, soil and water. In 1863 for example, G.P. Marsh wrote a book entitled "Man and Nature", which was later revised and republished several times under the title "The Earth as Modified by Human Action". This book created a national awareness toward watershed management. Several years later Kinney (1900) discussed the problems associated with water, forest fires, and exploitation of forest lands in Southern California.





Such reports had a significant impact on U.S. land policy formulation and on ensuing legislation.

It is evident from the wording of legislation authorizing the reservation of forested public lands that the water-controlling function of the forest was to be regarded as equally important as its capacity to supply timber. Thus, one clause in the Act of June 4, 1897 reads

"...no public reservation shall be established except to improve and protect the forest within the reservation or for the purpose of securing favorable conditions of water flow and to furnish a continuous supply of timber." (Kittredge, 1948).

Some of the more important pieces of U.S. Federal legislation together with the names of the key people involved have been summarized concisely by Hewlett and Nutter (1969)

"A period of evaluation and alarming descriptions (Marsh's' book, 1863) led to the propaganda period of forest influences (1877-1910). Forest influences played a large role in forestry, conservation and public land policies. Fernow, Hough, Pinchot, Roth, and Roosevelt helped to formulate policies which produced many acts of Congress related to forests and water: Weeks Law (1911); Forest Experiment Stations authorized by McSweeney-McNary Act (1928); New Deal of the 30's, including the CCC Program; The Flood Control Act (1936); Soil Conservation Service (1936). Public Law 566 (Small Watershed Act of 1954) forced involvement of local people in watershed management. The Senate Select Committee (1958-61) found that training, planning, and pollution were the greatest water problems. Since then a flood of acts aimed at water resources planning, conservation, and development have been passed. Several important ones were the Water Resources

---

<sup>1</sup> Marsh, G.P. 1863. Man and Nature. Scribner and Sons, New York, NY. (Later titled Earth as Modified by Human Action).



Research Act (1965), Water Pollution Control Act (1964), and the Water Resources Planning Act (1966)."

In Canada, forest-water relations research has not enjoyed the recognition accorded this field in the United States. Nevertheless, its importance was recognized as early as 1910 when legislation was passed to establish the Rocky Mountains Forest Reserve in the Saskatchewan River headwaters of Alberta as a watershed protection zone (Alberta Energy and Natural Resources, 1979).

Several collective terms have been used to describe forest-water relations. In older literature, the term "forest influences" is used. Forest influences have been defined to include all effects resulting from the presence of forest or brush upon climate, soil water, runoff, streamflow, floods, erosion, and soil productivity (Kittredge, 1948). It has been replaced by "forest hydrology" which is

"a branch of hydrology that deals with the effects of forests and associated wildland vegetation on the water cycle, including the effect on erosion, water quality, and the microclimate" (Hewlett and Nutter, 1969).

This term has been used interchangeably with "watershed management" which has been defined as

"Application of business methods and technical principles to the handling of all the renewable resources in a watershed to assure maximum supplies of useable water, desirable waterflow, prevention





and control of erosion, and the reduction of flood and sediment damages." (Society of American Foresters, 1958).

An alternative definition of watershed management is: "The management of land for optimal production of water, with due attention being given to soil stability and to the other resources of the land." (Jeffrey, 1969).

Generally speaking, "forest hydrology" refers to the scientific-technical basis for forest watershed management, and "watershed management" refers to the management of land for water production itself (Jeffrey, 1969). Other terms such as "wildland hydrology" and "land use hydrology" are also used, but in the forest environment context they are synonymous with "forest hydrology".

Forest hydrology then can be considered as the study of hydrologic processes such as precipitation, interception, overland flow, infiltration, evapotranspiration, groundwater flow, streamflow, erosion, sedimentation and water quality in a forest setting. Its subject matter also includes study of the side effects of forestry operations (timber harvesting, regeneration, tree planting, vegetation type conversion, and the application of fertilizers and pesticides), fire and grazing on water supply, floods, erosion, and water quality.

The scope of watershed management includes management of the forest land for one or more of the following specific objectives: optimum water yield, maximum water yield, flood



reduction, and maintaining water quality<sup>2</sup> by minimizing erosion and stream sedimentation. Typically such management is conducted in high- to medium-water yielding source or headwaters areas of river basins. Generally such areas are located in mountainous or hilly terrain, and are subject to greater precipitation than the plains below.

Forest hydrology and forest watershed management research have been pursued vigorously during the twentieth century, particularly in the United States. An excellent summary of American experience and results is provided by Anderson et al. (1976). Several important textbooks have been published both in North America (Kittredge, 1948; Colman, 1953; Hewlett and Nutter, 1969; and Satterlund, 1972) and in Europe (Geiger, 1950; Molchanov, 1960; and Rakhmanov, 1962). Several manuals (Food and Agriculture Organization of the United Nations, 1976a, 1976b, 1977; U.S. Forest Service, 1974) were made available, to assist the practicing forest manager. Two important international symposia on forests and water were also held (Sopper and Lull, 1967; Talât and Dunford, 1970). Several other symposia were organized at the local level (American Society of Agricultural Engineers and American Society of Civil Engineers, 1970; Csallany et al., 1972; Krygier and Hall, 1971; Society of American Foresters and Oregon State

---

<sup>2</sup> Maintaining water quality through erosion and sediment control is an extremely important objective in watershed management and is the primary function of many protection watersheds. However, the subject matter is beyond the scope of this paper and will not be discussed in detail.



University, 1963, 1966). Another international symposium - on the results of research on representative and experimental basins - was held in Wellington, New Zealand (International Association of Scientific Hydrology and UNESCO, 1970). Although it did not deal exclusively with forests/water problems, the subject matter of the symposium was highly relevant.

Tables 1, 2 and 3 are taken from Anderson et al. (1976) and from Hibbert (1967) and summarize the results from much of the research referred to above. Table 1 shows the increases in water yield following forest cutting in various parts of the United States and in other countries.

The Emmenthal watershed study begun in 1900 predates the studies referred to in Table 1 and involved two small watersheds in the Emmenthal Mountains of Switzerland. One watershed was completely forested and the other mostly pastureland. The objective was to determine the influence of the forest on the water balance. Although differences (246 mm) in streamflow between the two watersheds were detected, it was not possible to attribute these differences to the influence of forest cover alone (Colman, 1953). However, the study was the first attempt to solve a forest hydrology problem using entire watersheds and scientific methods.

The Wagon Wheel Gap experiment in Colorado (Table 1) was begun in 1910 and is significant because it was the first time that the control (paired) watershed method was used. This method requires measurement of streamflow from a





Table 1. Increases in water yield following forest cutting, by forest type, geographic location and type of cutting. (Adapted from Anderson et al., 1976; and Hibbert, 1967).

Watershed area (ha)	Mean annual precipitation (mm)	Mean annual stream-flow (mm)	Treatment	Percent of area or basal area (b) removed	Regrowth	Water yield increases by years after treatment (mm)				
						1	2	3	4	5
Mixed Hardwoods, Coweeta, Western North Carolina										
16	1829	787	Clearcut	100	Yes	366	277	277	249	201
13	1905	762	Clearcut	100	No	427	330	297	290	284
9	1803	610	Clearcut	100	No	127	94	58	112	79
34	2057	1270	Clearcut	50	Yes	198	155	130	112	99
28	2007	1219	Selection cut	22b	Yes	99	56	71	28	38
86	1854	1067	Selection cut	30b	Yes	Averaged 25 per year				
29	2032	1295	Selection cut	35b	Yes	Averaged 55 per year				
20	1956	1041	Selection cut	27b	Yes	Non significant				
9	1829	838	Riparian cut	12	Yes	Non significant				
Northern Hardwoods, Central New Hampshire										
16	1219	889	Cleared	100	No	343	274	239		
Mixed Hardwoods, Northern West Virginia										
24	1448	762	Cleared	100	No	262				
34	1524	584	Clearcut (except for culls)	100 (83b)	Yes	130	86	89	15	56
24	1448	762	Clearcut	50	No	155	147			
15	1499	660	Selection cut	36	Yes	64	36	8	30	-5
36	1473	762	Selection cut	22	Yes	18	3	-18	-41	18
34	1499	635	Selection cut	14	Yes	8	33	8	8	0
Oak Type, Central Pennsylvania										
43	940	330	Clearcut	20	No					69



Table 1. Increases in water yield following forest cutting, by forest type, geographic location and type of cutting (Adapted from Anderson et al., 1976; and Hibbert, 1967).

Watershed area (ha)	Mean annual precipitation (mm)	Mean annual stream-flow (mm)	Treatment	Percent of area or basal area (b) removed	Regrowth	Water yield increases by years after treatment (mm)				
						1	2	3	4	5
Douglas-fir, Western Oregon										
96	2286	1448	Clearcut	100	Yes	462	457			
101	2286	1448	Clearcut	30	Yes	150	163	150	297	226
Aspen and Conifers, Wagon Wheel Gap, Colorado										
81	533	155	Clearcut	100	Yes	36	48	25	20	13
Lodgepole Pine and Spruce - Fir, Fool Creek, Colorado										
289	762	279	Clearcut	40	Yes	84	132	94	117	137
Mixed Conifers, Arizona										
471	686	81	Clearcut	16	Yes	30				
100	813	86	Selection cut	32	Yes	13	51	41	48	30
129	813	86	Selection cut	45	Yes	Non significant				
Utah Juniper, Central Arizona										
131	483	23	Cabled, burned seeded to grass	100	Yes	Non significant				
Chaparral, Central Arizona										
38	660	56	Herbicide	90	Yes	86	76	66	249	361
19	660	56	Herbicide	40	Grass	76	23	46		
Mixed Conifers and Hardwoods, Kariabuti, Japan										
3	2616	2075	Clearcut	100	No	110 (average for 3 years)				



Table 1. Increases in water yield following forest cutting, by forest type, geographic location and type of cutting (Adapted from Anderson et al., 1976; and Hibbert, 1967).

Watershed area (ha)	Mean annual precip- itation (mm)	Mean annual stream- flow (mm)	Treatment	Percent of area or basal area (b) removed	Regrowth	Water yield increases by years after treatment (mm)				
						1	2	3	4	5
Oak-Woodland, Central California										
5	635	104	Chemical kill	100	Grass	102	201	102		
High Montane and Bamboo, Kericho Sambret, Kenya, East Africa										
688	1905	416	Clearcut	34	Tea	103				
High Montane and Bamboo, Kimakia A, Kenya, East Africa										
35	2014	568	Clearcut	100	Vegetables	457	229	178		





Table 2. Effects of reforestation and afforestation on water yield (Adapted from Anderson et al., 1976; and Hibbert, 1967).

Location	Forest cover before planting	Pretreatment mean annual....		Conversion planting by extent and type	Reduction in water yield for given year (mm)
		Precip- itation (mm)	Stream- flow (mm)		
Ohio	30% hardwoods	965	305	71% pine	135 (19 yr)
Western Tennessee	23% hardwoods	1270	254	65%, mostly pine	76 to 152 (16 yr)
Central New York (3 watersheds)	1. Mixed hardwoods	965	533	47%, conifers	107 (24yr)
	2. do.	1041	610	58%, conifers	173 (23 yr)
	3. do.	1041	635	58%, conifers	130 (23 yr)
Eastern Tennessee	65% mixed hardwoods and pine	1194	457	34%, mostly pine	0
Chenango River Basin, New York	Abandoned farm land	1143	635	7%, conifer plantations (10% second growth hardwoods)	25 (42 yr)
Western North Carolina	Hardwoods: Watershed 1 Watershed 17	1727 1930	787 686	100%, white pine 100%, white pine	142 (10 yr) 277 (11 yr)
Jonkershoek, South Africa	Sclerophyll scrub		475	53%, pine	104 (4-yr mean) 16-20 yrs
Bosboukloof	(chaparral type)		490	98%, pine	142 (4-yr mean) 8-12 yrs
Biesierlei					



Table 3. Effects of reforestation on peak flows from selected experimental watersheds  
(Adapted from Anderson et al., 1976).

Watershed location	Area (km <sup>2</sup> )	Watershed condition		Effect on peak flows
		Before treatment	After treatment	
Shackham Brook area Near Truxton, N.Y.	8.08	25% deciduous 1% coniferous 74% pasture and crops	27% deciduous 57% coniferous 16% pasture and crops	From 1939 to 1957 peak flows were reduced by 41% ranging from 66% in November to 16% in April.
White Hollow Water- shed Mason Co., Tenn.	6.94	66% poorly stocked mixed hardwood and pine 4% cultivated 4% cultivated 26% abandoned land	100% mixed hardwood and pine	From 1935-36 to 1942-49, summer peak discharges were reduced from 73% to 95%, dependent on initial soil wetness and rainfall intensity. Winter peaks were reduced from 0% to 28%, depending on amount surface runoff.
Pine Tree Branch Watershed, Henderson Co., Tenn.	0.36	23% deciduous 16% cultivated 19% pasture 50% idle 2% miscellaneous	33% deciduous 65% coniferous 2% miscellaneous	From 1941-45 to 1951-60, summer peaks were reduced 92% to 97%, winter peaks 71% to 92%, depending on rainfall intensity and soil wetness.
Watershed 172 Coshocton, Ohio	0.18	29% woodland 51% pasture 20% idle	43% natural woodland 57% forest plantation (pine and locust)	From 1938 to 1957, average growing season peaks were reduced by 59%; dormant season peaks were reduced by 69%. (Mean peaks were 0.38 and 0.503m <sup>3</sup> /s/km <sup>2</sup> in growing season, respectively.) No effect was found on peaks from extreme storm occurrences (data were insufficient for rigorous analysis).



control sub-watershed and from an adjacent to-be-treated sub-watershed. Flow data are collected for a calibration period of, preferably, 10 or more years, and a statistical relationship obtained between the two sets of flow data. A treatment such as commercial logging and associated road construction is imposed on one sub-watershed. This marks the end of the calibration phase and the beginning of the post-treatment period. Flow data are obtained from both sub-watersheds for some minimum period following treatment, and a statistical relationship obtained. If the relationship is significantly different from that determined for the calibration period data, then this is regarded as evidence that the treatment has affected streamflow. This method was to be the basis for much of the forest hydrology research that followed. For Wagon Wheel Gap, the investigators showed conclusively (Fig. 1) that removing 100 percent of the aspen and Douglas fir resulted in a measurable increase in water yield.

Data (Table 1) from two different watersheds will be used to illustrate the great variability in results due to geographic location, climatic and other factors. In 1940, one subbasin of the Coweeta watershed in North Carolina, 16 ha in extent and supporting mixed hardwoods, was 100 percent clearcut. Located in the humid mountain region of the United States, it has a mean annual precipitation (all rain) of 1829 mm and a mean annual streamflow of 787 mm. During the first five years following cutting, water yield increases





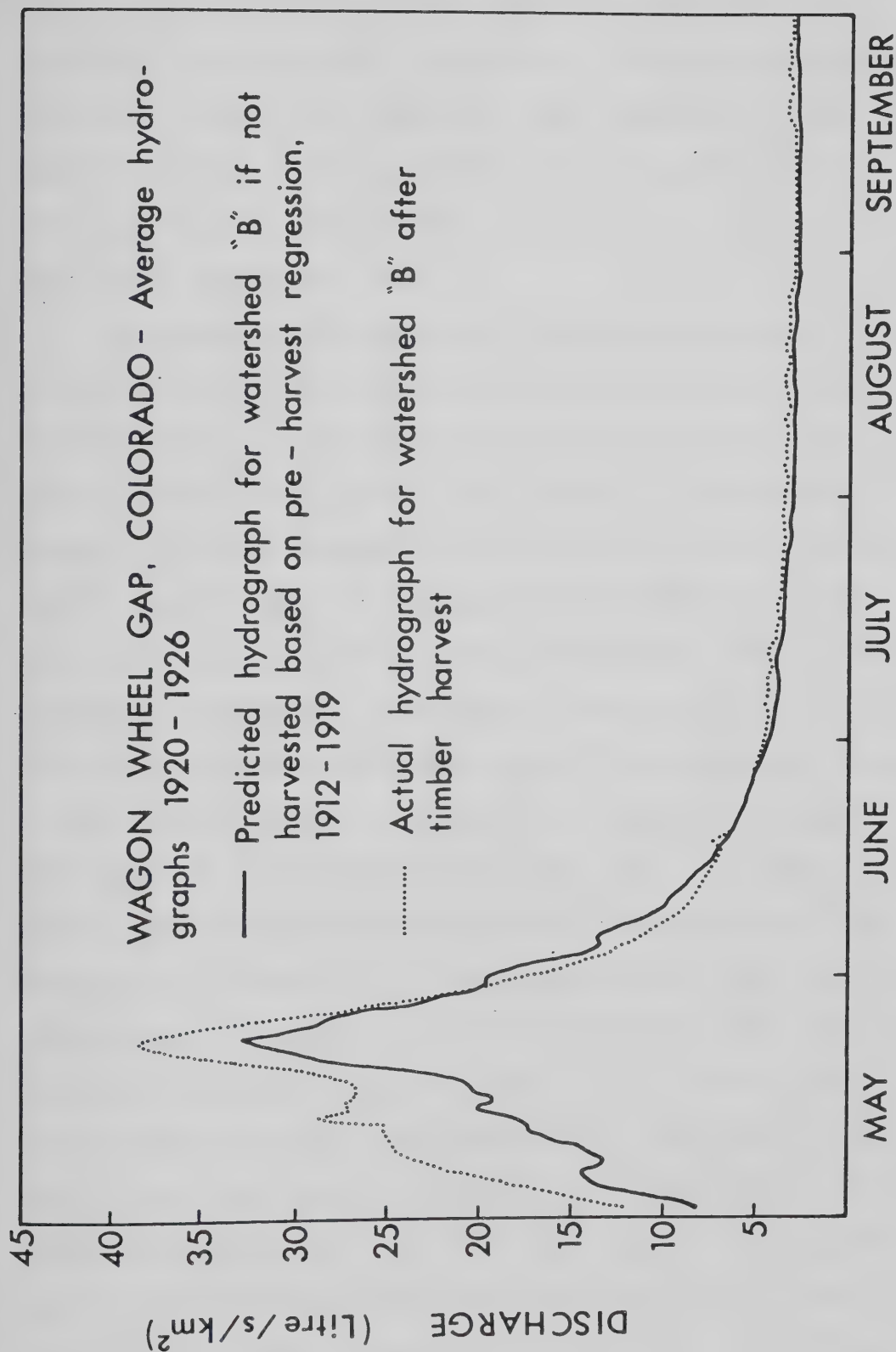


Figure 1. Hydrographs for Wagon Wheel Gap watershed, Colorado (Adapted from Bates and Henry, 1928).



were recorded as 366, 277, 277, 249, and 201 mm. The first value represents a 66 percent and the last a 31 percent increase in water yield. Evidently, the effect diminishes as regrowth occurs. The experiment was repeated in 1962 and the results for the first year following treatment were identical to the corresponding year of the earlier experiment (Hibbert, 1967).

The Fraser watershed study in the high-elevation zone of the Colorado Rocky Mountains consists of Fool Creek and East St. Louis Creek where the latter serves as control. Mean precipitation for the area (Table 1) is 762 mm, 75 percent of which occurs as snow. The mean annual streamflow is 279 mm. In 1954, 40 percent of the lodgepole pine, spruce-fir forest on Fool Creek watershed, which is 289 ha in area, was clearcut. Alternate clearcut strips 20, 40, 60, and 121 m wide were extended up and down slope and bounded at the ends by contour roads. This treatment produced increases in water yield of 84, 132, 94, 117, and 137 mm during each of the next five years. These figures are considerably lower than those from Coweeta, but the highest values for both Coweeta and Fool Creek are about 18 to 20 percent of mean annual precipitation. In the Colorado study the smallest increase (32 percent) in water yield occurred during the first year following cutting and the largest (71 percent) during the fifth year. The effect is not diminished over a short time period as is the case in the Coweeta experiment. In fact, increases in flow of 51 to 102 mm from



Fool Creek have been sustained for 17 years (Fig. 2), and are expected to persist for considerably longer (Anderson et al. 1976). The main factor at Fraser is the considerable length of time required for coniferous subalpine forests to grow to maturity. In contrast, at Coweeta where the increase in water yield diminishes rapidly with time, the climate is more favorable to rapid regrowth of forest cover.

The mechanism by which increased water yields are generated differ between the two locations. In Coweeta extra water becomes available through reduction in transpiration. In Colorado, the primary cause for increased water yields from subalpine forests is the combined action of snow redistribution and reduced evapotranspiration (Leaf, 1975).

Table 2 summarizes results from studies investigating the effects of reforestation and afforestation (establishing a forest where no forest existed before). In nearly every case there is a reduction in water yield. The decreases range from 0 to 277 mm and appear to be effective for as long as the new forest cover exists. Factors contributing to water yield reduction may include: increased interception and infiltration rates, diminished overland flow, increased detention storage, and increased transpiration. Reforestation may also lead to reduction in peak flows (Table 3) from a watershed. The reduction varies with the type of cover that existed before conversion, the proportion of the watershed planted, and with the season of the year.





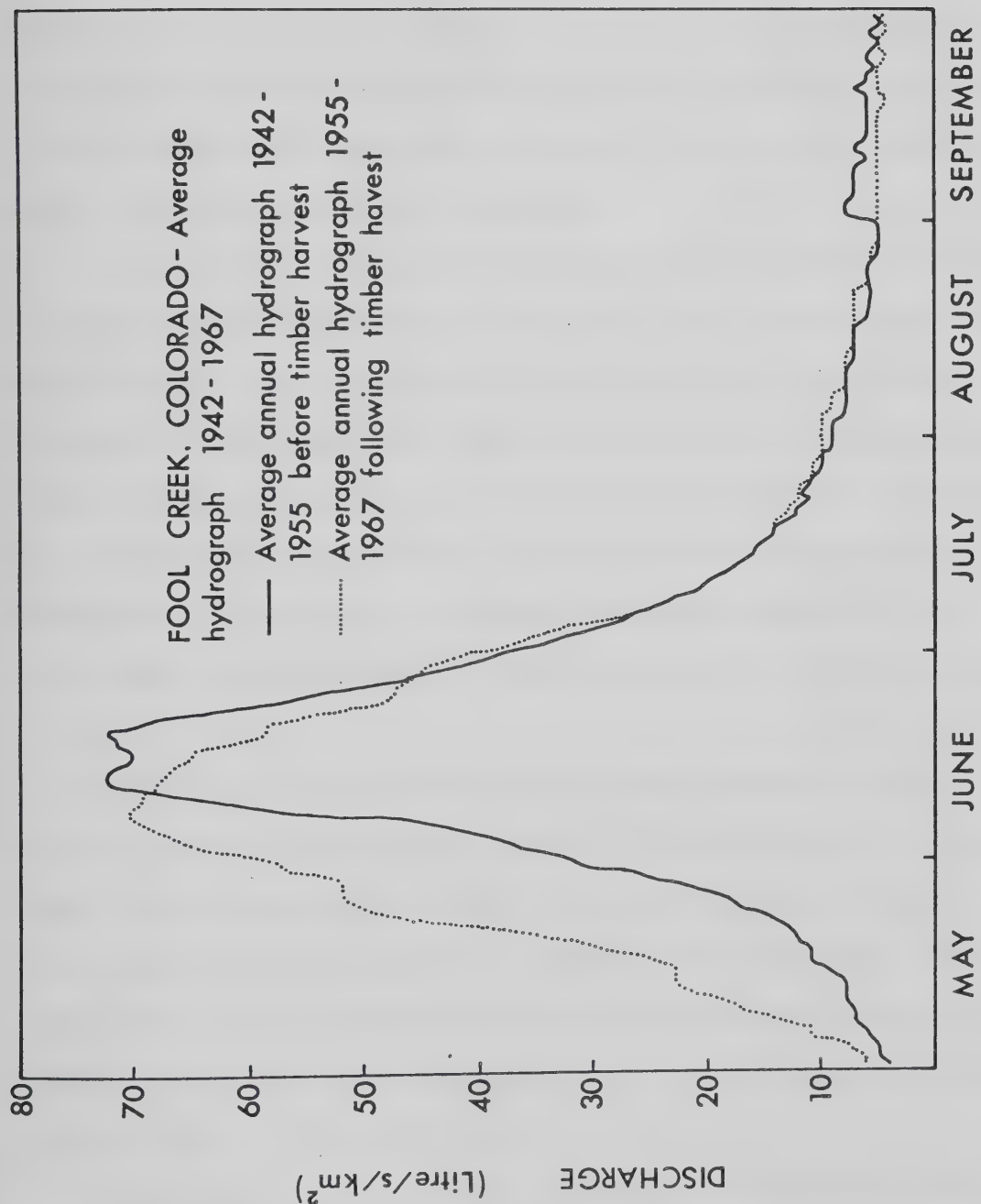


Figure 2. Hydrographs for Fool Creek watershed, Fraser, Colorado (Adapted from Leaf, 1975).



The effects of forest cover removal on peak flows are still unclear. Anderson et al. (1976) give details of many studies where this factor has been investigated and they are repeated here. Two examples are taken from Coweeta. The first is a 13 ha, 100 percent clearcut watershed where no increase in maximum peak discharge was detected. The second, a 44 ha watershed was also clearcut 100 percent, and the peak flows increased by 9 percent.

A study of commercial logging on watersheds in West Virginia showed that the effects on storm peaks depended on the season. Eighty-six percent of the total wood volume was removed from a hardwood-forested watershed. Instantaneous peaks during the growing season increased by an average of 21 percent; in the dormant season they were apparently reduced by 4 percent. In Japan, clearcutting a 2.4 ha watershed increased peak runoff from heavy rains by about 20 percent.

Both forest and ground cover were removed from the Hubbard Brook Experimental Forest in New Hampshire. Summer peak flows increased considerably. For the six highest peak flows during June through September, 1966 through 1969 the peaks for a 16 ha denuded watershed averaged double the expected amount, with increases for the individual events ranging from -19 to +250 percent.

Clearcutting can either increase or decrease peak flow rates when snowmelt is involved. In another experiment at Hubbard Brook, clearcutting a small watershed increased peak



flows early in the snowmelt season by as much as 35 percent and decreased them as much as 66 percent later in the season.

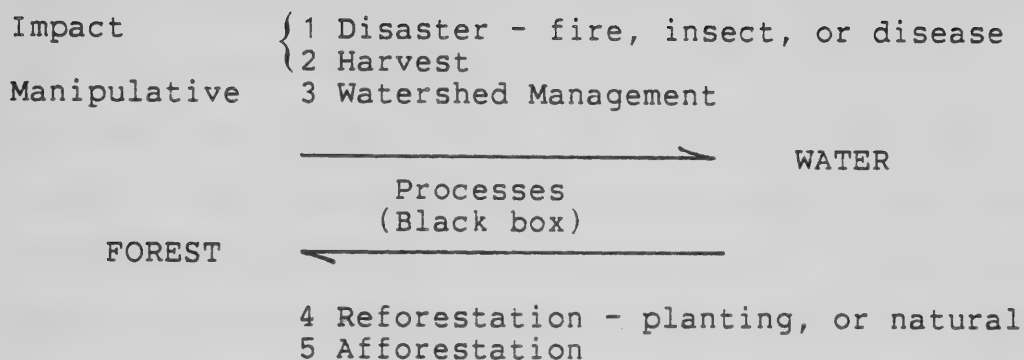
At the H.J. Andrews Experimental Forest in central Oregon during the 1965-69 period, the peaks for 84 percent of the storms were greater in the clearcut watershed than in the uncut control. Other studies show that clearcutting watersheds in Oregon may produce an increase in peaks from fall storms of 90 percent and from winter storms of 28 percent. (Anderson et al. 1976)

At Fraser, Colorado the treatment referred to earlier produced no significant change in the average peak flows (Leaf, 1975), although peak discharges from snowmelt were greater than predicted, increasing by 50 and 45 percent during the first and third years following treatment, respectively. The peak for the second year was 23 percent less than had been expected. (Anderson et al. 1976)

Given the results from the investigations described above together with results published elsewhere, it is possible to illustrate most of the facets of forest hydrology and watershed management in the form of a reversible quasi-equilibrium equation:







The events shown above the equation result in reduced forest cover and increased water yield or a shift in equilibrium to the right. For events listed below the equation, the reverse is true.

It will be observed that the watersheds referred to so far are all quite small - only one exceeds 500 ha in area. Therefore, the results to be summarized are applicable primarily to small watersheds. It appears that removing forest cover affects hydrological processes in the following ways:

1. decreases interception (no forest canopy);
2. reduces transpiration (no trees);
3. increases evaporation (reduced ground protection);
4. reduces soil water deficits (decreased draft on soil water);
5. increases water yield, the absolute increase being greater in humid than in dryer regions;
6. increases peak flows;



7. changes the aerodynamic effect of the forest (wind flow patterns and velocities are altered which has important implications for snow redistribution);
8. in areas where snow forms a significant part of the precipitation, increases snow accumulation in the open areas and reduces it in the adjacent forest. (Snow in the open is also subject to increased sublimation. Under certain sheltered conditions, snow tends to remain longer in the openings than in the adjacent forest);
9. water yield increases are usually greatest during the first few years following forest cover removal. The effect is reduced as the area becomes restocked with trees. In humid areas where plants grow rapidly, the increase in water yield may be significantly reduced within a few years after forest clearing. In areas where snow is an important factor and where plant growth is slow, the effects may remain for more than 30 years.

When regrowth is established, or when reforestation or afforestation are effected, the foregoing processes are reversed. This is a generalization, but there are usually increases in interception, transpiration, infiltration rate, and detention storage, as well as reductions in water yields and peak flows. As the forest canopy becomes more uniform in height the snow depth under the canopy also tends to become more uniform.



Another important finding from many studies is that Hortonian overland flow is not a significant process on forested watersheds except on and in the vicinity of logging roads and exposed soils. Usually infiltration capacity of soils under forest exceeds the rainfall intensity by a comfortable margin.

In spite of the progress made in the fields of forest hydrology and watershed management, many problems remain. Most important perhaps is the insufficient attention paid to the necessity of extrapolating results from small watersheds to large ones for land management purposes. The problem is compounded by contradictions between results reported for small watersheds and those obtained for large river basins. Russian investigators (Rakhmanov, 1962, 1970a, 1970b; and Bochkov, 1970) used statistical procedures to show that a positive relation exists between percent forest cover and streamflow for large river basins. In the case of the Upper Volga Basin study (Rakhmanov, 1970b) this conclusion was based on data (Fig. 3) from 53 basins ranging in size from 248 to 13,528 km<sup>2</sup>. However, the positive relationship discovered by Rakhmanov and Bochkov exists because more trees grow where water and climate are favorable; it does not imply that water yields are reduced when forest cover is decreased.

There are two instances where results from large basins have supported conclusions drawn from small watershed studies. The first concerns destruction of a forest by





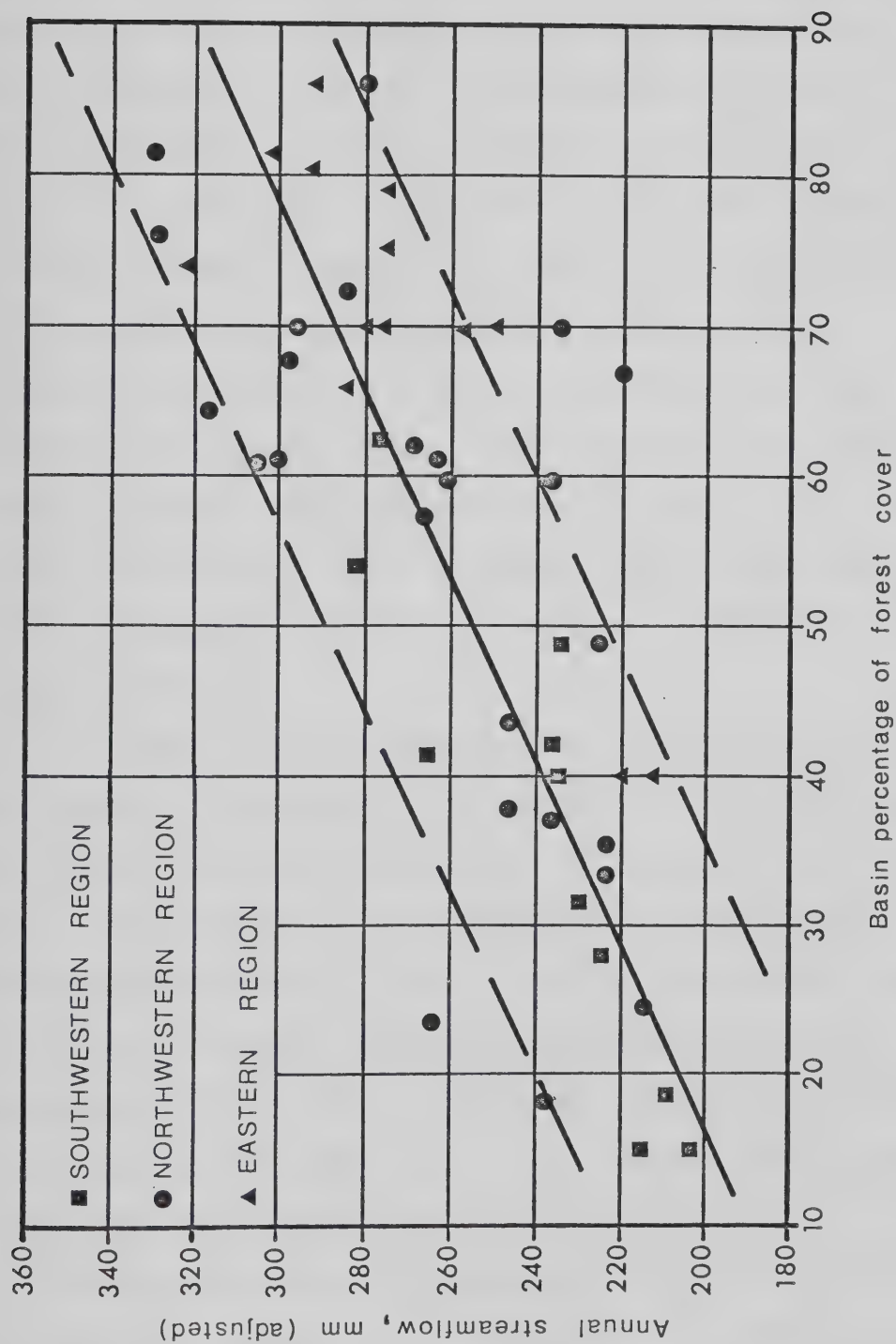


Figure 3. Relation of mean annual streamflow to forest cover adjusted for effect of latitude. Upper Volga Basin. (After Rakhmanov, 1970b).



insects (Love, 1955), and the second involves long term recovery of forest vegetation in the Sacandaga River drainage, New York (Hibbert, 1967). An outbreak of Engelmann spruce beetle on the White River Plateau of western Colorado killed Engelmann spruce and lodgepole pine on 30 percent of a 1974 km<sup>2</sup> drainage of the White River. The increase in average annual streamflow of 58 mm during the years following the outbreak was attributed to reduced interception of snow and reduced transpiration by beetle-killed trees (Love, 1955). Results from the New York study (Hibbert, 1967) showed that increasing the forest basal area from 17 to 28 m<sup>2</sup>/ha on the 1272 km<sup>2</sup> Sacandaga River watershed over 38 years caused a reduction in water yield of 196 mm.

Although a considerable amount of information is available on the behavior of watersheds, it is a remarkable fact that there are no examples of watersheds, large or small, being managed for increased water production. Forest watershed management today is almost exclusively protective in nature, directed primarily to preventing erosion and maintaining water quality. However, some estimates are available on the potential for increasing water yield in the United States (Table 4).

From the foregoing discussion it is evident that considerable research still remains to be done and should be directed to solving the following problems:

1. develop extrapolation procedures so that results from



Table 4. Estimated potentials for increased water yields from forest and range lands in the United States through programs of vegetative management (Adapted from Sopper, 1971).

Area	Total (X1000km <sup>2</sup> )	% treatable	Potential increase from uncut base (X10 <sup>6</sup> m <sup>3</sup> )	Potential increase under present forest condition (X10 <sup>6</sup> m <sup>3</sup> )
<b>Northeast</b>				
(New England, Middle Atlantic, Lake and Central States)				
Commercial forest	696	53	3207	2899
<b>Southeast</b>				
(South Atlantic and Gulf States)				
Commercial forest	813	58	3639	3392
TOTAL (East)	1509	56	6846	6291
<b>Pacific Northwest</b>				
(Eastside portions of Oregon and Washington)				
Commercial forest	93	61	210	197
<b>California - excluding North Coast</b>				
Commercial forest	65	70	234	160
Phreatophyte area	12	5	12	12
Chaparral	32	30	505	505
Woodland - grass	36	50	456	456
<b>Northern Rocky Mountains</b>				
(Idaho, Montana, Western S. Dakota and Wyoming)				
Commercial forest	154	68	1419	1233
Other	12	30	49	49
<b>Southern Rocky Mountains</b>				
(Arizona, Colorado, Nevada, New Mexico, and Utah)				
Commercial forest	105	58	690	654
Phreatophyte area	65	15	1110	1110
Chaparral	24	25	357	357
Other	304	14	370	370
TOTAL (West)	902	38	5412	5103
TOTAL (48)	2411	49	12258	11394

Source: Reigner, I.C., R.C. Maloney, and E.G. Dunford. 1969. Report on file.  
USDA Forest Service, Washington, D.C.



- small experimental watersheds can be applied to
- a. similar basins in the same region,
  - b. basins with different characteristics,
  - c. large river basins;
2. in the absence of Hortonian flow, obtain a better understanding of subsurface flow as influenced by geology, vegetation, landform, and other important factors;
  3. develop improved methods of routing flow through the subsurface portion of the watershed.

Watershed experiments are costly and time-consuming undertakings. Because of this, and the availability of powerful computers, researchers are turning increasingly to watershed simulation models for answers to their watershed problems. Nevertheless, gauged watersheds are still necessary to provide field data against which model outputs can be checked. This thesis is an attempt to find solutions to the subsurface flow problems described in 2 and 3 above, in the particular setting of a forested foothill or mountain watershed, using computer simulation models.

## **B. Development Of Forest Hydrology And Watershed Management In Alberta**

The Saskatchewan River system which rises on the east slopes of the Rocky Mountains of Alberta is an important source of water for the prairie region of Alberta,





Saskatchewan and Manitoba. About 87 percent of the drainage area is located on the plains, the remainder lies within the foothills and mountains of Alberta. However, this smaller portion (13 percent) contains the upper headwaters of the Saskatchewan River system and contributes 87 percent of the total annual flow (Hanson, n.d.).

The importance of these forested headwaters was recognized as early as 1910 when the Dominion Government established the Rocky Mountains Forest Reserve, an area of about 23150 km<sup>2</sup>. The Forest Reserve contains most of the Saskatchewan River headwaters area not included in the National Parks (Fig. 4).

Later, discussions between the Canadian Government and the Province of Alberta led to the formation in 1947 of a joint federal-provincial agency, the Eastern Rockies Forest Conservation Board. Its task was two-fold:

1. to operate a program designed to protect forests from fire, insects, disease and other damage;
2. to conserve, develop and manage forests to obtain the optimum flow of water (optimum quality, quantity and timing) in the Saskatchewan River and its tributaries (Alberta Energy and Natural Resources, 1979).

After a decade of operation, the Board faced several problems: its ability to function effectively was hampered by lack of basic data from research, local water shortages were becoming more common, and there were conflicts in



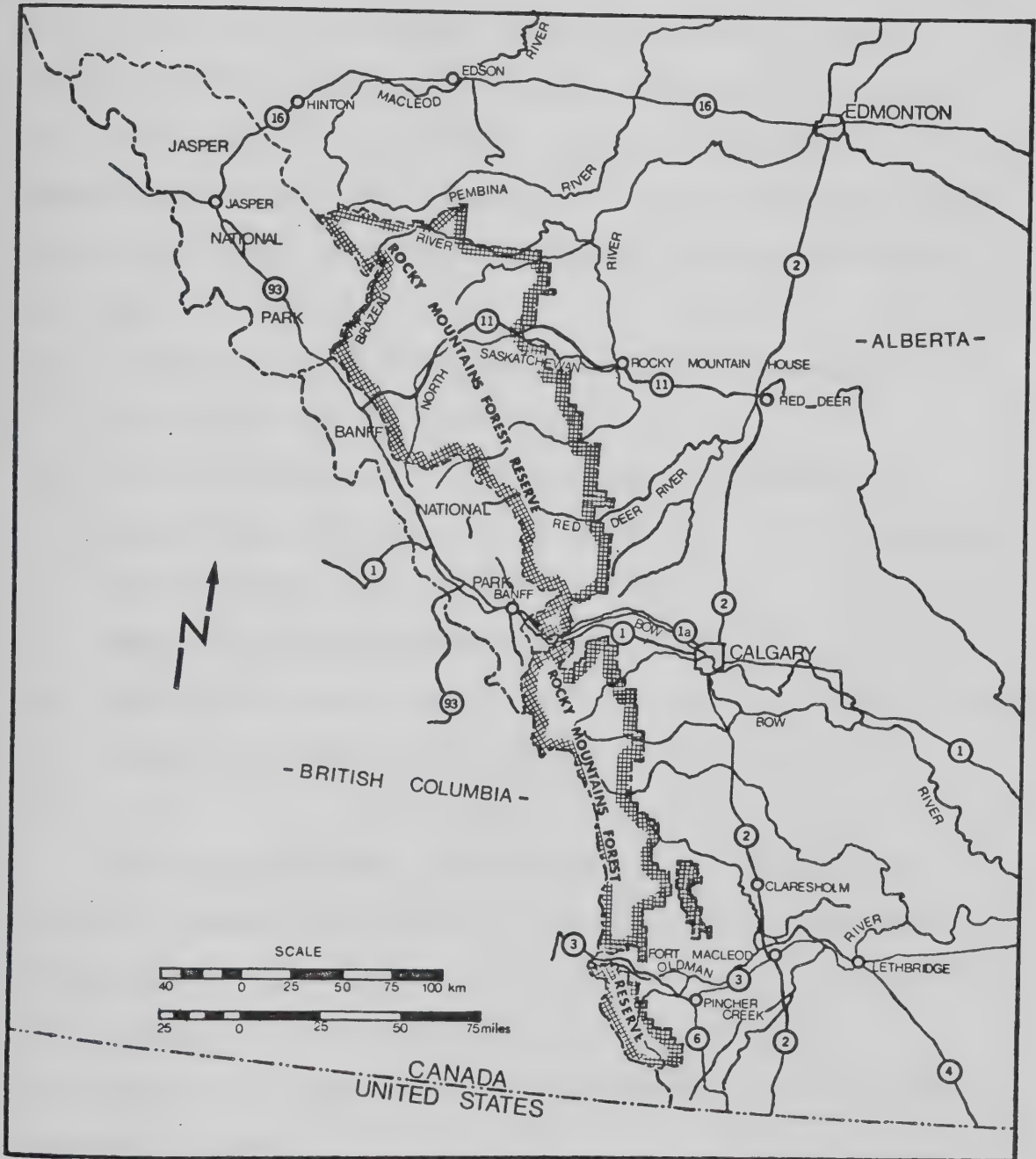


Figure 4. Map showing Rocky Mountains Forest Reserve (Adapted from maps published by the Alberta Government).



demand for available water supplies downstream (Redmond, 1964).

In 1959, senior federal and provincial authorities met to examine these problems. They agreed that a special Committee - the Technical Advisory Committee - be formed to define research and management problems related to watershed management on the east slope of the Rocky Mountains. This Committee would carry out a research program which would provide:

1. a better understanding of hydrologic processes both locally and in the entire area;
2. evaluation of newly developed and old methods of protecting and maintaining watersheds while forests and other resources are being utilized;
3. means of restoring damaged watersheds;
4. methods of improving streamflow (quantity, quality, and timing) from the watershed.

This program came to be known as the East Slopes (Alberta) Watershed Research Program. It was also agreed that most of the research should be carried out within the Rocky Mountains Forest Reserve, and that small representative watersheds be selected for intensive study (Redmond, 1964).





Jeffrey<sup>3</sup> was perhaps the first to attempt a problem analysis and to suggest methods by which stated research program objectives might be attained. Subsequently, three representative basins were selected for study. Marmot Creek Basin (940 ha in area) was established to study the hydrology of spruce-fir forests. Deer Creek Basin (544 ha) was selected as representative of lodgepole pine forest, and Streeter Basin (598 ha) was chosen for research into montane aspen forest and associated grasslands. These three vegetation types comprise most of the Forest Reserve area which lends itself to any type of vegetation manipulation for the purpose of altering water yield and regime.

Deer Creek Basin was later withdrawn from the Watershed Research Program because the commercial harvest objectives set for the lodgepole pine basin had been realized elsewhere on the East Slopes. It was established that harvesting lodgepole pine and spruce-fir does increase streamflow (Swanson, 1977; Swanson and Hillman, 1977).

During the decade 1960 to 1970 meteorological, groundwater, hydrometric and other instrumentation networks for the three basins were completed (Jeffrey, 1964, 1965; East Slopes (Alberta) Watershed Research Program, 1966). In 1969, when the Program was expanded to include the entire province of Alberta, its name was changed to Alberta Watershed Research Program (AWRP) (Swanson, 1977). The AWRP

---

<sup>3</sup>Jeffrey, W. W. 1961. Prerequisites and priorities for watershed research in the Eastern Rockies, Alberta - a tentative initial appraisal. Can. Dep. For., For. Res. Br., Calgary, Alberta. Unpubl. rep.



has become the primary vehicle for conducting and overseeing forest watershed research in Alberta. It replaces the Eastern Rockies Forest Conservation Board which ceased to exist in 1973.

The expansion introduced other watershed experiments, located outside the Forest Reserve, into the program. Tri-Creeks Basin for example is being monitored to determine the impact of a pulp timber harvesting operation on lodgepole pine-foothills hydrology with special attention being devoted to maintaining water quality and preserving fish habitat. Spring Creek project was established to examine the hydrologic effects of converting aspen-spruce forest land for agricultural use.

The principal objectives for each basin are similar to the objectives of the AWRP as a whole: to establish the hydrology of the basin, to assess the effect of forest cover removal on water quality, yield and regime, and/or to develop vegetation manipulating schemes which will produce favorable changes in water quality, yield or regime. The common procedure adopted to attain these objectives is the paired watershed approach described earlier.

The program's first treatment, a "commercial" forest harvest, was carried out on Cabin Creek Basin, a subbasin of Marmot Creek. Another subbasin, Middle Creek Basin, which adjoins Cabin Creek subbasin, serves as control. Logging haul roads were constructed in Cabin Creek Basin during 1971-72. The commercial harvest itself was not carried out



until 1974. Data for evaluating the effects of road construction alone on sediment production in Cabin Creek were obtained during the intervening period. The commercial harvest on Cabin Creek Basin was completed in October, 1974. Six blocks representing 50 percent of the forested area in the subbasin were clearcut.

In 1976, the west subbasin of Streeter Basin was treated to improve range conditions for cattle and wildlife while maintaining or prolonging streamflow during the summer months. The hydrologic objectives were to be met by altering the vegetation so that a) snow would be concentrated in areas where sublimation and melt would be minimized, and b) infiltration of snowmelt would be enhanced by reducing snow accumulation in discharge areas and increasing it in recharge areas.

For this purpose a total area of about 55 hectares was treated. Patches 1 1/2 to 2 tree heights in width and 60 to 180 m in length were cut in the aspen stands. In shrub stands, strips of 3 to 5 m width were cleared (Golding, 1977).

A second treatment for Marmot Creek Basin commenced in 1977. In this case the objective is to alter the water regime or, more specifically, to delay the time of peak runoff and to prolong recession flow resulting from snowmelt. Middle Creek subbasin again serves as control. Treatment was carried out on Twin Creek subbasin and consisted of cutting 40 percent of the forested area in 2500



circular openings. The size of openings ranged from about 3/4 to 1 1/2 times the height of the adjacent trees (Golding, 1977). Treatment was completed in late 1979.

In August 1978, the Oldman River Basin Study Management Committee recommended that research areas be established in the Oldman River Basin, Southern Alberta to provide convincing data on whether vegetative manipulation would produce beneficial increases in water yield (Environmental Council of Alberta, 1979). Unlike the experiments described previously, this study would be conducted over a large area ( $> 260 \text{ km}^2$ ). The recommendation calls for tests of three different forest land management practices:

1. no vegetation manipulation;
2. harvesting using good commercial harvesting techniques as approved by the Alberta Forest Service;
3. vegetation manipulation for the sole purpose of increasing water yield. These practices would be monitored on three representative sub-basins.

The recommendation is an outcome of a report, prepared for the Oldman River Basin Study Management Committee (Northwest Hydraulics Consultants Ltd., Hyat Resource Services Ltd., Edmonton, Alberta. 1977) which examined the possibility of increasing water yields through watershed management in the upper Oldman River Basin. This report is one of several commissioned by the Committee, in response to water shortages in Irrigation Districts of southern Alberta,





to investigate alternatives for increasing water yields in the Oldman River Basin.

### C. The Watershed System

Forest watershed management and forest hydrology studies are usually conducted on small watersheds that provide flow during most of the year and are less than 25 km<sup>2</sup> in extent. The main reason for selecting small watersheds is that travel time and channel storage during storm periods are not the major factors in determining volume of direct runoff. If they were, then the land-use effects being measured would be masked by the channel storage effect.

A watershed system consists of the area contained within topographic divides, the precipitation falling on the area, water stored or detained by the watershed, and the discharge from its exit point. Vertically, the system extends high enough above the vegetation canopy to include both total precipitation and the aerodynamic effects of the canopy. It extends low enough to include all porous media and subsurface water influencing or contributing to channel flow within the watershed. Usually, it is assumed that the groundwater or phreatic divide coincides with the topographic divide, and that water enters the watershed as precipitation and leaves it as channel flow or is returned to the atmosphere. The second assumption implies that there is no subsurface inflow and outflow i.e. the watershed does



not leak. Such assumptions must be verified by appropriate subsurface investigations.

The hydrological processes governing water movement through a watershed are well documented. Many processes such as infiltration, flow through porous media, and open channel flow can be expressed in the form of one or more equations, the derivation of which is based on sound physical principles. Most hydrologists accept these relations when the processes are considered in isolation, but often disagree on how these processes should be integrated to describe the watershed system. A prime example of such a subject of disagreement is the movement of water from the land surface to the stream channel.

Hydrologists have long recognized that water moving from the ground surface to the stream channel follows three routes of travel: overland flow, interflow, and groundwater flow. Overland flow or surface runoff is that water which travels over the ground surface to the channel. Interflow is water which infiltrates the soil surface and moves laterally through the upper soil layers. Groundwater flow, also called base flow or dry-weather flow, occurs when the water table intersects the stream channel. Usually, the total flow is divided into two parts: storm, or direct, runoff and base flow. Direct runoff consists of overland flow and interflow, and baseflow is groundwater. This distinction is based on time of arrival in the stream channel rather than on the path followed (Linsley et al., 1958). The relative



importance of overland flow, interflow and groundwater flow has been the subject of much debate among hydrologists.

The classical concepts of infiltration and overland flow were first propounded by Horton (1933, 1936, 1945) nearly 50 years ago. He developed a negative-exponential decay function which determined the changes in infiltration capacity as a rainstorm progressed. Simply put, Horton's theory states that if the rainfall intensity exceeds the infiltration capacity, then the excess rainfall becomes overland flow which is the sole determinant in the stream hydrograph peak. Overland flow is assumed to occur over all parts of the watershed as a thin film or sheet.

These concepts were not seriously questioned until the 1960's when several investigators presented new insights into process and watershed behaviour. Hewlett (1961) observed no overland flow on a forested watershed at Coweeta, North Carolina. Further investigation also showed an absence of any large groundwater system to provide nonstorm streamflow. Using measurements of saturated and unsaturated flow through a steeply-inclined trough, Hewlett (1961) showed that unsaturated soil can serve as main storage or source for base flow. He concluded that: "up-slope rain charges the soil mantle in preparation for succeeding days and weeks of base flow, whereas downslope rain and channel interception will furnish most of the streamflow". Thus the areas immediately adjacent to small streams provide, through groundwater drainage, a





disproportionate percentage of stormflow relative to the total area of the watershed. This implies that, contrary to Horton's theory, only a small percentage of a watershed area contributes storm runoff, and that this area is effectively an extension of the existing channel network. After the storm has passed, the channel system eventually reverts to its original, perennial extent. Hewlett and Hibbert (1967) referred to this idea of a shrinking and expanding source area as the variable source area concept.

Betson (1964) developed a nonlinear mathematical infiltration capacity model to analytically equate the difference between rainfall and runoff to hydrologic variables. Discrepancies between observed and predicted results indicated that some important factor had been omitted during model development. Further investigation showed that the problem centred around the assumption that the total watershed area contributed runoff. The observed volume of runoff from the watershed had been converted to watershed inches using total drainage area. When adjustments were made for smaller contributing, or partial, areas, the rainfall-runoff relation occurred according to the infiltration capacity concept. Subsequently, it was determined that contributing areas for different watersheds supporting various cover types ranged from 4.6 to 86 percent. The "partial areas" idea helps to explain why infiltration capacity of much of the watershed is seldom exceeded during storms (Betson, 1964).



Ragan (1968) investigated the concept of partial area contribution to storm hydrographs by collecting detailed information in the vicinity of a 189 m length of a second order stream on a forested watershed. Measured inputs to the channel included flow entering the channel over an upstream structure, channel precipitation, baseflow prior to storms, flow from seeps, and lateral inflows (overland flow, interflow and groundwater flow). Outflow from the channel section was measured by a downstream control structure.

Ragan, too, found that only a small portion of the watershed contributed flow to the storm hydrograph. The contributing area, which is a function of storm duration and intensity was very localized - occupying only 1.2 to 3 percent of the total watershed area. During periods of low rainfall intensity most of the flow came from channel precipitation and rain falling on wet areas surrounding a series of seeps. During a period of high rainfall intensity, flow occurred as saturated porous media flow within the lower zone of the forest litter on hillsides, creating a larger contributing area. Interflow through mineral soil did not occur.

The idea that only a small portion of a watershed area contributes direct runoff has been supported by results from other studies. Dickinson and Whiteley (1970) computed the minimum contributing area for several storms on the Blue Springs Basin in southern Ontario and obtained values ranging from 1 to 50 percent, with the majority being less



than 10 percent.

The two concepts of contributing areas referred to in the preceding discussion differ in two ways. First, partial areas are considered to be more or less fixed in location on the watershed, whereas variable source areas expand and contract. Second, partial areas supply water to streams by means of overland flow, whereas the extended channels in variable source areas are believed to be fed by subsurface stormflow (Freeze, 1974).

Subsurface stormflow which commonly occurs in forested areas differs from true groundwater flow in that it flows to the stream channel before reaching the general groundwater zone. It is more likely to occur where: a) the land is sloping, b) the surface soil is permeable, c) a water-impeding layer is near the surface, and d) the soil is saturated (Whipkey, 1965).

Forest hydrologists (Hewlett, 1961; Hewlett and Hibbert, 1963, 1967; Hewlett and Nutter, 1970; Whipkey, 1965) have studied the subsurface flow mechanism in some detail. They believe that the bulk of the average upland hydrograph is accounted for through this process (Hewlett and Nutter, 1970). To counter the argument that flow velocities are too small for subsurface flow to contribute a significant volume to direct runoff, Hewlett and Hibbert (1967) suggested the concept of translatory flow - a flow produced by water displacement. This concept implies that "new" water does not have to traverse the soil mass between



the point of entry and the stream channel to produce an effect on streamflow. Instead, the water induces a "pulse" such as occurs when water is added to a soil column drained to field capacity. Water flows from the bottom (stream channel) almost immediately but it is not the same unit of water added at the top (storage). The evolution of the variable source area concept and subsurface stormflow theory can be traced through a series of papers listed in Hewlett (1974) and Whipkey (1965).

Dunne and Black (1970a,b) examined runoff-producing mechanisms on three heavily instrumented hillside plots on the Sleepers River watershed, northeastern Vermont. They concluded that the major portion of storm runoff is produced as overland flow on small saturated areas close to streams - a conclusion which supports the partial area concept of storm runoff production. Subsurface stormflow was not an important contributor to total storm runoff. Freeze (1972b) used a deterministic mathematical model to investigate mechanisms for generating streamflow. His conclusions, based on a number of simulations, were similar to those of Dunne and Black (1970a,b). Freeze also specified the conditions under which subsurface stormflow becomes large enough to contribute significant amounts to storm runoff, namely: convex slopes feeding steeply incised channels, and high soil permeabilities.

It appears then that there are two distinct schools of thought regarding streamflow generation in upstream source





areas of vegetated watersheds: one supporting the theory of overland flow from near-channel partial areas, and the other advocating the variable source area concept coupled with subsurface flow. However, as Hewlett (1974) points out, if one makes allowances for differences in concepts and terminology, the two ideas are essentially one and the same.

There is ample evidence in the more recent literature that some or all of the mechanisms described previously may be important in runoff generation. The relative dominance of each process is governed by both meteorological and watershed characteristics. Hortonian overland flow, for example, was the principal mechanism operating on a tropical rainforest watershed in Queensland, Australia (Bonell and Gilmour, 1978). High intensity rainfalls frequently exceeded the average resultant saturated hydraulic conductivities below 20 cm depth, which resulted in a perched water table and subsurface flow (including "pipe flow") within the top 20 cm of soil. Widespread saturation overland flow occurred when additional rain caused the perched water table to emerge at the soil surface. In this case the variable source area concept is not applicable (Bonell and Gilmour, 1978).

Certain soil conditions that prevail prior to storms and snowmelt may also be conducive to generation of extensive overland flow. During a field study in Yorkshire, England, Beven (1978) found that surface runoff occurred on large areas of poorly drained soils (which soon reached saturation) during storms.



In Canada, snow and ground frost are usually important factors governing runoff. Dunne et al. (1976) determined the runoff from hillside plots under boreal forest and on tundra in the Labrador subarctic, near Schefferville, Quebec. They found no evidence of subsurface flow, in the trenches prepared for this purpose, during the snowmelt period. The soil had been rendered impermeable by concrete frost, and runoff took place through the snowpack - primarily through a saturated layer of snow at the base of the pack.

In contrast to studies which show overland flow to be the primary source of storm discharge, there are other studies which indicate that subsurface flow is the only mechanism producing runoff (Beasley, 1976; Harr, 1977; Megahan, 1972; and Mosley, 1979). Beasley (1976) monitored 115 storms in northern Mississippi over a three year period and found that they produced little overland flow and subsurface flow above the B horizon. Subsurface flow over an impermeable clay layer was as much as 90 percent of rainfall during a calendar quarter. It usually began shortly after rainfall commenced, even when there was neither saturation at the point of outflow nor high antecedent soil moisture. Thus the translatory flow concept of Hewlett and Hibbert (1967) could not explain this quick response. Instead, the response is attributed to the presence of interconnected channels through the soil formed by decayed roots and animal burrows. This idea is shared by several other workers investigating subsurface flow phenomena (De Vries and Chow,



1978; Mosley, 1979; and Whipkey, 1965).

Mosley (1979) used dye tracer experiments on a forested watershed in New Zealand to show that water may move through macropores (root channels, pipes) at rates two orders of magnitude greater than the saturated hydraulic conductivity of the soil. Subsurface flow through the macropores and seepage zones in the soil was found to be the predominant mechanism of channel stormflow generation. Mosley also found that subsurface flow from lower slopes contributed to delayed flow. Runoff from partial and variable source areas did not contribute significantly to stream discharge, and translatory flow apparently was not an important runoff generating process on this watershed.

No overland flow was observed during a study on a steep, forested watershed in Oregon (Harr, 1977). Subsurface flow and channel interception accounted for 97 percent and 3 percent respectively of total stormflow. The rapid response to precipitation was attributed to translatory flow (Hewlett and Hibbert, 1967). Results from stormflows analyses showed agreement with the variable source area concept of runoff production.

Weyman (1973) measured saturated and unsaturated lateral soil water movement on a convex hillside in Somerset, England. He found no overland flow and concluded that saturated flow through non-capillary pore spaces dominated hillslope hydrographs. Weyman suggested that saturated conditions must be generated within the organic





horizons or within the non-capillary spaces of the lower soil horizons if lateral soil water flow is to provide storm runoff to the stream. Baseflow was dominated by unsaturated lateral flow.

It is evident from the results of many hillslope hydrology studies (Chamberlin, 1972; De Vries and Chow, 1978; Mosley, 1979; Plamondon et al., 1972; Weyman, 1973; and Whipkey, 1965) that macropores or non-capillary spaces in the form of root channels and animal burrows may be important factors in storm runoff generation. Plamondon et al. (1972) used a water balance procedure to determine saturated flow through macropores of the forest floor and soil matrix on a forested site in coastal British Columbia. They discovered that usually between 50 and 80 percent of the precipitation flowed through the macropores during storms.

In another experiment on the same watershed De Vries and Chow (1978) measured the water potential field during wetting and drainage phases of simulated rainfall events. Measurements were repeated with the forest floor intact, partly disturbed, and totally removed. It was inferred that the flashy response of streams to rainfall events was related to rapid subsurface stormflow through root channels. Where the forest floor was disturbed there was a tendency for less water to move through the root channels, and more water through the soil matrix. Consequently, the rate of subsurface flow was diminished. This condition probably



resulted from closure of root channel openings during disturbance to the forest floor.

If flow through macropores is indeed an important process in storm runoff generation, it is probable that Darcy's Law for flow through a porous medium will not apply in this case. Instead, the flow may be better described by turbulent flow equations. Furthermore, when flow takes place through the upper layers, including the litter layer, of the forest floor, it also is more likely to occur as turbulent rather than porous media flow. Often it will not be readily observed because it takes place below the visible coarse matrix of the litter, but over the more compact portion of the organic horizons.

In hydrograph analysis groundwater is customarily associated with base flow, but there is increasing evidence that groundwater may also contribute significantly to storm runoff as well. Using environmental tritium, Martinec (1975) demonstrated that a substantial part of snowmelt water did not leave the basin, although a quantitative water balance was maintained. The proportion of subsurface flow contributing to snowmelt discharge exceeded 50 percent. Apparently snowmelt water infiltrated into the ground and "old" subsurface water appeared in the discharge.

Similar results have been obtained by Sklash and his colleagues (Sklash et al., 1976; Sklash and Farvolden, 1979) using the Oxygen-18 isotope technique and specific conductance methods. They found groundwater to be a major



component in virtually all the runoff events they examined. Field observations and computer simulations (Sklash and Farvolden, 1979) suggest that very large and rapid increases in hydraulic head in the near-stream groundwater occur soon after the onset of rain. Computer simulations show the formation of a groundwater ridge adjacent to the stream in response to a rain event with the lag time brief and inversely related to the near-stream unsaturated zone thickness.

The same paper also provides a theoretical basis to explain the significant role of groundwater in storm and snowmelt runoff generation

"Along the perimeter of transient and perennial discharge areas, the water table and its associated capillary fringe lie very close to the ground surface. Soon after a rain or snow-melt event begins, infiltrating water readily converts the near-surface tension-saturated capillary fringe into a pressure-saturated zone or groundwater ridge (Ragan, 1968). This groundwater ridge not only provides the early increased impetus for the displacement of the groundwater already in a discharge position, but it also results in an increase in the size of the groundwater discharge area which is essential in producing large groundwater contributions to the stream. The response of the upland groundwater may become important at later times in the runoff event but has little influence in the early part of the runoff event.

The groundwater may discharge directly into the stream through the stream bed or it may issue from the growing near-stream and/or remote seep areas and flow as overland flow to the stream (as in the variable source area-overland flow theory). Following periods of drought during which the water table has fallen far below ground surface, intense storms may result in surface saturation from above and rain-like overland flow (partial area-overland flow) before the water table can emerge."



Results from these groundwater studies lend credence to the translatory flow concept of Hewlett and Hibbert (1967).

As new developments of the type described above unfold, it becomes necessary to make provision for them in field studies and hydrological analyses. For example, the variable source area concept is now widely accepted as a valid mechanism for generating streamflow. However, techniques to identify, map, and predict variable source areas in the field on a routine basis have yet to be developed.

This problem is receiving increasing attention as is evidenced from papers by Anderson and Burt (1978), Beven (1978), and Dunne et al. (1975). The first of these papers (Anderson and Burt, 1978) describes a field study in which an automatic tensiometer system was used to monitor soil water potential on a single hillside hollow - a location usually identified as a variable source area - and on an adjacent ridge. Soil water potential maps and flownets constructed from field data showed that, after a storm, convergent flow into the hollow took place. They also established that hollows are the major sources of slope discharge while ridge zones were much less important contributors.

While investigating comparative contributions of sideslope and headwater areas to stream discharge Beven (1978) also found that convergent hollows are important sources of streamflow. These areas of surface soil saturation were associated with ephemeral channels expanding





as variable contributing areas of surface flow during storm rainfall. The apparent saturated areas were mapped by direct observation in the field. Results from the study showed that the headwater areas will usually provide higher and earlier peak flows per unit area, and more total storm discharge than the sideslope areas.

Dunne et al. (1975) consider repeated field mapping to be the best method for determining the size, location, and variation of the saturated zone both during and between storms. This method should certainly be satisfactory for rainstorms but will be impractical where extensive snowpacks serve as the water supply. Other methods which can be used include:

1. mapping the saturated areas on the basis of soil colouring where the colour is indicative of waterlogged soils;
2. relating saturated areas to areas of "poorly drained" soils as shown on soil maps;
3. using plants as indicators of soil wetness;
4. relating baseflow, antecedent precipitation index, or water table elevation to mapped extent of saturated area.

The authors, describing areas for future research, stress the need for more field observations relating subsurface stormflow, return flow, and direct precipitation on saturated areas. The process of, and storage opportunities



for, saturation overland flow in runoff producing areas also needs to be investigated. Techniques are also required for estimating the seasonal variation of saturated areas.

To conclude this section on the watershed system, it is worth noting that several investigators who featured prominently in the development of the concepts outlined above have contributed to a book on hillslope hydrology (Kirkby, 1978). This book provides a most comprehensive description of the "state-of-the-art" of small watershed hydrology.

#### **D. Watershed And Hydrologic Modelling**

Comprehensive field studies of watershed systems can be expensive and time-consuming. Consequently, hydrologic and watershed models are used to overcome these limitations and to supplement field studies. A watershed model is really one type or class of model within the spectrum of a multitude of hydrologic models. Clarke (1973) defines a model as a simplified representation of a complex system being either physical, analog, or mathematical. Along with the development of hydrologic models, a new vocabulary has evolved. In their reviews of methods used in hydrologic investigations, Amorochio and Hart (1964) and Clarke (1973) clarified the definitions of many terms used in hydrologic modelling and data processing. The definitions which follow are taken from these two papers.



Hydrologic studies may be grouped under two areas of research: physical hydrology and systems investigations. Physical hydrology is concerned with physical processes such as those involved in water or energy transfer, whereas systems investigations deal with establishing relationships between variables, without concern for the physical mechanism involved.

Systems investigations fall into two categories called parametric hydrology and stochastic hydrology. Parametric hydrology is the development of relationships among physical parameters involved in hydrologic events and the use of these relationships to generate, or synthesize, non-recorded hydrologic sequences. Examples of methods used in parametric hydrology include correlation analysis, partial system synthesis with linear analysis, general system synthesis and general non-linear analysis. Some knowledge of the physical system is required when the first three methods are employed.

Stochastic hydrology is the use of statistical characteristics of hydrologic variables to solve hydrologic problems. A stochastic system differs from a probabilistic system, in that it is time dependent. There are two important methodologies in common use in stochastic hydrology: Monte Carlo methods, and the methods of transition probability developed under the general theory of Markov processes. The first group is valid for data which are statistically independent, and the second is applicable





where the state of a system at a particular time depends on previous states.

The different methods of systems investigations share two things in common, a) their dependence on historical records of parameter values, and b) the assumption of time invariance (stationarity) of the hydrologic systems. Both of these characteristics place definite theoretical limitations on the generality of the solutions.

Parametric hydrology is usually associated with system analyses or "black box" methods in which relationships are established between measured input and measured output by mathematical procedures. No attempt is made to describe the internal mechanisms of the system. In system synthesis, on the other hand, the investigator attempts to describe the operation of the system by a linkage or combination of components, whose presence is presumed to exist in the system and whose functions are known and predictable. The linkage of components must be made in such a manner that the correct output is produced whenever a specified input is applied. System synthesis falls within the realm of physical hydrology.

The nature of hydrologic or watershed models can be described in several ways. They may be "deterministic" or "stochastic", "conceptual" or "empirical", "lumped" or "distributed", and "linear" or "non-linear". If a model or process follows a definite law of certainty but not any law of probability, then it is described as deterministic. If



the concept of probability is involved, then the process or model is considered to be stochastic or probabilistic. A conceptual model is one in which the mathematical functions consider the physical processes acting on the input variables to produce the output variables. If the model is based on observation and experiment rather than on theoretical considerations, then it is empirical. A lumped model is space-independent, whereas a distributed model takes into account the spatial variability of input variables or model parameters.

The term linearity may have at least two meanings (Clarke, 1973). In the systems theory sense, a model is linear if the principle of superposition holds: that is, given that  $y_1(t)$ ,  $y_2(t)$  are the outputs corresponding to inputs  $x_1(t)$ ,  $x_2(t)$ , a model is linear if the output corresponding to input  $x_1(t) + x_2(t)$  is  $y_1(t) + y_2(t)$ . This is the sense in which linearity is most widely used in the hydrologic literature. Alternatively, the model may be linear in the statistical regression sense if it is linear in the parameters to be estimated.

Improved computer technology and the International Hydrological Decade (1965-1974) have provided the stimulus for a considerable amount of research in watershed and hydrologic modelling. Several mathematical or digital watershed models were published in the sixties and seventies, the best-known being the Stanford Watershed Model (SWM) (Crawford and Linsley, 1966). A flow chart for the SWM



is shown in Fig. 5.

This model, the parameters of which are optimized, can be used to simulate watershed response to weather modification and urban development; to design hydrometeorological networks; and to predict streamflow from ungauged watersheds. Streamflow is calculated at several locations in the stream channel called flowpoints. The area upstream from each flowpoint is divided into segments so that there are one or more segments for each recording rain gauge. The model continuously calculates streamflow at each flowpoint from rainfall in each successive watershed segment, and from flows measured or calculated at upstream flowpoints.

Major data inputs for the Stanford model are precipitation and potential evapotranspiration. Further meteorological data are required if the snowmelt subroutine is used. Available moisture and potential evapotranspiration data inputs are used together with cumulative frequency distributions of infiltration and evapotranspiration opportunity to determine detention, infiltration, interflows, and evapotranspiration.

Three subsurface water storages are defined: the upper zone, the lower zone, and groundwater storages. The upper and lower zone storages control overland flow, infiltration, interflow, and inflow to groundwater storage. The upper zone simulates the initial watershed response to rainfall and is of major importance for smaller storms and for the first few



# STANFORD WATERSHED MODEL IV FLOWCHART

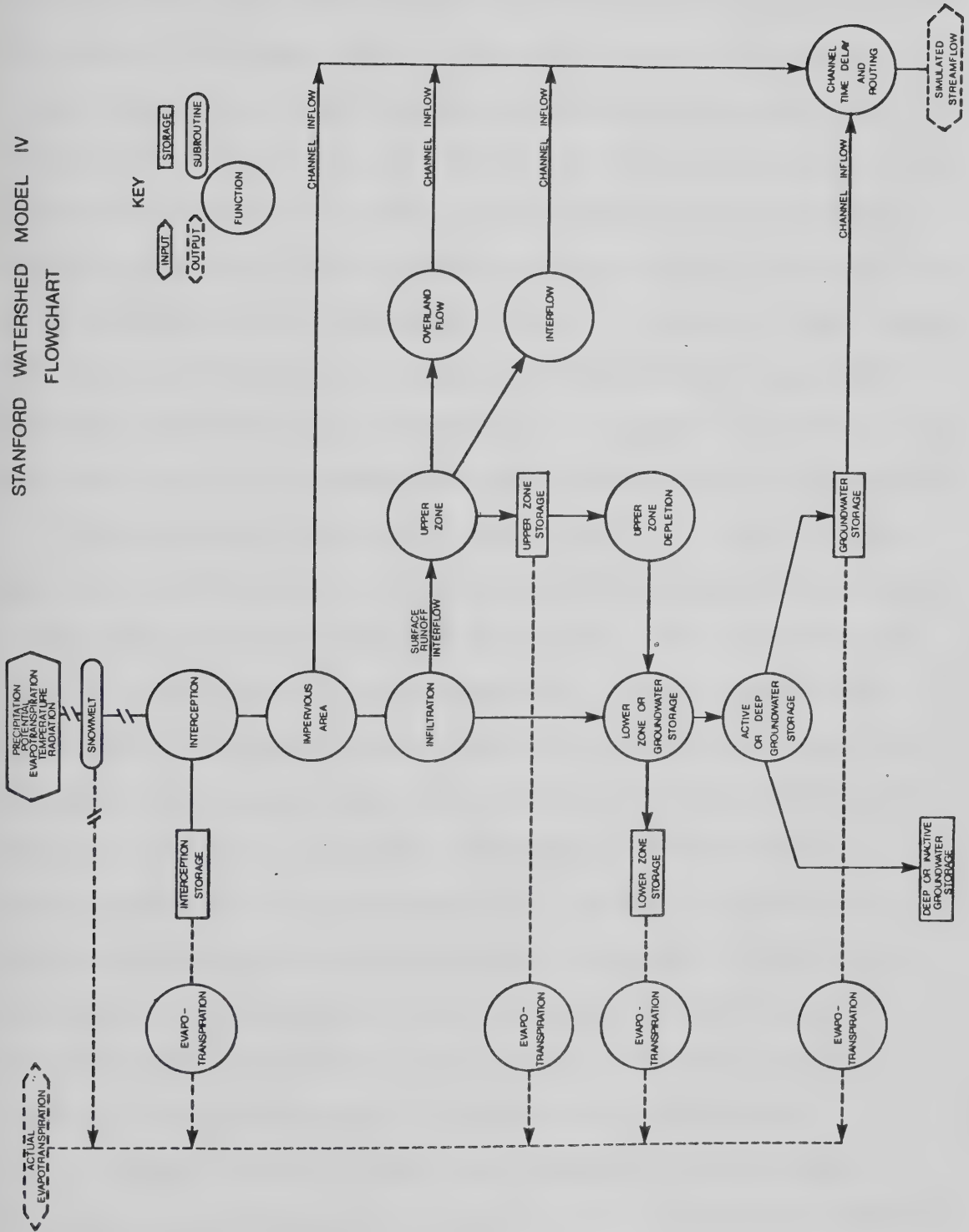


Figure 5. Stanford Watershed Model IV flowchart (After Crawford and Linsley, 1966).





hours of larger storms. The lower zone controls watershed response to major storms by controlling long term infiltration. Base flow to stream channels is supplied from groundwater storage. None of the soil water storages have fixed capacities, and evaporation and transpiration may occur from any of them. Streamflow hydrographs are the most important outputs from the Stanford model which has been tested using data from over 300 basins ranging in size from 0.65 to 800,000 km<sup>2</sup> (Linsley, 1976). If reliable input data and accurate streamflow records are available, agreement between observed and simulated flow is good with annual flow volumes within +5 percent and peak flows within +10 percent.

Another well-known hydrologic model is the Streamflow Synthesis and Reservoir Regulation (SSARR) model (Rockwood, 1958, 1968; US Army Corps of Engineers, 1971). SSARR is a deterministic hydrologic mathematical river system model designed to simulate flows from large basins. It uses basin storage routing procedures to convert precipitation excess over the basin to represent streamflow. Soil moisture, evapotranspiration, and base flow indices, together with empirically derived relationships, are used to determine soil moisture increases, soil moisture reductions, and baseflow contributions, respectively. The model also contains snow accumulation and snowmelt components.

Although SSARR is designed primarily for streamflow forecasting and reservoir regulation it can also be used in the development of design floods, or in the extension of



missing or broken records of streamflow. Examples of important applications of SSARR include simulations of flow from the Columbia River Basin in Western North America, and from the Lower Mekong River in Southeast Asia.

In contrast to the engineering approach evident in the Stanford and SSARR models, Freeze (1971) developed a completely physically based, theoretical hydrologic response model and used the entire set of equations of flow through heterogeneous, anisotropic porous media to obtain solutions to the transient, saturated/unsaturated flow problem for a groundwater basin.

In this model, the watershed or sideslope is defined in terms of a block-centred nodal grid (Fig. 6), and mesh spacings which can be varied. Inflows such as rainfall and outflows such as evaporation are simulated at specified boundary flux nodes. At other boundary nodes, boundary conditions may be imposed that specify hydraulic head or no-flow conditions. The basic information required to operate the model is related primarily to the properties of water, soil and the geologic formations, namely: the compressibilities of soil and water; porosity, specific permeability, density of water, and water content. The last four variables are functions of pressure head.

The fundamental equation of flow for the model is a nonlinear parabolic partial differential equation. An iterative numerical scheme that employs an implicit finite difference formulation, and known as the line successive



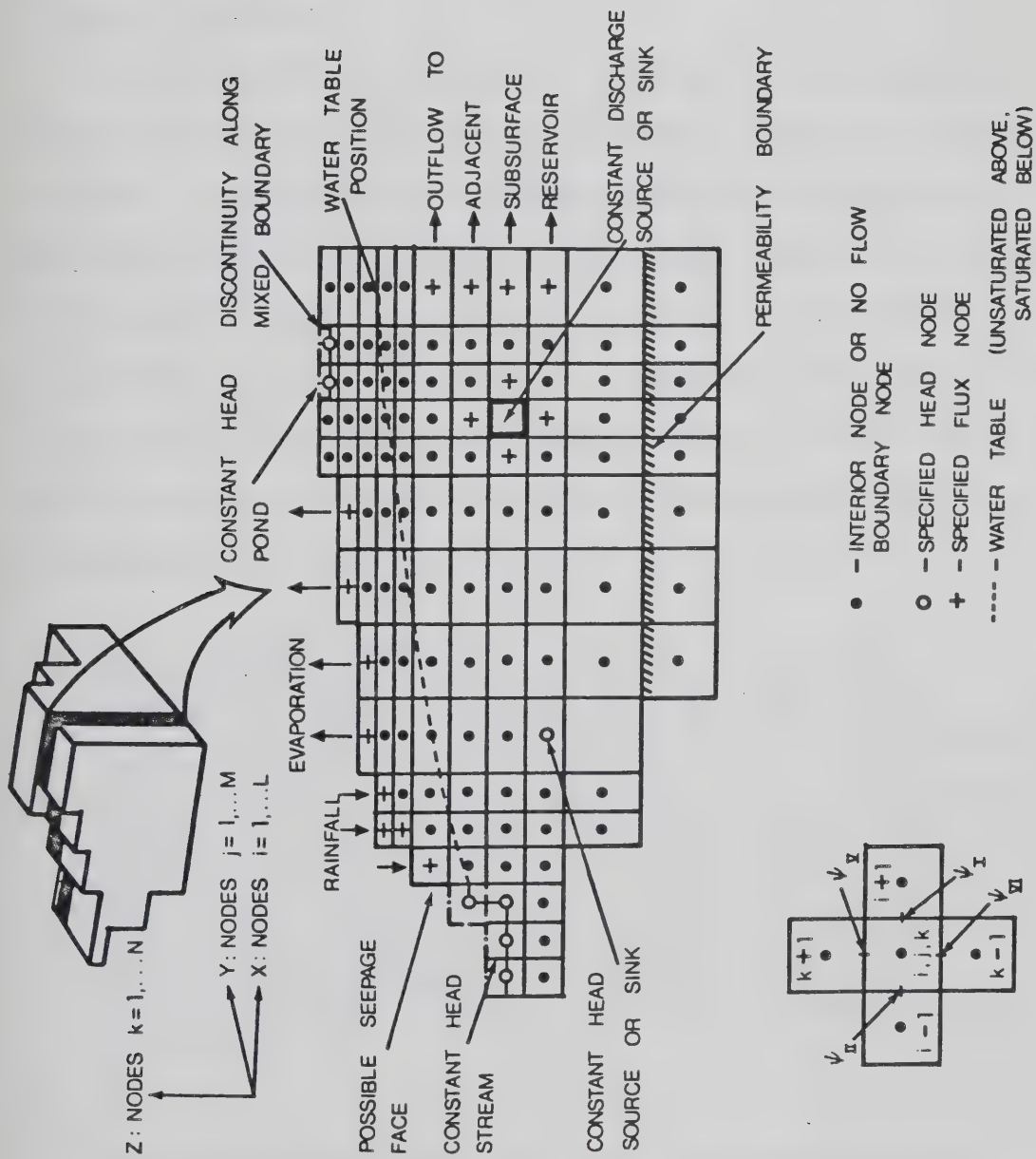


Figure 6. Block-centred nodal grid for subsurface flow model (After Freeze, 1971).





overrelaxation technique, was used to obtain solutions to the equation. Output takes the form of plots of pressure head, total head, and moisture content fields for any cross section at any time step. Base flow is determined from flownet analysis.

Freeze (1972a) subsequently coupled his subsurface flow model with a one-dimensional, gradually varied, unsteady channel flow model to study the mechanism of base flow generation and the nature of watershed response in streams dominated by base flow. The full set of nonlinear, hyperbolic partial differential equations for shallow water flow were solved using an explicit finite difference technique known as the single step Lax-Wendroff method. The combined model operates (Freeze, 1972a) as follows:

"...internal coupling is carried out by using the stream depth as the convergence quantity. The subsurface model is solved at each time step by using the stream depth from the previous time step as the specified head condition at the stream boundary. The calculated outflow from the subsurface system becomes the lateral inflow to the streamflow model for that time step, and a new stream depth profile is calculated. This new profile replaces the old to set the heads for a solution to second cycle subsurface. This alternating cycle is continued until the stream depth and the specified head boundary values converge to within a predetermined tolerance."

The uncoupled subsurface flow model was designed primarily as a research tool and has been applied to many hypothetical hydrologic situations. It has also been applied to the real world conditions of Reynolds Creek watershed,



Idaho (Stephenson and Freeze, 1974). Calibration of the model consisted of trial-and-error matching of computer output with field measurements of check parameters, during a series of simulations in which some of the input parameters were varied. Results from the field study indicate that, within the limitations of the model and data availability, the model adequately simulates natural conditions. However, because of: its extreme complexity, its requirements for large amounts of data, limitations in theoretical development, constraints on calibration procedures, and computer storage limitations, it cannot be considered suitable for routine operational use.

The interaction between biologically controlled and physically controlled hydrologic processes, particularly in interception, throughfall, evapotranspiration, snow accumulation, snowmelt, and soil water redistribution simulations, features prominently in some watershed models. Such models are most useful for investigating plant-water relationships, and for simulating the effects of land use on hydrologic processes for watersheds where vegetation is an important consideration.

The United States Department of Agriculture Hydrograph Laboratory model of watershed hydrology, USDAHL-74 (Holtan et al., 1975) was designed to serve the needs of agricultural watershed engineering. It employs plant growth indices in both evapotranspiration and infiltration simulations, and requires more detailed information on soil



physical properties - particularly in the plant root zone - than does either Stanford or SSARR models. Soils on each watershed are grouped by land capability classes to form hydrologic response zones for computing infiltration, evapotranspiration, and overland flow. Three zones are identified on a watershed: uplands, hillsides, and bottomlands, therefore the model can be categorized as a distributed one. Computations are based on the assumption that some of the runoff will cascade over successive zones.

The program calculates the extractions from a soil layer through evapotranspiration and free drainage, and then records the resulting increase in available storage during a given time interval. Reductions in available storage are computed when infiltration occurs from surface depression storage, or following rainfall or overland flow. Water inputs applied at rates in excess of the infiltration rate are routed as overland flow. Channel flows and subsurface return flows are routed by solving the continuity equation and a storage function using recession flow analysis.

A very detailed biophysical hydrologic model has been assembled by Huff and his colleagues from the Oak Ridge National Laboratory, Tennessee (Huff et al., 1977). It is called the terrestrial ecosystem hydrology model (TEHM), and is essentially a combination of two models that were developed independently: the Wisconsin Hydrologic Transport Model and an atmosphere-soil-plant water flow model (PROSPER). The first is based in part on the Stanford model.



In PROSPER, a water balance is applied to a stand of vegetation on a layered soil. The model, which is one-dimensional, uses a combined energy balance-aerodynamic method to derive an equation for evapotranspiration as a function of a resistance to vapor transfer which is characteristic of evapotranspiration surfaces. Because of the close parallel between the equations of flow for electricity and those of water flux through a soil-plant-atmosphere continuum, an electrical circuit analogy (Fig. 7) was developed so that standard methods for solving electrical circuit problems could be applied.

PROSPER has been used as a completely self-contained model to simulate evapotranspiration and annual drainage from a mature hardwood forest at Coweeta in the southern Appalachians (Swift et al., 1975). Because the movement of water between 90 cm depth and the stream is not simulated in PROSPER, the drainage term was equated to streamflow for annual periods. For the hardwood forest, simulated annual drainage was within 1.5 percent of measured streamflow. Simulations were also performed for a 16-year old white pine plantation and a 1-year old clearcut area. The model estimated a reduction in drainage of 20 cm for the plantation and an increase of 36 cm for the clearcut. These values correspond to measured annual streamflow changes of -20 and +38 cm respectively. The results from these simulations also indicated that summer evapotranspiration for hardwood and pine were identical, and that during winter





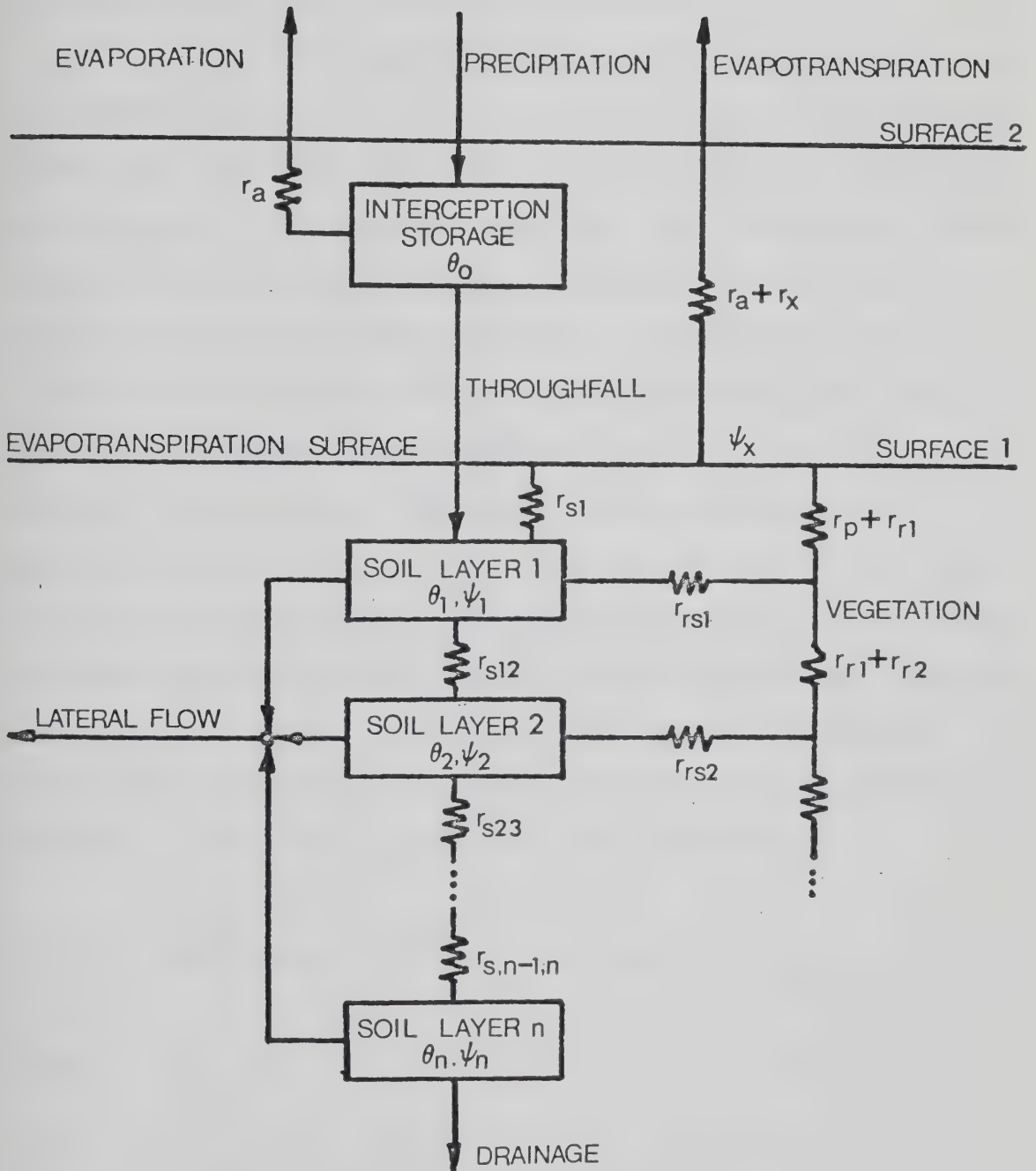


Figure 7. Schematic of PROSPER (After Huff et al., 1977).



and early spring, losses due to evapotranspiration were greater for pine. Simulations showed that evapotranspiration was considerably less, and soils much wetter, on the clearcut areas than on the forested areas.

The subsurface component of the TEHM takes into consideration the variable source area concept, by relating subsurface drainage rate and variable source area runoff. As Huff et al. (1977) explain, when the root (or surface) zone drainage rate exceeds a certain threshold value, the fraction of source areas draining to the channel increases linearly with drainage rate until a specified upper limit is reached. This upper limit defines the full extent of variable source areas. The lower limit represents the permanent part of the source areas that are linked to the stream in the basin, and will contribute subsurface drainage through the layers below the root zone at all times. Beneath the zones simulated in PROSPER, soil water transmission zones are defined in which soil hydraulic conductivity is related to soil water content by the expression

$$K(\theta) = K_{S_i} e^{a_i(\theta - \theta_s)} \quad 1 \leq i \leq 3 \quad (2.1)$$

where

$K(\theta)$	hydraulic conductivity at water content $\theta$ ,
$K_{S_i}$	saturated conductivity parameter,
$a_i$	curve fitting parameter,
$\theta$	water content,
$\theta_s$	water content at saturation,
$i$	section number of portion of $K$ vs. $\theta$ curve.



Hydrograph separation techniques are used to determine outflows from groundwater storage.

The channel flow portion of the model combines simulated flow components such as direct channel precipitation, impervious area runoff, runoff from permanent and variable source areas, and groundwater inflow from each portion of the watershed. It then generates hydrographs at specified points in the channel system.

Output from the TEHM consists of monthly and annual water balance summaries, and daily values of selected hydrologic variables for each watershed segment. Water flux terms such as infiltration, direct runoff, drainage to deeper soils, evapotranspiration, lateral subsurface flow, and net flux from the second to third soil layer, as calculated by PROSPER for each day are tabulated.

The monthly summary includes a "deep soil balance" term in addition to the terms which normally appear in water budget equations. This term is related to storage changes in the soil water transmission layers.

Four summaries appear in the annual summary: runoff, precipitation/evapotranspiration, moisture status, and water budget. The moisture status summary is intended as an index to total water content of a vertical column extending from canopy to bedrock, but it is more likely indicative of overall water storage in the unsaturated soil column (Huff et al., 1977).





The TEHM has been tested using data from the Walker Branch Watershed, a 97.5 ha drainage area located in the Ridge and Valley province of east Tennessee. A predominantly oak-hickory forest covers the basin. During simulations the model generated hydrographs for stormflow, base flow and total flow. The total flow data were compared with the observed hydrographs, while stormflow and baseflow were compared with quickflow and delayed flow, respectively. Quickflow and delayed flow were calculated by the method of Hewlett and Hibbert (1967). In all cases good agreement was obtained between simulated and observed results. Monthly and annual summaries were also provided by the model.

A special feature of the terrestrial ecosystem hydrology model is that it can be used in environmental chemistry studies. For this purpose TEHM is combined with subroutines for atmospheric transport, soil chemistry, exchange of heavy metals, a plant-growth model, and a mineral uptake model.

A number of hydrologic or watershed models have been developed specifically to meet the needs of forest hydrologists or watershed managers. Multiple regression and covariance analyses are perhaps the earliest and simplest examples of such models. Anderson (1960) used regression models to relate forest shade and radiation to snow accumulation and melt. The results indicated that shade could be maximized and back radiation minimized by cutting east-west strips in the forest, with successive cuts



proceeding toward the south. This idealized forest stand structure, referred to by Anderson as a wall-and-step forest (Fig. 8), would maximize both snow accumulation and delay in snowmelt, and therefore would be favourable for water production.

Leaf and Brink (1973a) developed a snowmelt simulation model for Colorado subalpine watersheds and used it (Leaf and Brink, 1972, 1973a) to simulate the probable effects of timber harvesting on snowmelt in the subalpine forest. The model was subsequently expanded (Leaf and Brink, 1973b) to simulate the total water balance on a continuous, year-round basis. It was designed to simulate watershed management practices and their effects on hydrologic systems.

For simulation purposes, the study basin is divided into several hydrologic response units. Hydrologic responses are computed for each unit, then weighted according to their respective areas and combined to produce a composite record of hydrologic system behaviour on a watershed basis. Input to the response system is derived from snowmelt and rainfall. Once evapotranspiration requirements have been satisfied, additional input satisfies soil mantle recharge requirements. When field capacity is reached, residual input becomes water available for streamflows. Excess water is not routed through the soil mantle.

For this model, the structure and properties of the forest stand play an important role in the simulation process (Leaf and Brink, 1973b). Forest cover density, for



# PROGRESSIVE CUTS

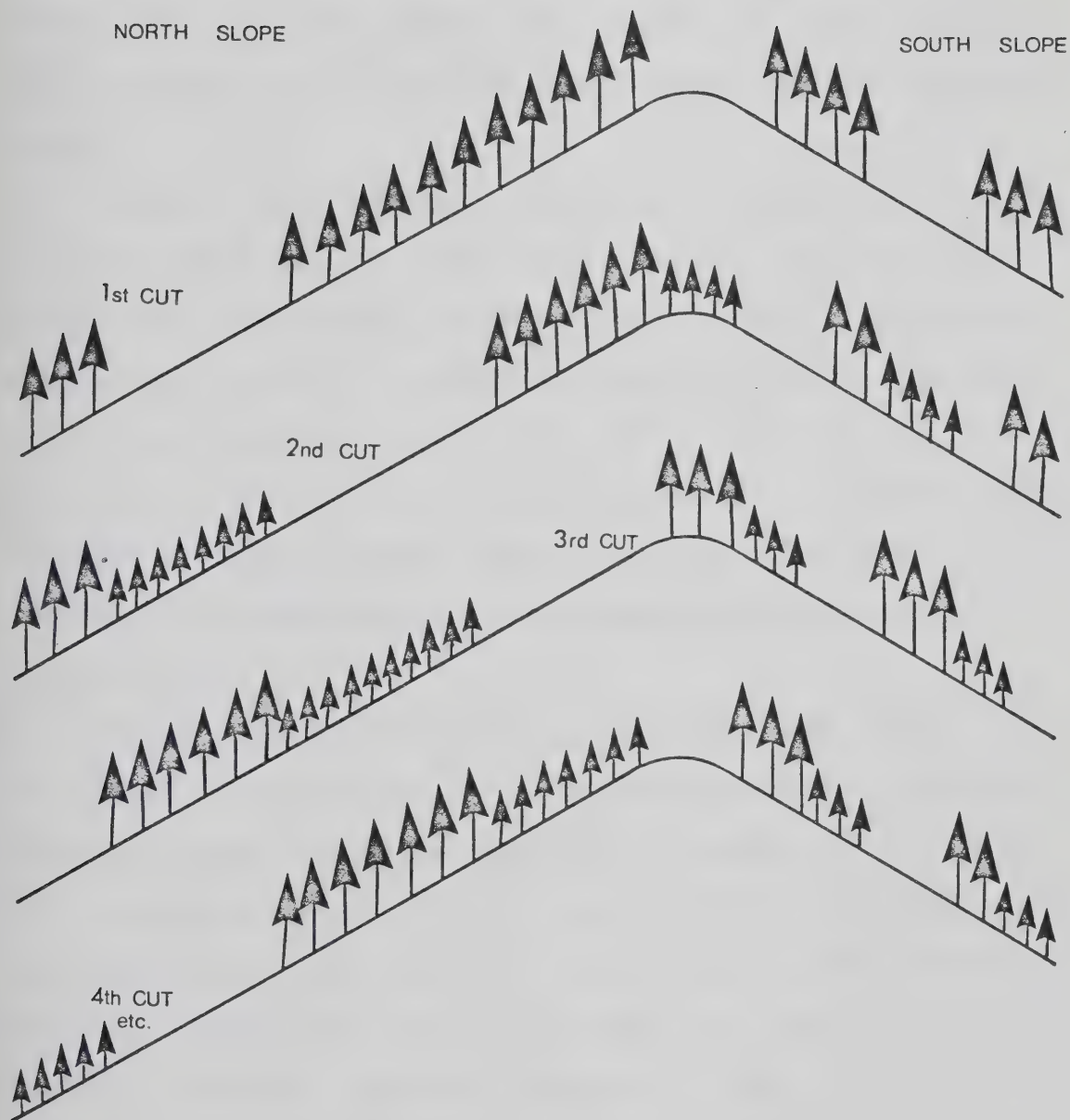


Figure 8. Wall-and-step forest - a cutting pattern for improved water yield from snow zone forests (After Anderson, 1960).



example, is used to determine the amount of snow intercepted by the forest canopy and vaporized from it. It is also required to compute evaporation from the snowpack beneath the trees. Reflectivity of the forest stand is a function of forest density, and is used to calculate evapotranspiration from forest and open areas. Cut blocks and other clearings are simulated by setting the forest cover density equal to zero.

The Colorado subalpine hydrologic simulation or water balance model serves as the core system of the Land Use Model also developed by Leaf and Brink (1975). The latter model was designed to extend the capabilities of the former over a much longer time period - from a few years to 120 years or more (the rotation age of subalpine forests). The package provides greater flexibility for simulating a variety of timber harvesting and weather modification combinations.

The interactions between timber management and watershed management in the subalpine forests of Colorado have also been simulated (Leaf and Alexander, 1975). This was accomplished by linking timber models for lodgepole pine and spruce-fir forests to the water balance and land use models. Linkage was achieved through the forest cover density variable. Projected changes in water yield were obtained for several different forest management practices. The investigators concluded that this method for projecting long-term yields of both wood and water shows that the





strategies for optimum water production are compatible with the conversion of old growth forests to managed stands for timber production. The major disadvantage of both the land use and the timber/water model is the inability to verify the long-term projection during the short term.

Another model designed to predict long-term timber and water yields from snow pack zones of lodgepole pine subalpine watersheds along the Colorado Rocky Mountain Front Range was developed by Betters (1975). The model operates on an annual time scale and incorporates several empirical relationships to simulate forest growth and water production on a watershed. Precipitation, potential and actual forest evapotranspiration, soil water holding capacity, and proposed timber-harvesting schedule are the most important variables and parameters used by the hydrologic submodel.

Past records of timber inventory and runoff values for Little Beaver Creek and Fool Creek were used to test the model. Both watersheds have long-term streamflow records. Results from the tests indicated that the predicted timber inventory estimate was 8 percent higher than the actual timber inventory estimate. On Beaver Creek, the observed water yield exceeded the predicted yield by 13 percent. Two time periods were simulated for Fool Creek - before harvest and after harvest. Predicted water yields exceeded observed by 16 and 10 percent, respectively.

Simulations showed that on a per hectare basis, after harvest the water yield from the uncut portion of a subunit



decreases. The net result, however, is an increased yield because the large increase in snowpack combined with reduced evapotranspiration on the cut area exceeds the loss sustained on the uncut portion (Table 5).

To date there have been few attempts to simulate the effects of forest succession on water yield. Forest succession is the gradual replacement of one forest tree species or plant community by another. Jaynes (1978) developed a lumped, deterministic model (ASPCON) to simulate the hydrologic impacts of forest succession in the Rocky Mountain area of Utah. The model calculates weekly water budgets throughout one water-year, using inputs of precipitation and air temperature. The model predicted (Table 6) a net loss of 8.6 cm in streamflow when aspen assumed dominance over grass-forb<sup>4</sup> cover. An additional loss in streamflow of 11.7 cm was predicted when conifers replaced the aspen.

Attempts to incorporate relatively new hydrological concepts into hydrologic or watershed models are exemplified by the work of Beven and Kirkby (1979). They formulated a physically based, deterministic model that provided for simulation of variable source areas. The model was designed to predict the hydrologic response of ungauged basins without resorting to optimization procedures. Only information derived directly from the basin itself was used. Application of the model to an 8 km<sup>2</sup> watershed showed that

---

<sup>4</sup>An herb other than grass



Table 5. Impact of timber removal on simulated snow distribution, evapotranspiration, and water available for runoff on the Fool Creek Watershed (Adapted from Betters, 1975).

Subunit	Area, ha	Elevation, m	Aspect	Before Harvest (15 yrs)				After Harvest (7 yrs)			
				Potential Evapotranspiration, cm	Actual Evapotranspiration, cm	Snow-pack, cm	Water Available for Runoff, m <sup>3</sup>	Area, ha	Actual Evapotranspiration, cm	Snow-pack, cm	Water Available for Runoff, m <sup>3</sup>
98E55	15.8	2987	E	94	26.7	23.6	31084	11.7	uncut 26.7 cut 5.6	21.3 30.2	20353 19243 39595*
98W55	8.5	2987	W	94	26.7	23.6	16776	3.6 4.9	uncut 26.7 cut 5.6	14.7 30.2	3947 23067 27014*
103E55	41.7	3124.2	E	91.4	26.2	28.7	103737	23.5 18.2	uncut 26.2 cut 4.8	21.8 36.1	43913 98310 142223*
103W55	39.3	3124.2	W	91.4	26.2	28.2	97693	19.0 20.2	uncut 26.2 cut 4.8	19.6 36.1	31208 109288 140372*
107E55	54.2	3261.4	E	86.4	24.6	32.8	168249	29.1 25.1	uncut 24.6 cut 3.3	24.6 41.9	67102 154188 221290*
107W55	49.8	3261.4	W	86.4	24.6	32.8	154434	35.6 14.2	uncut 24.6 cut 3.3	29.0 41.9	97323 86962 184285*
112N55	73.7	3413.8	N	88.9	25.1	37.8	261872	50.6 23.5	uncut 25.1 cut 4.1	32.8 48.5	154434 158258 312692*
114N55	6.1	3474.7	N	86.4	24.4	39.9	23190	3.6 2.4	uncut 24.4 cut 3.3	32.3 51.1	11102 17146 28247*

\* Total water available for runoff



Table 6. Water budget components for an average water-year on the Chicken Creek Watershed at different stages of succession (Adapted from Jaynes, 1978).

Vegetation <sup>1</sup> Status	Streamflow	Streamflow +ΔSM	Runoff <sup>2</sup>	QOF	QF	ΔSM <sup>3</sup>	ΔGWL	SEEP	TRAN	RINT	SINT	SVAP
	cm	cm	Percent	-----	-----	-----	cm	-----	-----	-----	-----	-----
98-1-1	54.1	59.2	49.6	8.4	39.9	5.1	4.6	17.5	24.4	2.5	0.0	4.3
90-9-1	54.1	58.2	48.7	7.9	40.1	4.1	4.6	17.5	25.1	2.8	0.3	4.3
80-19-1	53.1	57.2	47.9	7.6	39.6	4.1	4.3	17.5	26.2	2.8	0.3	4.1
70-29-1	52.3	55.6	46.6	7.1	39.1	3.3	4.8	16.8	28.2	2.8	0.3	4.1
60-39-1	51.6	54.4	45.5	6.9	38.9	2.8	4.6	16.8	29.7	3.0	0.5	3.8
50-49-1	51.6	53.4	44.7	6.6	39.1	1.8	4.6	16.8	30.5	3.0	0.5	3.8
40-59-1	51.3	51.3	43.0	6.1	39.1	0.0	4.8	16.8	32.3	3.0	0.5	3.6
30-68-2	50.8	50.8	42.6	5.8	39.1	0.0	4.6	16.8	32.8	3.3	0.8	3.6
20-78-2	50.5	50.5	42.3	6.6	38.1	0.0	4.3	16.5	33.3	3.3	0.8	3.3
20-68-12	46.2	46.2	38.7	4.6	36.1	0.0	4.3	15.0	38.6	3.6	1.3	3.3
20-58-22	42.9	43.2	36.2	3.0	34.0	0.3	4.1	14.0	41.9	3.8	1.8	3.0
20-47-33	41.9	41.9	35.1	2.3	33.8	0.0	4.6	13.5	42.7	4.1	2.5	3.0
20-36-44	40.9	40.6	34.0	1.8	33.3	-0.3	4.3	13.2	43.4	4.3	3.0	2.8
20-25-55	40.1	40.9	34.3	2.0	32.5	0.8	4.6	12.4	42.9	4.6	3.6	2.8
20-15-65	39.1	39.6	33.2	0.5	32.8	0.5	4.1	13.2	43.4	4.8	4.3	2.8
20-5-75	38.6	38.9	32.6	0.8	32.0	0.3	4.6	12.4	44.2	5.1	4.8	2.5

<sup>1</sup> Percent watershed areal cover composed of grass-forb, aspen, and conifer types, respectively.

<sup>2</sup> Runoff percent is equal to (Streamflow + SM)/precipitation.

<sup>3</sup> ΔSM and ΔGWL represent the net annual change in soil moisture and ground water level, respectively.





there was fairly close agreement between simulation output and observed values.

The variable source area concept has been incorporated into other hydrologic models - models designed specifically to evaluate the effects of forest land use on the hydrology of an area (Troendle, 1979; Chanasyk, 1980).

Troendle's (1979) simulator contains three main flow components: subsurface flow, channel interception, and impervious area overland flow. The simulation watershed is partitioned into a number of subbasins and each subbasin is subdivided into segments and horizons. The segments run from ridge-top to stream channel, and the horizons correspond to soil layers. After the system has been initialized, an explicit finite difference scheme is used to determine the volumetric water content of each element, at regular time intervals. During each iteration, a test is made for saturation in the surface layer beginning with the first segment next to the stream channel, and then proceeding upslope until an unsaturated element is detected. At this point, the saturated surface is considered to be part of the expanding channel system, and the remaining unsaturated portion of the slope is partitioned again for the next iteration. A reverse procedure is used during storm recession simulation, when channel contraction takes place. Tests are made on previously saturated zones beginning with ridge-top elements and proceeding towards the channel. If an element is unsaturated, it is added to the unsaturated slope



which is re-partitioned for the next iteration. This concept of expanding and contracting channels is the central idea behind the variable source area model.

Troendle (1979) compared results from his simulator with data from a 38 ha watershed, in north central West Virginia, without resorting to calibration. He found that simulated storm response varied from 45 to 125 percent, and averaged 89 percent of the streamflow. The simulated time to peak was about 4 percent below the observed time to peak. More than 90 percent of the simulated streamflow was of subsurface origin.

The idea of expanding and contracting stream channel systems for low order watersheds is also incorporated into Chanasyk's (1980) land use hydrologic model. The model, called SLUICES (Soils and Land Use affecting Interflow and Creating Effects on Streamflow), uses a square element grid system, together with seven easily obtainable or optimized parameters. The most sensitive of these parameters are: hydraulic conductivity, saturation moisture content, field capacity, and drainage coefficient. The model is also sensitive to antecedent soil moisture conditions and to evapotranspiration. Model operation is based on the existence of three storages: unsaturated flow storage, saturated flow storage, and overland flow storage. When the unsaturated storage is completely filled, it becomes saturated storage. Additional water creates overland flow conditions.



Chanasyk (1980) applied his model to the Jamieson Creek watershed, located near Vancouver, British Columbia. Agreement between recorded and simulated discharge hydrographs for seven storms ranged from very good to fair - depending on whether the storms were preceded by wet or dry antecedent conditions , respectively. He found that streamflow can be augmented by logging , and that the increase was proportional to the area clearcut.

It is evident from the preceding discussion that hydrologic and watershed modelling has advanced considerably during the past two decades. Extremely sophisticated mathematical models are currently available that can be used to simulate forest and watershed management situations. It is also clear that the simulation of certain processes, notably the subsurface flow components, needs to be improved if the goal of creating a completely physically based hydrologic or watershed model is to be achieved. Groundwater hydrologists, petroleum engineers, and soil physicists have paved the way to meeting this objective by deriving and solving the complicated mathematical expressions which describe subsurface flow.



## E. Development Of Subsurface Flow Equations And Methods For Obtaining Their Solutions

### Saturated flow

The equation for groundwater flow developed by Darcy (1856) from his experiments on water flow through filter sands may be considered as the forerunner of most of the subsurface flow equations developed subsequently. It can be written (Davis and DeWiest, 1966) as

$$Q = KA \left( \frac{H_1 - H_2}{dl} \right) = -KA \frac{dH}{dl} \quad (2.2)$$

where

Q	flow rate,
K	hydraulic conductivity,
A	cross sectional area of flow,
H <sub>i</sub>	energy per unit weight of fluid or hydraulic head; in the case of water = $Z + \frac{P}{\gamma}$ + arbitrary constant,
Z	elevation above an arbitrary datum plane,
P	pressure sustained by the fluid in the pores of the medium,
$\gamma$	specific weight of the fluid,
$dH/dl$	hydraulic gradient.

The Darcy equation is used together with the equation of continuity (Jacob, 1949) to obtain Laplace's equation for steady, incompressible flow

$$\frac{\partial^2 H}{\partial x^2} + \frac{\partial^2 H}{\partial y^2} + \frac{\partial^2 H}{\partial z^2} = 0 \quad (2.3)$$





where  $H$  is the hydraulic head.

This is an elliptic, second-order partial differential equation.

Fifty years after Darcy's Law was first formulated Thiem (1906) used Darcy's Law in terms of polar coordinates to determine the cone of depression for groundwater in the vicinity of a discharging well. However, it could be used only when steady state or equilibrium conditions prevailed.

Later, Theis (1935) used the analogy between heat flow and groundwater flow to develop an equation applicable under nonsteady or nonequilibrium conditions. The time variable is introduced into the equation, and an analogy is drawn between sources and recharging wells, and between sinks and discharging wells. The Theis equation can be used to determine drawdown before equilibrium conditions occur. The same fundamental differential equation and its solution were obtained by Jacob (1940) from Darcy's Law and the continuity equation. Jacob (1949) subsequently derived the three-dimensional form of the general differential equation for unsteady groundwater flow

$$\frac{\partial^2 H}{\partial x^2} + \frac{\partial^2 H}{\partial y^2} + \frac{\partial^2 H}{\partial z^2} = \frac{S}{K} \frac{\partial H}{\partial t} = \frac{\rho g}{K} (n\beta + a) \frac{\partial H}{\partial t} \quad (2.4)$$



where

H	hydraulic head,
S	storage coefficient,
K	hydraulic conductivity,
$\rho$	fluid density,
g	gravitational constant,
n	porosity,
$\beta$	compressibility of fluid,
a	compressibility of medium.

This is a parabolic partial differential equation. Cooper (1966) was able to verify Jacob's derivation and resolve certain contradictions by considering the Z (vertical) coordinate as a deforming coordinate.

Before the introduction of sophisticated computers, equations (2.3) and (2.4) or their polar coordinate equivalents were solved analytically by the methods developed by Thiem (1906) and Theis (1935). However, since the mid-fifties groundwater hydrologists have been turning increasingly to numerical methods for solutions to these equations. Freeze and Witherspoon (1966) used both mathematical and finite difference techniques to solve the Laplace equation [equation (2.3)] for a three-dimensional, nonhomogeneous, anisotropic regional groundwater basin. They compared the method of analytical separation of variables and Fourier Series technique employed in partial differential equations theory with a numerical finite difference approach, and found the numerical method more versatile, mathematically simpler, and better suited to computer-oriented methods of data storage.



Laplace's equation is the governing equation in the problem of steady seepage through a homogeneous earth dam and as such has been solved by means of finite difference and relaxation methods (Finnemore and Perry, 1968). Laplace's equation and a finite difference technique have also been used to predict the effect of a proposed reservoir on aquifer water levels (Remson et al., 1965).

Equation (2.4) also has been solved using numerical methods. Pinder and Bredehoeft (1968) used an alternating-direction implicit technique to solve the transient flow problem in the case of an aquifer in Nova Scotia. Their calculated values compared favorably with the analytical solutions for homogeneous, isotropic aquifers of simple geometry. The same iterative technique has been used to solve other practical (Trescott et al., 1970) and theoretical (Bredehoeft and Pinder, 1970) problems.

### Unsaturated flow

It will be observed that no attempt has been made to define the saturated and unsaturated zones or the water table. The omission is deliberate inasmuch as we wish to pursue a continuum approach to the subsurface flow problem. However, it is essential to differentiate between saturated and unsaturated flow, and to discuss factors related to this difference. This can be achieved best by first discussing the concept of potential.



For the equations discussed so far (2.2 to 2.4), the term 'H' is referred to as hydraulic head. It is also called piezometric head. Because this term has the dimension of energy per unit weight, H may be regarded as the potential energy of water at a point (Jacob, 1949). According to Remson et al. (1971)

"...The [total] potential at a point is a measure of the work required to transport a test body of water to that point from a specific reference state in a soil-water system which is in a state of rest. When described in terms of energy per unit weight of water, potential has the dimension length and is referred to as "head". The gradient of total potential is proportional to the water-moving forces..."

Evidently, the terms: hydraulic head, piezometric head, total potential, and piezometric potential can be used interchangeably. This concept is applicable to both saturated and unsaturated flow.

The total potential ( $\Phi$ ) at a point can be written (Remson et al., 1971) as

$$\Phi = \psi_g + \psi_p + \psi_o + \psi_a + \psi_t + \psi_c \quad (2.5)$$

where

$\psi_g$	gravitational potential,
$\psi_p$	hydrostatic pressure potential,
$\psi_o$	osmotic potential,
$\psi_a$	adsorption potential,
$\psi_t$	thermal potential,
$\psi_c$	chemical potential.





The gravitational potential is related to the position of the point and depends only upon its height above datum. Thus it is identical to the elevation head ( $z$ ) of that point.

The hydrostatic pressure potential is considered to be zero at the water table where pressure is atmospheric. Therefore all pressures in subsurface water are gauge pressures. Below the water table at static equilibrium, hydrostatic pressure potential increases with increasing depth. In the case of unsaturated media, the hydrostatic pressure potential is negative (i.e. it represents a suction) because a suction must be applied in order to withdraw water <sup>5</sup>.

The osmotic potential is related to the effect of two solutions of unequal concentrations being in contact through a semipermeable membrane. Water moves through the membrane from the less concentrated to the more concentrated solution, thereby increasing the pressure in the more concentrated solution. This pressure is termed the osmotic pressure potential.

Frequently, cations become dissociated from soil particles of clay size leaving the surface of the soil particle with a negative charge. The attraction of particles having opposite electrical charge results in an increased concentration of cations in the vicinity of the negatively charged particles. It is this increase in cations which

---

<sup>5</sup>This concept of treating suction as a negative hydrostatic potential for unsaturated conditions will be maintained in this study.



results in an osmotic force moving water into the space between the particles. The osmotic pressure potential is important in soils that shrink upon drying.

The adsorption potential is due to the attractive (adsorptive) forces between the matrix water and the matrix particles and are prominent only when the soil becomes extremely dry.

Thermal potential has appreciable effect only in the case of vapour diffusion or capillarity.

Chemical potential is due to the osmotic energy of ions free in the aqueous solution. This is distinct from the potential due to the osmotic energy described above.

If we assume isothermal conditions and uniform solute concentration, the total potential at a point becomes

$$\Phi = \psi_g + \psi_p + \psi_o + \psi_a \quad (2.6)$$

In the case of saturated flow the last two terms on the right hand side ( $\psi_o$  and  $\psi_a$ ) are disregarded. For unsaturated flows, all the terms are retained. However, for soil-moisture ranges usually encountered in the field,  $\psi_a$  can be neglected. In soils that shrink on drying  $\psi_o$  assumes greater significance than  $\psi_p$ ; in nonshrinking soils the reverse is true. Generally speaking, the last three terms on the right hand side of equation (2.6) cannot be evaluated separately, so commonly they are lumped together and referred to collectively as the "capillary" potential. The



basic idea of capillary potential which, together with "capillary conductivity," forms the basis of modern soil water physics was first set forth by Buckingham (1907).

For the remainder of this treatise, the following definition of total potential ( $\Phi$ ), and notation, will be used

$$\Phi = \psi + z \quad (2.7)$$

where

$\psi$             hydrostatic pressure potential (or pressure head),  
 $z$             gravitational potential (or elevation head).

The extension of Darcy's Law to unsaturated flow was first proposed by Richards (1931) who assumed that the conductivity  $K$ , as well as the water content could be treated as (non-hysteretic) functions of pressure potential ( $\psi$ ). If the soil water is assumed incompressible, the general equation for unsaturated, unsteady flow can be written as

$$\frac{\partial}{\partial x} [K(\psi) \frac{\partial \Phi}{\partial x}] + \frac{\partial}{\partial y} [K(\psi) \frac{\partial \Phi}{\partial y}] + \frac{\partial}{\partial z} [K(\psi) \frac{\partial \Phi}{\partial z}] = \frac{\partial \theta}{\partial t} \quad (2.8)$$

where

$K(\psi)$         hydraulic conductivity as a function of  
                  pressure potential ( $\psi$ ),  
 $\Phi$             total potential,  
 $\theta$             volumetric soil water content.



This equation, sometimes referred to as the Richards equation, is highly nonlinear. Since most of the solutions for unsaturated flow problems have been obtained using the one-dimensional case, it is useful to write the equation for vertical soil water movement

$$\frac{\partial}{\partial z} [K(\psi) \frac{\partial \Phi}{\partial z}] = \frac{\partial \theta}{\partial t} \quad (2.9)$$

Since  $\Phi = \psi + z$  (equation 2.7), we can write

$$\frac{\partial}{\partial z} [K(\psi) \frac{\partial (\psi + z)}{\partial z}] = \frac{\partial \theta}{\partial t} \quad (2.10)$$

or

$$\frac{\partial}{\partial z} [K(\psi) \frac{\partial \psi}{\partial z} + K(\psi)] = \frac{\partial \theta}{\partial t} \quad (2.11)$$

Childs (1936) hypothesized that water movement in the unsaturated zone is determined by the moisture concentration gradients, which implies that water moves according to a diffusion equation

$$\frac{\partial c}{\partial t} = -k \frac{\partial^2 c}{\partial x^2} \quad (2.12)$$

where

c            moisture concentration,  
k            diffusion coefficient (constant),  
σ            weight of dry matter per unit volume.





When  $\psi$  and  $K$  are single-valued functions of  $\theta$ , equation (2.11) becomes

$$\frac{\partial}{\partial z} [D \frac{\partial \theta}{\partial z} + K(\theta)] = \frac{\partial \theta}{\partial t} \quad (2.13)$$

where  $D = K(\theta) \partial \psi / \partial \theta$  or moisture diffusivity (Childs and Collis-George, 1950).

The term diffusivity and the symbol  $D$  are used because the form of the equation is the same as that of Fick's Law of diffusion; there is no implication that molecular diffusion is or is not involved as a mechanism (Miller and Klute, 1967). Equation (2.13) is commonly used as an alternative to equation (2.11).

In order to introduce one further concept related to unsaturated flow, the right hand side of the foregoing equations will be written as

$$\frac{\partial \theta}{\partial \psi} \frac{\partial \psi}{\partial t} \quad (2.14)$$

The term  $\partial \theta / \partial \psi$  is defined as the specific moisture capacity  $C(\theta)$  and represents the slope of the water retention or moisture characteristic curve ( $\theta$  vs  $\psi$ ).

It is evident from the preceding discussion that the main difference between saturated and unsaturated flow is the dependence of  $K$ ,  $\psi$ , and  $C$  on soil water content in the unsaturated case. At saturation,  $\psi$  is no longer a function



of  $\theta$ ,  $K$  is a constant, and  $C=0$ .

A basic feature of unsaturated flow problems is that  $K$  and  $\psi$  are not single-valued functions of  $\theta$  (although the opposite assumption is often made). This phenomenon is termed 'hysteresis', and implies that a wetting soil will have a characteristic curve different from that of the same soil when it is drying. Furthermore, there may be any number of intermediate or scanning curves which are governed by the soil water content at the time when change (from wetting to drying, or from drying to wetting) occurs. Usually the term 'characteristic curve' is reserved for the limiting wetting and drying curves.

The first serious attempt to solve the unsaturated flow equation appears to be that of Klute (1952). He used an iterative procedure to obtain moisture content distributions in semi-infinite columns of sand and clay after varying time intervals, in the case of horizontal flow. Philip (1957) also used an iterative method to solve the one-dimensional, horizontal flow equation, and described a numerical procedure to solve the vertical, unsaturated flow problem.

Hanks and Bowers (1962) were perhaps the first to investigate layered soils using the unsaturated flow equation, which they solved by means of the Crank-Nicolson implicit finite difference technique. The effects of continuous rainfall on soil water content were examined by Rubin and Steinhardt (1963). They used a linear extrapolation-based linearization of the finite difference



equation to solve the Richards equation, and concluded that ponding at the surface results only if rain intensity exceeds the soil's saturated hydraulic conductivity. Whisler and Klute (1965) and Rubin (1967) took hysteresis into consideration when evaluating unsaturated flow problems. This represented a significant advance in unsaturated flow analysis. An explicit-implicit difference scheme was used by Wang and Lakshminarayana (1968) to investigate unsteady soil water movement in a nonhomogeneous unsaturated soil.

Freeze (1969) reviewed the more important papers dealing with application of numerical methods to the unsaturated flow equation, and tabulated the significant features of each paper. He presented a mathematical model for one-dimensional, vertical, unsteady infiltration or evaporation above a recharging or discharging groundwater flow system. Freeze also used hypothetical cases to examine the effects of soil type, rainfall intensity and duration, antecedent soil water conditions, groundwater recharge or discharge rate, depth to water table, and depth of ponding, on the saturated-unsaturated flow system.

Hanks et al. (1969) used a modification of the procedure developed by Hanks and Bowers (1962) to estimate one-dimensional infiltration, redistribution, evaporation, and drainage of water from soil - taking hysteresis into account. They found good agreement between measured and calculated values.



Molz et al. (1968), modelling the effect of a single plant on water transfer, introduced the concept of potential soil-moisture availability which they defined as a measure of the capacity of a soil to transmit water to a root site. They developed a differential equation describing radial flow of soil water to a single vertical sink or root. The soil moisture flux was determined from this equation using Euler's method.

In contrast to the microscopic approach - described above - of simulating the influence of plants on soil water transfer (Molz et al. 1968), there is the macroscopic approach (Molz and Remson 1970, 1971). In this case water transfer and extraction from an entire root zone is considered. Molz and Remson (1970, 1971) introduced an extraction term to the one-dimensional form of Richards' equation and used the Douglas-Jones predictor-corrector finite difference method to solve the modified equation.

### **Saturated and unsaturated flow in an integrated subsurface flow system**

Luthin and Day (1955) were among the first to model unsaturated and saturated flow systems as a single entity. They induced lateral flow through a sand-filled tank by maintaining a small difference in head between constant reservoirs. Flow nets were obtained by means of Laplace's equation, in which  $K=K(x,y)$ , and which was solved by a relaxation method of numerical analysis.





The integrated approach to unsaturated-saturated flow systems was also used by Bouwer and Little (1959). In this case solutions to the two-dimensional steady flow problem were obtained by use of an electrical resistance network for relaxing the system.

Freeze (1967, 1969) used a mathematical model to examine the mechanisms which control the relations between the unsaturated flow processes of infiltration and evaporation and the saturated processes of recharge and discharge. One-dimensional vertical, unsteady flow problems involving saturated-unsaturated systems were solved by means of a numerical difference technique.

The next important advance in the continuum approach occurred when Rubin (1968) solved the Richards equation for two-dimensional transient flow in rectangular unsaturated or partly unsaturated soil slabs. The equation was solved by means of alternating-directions, implicit difference methods.

Other workers who have featured prominently in the development of the integrated saturated-unsaturated flow system concept include Taylor and Luthin (1969), Hornberger et al. (1969), and Verma and Brutsaert (1970).

The most comprehensive treatment of the unsaturated and saturated flow systems as a continuum is undoubtedly that of Freeze (1971). He devised a three-dimensional model that simulated saturated-unsaturated transient flow in small nonhomogeneous, anisotropic basins. The model can be



collapsed to simulate two-dimensional flow, and can also accommdate hysteresis. Solution of the Richards equation was obtained using an implicit iterative method called the line successive overrelaxation (LSOR) technique. Freeze's model was discussed in some detail in the preceding section.

Details of many of the numerical methods referred to in the foregoing discussion can be found in Remson et al. (1971).



### III. STRATEGY FOR MODEL DESIGN

As stated previously, the primary objectives of this study are: a) to develop a subsurface flow model in which vegetation appears as an integral part, and b) to use the model to simulate the effects of a variety of vegetation patterns on soil water and streamflow.

The simplest approach is to consider the subsurface system as the core, and other process components, such as infiltration, evapotranspiration and seepage, as inputs and outputs of the hydrologic simulation model. Inflows are regarded as gains or additions to, and outflows represent losses from, the system. A schematic diagram of the conceptual model is shown in Fig. 9. This simple model must relate to the physical watershed system.

Given the complexity of soils and geology of most watersheds, a two-dimensional profile provides the best configuration for simulating subsurface flow (Fig. 10). Two-dimensionality implies that a given section has unit width, say 1 m. A section so defined for simulating subsurface flow is assumed to supply generated streamflow to the adjacent 1 m of stream channel running perpendicular to the section. If the section is expanded uniformly in the third dimension, then the total outflow from this uniform "slice" is obtained by multiplying the outflow from the unit section by the length of channel adjacent to the slice. A simple example is a long uniform valley formed by escarpments (Fig. 11). This geomorphic pattern is often



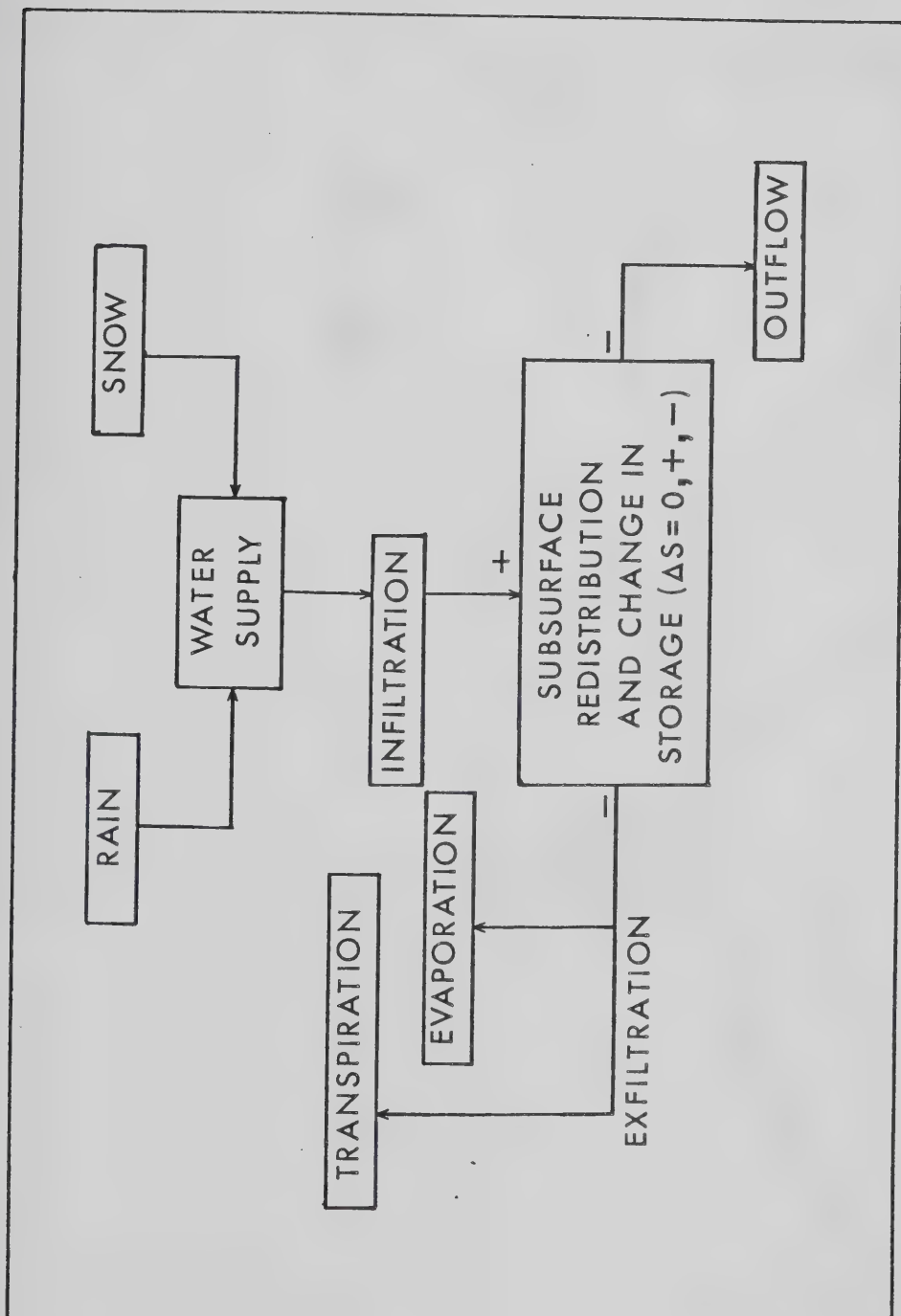


Figure 9. Conceptual hydrologic model.





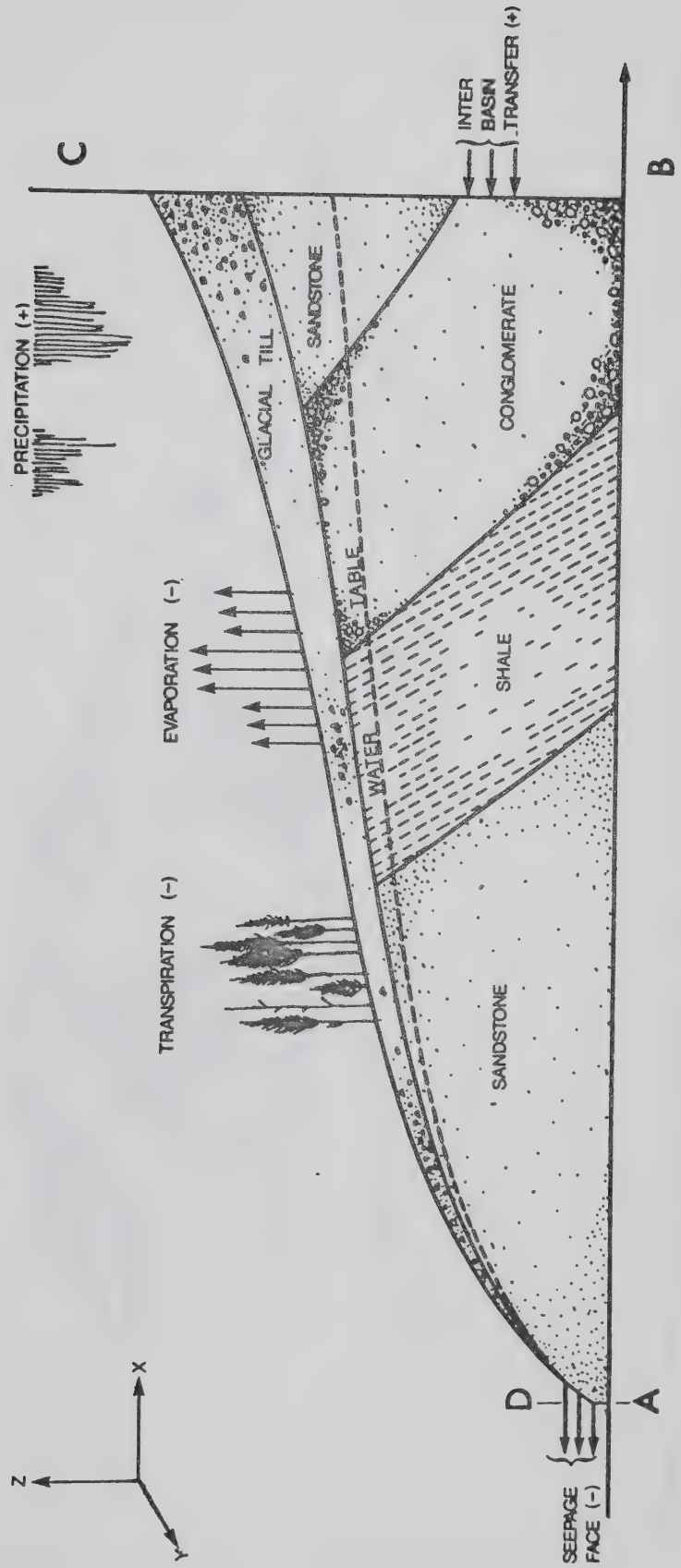


Figure 10. Two-dimensional hillslope profile for simulating subsurface flow.



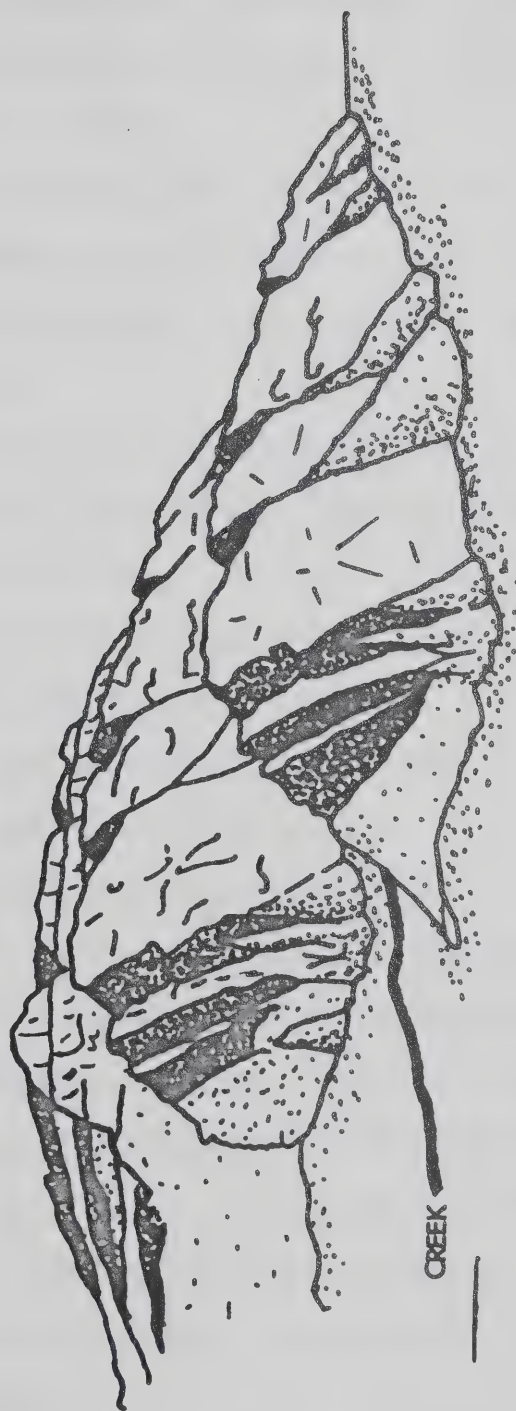


Figure 11. Uniform valley formed by escarpments.



encountered in the Front Ranges of the Rocky Mountains.

The process of extending a two-dimensional problem to an entire three-dimensional watershed is fraught with difficulties. Conceptually, though, it is simple and involves four main steps:

- a) divide the watershed into several slices or segments based on geology, soils, vegetation, precipitation-elevation relationships, and other factors;
- b) carry out subsurface flow simulations using the two-dimensional, unit width representation (section), and generate outflow;
- c) use results from b) to determine the outflow to stream channel from each entire segment;
- d) route generated channel flows through the watershed using a standard routing procedure.

Part a) can be readily accomplished if suitable data and detailed maps of the watershed to be simulated are available. Part b), the successful completion of which forms the main thrust of this thesis, is the most difficult step to resolve. It entails a statement of assumptions concerning the physical situation; the derivation and solution of the equations of flow through porous media; and the development of a mechanism for simulating outflow from the seepage face to the stream channel.

The first necessary assumptions relate to defining the limits of the subsurface flow system. A datum is selected to



coincide with a lower impermeable boundary or basement (the x-axis AB in Fig. 10) across which no flow takes place. The position of this boundary is determined, preferably, from geologic maps. Vertical impermeable boundaries BC and DA (Fig. 10) define the upslope and downslope limits of the subsurface system. The presence of a no-flow boundary at BC implies that the phreatic divide coincides with the topographic divide. If it is further assumed that water does not move transversely (in the y-direction), then it is evident that no positive or negative leakage can occur into or out of the segment. All water leaving the basin does so via the stream channel or the atmosphere. Water is free to move across the upper boundary (ground surface CD in Fig. 10) in either direction. It can also be transferred from the system interior by means of plants, pumping wells, or tile drains.

Plants, especially trees, consume large quantities of water; often the volume of water that leaves a watershed as evapotranspiration exceeds the total volume of streamflow. During transpiration water does not cross the upper boundary directly, but is 'piped' up the stems and lost to the atmosphere through the leaves. For simulation purposes, it is useful to draw an analogy between transpiring trees and pumping wells. In the latter case, water is withdrawn from the saturated zone and discharged above ground; the well is considered to be a sink in the system. Analytical methods are available to determine the effects of pumping wells or





sinks on the groundwater reservoir.

Plants extract water, usually from the unsaturated zone, by means of an extensive root system. Research with forest trees (Kramer, 1969) indicates that water may be absorbed by trees at distances of several metres from their stems. Veihmeyer and Hendrickson (1938, cited by Kramer, 1969) found that water 6 or 7 m from fruit trees is absorbed. The rooting depth varies with plant species. In most cases, the root zone is considered to be the upper 1 or 2 m of soil. However, some phreatophytes such as salt cedar (Tamarix chinensis Lour.) are capable of extracting water from depths of 6 m (Horton and Campbell, 1974), while the roots of mesquite (Prosopis juliflora) can penetrate as deep as 18 m into alluvium (Kearney and Peebles, 1951; cited by Horton and Campbell, 1974).

In order to simulate water withdrawal by trees, a series of sinks is introduced into the model near its upper boundary. The location of a sink in a finite element mesh corresponds to a tree rooting depth of 1 to 2 m in the physical system. Each sink has a rate-of-withdrawal value assigned to it and represents the influence of a number of trees on subsurface water. When trees are harvested, simulation is achieved by deleting a suitable number of sinks from appropriate locations. Conversely, when regrowth occurs the sinks are restored. However, the rate-of-withdrawal value assigned to sinks representing the young trees will be less than that assigned to sinks



representing mature trees before harvest. This method allows for considerable flexibility since the differences in water demand due to species, age, and forest management practices are simulated. The basic assumption here is that trees can be simulated using sinks in the manner described. The main limitation is the lack of information regarding consumptive use by different tree species at different ages.

Although it is recognized that great differences in properties may exist within the same soil type or geologic stratum, it is extremely difficult to map these spatial variations. Consequently, for simulation purposes, it is assumed that each soil type or geologic stratum is homogeneous.

The remaining assumptions concerning the model are related to its mathematical development. In the saturated region, flow is laminar and Darcian; inertia forces, velocity heads, temperature gradients, osmotic gradients, chemical concentration gradients are all assumed to be negligible. Water, the soils and geologic formations are assumed to be incompressible. In the unsaturated zone, it is assumed that the soils are non-swelling and that the air phase is continuous and always in connection with constant external atmospheric pressure (Freeze, 1971). The implications of these assumptions are alluded to in the last section (IIE) of the preceding chapter.

The general equation of flow through porous media (equation 2.8) used in simulating water flow through a



hillside section is usually solved by application of numerical techniques. Such techniques involve a) discretization of a continuous domain, and b) generation of a set of linear algebraic equations. Discretization is the procedure whereby a continuous domain  $D$  is divided into a number of subareas for the purpose of solving ordinary or partial differential equations. Approximations to a continuous solution may be defined at isolated points by finite differences or, alternatively, defined over the entire domain by application of the finite element method. The solution in this case is the pressure potential at each point defined in the domain.

The task of obtaining solutions for the parabolic partial differential equation of flow through porous media requires consideration of both initial and boundary conditions. The initial condition is the value of the function for the posed problem at starting time,  $t_0$ . The boundary conditions are either the value of the function, its normal derivative, or a linear combination of the function and its normal derivative on the boundary (Pinder and Gray, 1977). When the value of the function, such as constant pressure potential, is known, the boundary condition is referred to as a Dirichlet type boundary condition. If the normal derivative of the function is given, then the boundary condition is known as a Neumann type. Thus a vertical, impermeable or no-flow boundary forming a watershed divide exemplifies a Neumann type



boundary condition since  $\partial\psi/\partial x = 0$ , i.e. the hydraulic gradient in the x-direction is zero, so the flux across the boundary is also zero.

Since the equation of flow for this problem cannot be solved easily by analytical means, both the finite element and finite difference methods will be employed to develop and solve the necessary approximating equations during simulation. The finite element approximation will be applied to the spatial aspect of the problem, while the time derivative will be replaced by an appropriate finite difference representation.

The finite element method has several advantages over finite difference techniques when applied to a continuum (Desai and Abel, 1972; Remson et al, 1971; and Rodarte, 1978):

1. It is not necessary to develop special expressions to define the boundary conditions. Close agreement with complex real boundaries are obtained.
2. The dimensions of elements can be fixed arbitrarily. Thus, large elements can be used where a function changes gradually. When a function changes rapidly, such as in the near-surface regions of a simulated watershed, small elements are used. Irregular and complex configurations can be analyzed or simulated quite easily.
3. Anisotropy and heterogeneity can be routinely considered in the calculations.





4. It is possible to set up equations that produce positive-definite matrices which can be reduced to band form and solved with a minimum of storage and computation time.

Application of the finite element and finite difference methods to the governing equations should yield solutions for simulated time intervals of, say, one day (since we are primarily interested in snowmelt and rainfall runoff events, and seasonal recession flows). The field of pressure potential which constitutes the solution at time,  $t$ , conveys information about the direction of flow within the profile, and the position of the water table. An additional algorithm is required to provide values of outflow generated at the seepage face. For this purpose an iterative scheme, developed by Neuman (1973) and described in the next chapter, will be used.

The definition and solution of a simulated watershed section problem requires information regarding the geometry of the watershed, the hydraulic properties of the media, boundary fluxes, sinks, and streamflow data against which generated outflows can be compared. Thus, input data for the model will include some or all of the following:

- a) finite element mesh geometry of the entire vertical section,
- b) output from a snowmelt model to provide positive upper boundary fluxes during spring snowmelt periods,
- c) hydraulic properties of soil and geologic strata,



- d) amount, intensity, and duration of rainfall,
- e) climate data required to compute evaporation,
- f) values of consumptive use by trees, based on species, age and perhaps other factors such as diameter at breast height (dbh), crown cover density, or height; consumptive use values are assigned to sinks located at near-surface points in the finite element mesh,

The foregoing information provides both the initial and the boundary conditions of the problem.

Output from the model will consist of daily values of:

- a) pressure potential ( $\psi$ ) at points defined throughout the entire domain,
- b) total potential ( $\Phi$ ),
- c) volumetric water content ( $\theta$ ),
- d) water table position,
- e) outflow from seepage face (generated streamflow).



#### IV. MATHEMATICAL DEVELOPMENT OF SUBSURFACE FLOW MODEL

##### A. Governing Equations

The full general equation for three-dimensional transient, saturated-unsaturated flow through porous media can be written (Freeze, 1971) as

$$\begin{aligned} & \frac{\partial}{\partial x} \left[ \frac{g\rho^2(\psi)k_{xx}(F,\psi)}{\mu} \frac{\partial \psi}{\partial x} \right] + \frac{\partial}{\partial y} \left[ \frac{g\rho^2(\psi)k_{yy}(F,\psi)}{\mu} \frac{\partial \psi}{\partial y} \right] \\ & + \frac{\partial}{\partial z} \left[ \frac{g\rho^2(\psi)k_{zz}(F,\psi)}{\mu} \left\{ \frac{\partial \psi}{\partial z} + 1 \right\} \right] \\ & = \frac{[\rho(\psi)\theta(F,\psi)\{a'(F) + e(F,\psi)\beta'(F)\} + \rho(\psi)C(F,\psi)]}{e(F,\psi)} \frac{\partial \psi}{\partial t} \end{aligned} \quad (4.1)$$

where

$x, y, z$	coordinate directions, L;
$\psi$	pressure potential, L;
$g$	acceleration due to gravity, $LT^{-2}$ ;
$\mu$	viscosity of water, $FTL^{-2}$ ;
$\rho$	density of water, $FT^2L^{-4}$ ;
$k_{ii}$	intrinsic, or specific permeability, $L^2$ ;
$e$	porosity, dimensionless;
$\theta$	volumetric moisture content, dimensionless;
$F$	geologic formation or soil strata, dimensionless;
$C = \partial\theta/\partial\psi$	specific moisture capacity, $L^{-1}$ ;
$a' = a\rho g$	vertical compressibility of formation, $L^{-1}$ ;
$a$	coefficient of vertical formation compressibility, $L^2F^{-1}$ ;
$\beta' = \beta\rho g$	compressibility of water, $L^{-1}$ ;
$\beta$	coefficient of water compressibility, $L^2F^{-1}$ ;
$t$	time, T.

If the foregoing expression is written in vector notation it simplifies (Pinder and Gray, 1977) to



$$\vec{\nabla} \cdot [\vec{K} k_{rw} \cdot (\vec{\nabla} \psi + \vec{k})] = C \frac{\partial \psi}{\partial t} + \theta S_s \frac{\partial \psi}{\partial t} \quad (4.2)$$

where

$\vec{K} = \rho g k_{ii} / \mu$  saturated hydraulic conductivity tensor,  $LT^{-1}$ ;  
 $k_{rw}$  relative permeability of water, dimensionless;  
 $\vec{k}$  unit vector in the vertical direction;  
 $S_s$  specific storage,  $L^{-1}$ .

## B. Finite Element Simulation

The finite element method was developed in the 1950's to solve complex structural engineering problems. Since that time it has been successfully applied to problems in: soil and rock mechanics, heat conduction (Desai and Abel, 1972), surface and subsurface hydrology (Pinder and Gray, 1977), and in simulating water uptake by plants (Feddes et al, 1976). It has also been used to describe the geometry and position of cells in fossil and living plants (Niklas, 1977).

The following development of a finite element model for simulating unsteady, saturated-unsaturated flow of a single fluid through porous media is taken from Pinder and Gray (1977), and from Neuman (1973). The basis for the finite element model is Galerkin's method of weighted residuals. It is essentially a scheme for solving differential equations using integral approximations. We first consider the time independent equation

$$Lu = f \quad \text{in } B \quad (4.3)$$

where  $u$  is an unknown function,  $f$  is a known function,  $L$  is





the operator, and  $B$  is a bounded domain. Let  $u$  be approximated by a function  $\hat{u}(x)$  which consists of a linear combination of suitable functions and satisfies appropriate boundary conditions of the boundary value problem. For example, we might try

$$\hat{u}(x) = \phi_1(x) + \sum_{j=2}^M a_j \phi_j(x) \quad (4.4)$$

where  $\phi_1(x)$  is chosen to satisfy the essential boundary condition and the coordinate or basis functions  $\phi_j(x)$  (also called bases) satisfy the corresponding homogeneous boundary condition. Usually  $\phi_1(x)$  is not written explicitly, but is incorporated in the series

$$\hat{u}(x) = \sum_{j=1}^M a_j \phi_j(x) \quad (4.5)$$

Let a residual  $R$  be defined by

$$R(x) = L\hat{u} - f(x) \quad (4.6)$$

Inserting the trial function, we have

$$R(x) = L\left[\sum_{j=1}^M a_j \phi_j(x)\right] - f(x) \quad (4.7)$$

The residual (or error) function  $R(x)$  will be zero for the exact solution, but not for the approximation. In the method of weighted residuals, the residual is minimized by setting



the inner product of the residual function and a weighting function  $w_i$ , equal to zero:

$$\int_B R(x) \cdot w_i dx = 0 \quad (i=1,2,\dots,M) \quad (4.8)$$

This equation can more conveniently be written as

$$\langle R(x), w_i \rangle = 0 \quad (i=1,2,\dots,M) \quad (4.9)$$

There are several weighted residual techniques which can be used to obtain the solution to a set of differential equations. They include the collocation, subdomain, least squares, and Galerkin's, methods. The method selected governs the choice of the weighting function,  $w_i$ . In the Galerkin method, which was selected for this study, the coordinate functions  $\phi_j(x)$  also serve as the weighting functions  $w_i(x)$ . When the coordinate functions are inserted, the previous equation becomes

$$\langle R(x), \phi_i \rangle = 0 \quad (i=1,2,\dots,M) \quad (4.10)$$

In order for the residual to be minimized,  $R(x)$  must be orthogonal to all the functions  $\phi_i(x)$ .

The principle of the finite element method is that the coordinate functions, which are usually polynomials, are piecewise continuous over subdomains called finite elements. Nodes are located along the boundaries of each element and



each coordinate function is identified with a specific node i.e.  $\phi_i(x)$  has a value of unity at node  $i$ , but goes to zero at all other nodes. The elements may be one-, two-, or three-dimensional; linear, quadratic or cubic in space and/or time; rectangular, triangular or tetrahedral in shape. They may have either straight or curved sides. These examples are only a few from a large number of possible elements.

The preferred element for this model is the linear triangular element because it is well suited for use on irregular boundaries and concentrates coordinate functions in those regions of the domain where a rapidly varying solution is anticipated. Coordinate functions may be formulated in terms of either global or local coordinates. For triangular finite elements the local (or area) coordinate system is used because element integrations are thereby greatly facilitated. The development of coordinate functions using area coordinates for triangular elements and integration of the resulting expressions are described in Appendix A.

The general expression for coordinate functions for linear triangular elements is

$$\phi_i = a_i + b_i x + c_i y \quad (4.11)$$

where  $a_i$ ,  $b_i$ , and  $c_i$  are constants identified with the  $i$ th node and the  $i$ th coordinate function. When they are



expressed in terms of triangular area coordinates,  $L_i$ , the coordinate functions become

$$\phi_i = L_i = [(x_j y_k - x_k y_j) + (y_j - y_k)x + (x_k - x_j)y] / 2A_e \quad (4.12A)$$

$$\phi_j = L_j = [(x_k y_i - x_i y_k) + (y_k - y_i)x + (x_i - x_k)y] / 2A_e \quad (4.12B)$$

$$\phi_k = L_k = [(x_i y_j - x_j y_i) + (y_i - y_j)x + (x_j - x_i)y] / 2A_e \quad (4.12C)$$

where  $A_e$  is the element area.

The foregoing procedures will now be applied to the governing equation, 4.2. Let the pressure potential,  $\psi$ , be approximated by

$$\psi \sim \hat{\psi} = \sum_{j=1}^N P_j(t) \phi_j(x, y) \quad (4.13)$$

The two-dimensional form of equation 4.2 is

$$\bar{\nabla}_{xy} \cdot (\bar{K} k_{rw} \cdot \bar{\nabla}_{xy} \psi) + \bar{\nabla}_{xy} \cdot (\bar{K} k_{rw} \cdot \bar{k}) - [C + \frac{\theta S_s}{e}] \frac{\partial \psi}{\partial t} = 0 \quad (4.14)$$

and Galerkin's method requires that the coefficients  $P$  be determined such that

$$\langle L \hat{\psi}, \phi_i \rangle = 0 \quad (i=1, 2, \dots, N) \quad (4.15)$$

or





$$\begin{aligned}
& \langle \vec{\nabla}_{xy} \cdot (\vec{K} k_{rw} \cdot \vec{\nabla}_{xy} \sum_{j=1}^N P_j(t) \phi_j(x, y), \phi_i \rangle + \langle \vec{\nabla}_{xy} \cdot (\vec{K} k_{rw} \cdot \vec{k}), \phi_i \rangle \\
& - \langle [C + \frac{\theta S_s}{e}] \frac{\partial (\sum_{j=1}^N P_j(t) \phi_j(x, y))}{\partial t}, \phi_i \rangle = 0
\end{aligned} \quad (4.16)$$

Application of Green's theorem eliminates the second derivative, and reduces the governing equations to the form

$$\begin{aligned}
& \langle \vec{K}'(\psi) \cdot \vec{\nabla}_{xy} P_j \phi_j, \vec{\nabla}_{xy} \phi_i \rangle + \langle [C + \frac{\theta S_s}{e}] \phi_j \frac{dP_j}{dt}, \phi_i \rangle \\
& = \int_{\Gamma} \vec{n} \cdot \vec{K}'(\psi) \cdot [\vec{\nabla}_{xy} \psi + \vec{k}] \phi_i ds
\end{aligned} \quad (4.17)$$

where  $\vec{K}' = \vec{K} k_{rw}$  and  $\vec{n}$  is an outwardly directed unit normal vector on the surface,  $\Gamma$ .

This equation may also be expressed in matrix form as

$$[A]\{P\} + [B]\left\{\frac{dP}{dt}\right\} = \{F\} \quad (4.18)$$

where the elements of matrices  $[A]$ ,  $[B]$ , and  $\{F\}$  are

$$a_{ij} = \langle \vec{K}'(\psi) \cdot \vec{\nabla}_{xy} \phi_j, \vec{\nabla}_{xy} \phi_i \rangle,$$

$$b_{ij} = \langle [C + \frac{\theta S_s}{e}] \phi_j, \phi_i \rangle,$$

$$f_i = \int_{\Gamma} \vec{n} \cdot \vec{K}'(\psi) \cdot [\vec{\nabla}_{xy} \psi + \vec{k}] \phi_i ds$$

In general, for the subsurface flow problem,  $[A]$  is symmetric and  $[B]$  is a diagonal matrix.

The earlier assumption that the compressibilities of water, soil, and geologic formations are equal to zero



causes the specific storage,  $S_s$ , also to become zero. Thus  $b_{ij}$  reduces to

$$b_{ij} < [C] \phi_j, \phi_i > \quad (4.19)$$

Considering first the steady state problem, equation 4.18 reduces to

$$[A]\{P\} = \{F\} \quad (4.20)$$

When triangular finite elements are used, the information obtained from integration over each element is stored in a 3x3 element coefficient matrix as

$$\left[ \begin{array}{cc} K_{xx} < \frac{\partial \phi_1}{\partial x}, \frac{\partial \phi_1}{\partial x} > + K_{yy} < \frac{\partial \phi_1}{\partial y}, \frac{\partial \phi_1}{\partial y} > & K_{xx} < \frac{\partial \phi_1}{\partial x}, \frac{\partial \phi_2}{\partial x} > + K_{yy} < \frac{\partial \phi_1}{\partial y}, \frac{\partial \phi_2}{\partial y} > \\ & K_{xx} < \frac{\partial \phi_1}{\partial x}, \frac{\partial \phi_3}{\partial x} > + K_{yy} < \frac{\partial \phi_1}{\partial y}, \frac{\partial \phi_3}{\partial y} > \\ K_{xx} < \frac{\partial \phi_2}{\partial x}, \frac{\partial \phi_1}{\partial x} > + K_{yy} < \frac{\partial \phi_2}{\partial y}, \frac{\partial \phi_1}{\partial y} > & K_{xx} < \frac{\partial \phi_2}{\partial x}, \frac{\partial \phi_2}{\partial x} > + K_{yy} < \frac{\partial \phi_2}{\partial y}, \frac{\partial \phi_2}{\partial y} > \\ & K_{xx} < \frac{\partial \phi_2}{\partial x}, \frac{\partial \phi_3}{\partial x} > + K_{yy} < \frac{\partial \phi_2}{\partial y}, \frac{\partial \phi_3}{\partial y} > \\ K_{xx} < \frac{\partial \phi_3}{\partial x}, \frac{\partial \phi_1}{\partial x} > + K_{yy} < \frac{\partial \phi_3}{\partial y}, \frac{\partial \phi_1}{\partial y} > & K_{xx} < \frac{\partial \phi_3}{\partial x}, \frac{\partial \phi_2}{\partial x} > + K_{yy} < \frac{\partial \phi_3}{\partial y}, \frac{\partial \phi_2}{\partial y} > \\ & K_{xx} < \frac{\partial \phi_3}{\partial x}, \frac{\partial \phi_3}{\partial x} > + K_{yy} < \frac{\partial \phi_3}{\partial y}, \frac{\partial \phi_3}{\partial y} > \end{array} \right] \quad (4.21)$$

The components of these matrices are solved using the



following relations

$$\left\langle \frac{\partial \phi_i}{\partial x}, \frac{\partial \phi_j}{\partial x} \right\rangle + \left\langle \frac{\partial \phi_i}{\partial y}, \frac{\partial \phi_j}{\partial y} \right\rangle = \frac{1}{4A_e} ((y_j - y_k)(y_k - y_i) + (x_k - x_j)(x_i - x_k)) \quad (4.22)$$

and

$$\left\langle \frac{\partial \phi_i}{\partial x}, \frac{\partial \phi_i}{\partial x} \right\rangle + \left\langle \frac{\partial \phi_i}{\partial y}, \frac{\partial \phi_i}{\partial y} \right\rangle = \frac{1}{4A_e} ((y_j - y_k)^2 + (x_k - x_j)^2) \quad (4.23)$$

The next step is to assemble the element information into a global matrix, [A], by summing, for a given node, the contributions to that node from each element coefficient matrix. If the transient problem is considered, the global matrix [B] must also be assembled. This is done in much the same way as was matrix [A]. However, the element coefficient matrix in this case has the form

$$\begin{bmatrix} \langle \phi_1, \phi_1 \rangle & \langle \phi_1, \phi_2 \rangle & \langle \phi_1, \phi_3 \rangle \\ \langle \phi_2, \phi_1 \rangle & \langle \phi_2, \phi_2 \rangle & \langle \phi_2, \phi_3 \rangle \\ \langle \phi_3, \phi_1 \rangle & \langle \phi_3, \phi_2 \rangle & \langle \phi_3, \phi_3 \rangle \end{bmatrix} \quad (4.24)$$

The integrals are solved by means of the expressions

$$\langle \phi_l, \phi_l \rangle = A_e/6 \quad (l=i, j, k) \quad (4.25)$$

and

$$\langle \phi_l, \phi_m \rangle = 0 \quad (l=i, j, k), \quad m=i, j, k; \quad l \neq m \quad (4.26)$$



### C. Application Of Finite Difference Approximations To Time Domain

There are several methods available for replacing the time derivative in equation 4.18 with a finite difference approximation. The most general is the weighted average approximation

$$[A](\epsilon\{P\}^{t+\Delta t} + (1-\epsilon)\{P\}^t) + \frac{1}{\Delta t} [B](\{P\}^{t+\Delta t} - \{P\}^t) = \epsilon\{F\}^{t+\Delta t} + (1-\epsilon)\{F\}^t \quad (0 \leq \epsilon \leq 1) \quad (4.27)$$

where  $t$  is the time, and  $\Delta t$  is the time step.

When  $\epsilon=0$ , an explicit finite difference scheme results. This method is the simplest to solve but is only conditionally stable. The explicit scheme is

$$([A] - \frac{1}{\Delta t} [B])\{P\}^{t+1} = \frac{1}{\Delta t} [B]\{P\}^t + \{F\}^t \quad (4.28)$$

An unconditionally stable, first-order correct scheme is obtained when  $\epsilon=1$ , and equation 4.27 becomes

$$([A] + \frac{1}{\Delta t} [B])\{P\}^{t+\Delta t} = \frac{1}{\Delta t} [B]\{P\}^t + \{F\}^{t+\Delta t} \quad (4.29)$$

This scheme is usually referred to as the implicit or backward finite difference method.

A time-centred scheme results when  $\epsilon=1/2$ . Commonly referred to as the Crank-Nicolson implicit method, it is





second-order accurate and usually neutrally stable. It can be written as

$$\begin{aligned} & \frac{1}{2}[A]({\{P\}}^{t+\Delta t} + {\{P\}}^t) + \frac{1}{\Delta t}[B]({\{P\}}^{t+\Delta t} - {\{P\}}^t) \\ &= \frac{1}{2}({\{F\}}^{t+\Delta t} + {\{F\}}^t) \end{aligned} \quad (4.30)$$

Because of the dependence of both  $\bar{K}'$  and  $\theta$  on pressure potential, equation 4.18 is highly nonlinear, and the set of nonlinear algebraic equations it represents must be solved using an iterative procedure. A solution may be obtained by combining the finite element method with either the time-centred or the backward difference scheme. In this case, a backward difference scheme for time-centred coefficient matrices is used. (Pinder and Gray, 1977; Neuman, 1973). It is effectively an under-relaxation technique and has the advantage of damping oscillations that frequently occur when solving highly nonlinear systems. This iterative scheme also overcomes the problem of obtaining solutions that arises when the specific storage,  $S_s$ , is zero.

The fully implicit backward difference formula for this problem is

$$\begin{aligned} & ([A]^{t+1/2\Delta t} + \frac{1}{\Delta t}[B]^{t+1/2\Delta t}){\{P\}}^{t+\Delta t} \\ &= \frac{1}{\Delta t}[B]^{t+1/2\Delta t}{\{P\}}^t + {\{F\}}^{t+1/2\Delta t} \end{aligned} \quad (4.31)$$



where  $t$  represents the time, and  $\Delta t$  is the time step.

Equation 4.31 may be expressed as

$$[G]^{t+1/2 \Delta t} \{P\}^{t+\Delta t, m+1} = \{D\}^{t+1/2 \Delta t} + \{F\}^{t+1/2 \Delta t} \quad (4.32)$$

where

$$[G]^{t+1/2 \Delta t} = [A]^{t+1/2 \Delta t} + \frac{1}{\Delta t} [B]^{t+1/2 \Delta t}$$

$$\{D\}^{t+1/2 \Delta t} = \frac{1}{\Delta t} [B]^{t+1/2 \Delta t} \{P\}^t$$

and  $m$  is the iteration number.

Several steps are required to complete the iterative procedure which provides the solution to this equation.

1. The initial conditions for the problem are described at each node. They include initial volumetric water content  $\theta = \theta(\psi)$ , and initial hydraulic conductivity  $\bar{K}' = \bar{K}'(\psi)$ . Thus initial pressure potential,  $\psi$  (and  $\{P\}^t$ ), is also prescribed.
2. An initial estimate of pressure potential at the end of the first time step,  $\{P\}^{t+\Delta t}$ , is obtained by solving the expression

$$[G]^t \{P\}^{t+\Delta t} = \{D\}^t + \{F\}^t \quad (4.33)$$

rather than solving equation 4.32.

3. This estimate is used together with the relation



$$\{P\}^{t+1/2\Delta t} = (\{P\}^t + \{P\}^{t+\Delta t})/2 \quad (4.34)$$

to determine  $\{P\}^{t+1/2\Delta t}$

4. The values of  $\{P\}^{t+1/2\Delta t}$  govern the values of  $\bar{K}'$ ,  $C$ , and  $\theta$  which appear in coefficients  $a_{ij}$  and  $b_{ij}$  (equation 4.18). New values of  $\bar{K}$ ,  $C$ , and  $\theta$  are determined from  $\{P\}^{t+1/2\Delta t}$  and the resulting updated coefficient matrices are used in equation 4.32 to obtain an improved value for  $\{P\}^{t+\Delta t}$ .
5. The iterative procedure (steps 3 and 4) is repeated until the difference between successive iterations is within satisfactory limits i.e.

$$|P_i^{t+\Delta t, m+1} - P_i^{t+\Delta t, m}| < E \quad (i=1, 2, \dots, N) \quad (4.35)$$

where  $E$  is the specified difference criterion.

6. When this condition is met,  $\{P\}^t$  is updated to  $\{P\}^{t+\Delta t}$ , and the iterative cycle is initiated once again for the next time step, solving first for  $\{P\}^{t+2\Delta t, 1}$ .
7. For constant-sized time steps beyond the initial time step, the following relation is used to obtain a first estimate of  $\{P\}^{t+1/2\Delta t}$

$$\{P\}^{t+1/2\Delta t} = \{P\}^{t+1/2} / 2 (\{P\}^t - \{P\}^{t-\Delta t}) \quad (4.36)$$



The matrices generated by using the finite element method are usually sparse and banded, a condition which permits considerable saving in core-storage and computational effort (Pinder and Gray, 1977). There are several methods available for reducing matrices to a form suitable for extracting the solution,  $\{P\}$ . The method selected for this problem entails column by column decomposition of the matrices, and is referred to as the Cholesky method. The theory, procedure, and the algorithms necessary to implement the Cholesky method are given in Elwi and Murray (1977).

#### **D. Treatment Of Boundary Conditions, Sinks, And Seepage Faces**

The boundary conditions are handled through the line integral in  $\{F\}$ . This integral is non-zero only along the domain boundary,  $\Gamma$ , where it represents the component of flow normal to  $\Gamma$ . For a no-flow boundary condition,  $\{F\}$  is set to zero at each of the relevant boundary nodes. If  $\{P\}$  is known for a given node (Dirichlet-type boundary condition) then the equation for that node is condensed or partitioned from the matrices.

It appears that no provision for sinks has been made in equation 4.18. Strictly speaking a term,  $\{Q\}$ , for sinks should appear on the right hand side of the equation. However, for computation purposes  $\{Q\}$  has, in effect, been absorbed by  $\{F\}$  such that





$$\{F\}' = \{F\} + \{Q\} \quad (4.37)$$

Since  $\{F\}$  is zero for all interior nodes, and  $\{Q\}$  has non-zero values only at specified interior nodes, it is feasible to use  $\{F\}$  to define both  $\{Q\}$  and  $\{F\}$  without changing the definitions and assumptions related to the vector,  $\{F\}$ .

Consideration must also be given to proper simulation of outflow from seepage faces during iteration. For this purpose, the approach devised by Neuman (1973) will be used. This method predicts the location of the seepage face at time  $t^{n+1}$ , given its position at  $t^n$ . It works as follows: at time,  $t^n$ , the seepage face is defined and the pressure potential,  $P$ , is set to zero at all points along the seepage face. At points where  $P < 0$ , the inward-directed normal flux,  $Q$ , is prescribed as zero. The solution to the governing equations should then yield  $Q < 0$  (outflow) when  $P = 0$ , and  $P < 0$  when  $Q = 0$ . If, however, results show  $Q > 0$  at a point where  $P = 0$ , then  $Q$  is set equal to zero, and the point treated as a no-flow portion of the boundary. Similarly, if  $P > 0$  where  $Q = 0$ , the corresponding value of  $P$  is set to zero and the point treated as a constant potential point during the next iteration. Iteration is continued until results are compatible.



## V. SIMULATIONS: RESULTS AND DISCUSSION

### A. Unsaturated Flow

#### Model validation

The credibility of a physically based mathematical model should be established before it is used to simulate the complex, dynamic systems of the real world - systems in which not one, but several processes may be active at the same time. One has first to ask himself the question: "Is the model responding correctly, in a qualitative way, to the boundary and initial conditions imposed upon it ?" Applied to a specific hydrologic process, the question might be re-phrased as: "Does the model respond with reduced water content, lower potentials, and steep potential gradients, near the ground surface during times of high evaporative demand ?" Alternatively, one might pose the question: "Can the model show an advancing wetting front, and a decay function for infiltration rate, during infiltration ?" Such relationships were established long ago (Horton 1933, for example) through extensive field observations and laboratory experiments; they are described in many soils and hydrology text books.

Once it has been determined that the physically based mathematical model can, indeed, simulate isolated processes, then it is feasible to use the model to examine such processes within the context of an integrated system, such



as a watershed or a hillslope.

It is the intent, in the following simulations, to have the subsurface flow problem evolve from a very simple case of infiltration, evaporation, or transpiration for a single, unsaturated medium, to more complicated situations in which saturated-unsaturated flow systems, several media, and the seepage face are considered.

### One-dimensional, vertical infiltration and evaporation

The first simulation concerns one-dimensional flow through unsaturated clay soil. This problem was considered first because it is very simple. The volume of soil involved is small enough that the usual assumptions, that the soil is homogeneous and has uniform properties, are probably correct in this case. Furthermore, a solution to the problem has been obtained by other investigators (Beven, 1975; Philip, 1957). Philip solved the problem using an analytical technique, and Beven arrived at essentially the same result by means of a finite element method.

In each case, flow through Yolo Light Clay was simulated. This soil, which is an agricultural soil in California, consists of 23.8 percent sand, 45 percent silt, and 31.2 percent clay, with a pore space of 50 percent (Moore, 1939). The unsaturated hydraulic conductivity is related to pressure potential by the expression  $K=0.00463/(\psi^2+400.0)$ , where  $\psi$  is the pressure potential (Rubin, 1968). Thus, saturated  $K$  is  $1.16 \times 10^{-5}$  cm/sec.



A mesh of unit width with no-flow boundaries on either side (Fig. 12a), suggested by Beven (1975), was constructed for the one-dimensional problem. Note that z-coordinates for all but two of the nodes are negative. This has no effect on the total potential at one node relative to the total potential at other nodes. The only difference between results from a positive coordinate system, referenced from the bottom of the soil column, and the results from this system, is that the total potential at all nodes in the negative system is 10 cm higher than the potential at the corresponding nodes in the positive system. Initial pressure potentials were set everywhere equal to -660 cm ( $\theta=0.240$ ), except at the surface nodes where they were maintained at saturation ( $\psi=0$  cm). These initial and boundary conditions correspond to those of Beven and Philip.

The results produced by SUBFEM at the end of 10,000 sec, using a time step of 500 sec (Fig. 12b) compare favorably with Beven's (1975) finite element solution and Philip's (1957) analytical solution. In all three cases water penetrated to a depth of about 8 cm. Some differences are inevitable since the functional relationship between  $\theta$  and  $\psi$ , and between  $K$  and  $\psi$ , used in SUBFEM are different from those used in Beven's and Philip's simulations. However, the retention curves do have certain data points in common. Convergence occurred fairly rapidly in the one-dimensional simulation - to a difference in potential of 0.01 cm after 4 to 8 iterations.





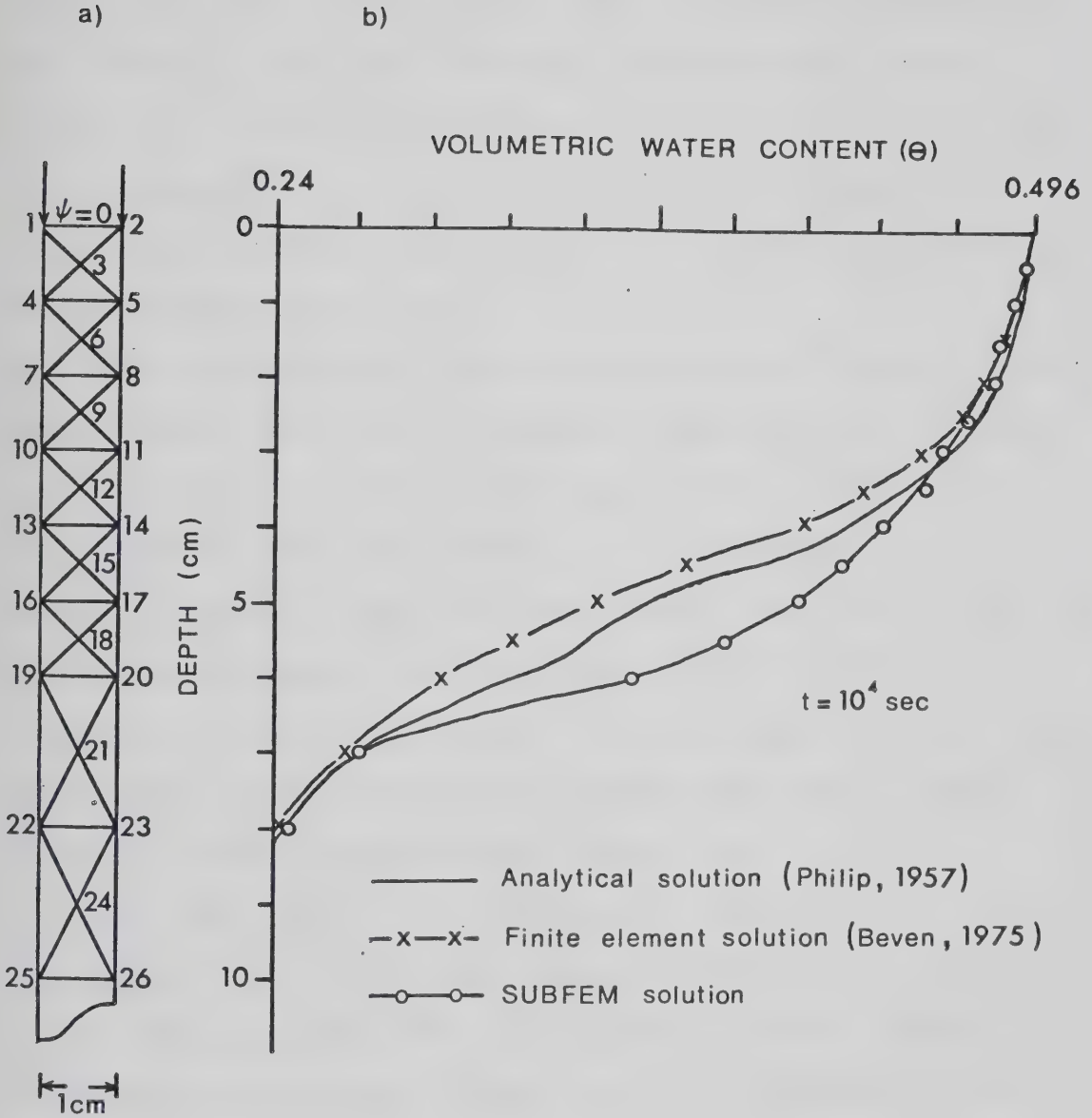


Figure 12. a) Finite element discretization for one-dimensional infiltration into Yolo Light Clay (After Beven, 1975).  
 b) Comparison of SUBFEM solution with those obtained by Philip (1957) and Beven (1975).



The isopotential lines for the soil column, after 10,000 sec, are shown in Fig. 13a. The highest potential (0 cm) occurs at the upper boundary and the lowest (-660 cm) at a depth of 10 cm. This confirms that vertical infiltration is taking place, i.e. in the direction of decreasing potential. The flow lines or streamlines run perpendicular to the isopotential lines

Field capacity is defined as the water content of soil after gravity drainage is complete, usually at a tension of  $1/3$  atmosphere, or -343 cm of water. After 10,000 sec of infiltration, the soil column is at field capacity, or wetter, down to a depth of about 6.7 cm. The lowest point at which field capacity is attained is in the region of steepest potential gradients - between depths of 6 and 8 cm (Fig. 13a). It is also in the region where the greatest changes in water content occur (Fig. 13b).

The zone where water invades and advances into originally dry soil is known as the wetting front zone. It is the zone in which the greatest water-moving forces, resulting from potential gradients, are produced (Hillel, 1980). For this problem, it corresponds to depths 6 to 8 cm, where the isopotential lines are close together and the potential gradient is 199 cm/cm (Fig. 13a). In contrast, the isopotential lines between 0 and 6 cm depth are more widely spaced, yielding a potential gradient of 34 cm/cm.

In order to evaluate transient behaviour of the simulated flow, the position of the wetting front is plotted



Vertical exaggeration : 0.5x horizontal scale

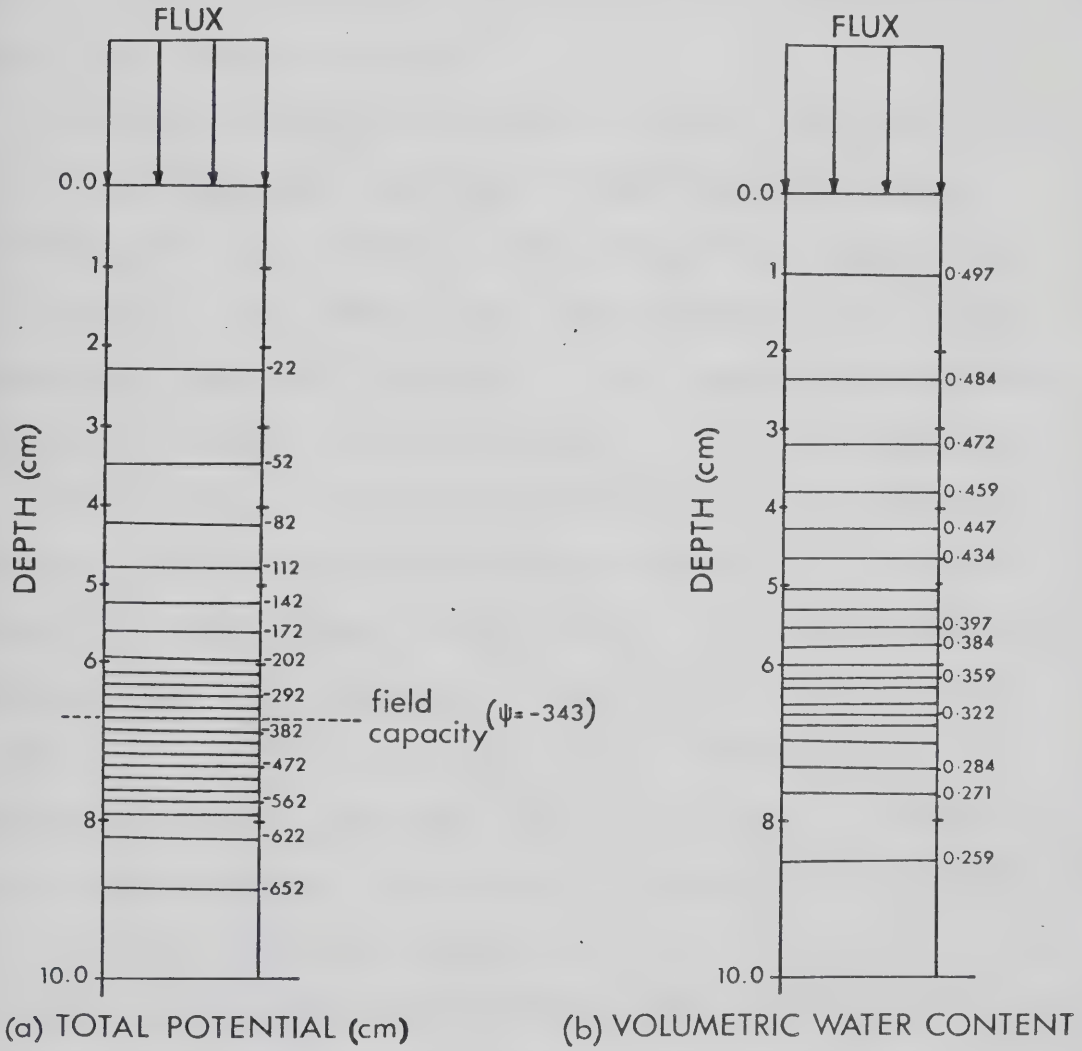


Figure 13. One-dimensional, vertical infiltration - total potential (a) and volumetric water content (b) after 10,000 sec.



over time (Fig. 14). Here, the wetting front is defined arbitrarily as the depth at which the water content is at field capacity. The curve shows a smooth progression of the wetting front from the surface at  $t=0$  sec, to a depth of nearly 7 cm after 10,000 sec. This is the "advancing wetting front" referred to earlier.

If the flux across the upper boundary is plotted over time, the resulting curve can be described by a decay function (Fig. 14). This is the infiltration capacity curve for the soil, and theoretically should become horizontal (constant) when the infiltration rate equals the saturated hydraulic conductivity of the soil ( $1.16 \times 10^{-5}$  cm/sec).

A transient, one-dimensional evaporation simulation was also run. It differed from the infiltration run only with respect to the boundary conditions at the surface nodes. A negative flux corresponding to an evaporation rate of 5 mm/day was specified for these nodes, instead of the constant pressure potential ( $\psi=0$ ) condition that applied during infiltration. The choice of 5 mm/day is reasonable as it is a rate commonly attained on warm, windy days in the mountains and foothills of Alberta. The initial conditions remained the same as for the infiltration problem.

At the beginning of the simulation, the water content ranged from 0.496 (saturation) at the surface to 0.250 at 0.5 cm depth. For the same depth increment, the pressure ranged from 0 to -660 cm. This is equivalent to a potential gradient of 1320 cm/cm in the downward direction.





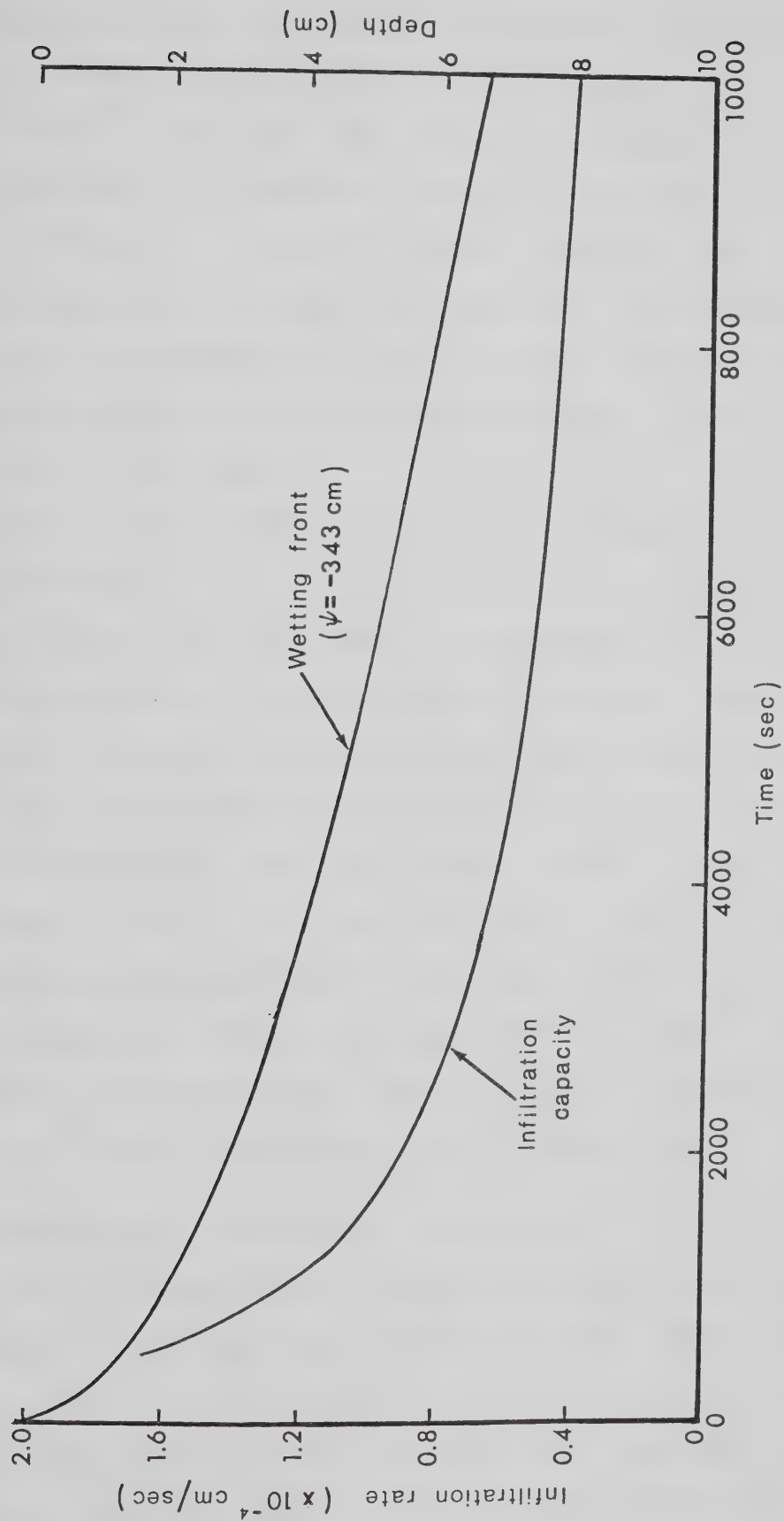


Figure 14. One-dimensional, vertical infiltration - advancing wetting front and infiltration capacity.



Consequently, when the simulation proceeds, there should be some evidence that drainage is taking place.

After 10,000 sec, the combined influence of evaporation and drainage had produced a potential gradient in the upper 1/2 cm of soil, of about 60 cm/cm. downward (Fig. 15a). This is considerably less than the gradient in the same depth increment at the start of the simulation. The gradient's downward direction indicates that drainage is the dominant process in this case.

Both total potential (Fig. 15a) and water content (Fig. 15b) show little change from initial conditions at depths below 4 or 5 cm. This is consistent with field observations which show that water draining from the surface, wets progressively deeper layers with time.

At the beginning of the simulation, water content was uniform throughout the soil column, except in the surface increment. After 10,000 sec, the water content in this increment approached that of the rest of the column. For the soil column as a whole, the water content tends to decrease slightly with depth (Fig. 15b). It is not possible in this case to discern the effects due to evaporation.

### **Two-dimensional, horizontal infiltration**

The two-dimensional, infiltration problem was selected because it, too, has been solved by others (Beven, 1975; Rubin, 1968). In this case horizontal infiltration into a 10-cm high block of Yolo Light Clay was simulated. The total hydraulic potential ( $\Phi$ ) at the infiltration face was



Evaporation : 5mm/day

Vertical exag: x0.5

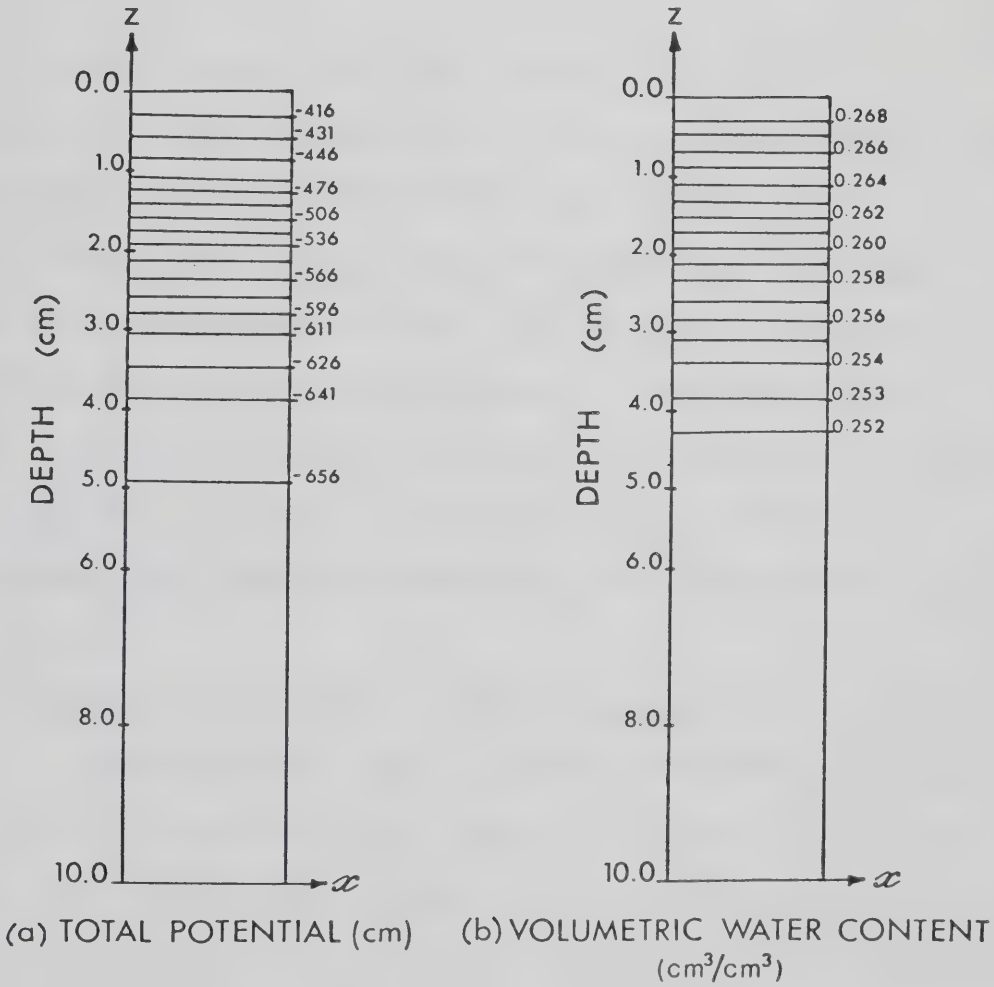


Figure 15. One-dimensional evaporation - total potential (a) and water content (b) after 10,000 sec.



maintained at  $-13$  cm, while the rest of the block was initially at  $\psi = -568$  cm (Beven, 1975). The  $K$  vs  $\psi$  relation, and the water retention curve were the same as for the one-dimensional problem. A time period of approximately 6 hours (22,000 sec) was simulated using Beven's (1975) finite element discretization (Fig. 16), and a time step of 1,000 sec.

Figure 17 shows the total potential field for this problem, obtained using Beven's finite element model (Fig. 17a), Rubin's method (Fig. 17b), and SUBFEM (Fig. 17c). Rubin (1968) employed the alternating-direction, implicit difference technique to obtain his solution. The three solutions show quite good agreement - the equipotential lines for each are almost vertical, and indicate horizontal flow from left to right. No difficulties related to convergence and numerical stability were encountered for this problem.

A comparison of the block's volumetric water content (Fig. 18) determined by Rubin (1968) and SUBFEM indicates that after 6 hours the water content is about 3 to 8 percent higher for the SUBFEM simulation. The difference may be attributed to the  $\theta$  vs  $\psi$  relation used in SUBFEM, which is different from that used in Rubin's (1968) simulation. Another factor could be the slightly greater simulation period (6 hours 7 minutes) used in SUBFEM, compared with 6 hours used by Rubin. In SUBFEM, the volumetric water content corresponding to the initial pressure potential ( $-568$  cm) is





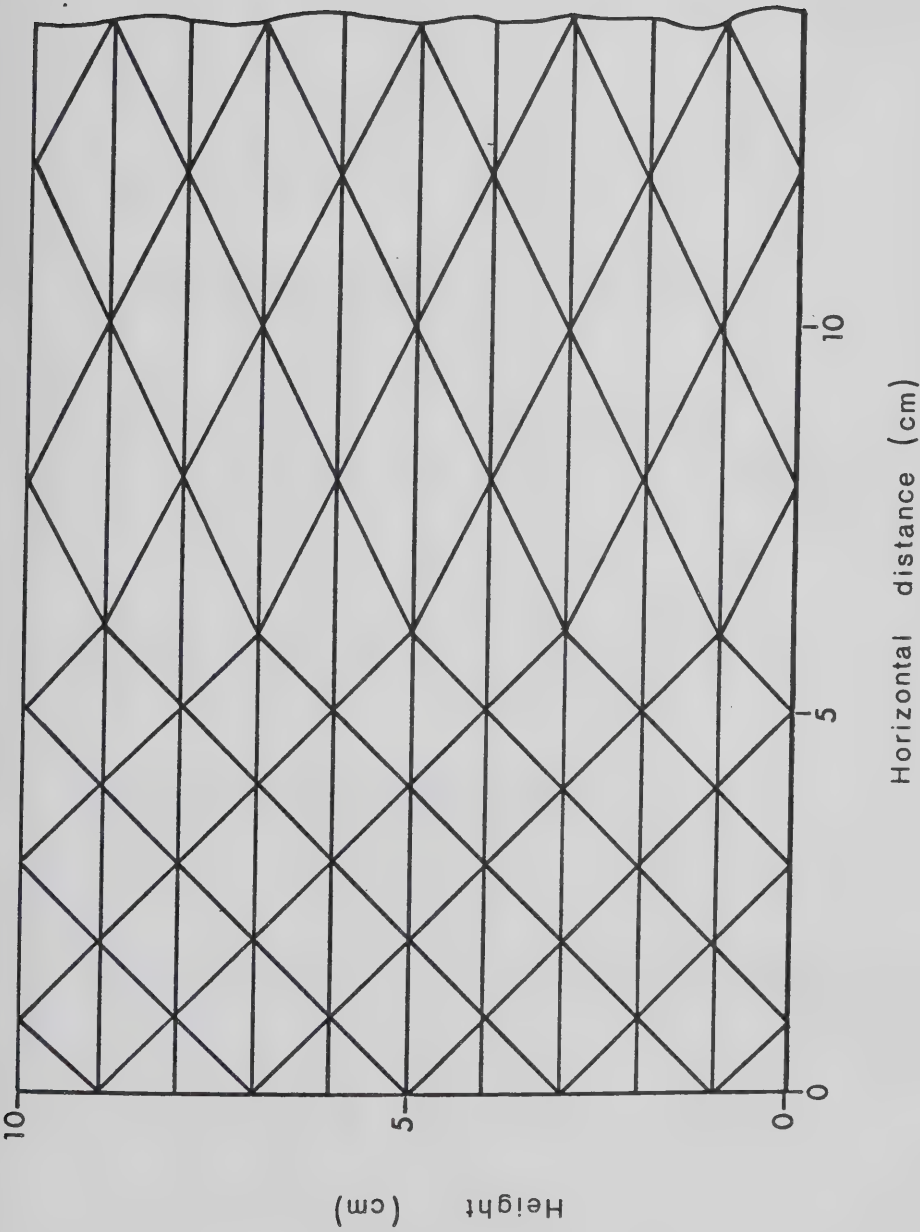


Figure 16. Finite element discretization for two-dimensional horizontal infiltration into a block of Yolo Light Clay (After Beven, 1975).



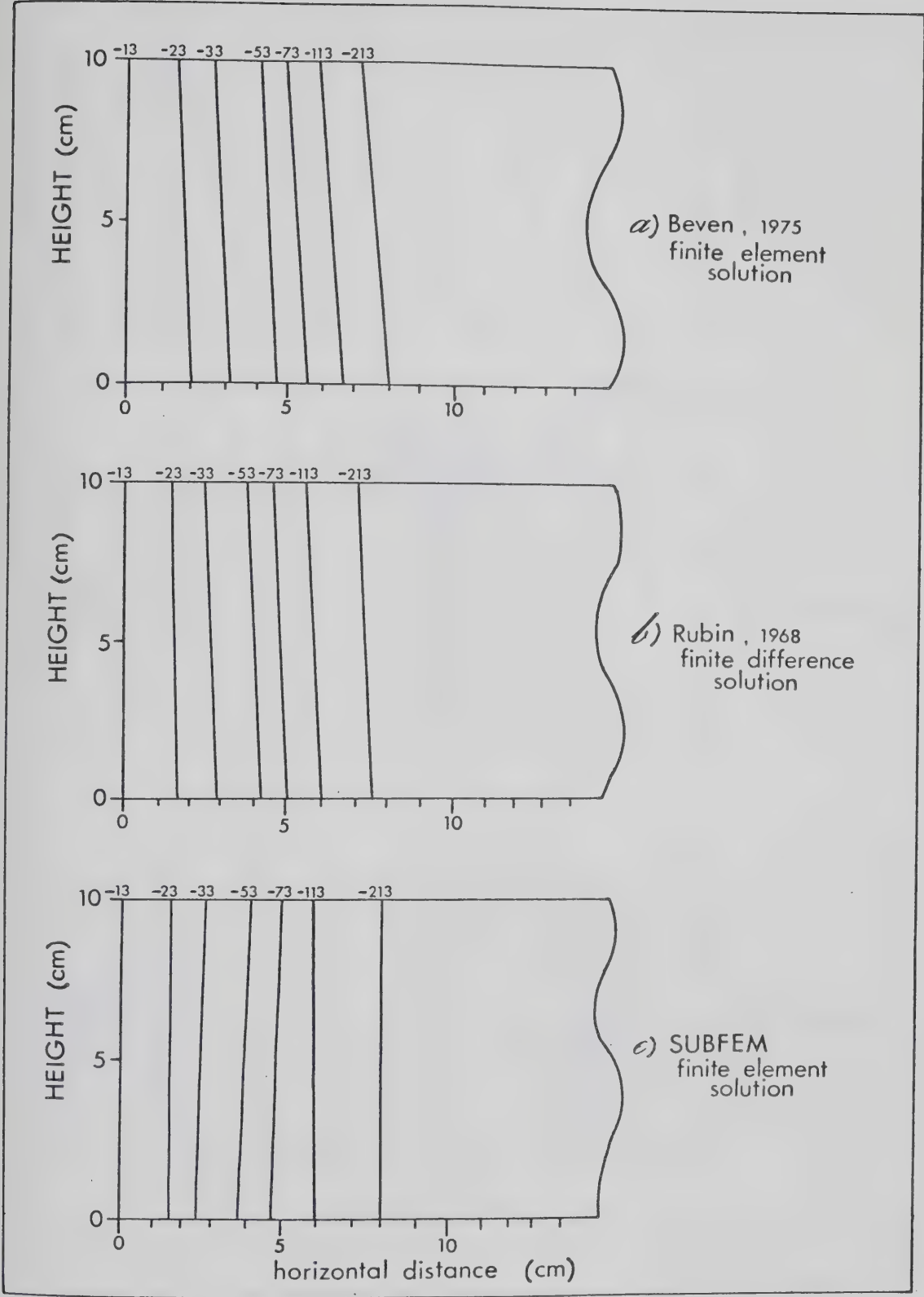


Figure 17. Two-dimensional, horizontal infiltration - total potential after 6 hr.



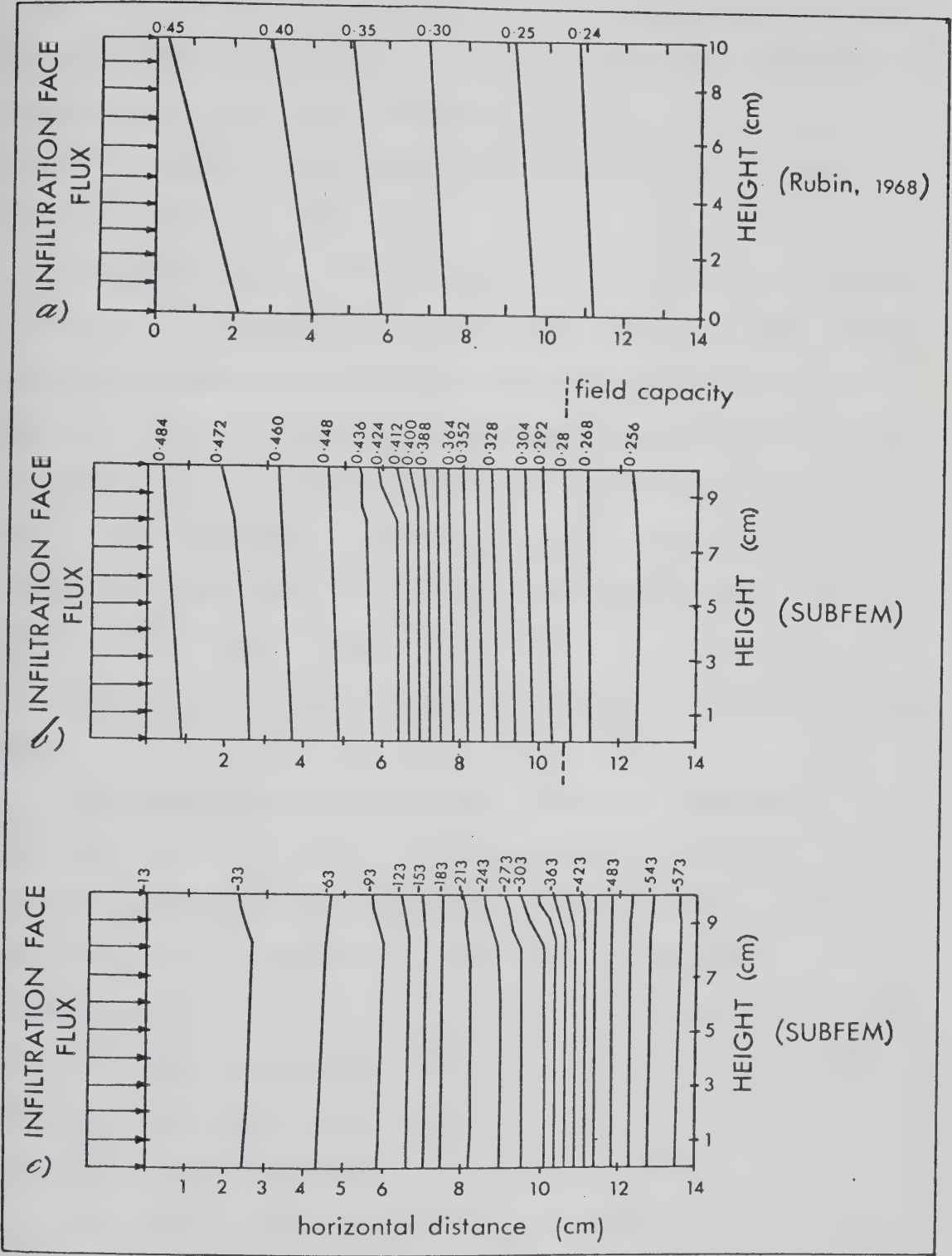


Figure 18. Two-dimensional, horizontal infiltration - water content [a) and b)] and total potential [c)] fields after 6 hr.



0.255, but in Rubin's simulation it was 0.238. It is also possible that a lower limit for the convergence criterion in SUBFEM would have produced solutions that were closer to those of Rubin. After 6 hours, water had advanced about 13 cm into the block (Fig. 18).

The soil is at field capacity at a horizontal distance of about 11 cm from the infiltration face (Fig. 18b). This gives us a reasonable indication of the position of the wetting front. The potential gradient between 10 and 12 cm is about 90 cm/cm, and between 0 and 10 cm, 29 cm/cm (Fig. 18c). This relation, or pattern, is very similar to conditions described for the vertical infiltration problem which showed steep potential gradients in the vicinity of the wetting front, and lower gradients near the infiltration face.

The advancing wetting front curve for horizontal infiltration (Fig. 19) is very similar to that for vertical infiltration (Fig. 14). After 10,000 sec, the wetting front had advanced 6.7 cm into the vertical column. The corresponding value for horizontal infiltration is 7.1 cm. The infiltration capacity curve for horizontal flow (Fig. 19) resembles the one for vertical flow (Fig. 14) in that it portrays a decay function.

The results obtained so far, for vertical and horizontal infiltration, suggest that SUBFEM can simulate, qualitatively at least, both isolated and interacting hydrologic processes such as infiltration and drainage. The





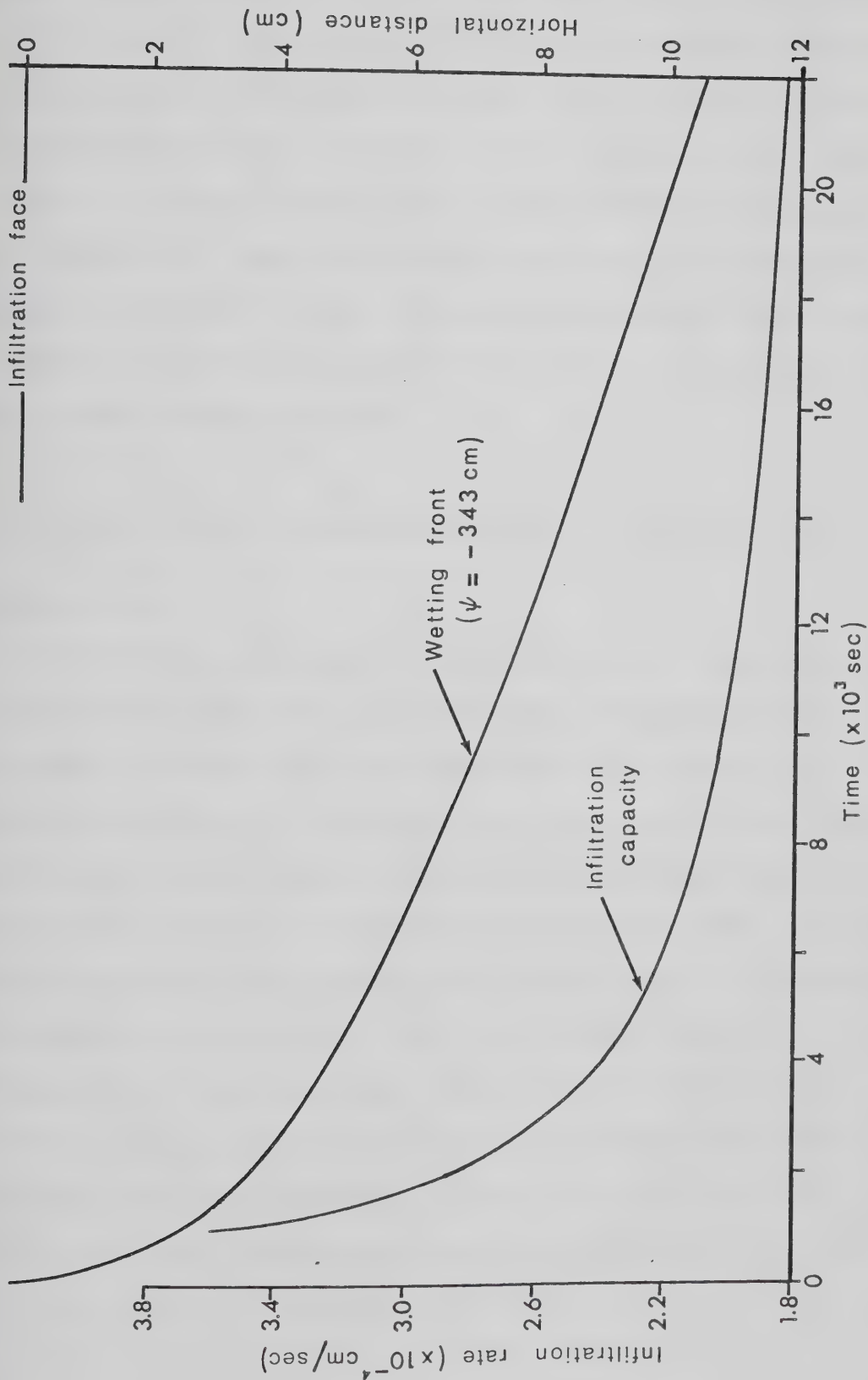


Figure 19. Two-dimensional, horizontal infiltration - advancing wetting front and infiltration capacity.



solutions are generally consistent with those obtained by other investigators and also with observations from field and laboratory experiments. The other researchers employed finite element, finite difference, and analytical techniques to achieve the same solution. On the basis of the foregoing results, it would appear that, since SUBFEM can simulate in a limited way, real hydrologic conditions, its validity has been established in part. Thus we can proceed, with some measure of confidence, to use the model to try and solve more complicated problems.

## Evaporation and transpiration from a large box of soil

### Evaporation

A run was performed to determine model response to evaporation simulation. In this case, evaporation was assumed to occur from Yolo Light Clay soil contained in a large, open box or container 30 m long, 1.8 m high, and of arbitrary width. The system might be considered as an extended lysimeter. A simple finite element mesh, consisting of 64 nodes and 90 elements, was used (Fig. 20). No-flow boundaries exist at  $x(z,t)=0$ ,  $x(z,t)=3000$ , and  $z(x,t)=0$  cm. Evaporation (negative flux) nodes are located at the surface, and an evaporation rate of 5 mm/day was specified. Initial conditions were set so that  $\psi(x,z,0)=-500$  cm ( $\theta=0.260$ ). The problem was run for a simulated time interval of 240 hr using a time step of 12 hr.



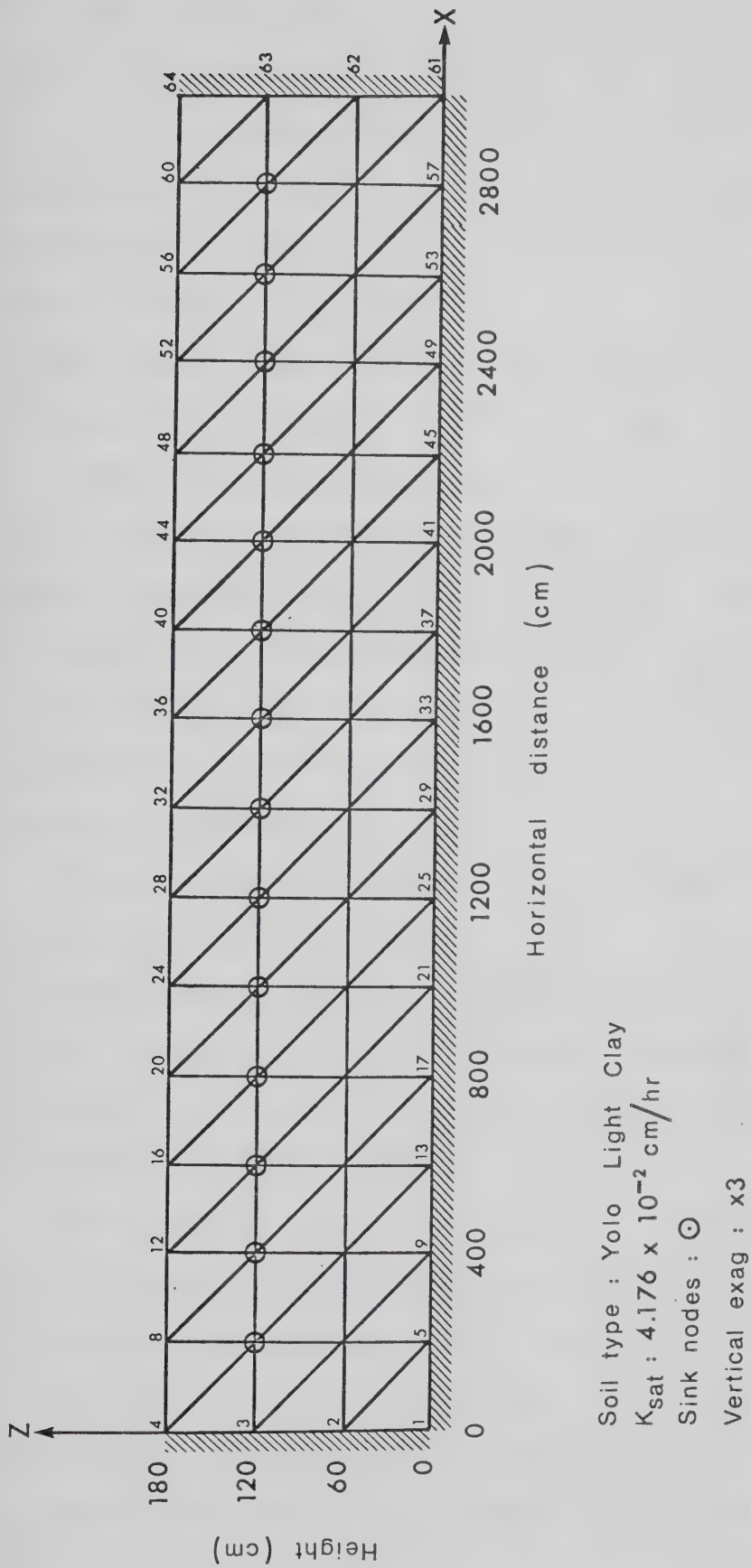


Figure 20. Finite element discretization for evaporation, transpiration, and evapotranspiration from a flat section of Yolo Light Clay.



The results show (Fig. 21) that for this problem, effects of evaporation on the soil are limited to the upper 60 or 70 cm. No changes were produced in the lower portion (heights 0 to 110 cm) of the profile. Pressure potential values after 10 days (Fig. 21a) ranged from -3330 cm at the surface to -500 cm at depth 70 cm below the surface. At the surface nodes, differences between pressure potentials over consecutive time steps tended to increase with time.

Steep potential gradients, up to 40 cm/cm, exist in the upper 70 cm of soil (Fig. 21b). They arise in order to sustain the evaporation rate at 5 mm/day, compensating for the reduction in the hydraulic conductivity which occurs as the soil dries out. The gradients are directed upward which is consistent with the direction of water movement in response to evaporation.

After 10 days of evaporation, the water status of the soil has changed significantly (Fig. 21c). At the surface, the water content has been reduced by 10 percent. Below the surface, reduction in water content decreases with depth for about 70 cm, below which point uniform moisture conditions ( $\theta=0.260$ ) prevail.

The boundary conditions, coupled with the fact that evaporation was not imposed on the surface corner nodes, have a pronounced effect on the shape of the isolines (Fig. 21). The isolines bend sharply near the lateral boundaries and intersect the surface at right-angles. The total potential lines (Fig. 21b) indicate that water is drawn away





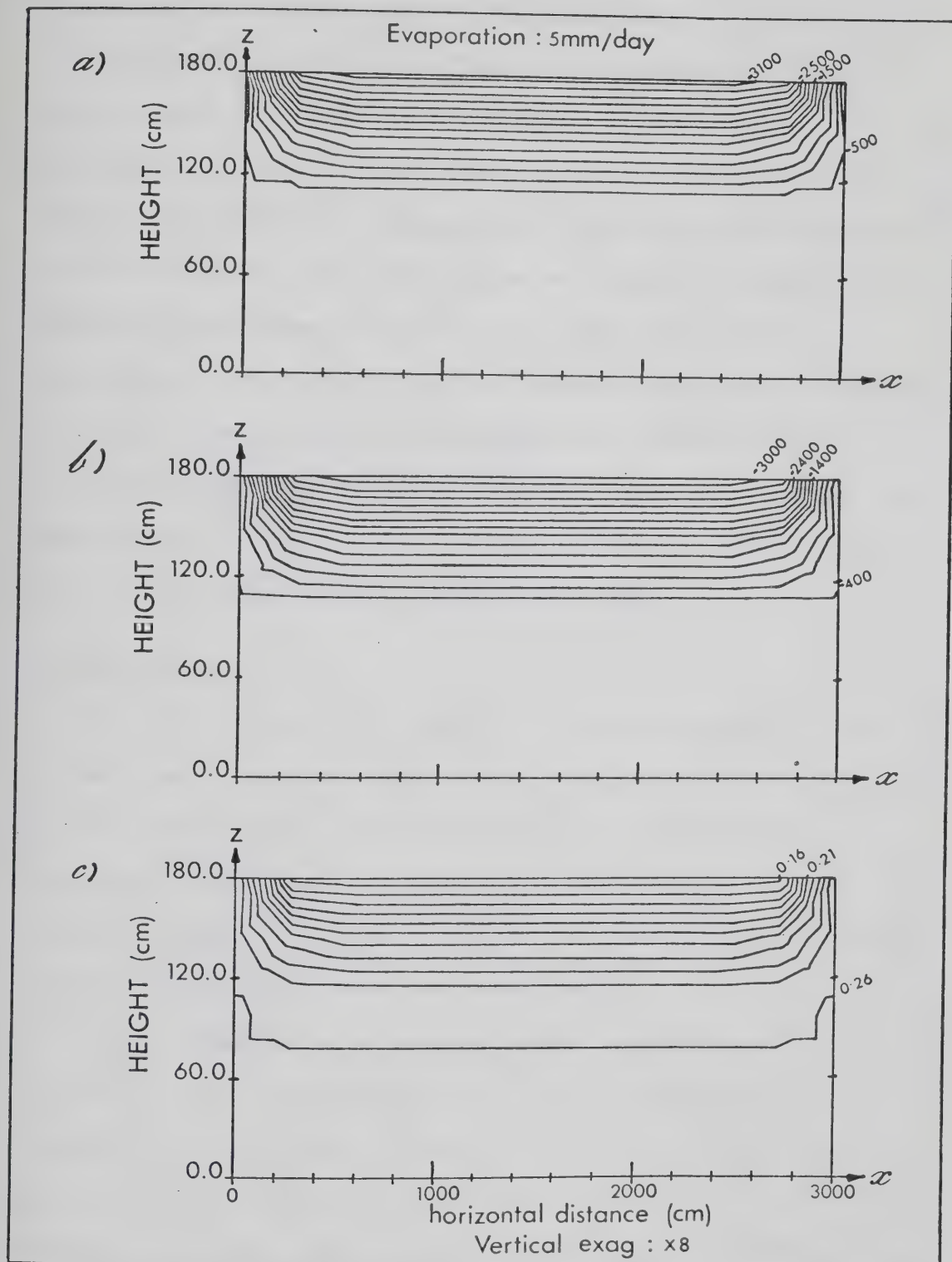


Figure 21. Evaporation from a flat profile - pressure potential (a), total potential (b), and water content (c), after 240 hr.



from these boundaries during evaporation.

The isolines shown in Figure 21 display a symmetric pattern about the 1500 cm horizontal distance mark. Supplementary simulations suggest that, if the box is tilted, this symmetry disappears. Positions downslope from the 1500 cm mark then tend to be wetter, and positions upslope dryer, than the mid-slope positions. These supplementary simulations also revealed that the proportion of the profile affected by evaporation increases with saturated hydraulic conductivity. If the conductivity is great enough, water may be removed from the bottom of a profile, even during the first time step.

### **Transpiration**

For the purpose of simulating transpiration, it was assumed that trees are planted in the box used in the previous simulation, and that the box is otherwise completely sealed to prevent soil evaporation. It was further assumed that the trees are of sufficient size and number to transpire 5 mm of water per day.

A few changes only are required to convert the simulation for the previous run from an evaporation to a transpiration problem. Transpiration is simulated by activating sink nodes at depth 60 cm below the surface, and assigning to them appropriate values that correspond to transpiration rates of 5 mm/day. Since no evaporation is occurring, fluxes at the surface nodes are set to zero.



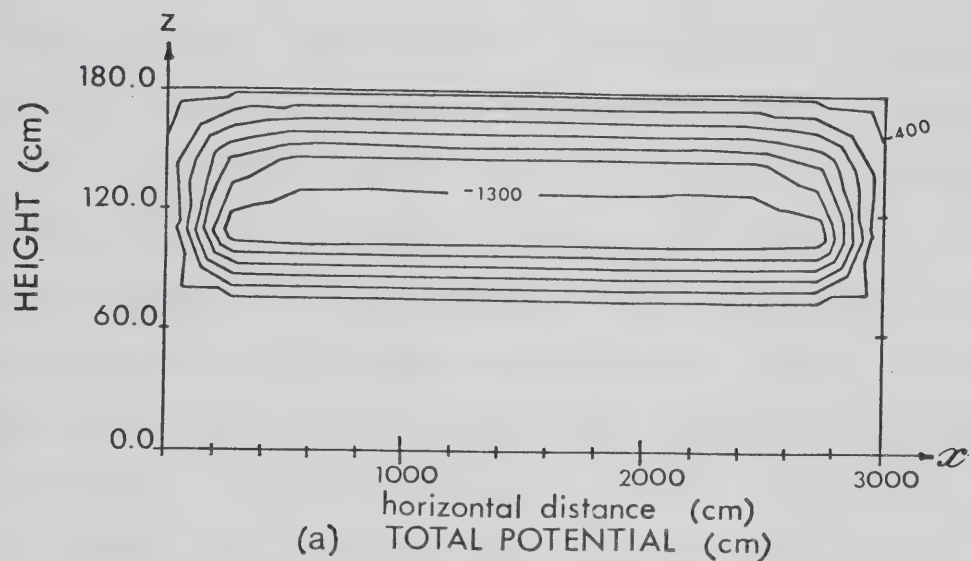
The results indicate (Fig. 22) that transpiration affects a greater volume of soil than does evaporation (Fig. 21), under the same conditions. The volume affected extends down to about 110 cm below the surface. The lower 70 cm are not affected. After 10 days, the lowest total potential (-1447 cm) was attained at the sink nodes (trees), 60 cm below the surface.

Because tree roots are completely surrounded by moist soil, they have access to water in every direction. In contrast, evaporation is controlled by surface conditions, and water has to be extracted from ever-increasing depths. As the surface soil dries out, it transmits water less readily, even if water is available at lower depths. Consequently, more water is removed from the surface layers. This is reflected in the low pressure potential (-3330 cm) values at the surface for the evaporation problem. The lowest pressure potential achieved for the transpiration problem was -1567 cm. Differences between the evaporation and transpiration problems are further reflected in the potential gradients. Evaporation produced gradients of up to 40 cm/cm - twice the average gradient (about 20 cm/cm) for the transpiration problem.

The isopotential lines (Fig. 22a) are almost concentric about the row of sink nodes, which implies that water is drawn inwards from the surface, the lateral boundaries, and from the soil below. The potential gradients are slightly steeper (22 cm/cm) below the sink nodes than they are above



TRANSPIRATION FROM A FLAT PROFILE (5mm/day)



Vertical exag : x8

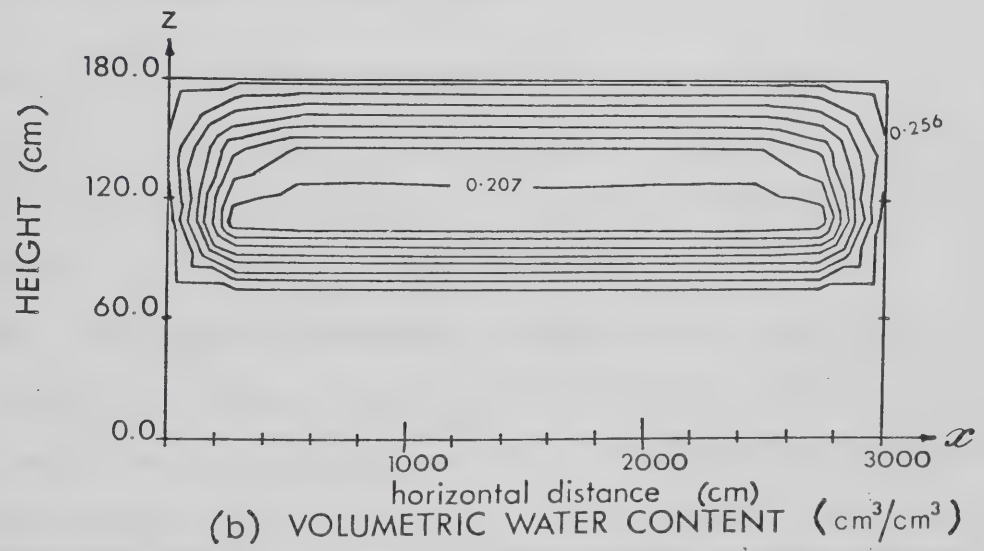


Figure 22. Transpiration from a flat profile - total potential (a) and water content (b) after 240 hr.





them (18cm/cm).

Data for individual time steps indicate that transpiration did not affect the surface until after about 3 days.

After 10 days, the volumetric water content in the vicinity of the sink nodes had decreased by about 6 percent (Fig. 22b). The reduction decreases away from the sink nodes toward the lateral boundaries and to depth of about 110 cm below the surface. At these points there is little or no change from the initial conditions ( $\theta=0.260$ ). There is also a reduction in water content above the sink nodes ranging from 6 percent at the sink nodes to about 0.4 percent at the surface. These data suggest, what is self-evident in the field, that during transpiration, trees remove water from the soil surrounding their roots.

### Evaporation plus transpiration

The box described in the two previous experiments is opened up for this simulation to permit evaporation and transpiration to occur simultaneously. In every other respect, the three problems of evaporation, transpiration, and evaporation plus transpiration, are identical.

Both the surface and the sink nodes are activated for the evaporation plus transpiration simulation. The 5 mm/day water withdrawal rate used previously is divided equally between evaporation and transpiration so that each occurs at the rate of 2.5 mm/day.



The plot of total potential for evapotranspiration (Fig. 23a) shows features that were evident when evaporation and transpiration were treated separately. For example, the lowest total potential (-1690 cm) occurs at the surface which was also the case in the evaporation simulation (Fig. 21b). The effects of evapotranspiration extend to a depth of about 110 cm - the same depth as for the transpiration simulation (Fig. 22a).

The potential gradient produced by evapotranspiration (11 cm/cm) is only 1/4 of the gradient resulting from evaporation (Fig. 21b), and half the gradient resulting from transpiration (Fig. 22a). The isopotential lines indicate that flow is directed upward, and away from the lateral boundaries.

The reduction in volumetric water content at the surface is greater for evapotranspiration (Fig. 23b) than for transpiration (Fig. 22b), but less than for evaporation (Fig. 21c). The reduction decreases almost linearly with depth.

### Evapotranspiration from sloping profiles

If it were possible to tilt the box to, say, an angle of 20°, and open the downslope end so that water is free to move out, we would have a very crude representation of a two-dimensional, unsaturated flow system for a forested hillslope.

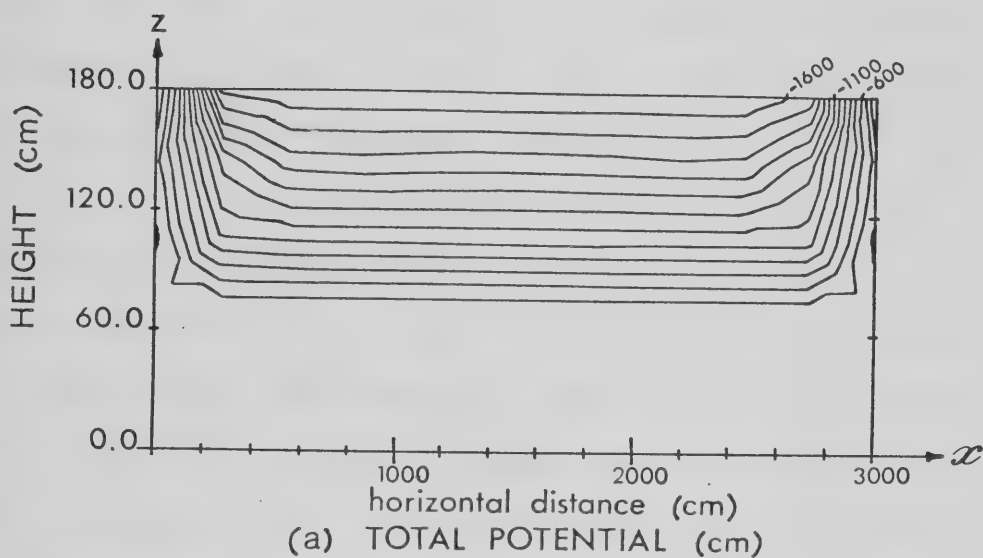
These added complexities can be accommodated within the context of the previous problem by simply changing the



# COMPLETELY FORESTED

Evaporation : 2.5mm/day

Transpiration : 2.5mm/day



Vertical exag : x8

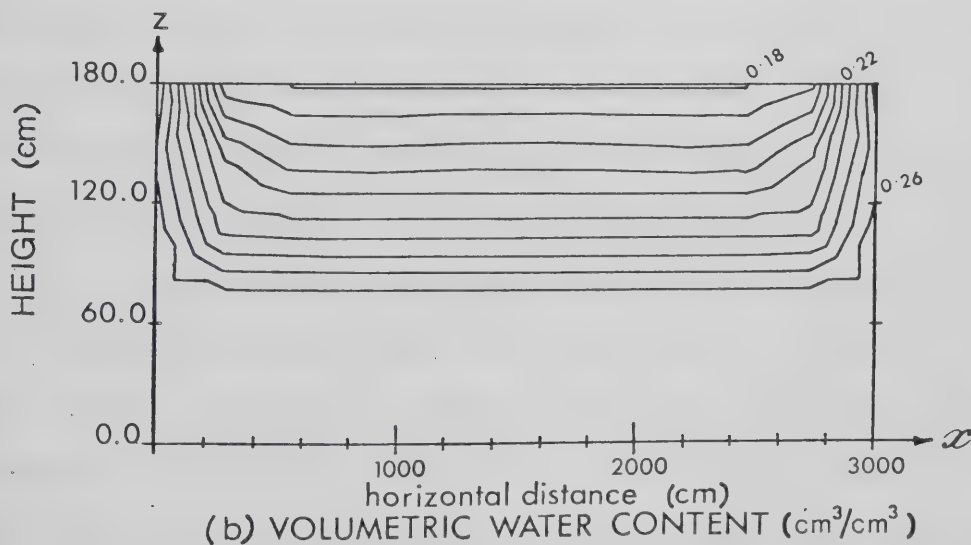


Figure 23. Evapotranspiration from a flat profile - total potential (a) and water content (b) after 240 hr.



z-coordinates and redefining the downslope (left) no-flow boundary as a negative flux (evaporation) boundary.

Until now, for vertical and horizontal flow, the same coordinate system has been used to compute the solution and to plot the isolines. However, for sloping profiles the procedure is different. The original coordinate system, in which the nodes are stacked in vertical columns of four (Fig. 20), is still used to obtain the solution, but is modified for plotting purposes. The z-coordinates are effectively restored by transformation to those describing a flat profile and the system is then rotated through the slope angle. The columns of nodes are, subsequently, no longer vertical (Fig. 24). This change was instituted so that the entire plotting space on the AED 512 colour graphics terminal could be utilized. If the original coordinate system is used for plotting, then the available plotting area is much reduced. In all plots, the pronounced vertical exaggeration results in some distortion of isolines, particularly near lateral boundaries.

The isopotential lines for the sloping system (Fig. 24a) indicate that flow patterns are quite different from those in the horizontal system (Fig. 23a). Although water movement is directed primarily toward the surface in each case, flow in the sloping profile has a downward component as well. Throughout the sloping profile water moves in response to gravitational potential; near the surface and downslope face, it moves also in response to forces produced

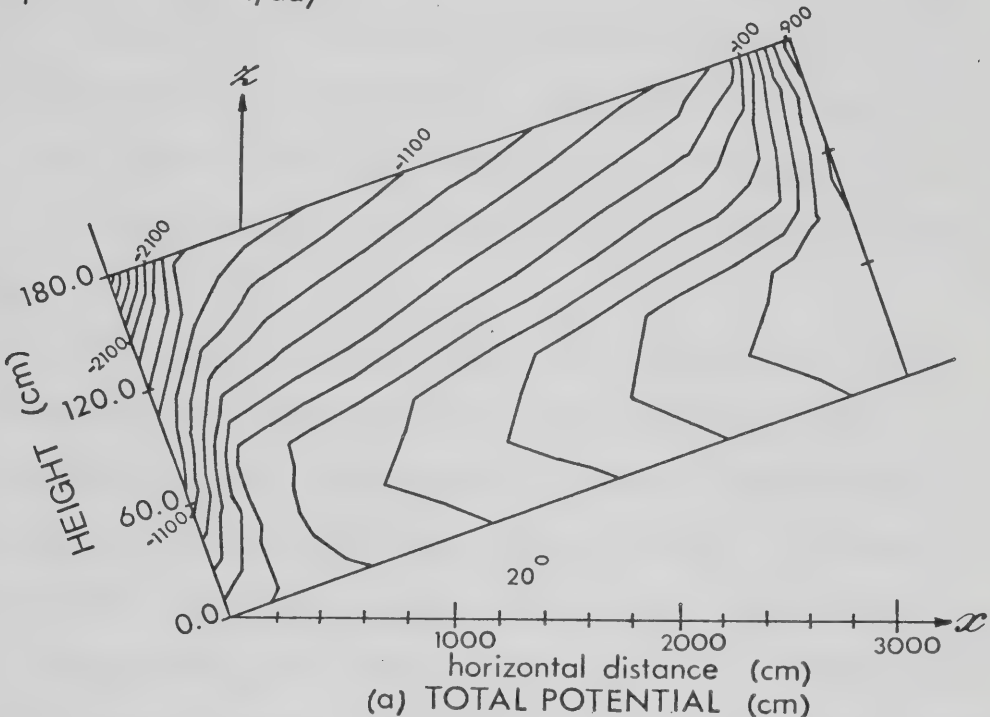




FORESTED SLOPE SIMULATION

Evaporation : 2.5mm/day

Transpiration : 2.5mm/day



Vertical exag: x9

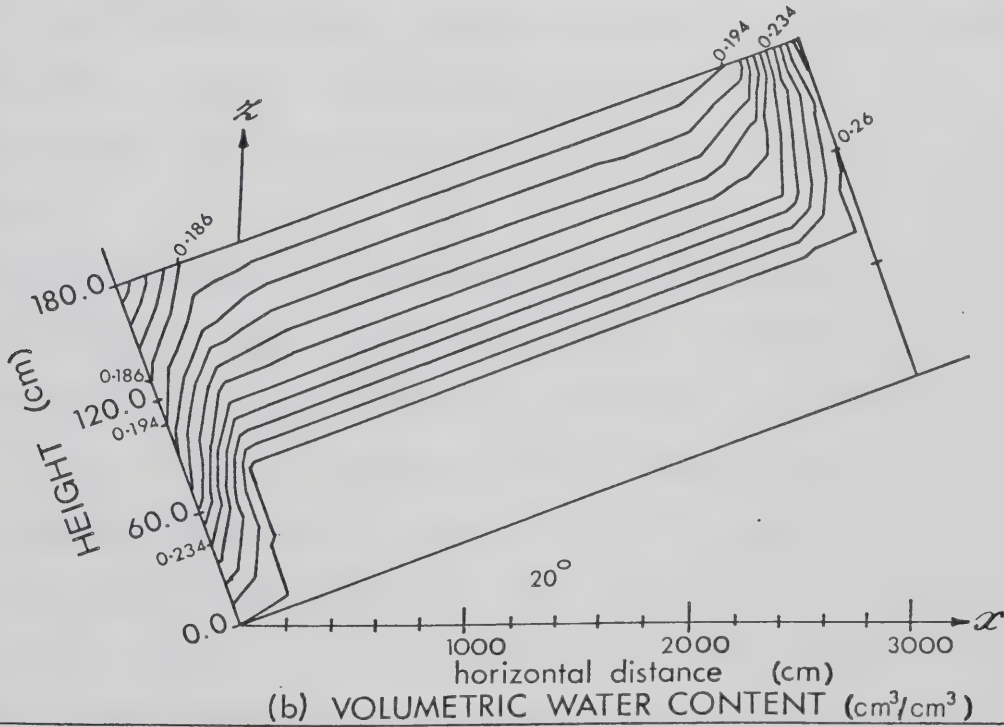


Figure 24. Evapotranspiration from a sloping profile - total potential (a) and water content (b) after 240 hr.



by evaporative demand.

The sharp breaks in the isopotential lines at a depth of about 110 cm below the surface marks the limit of the surface evaporation and transpiration effects. Below this depth, flow toward the downslope face is indicated. At the bottom of the profile (0 to 30 cm) flow is toward the basal boundary.

Soil water depletion patterns for the sloping (Fig. 24b) and horizontal systems (Fig. 23b) are very similar. In both situations, the isolines are evenly spaced and parallel to the surface, indicating that water content increases uniformly with depth. At about 110 cm below the surface, it remains unchanged at 26 percent. The only real differences in water content between the horizontal and inclined systems result from evaporation at the downslope face of the sloping profile. Water content was reduced by about 10 percent at the node where the downslope face joins the surface boundary.

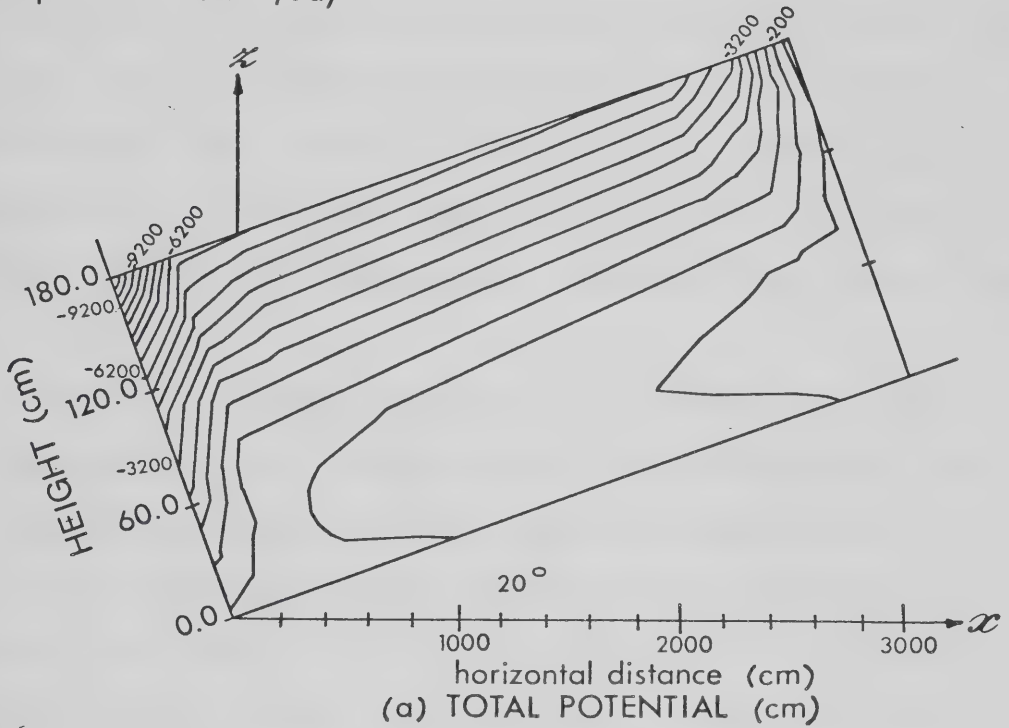
Evapotranspiration from the same profile over a 20-day period, under the same conditions, was also simulated. Results indicate (Fig. 25) that the effects of evaporation after 20 days are still confined to the upper 110 cm of soil. However, movement of water above this depth is in a direction almost perpendicular toward the surface (Fig. 25a). Water content has been reduced by an additional 7 percent at the surface, and by about another 5 percent at depth 60 cm below the surface (Figs. 24b and 25b).



# FORESTED SLOPE SIMULATION

Evaporation : 2.5mm/day

Transpiration : 2.5mm/day



Vertical exag : x9

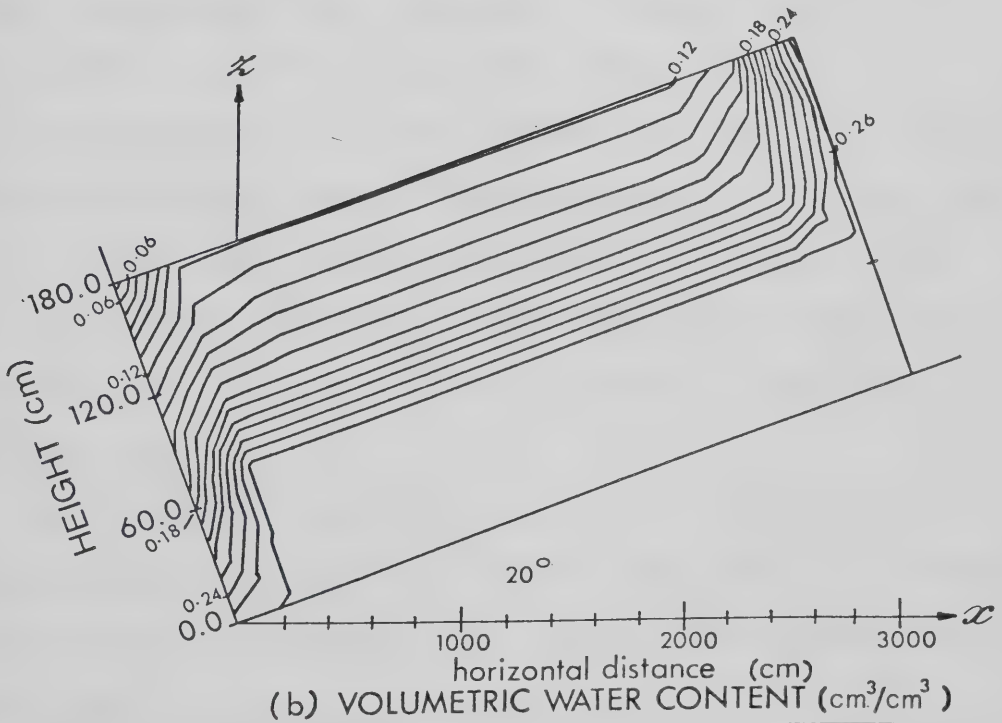


Figure 25. Evapotranspiration from a sloping profile - total potential (a) and water content (b) after 480 hr.



In the next four sets of experiments, the effects of locating trees on portions of the slope only will be examined. The soil, initial conditions, boundary conditions, time step size, and simulation period will all remain the same as before. An evaporation rate of 2.5 mm/day will again be assumed for the entire slope. The only changing input variables will be the number and placement of activated sink nodes.

Trees on the lower slope are simulated by activating only those sink nodes located below the midslope position. The 10-day simulation in this instance produced quite distinctive features in both the upslope and downslope regions of the profile (Fig. 26). Upslope, the effects of evaporation are evident down to a depth 70 cm below the surface. Downslope, the influence of evapotranspiration is manifest down to 110 cm below the surface.

The equipotential lines signify that, uphill from the midslope position, water is moving upward in the top 70 cm of soil. Below this level, it is moving downslope (Fig. 26a). On the downhill side of the midslope position, water is moving upward in the top 110 cm of soil, and moving downslope below.

After 10 days, the reduction in soil water content is greater downslope than it is upslope (Fig. 26b). At a depth of 60 cm below the surface, for example, the upslope water content remains virtually unchanged from the initial condition of 26 percent. The downslope water content at this





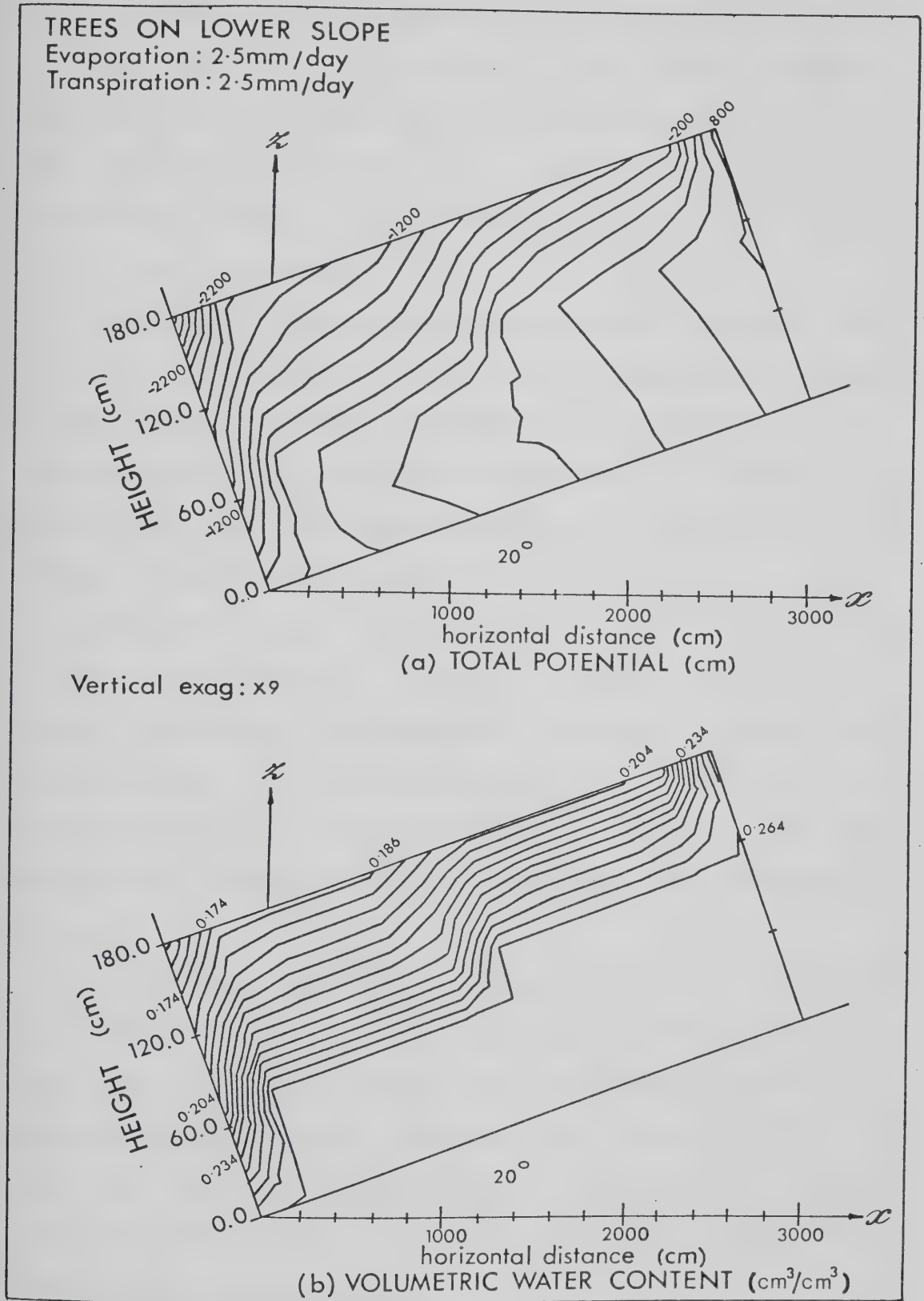


Figure 26. Trees on lower slope - total potential (a) and water content (b) after 240 hr.



depth, however, has been reduced by 4 percent to 22 percent.

When data for this simulation (Fig. 26) are compared with those for the completely forested slope (Fig. 24), the most noticeable difference between them is the step-like change which occurs at the midslope position when trees are on the lower slope only.

Results from the corresponding 20-day simulation (Fig. 27a) show that, after 20 days, flow in the upper the portion of the profile is almost perpendicular to the slope. The regions affected by downslope evapotranspiration and upslope evaporation (Fig. 27) remain essentially the same as for the 10-day simulation (Fig. 26).

Over the second 10-day period, volumetric water content at the surface has been reduced by an additional 4 to 6 percent (Fig. 27b). The reduction downslope is greater than upslope. Above the midslope position, at a depth of 60 cm below the surface, reduction in water content is less than one percent. Downslope, at the same depth, the decrease is 4 percent.

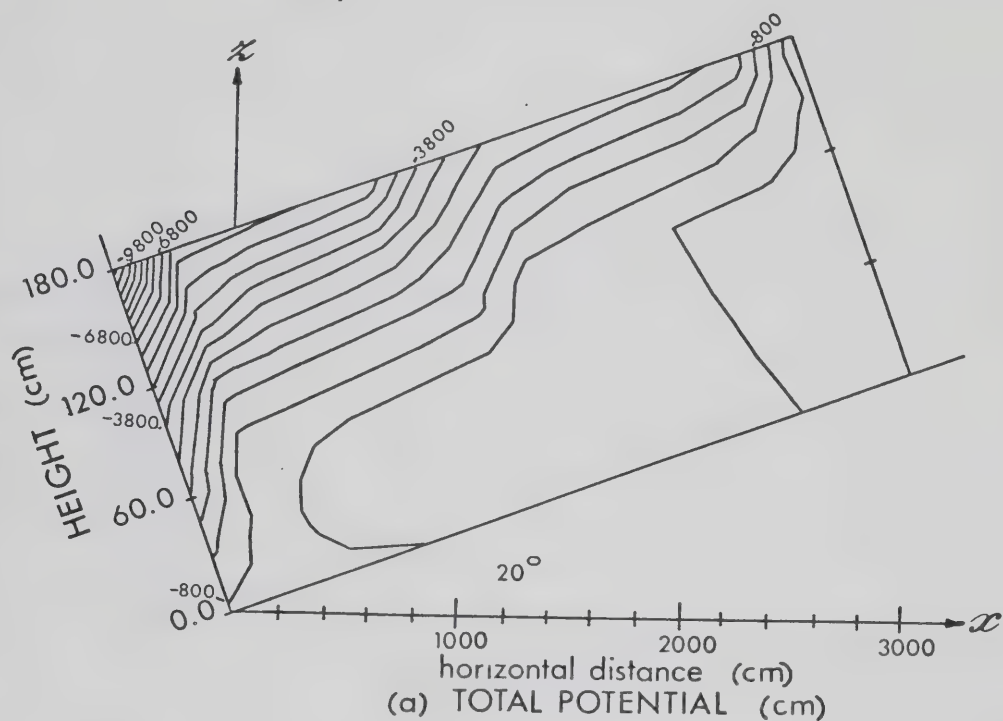
For the next simulation, trees are located on the upper slope only. This effect is achieved by activating the sink nodes above the midslope position, and de-activating them elsewhere. It is evident from the total potential field (Fig. 28a) for this system, that the response is analogous to that of the previous simulation, in which trees were located on the lower slope.



## TREES ON LOWER SLOPE

Evaporation: 2.5mm/day

Transpiration: 2.5mm/day



Vertical exag: x9

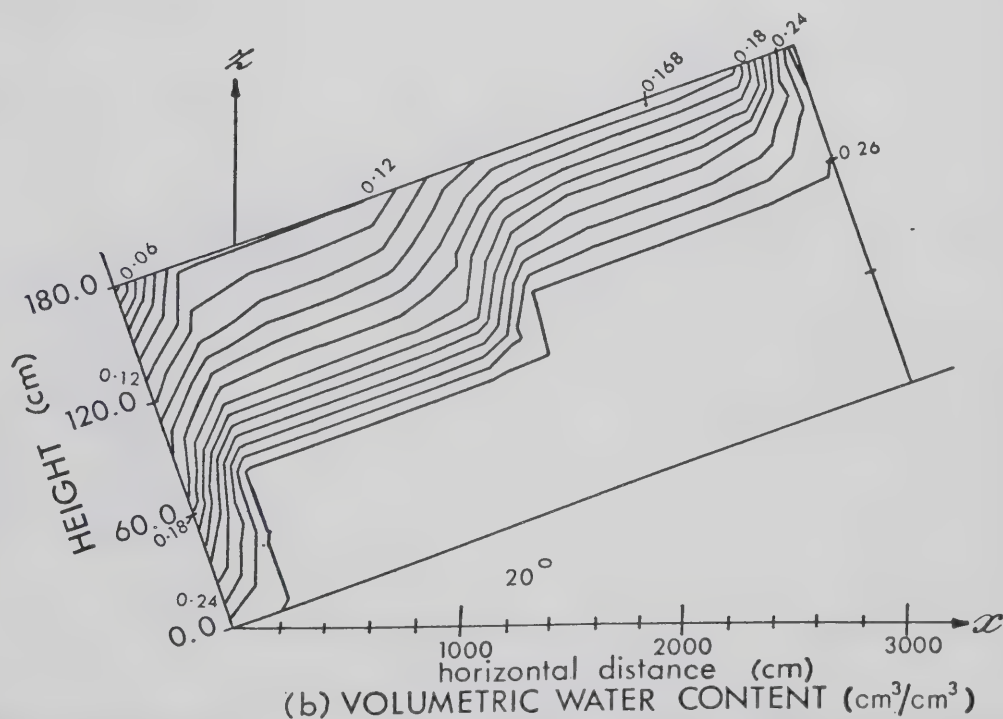


Figure 27. Trees on lower slope - total potential (a) and water content (b) after 480 hr.



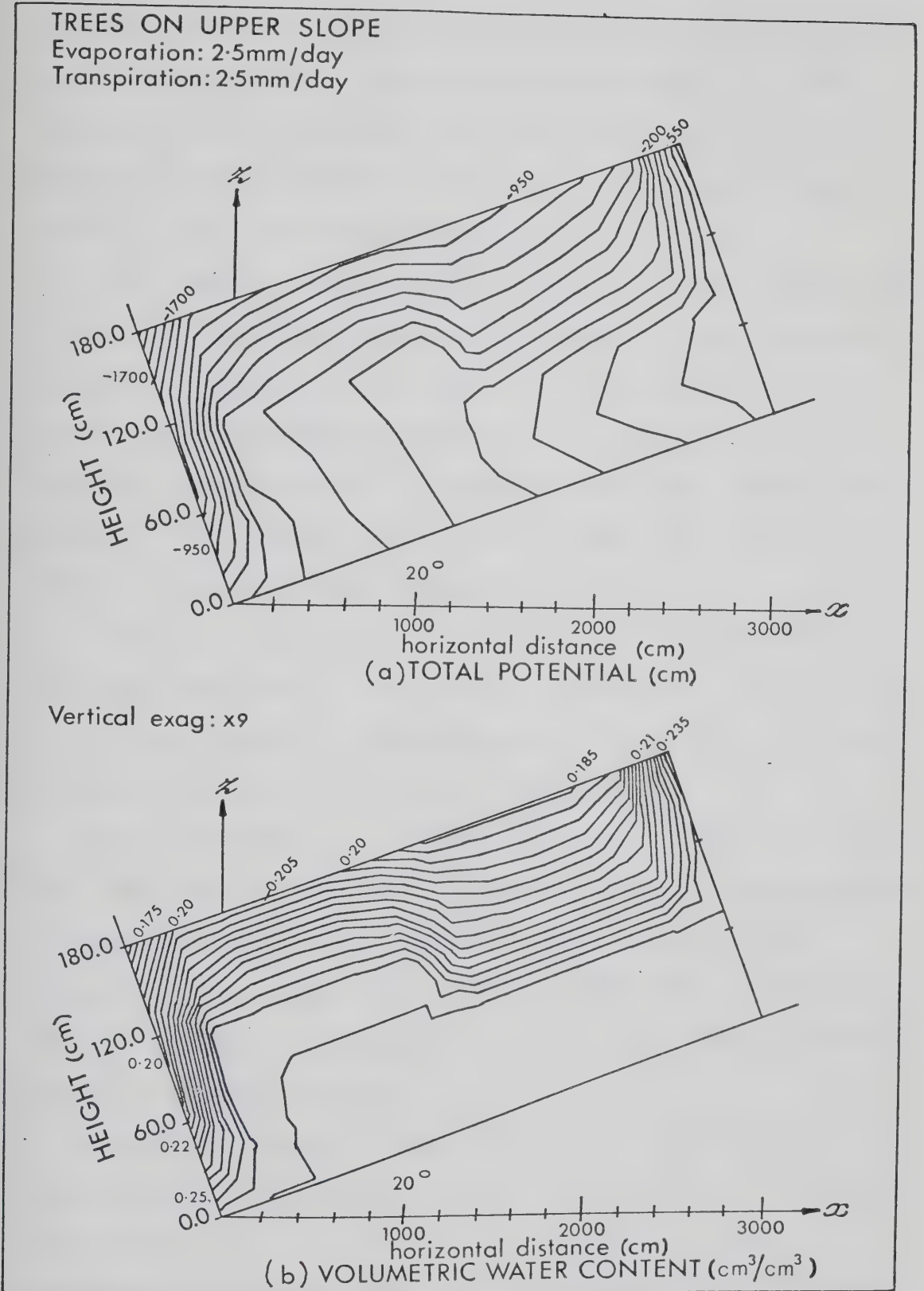


Figure 28. Trees on upper slope - total potential (a) and water content (b) after 240 hr.





The effects of evapotranspiration extend to about 110 cm below the surface, while downslope evaporation affects only the top 70 cm of soil. In these regions flow is directed upward toward the surface. Below these affected regions, flow is directed downslope (Fig. 28a).

Soil water content, after 10 days, is less uphill from the midslope position than it is downhill. The difference is about 2 or 3 percent (Fig. 28b). At the surface, water content has been reduced by about 7.5 percent at upslope locations, and by about 5.5 percent downslope. Lowest water content (0.165) occurs at the point where the surface boundary joins the lower lateral boundary.

The step-like change in data at the midslope position which was observed in the previous simulation (Figs. 26 and 27) is also present in this simulation (Fig. 28). In this instance, however, the step is reversed.

The isopotential lines for the 20-day simulation (Fig. 29a) indicate that the soil regions affected by evaporation and evapotranspiration are the same as for the 10-day simulation (Fig. 28a). They indicate that flow in these regions is upward and perpendicular to the slope; elsewhere flow is directed downslope.

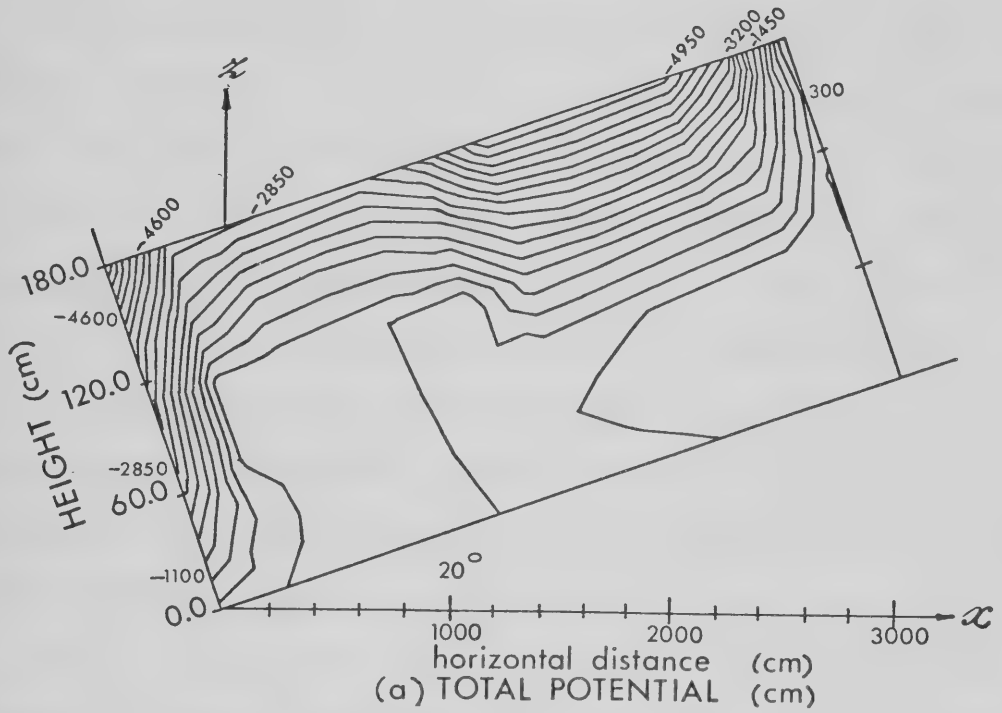
During the second 10-day period, soil water content at the surface is reduced by 6.5 percent in the evapotranspiration zone and by 4.5 percent in the evaporation zone (Fig. 29b). The net effect is a 4 percent difference in surface moisture content, between the two



## TREES ON UPPER SLOPE

Evaporation: 2.5mm/day

Transpiration: 2.5mm/day



Vertical exag: x9

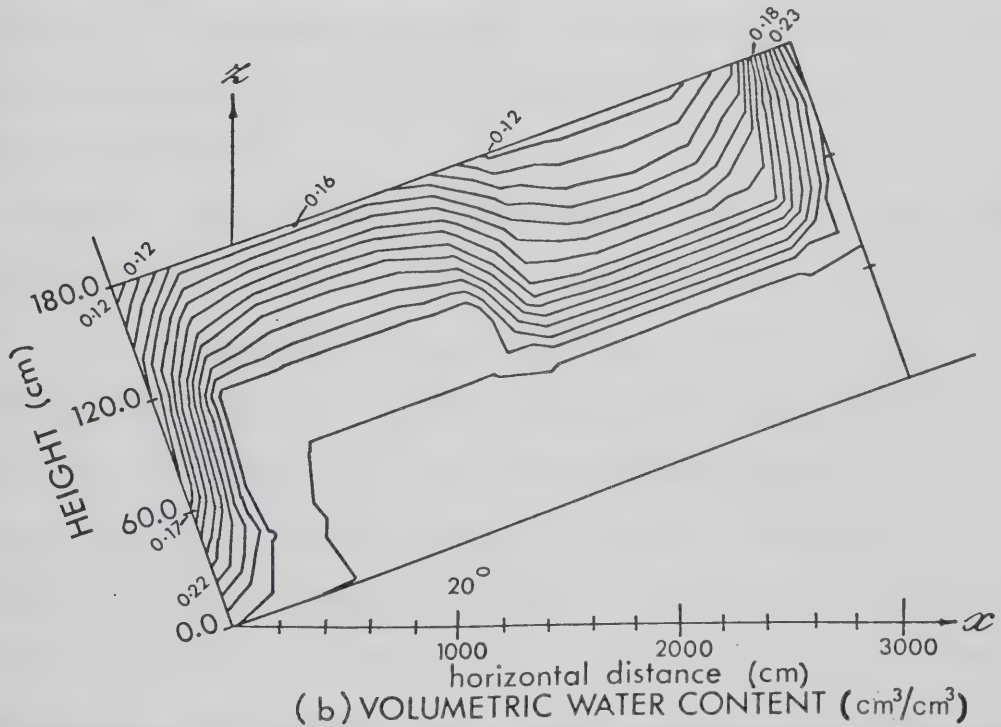


Figure 29. Trees on upper slope - total potential (a) and water content (b) after 480 hr.



zones. At depth 60 cm below the surface the difference is 7 percent.

When all the sinks for the slope are de-activated, a "clearcut" condition is created and transpiration no longer occurs. The results from this simulation, shown in Fig. 30, are similar in some respects to those obtained for the flat profile evaporation simulation (Fig. 21). In each case, after, 10 days, the effects of evaporation have reached a depth of 70 cm below the surface; above this level flow is directed upward toward the surface. For the clearcut condition on the sloping profile, flow below the 70 cm depth is directed downslope.

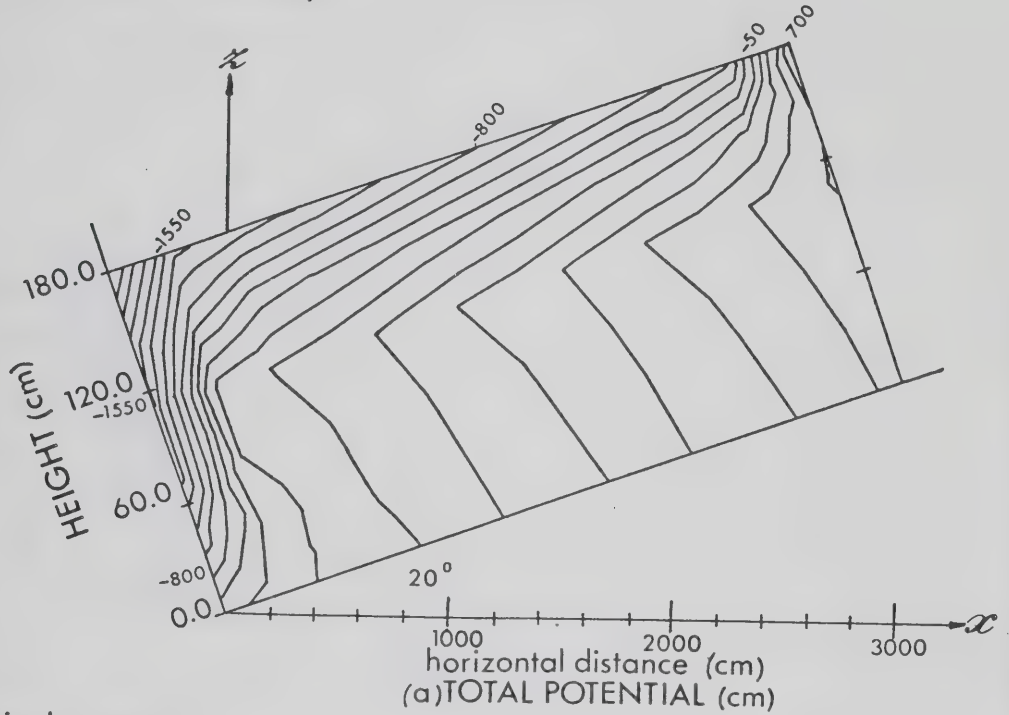
After 10 days, soil water content at the surface has decreased by about 5 percent (Fig. 30b). For most of the profile, it increases uniformly with depth to about 70 cm below the surface. Below this depth, the water content remains unchanged.

Results for the 20-day simulation (Fig. 31) show that, after 20 days, the effects of evaporation have not extended below the 70 cm depth. Above this depth, flow is perpendicular (upward) to the slope. Below, flow is still directed downslope (Fig. 31a). The surface soil water content has been reduced further by about 4 percent, bringing the total reduction from initial conditions at the surface to 10 percent (Fig. 31b). A decline in soil water content below the surface soil layer is also apparent, but it decreases with depth.



# CLEARCUT SIMULATION

Evaporation: 2.5mm/day



Vertical exag: x9

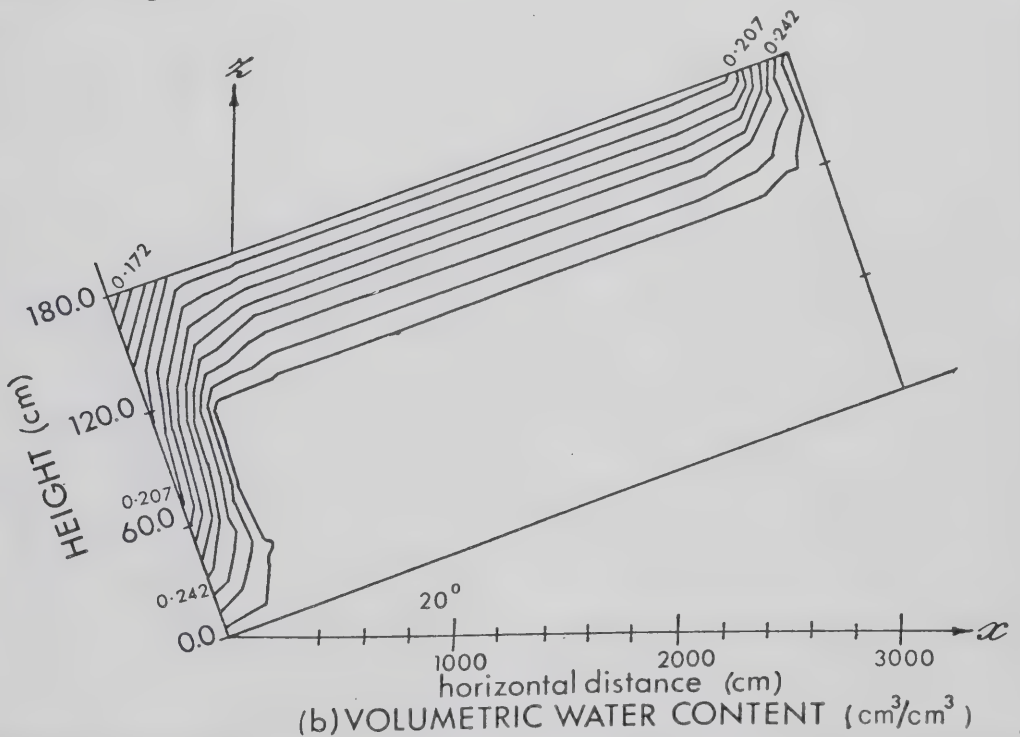


Figure 30. Clearcut simulation - total potential (a) and water content (b) after 240 hr.





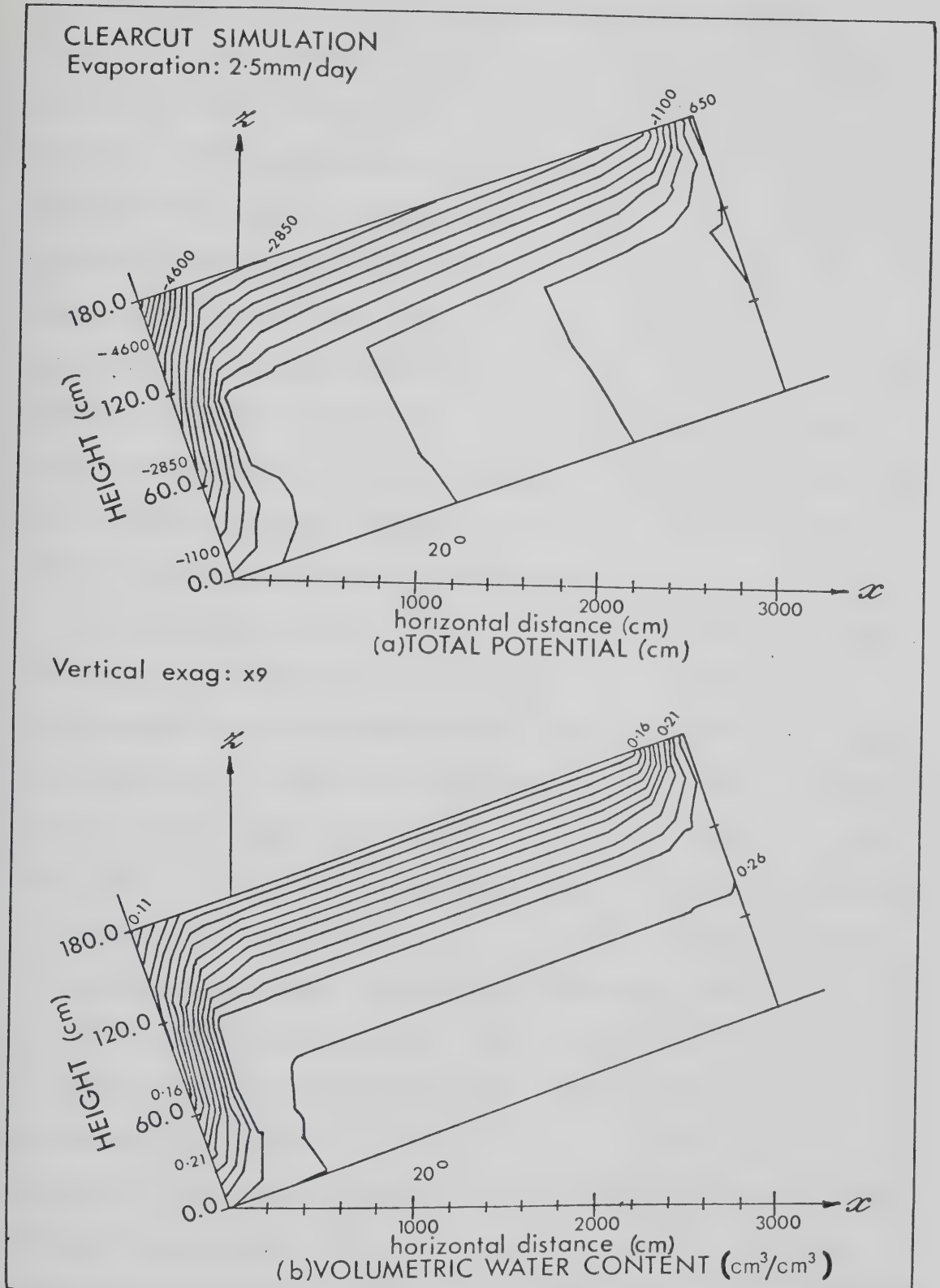


Figure 31. Clearcut simulation - total potential (a) and water content (b) after 480 hr.



The preceding four sets of simulations serve to illustrate the possible effects of three different logging patterns on soil water flow and storage in a forested hillslope. The undisturbed forest (Figs. 24 and 25) can be compared with logging on the upper slope (Figs. 26 and 27), logging on the lower slope (Figs. 28 and 29), and with clearing of the entire slope (Figs. 30 and 31). The simulations are very simplistic in that they contain fixed evaporation and transpiration rates for relatively long periods of time. No attempt is made, either, to accommodate the increase in ground surface evaporation which usually occurs when an area is cleared of trees.

In spite of these limitations, the response for each simulation is distinct, and reflects in a reasonable way, what happens in the corresponding field situation. If soil water content for clearcut conditions (Fig. 30b) is compared with soil water content for the completely forested slope (Fig. 24b), it is clear that removing the trees has resulted in a reduction in the drain on soil water. Under forested conditions, soil water content is diminished down to a depth of 110 cm below the surface. Under clearcut conditions, only the top 70 cm of soil is affected. In this region, at corresponding depths in the profile, soil water content is higher for the clearcut than for the forested slope. These simulations confirm, what has often been observed in the field, that removing trees results in an increase in soil water content. In some instances, especially where high



water-tables are present, the increase may be so great that it is difficult to restock the cleared sites with new trees.

Patch logging and strip-cutting are two methods which have been used frequently in the past to provide a suitable environment for growing the next generation of trees at the same time as mature trees are removed. Such methods are characterized by patches or strips of cleared or open areas alternating with strips or patches of trees.

In order to simulate effectively the influence of these logging methods on soil water, the slope length used in previous simulations must be increased. By increasing the length to 100 m, two cut strips, each 20 m wide running across the slope and alternating with three forested strips also 20 m wide, can be accommodated. This configuration could be adapted quite easily to simulate the "wall-and-step" forest illustrated in Fig. 8. Except for the mesh size, all other conditions remain the same as before. The finite element mesh for this simulation contains 204 nodes and 300 elements.

The strip locations and the effects of this configuration on flow patterns are displayed in Fig. 32a. Below 120 cm from the surface, flow is everywhere parallel to the slope. In the top 60 cm, flow is directed toward the surface. In this region, under the open strips, flow is almost perpendicular (upward) to the slope, whereas under forest it is inclined at an angle to the surface. Between depths 60 and 120 cm, two fairly distinct flow patterns are



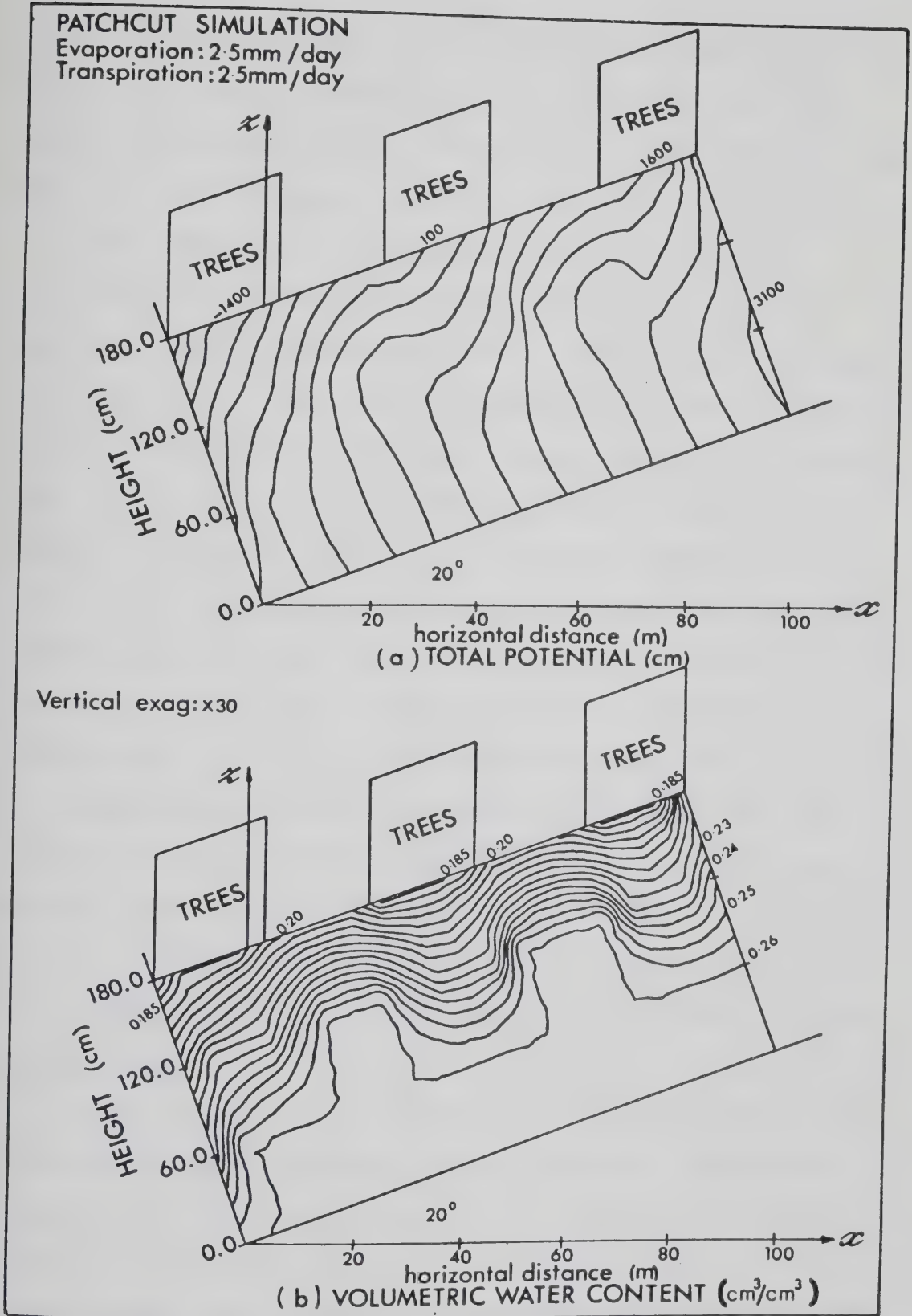


Figure 32. Patchcut simulation (two cut strips and three forested strips - total potential (a) and water content (b) after 240 hr.





evident. Under the open strips, water runs parallel to the slope, but tends to move upward beneath the trees. This result is consistent with the fact that trees have a greater effect on water movement at depth, than does evaporation.

Soil water depletion patterns for the patchcut configuration are quite pronounced (Fig. 32b), and are consistent with results obtained for previous simulations. Under the trees, soil water is depleted, to some extent down to a depth of 120 cm below the surface. For the cut strips, only the top 60 cm is affected (by evaporation). At the surface, soil water content is 2 percent greater for the open than for the forested strips. The reduction in water content decreases with depth for both sites. At depth 60 cm below the surface, soil water content is 26 percent under the open and about 23 percent under the forested strips.

Comparison of the plots shown in Figure 32 with the original data show that, although they are accurate over most of the region, the plots are not accurate in the vicinity of the lateral boundaries. The discrepancy can be attributed to plot distortion caused by the large vertical exaggeration.

If the positions of the open and forested strips are exchanged so that there are two forested and three open strips, then the flow patterns and water content fields are also exchanged (Figs. 32 and 33). The flow patterns under trees in Fig. 32a are the same as those under trees in Fig. 33a, even though the trees are on different parts of the



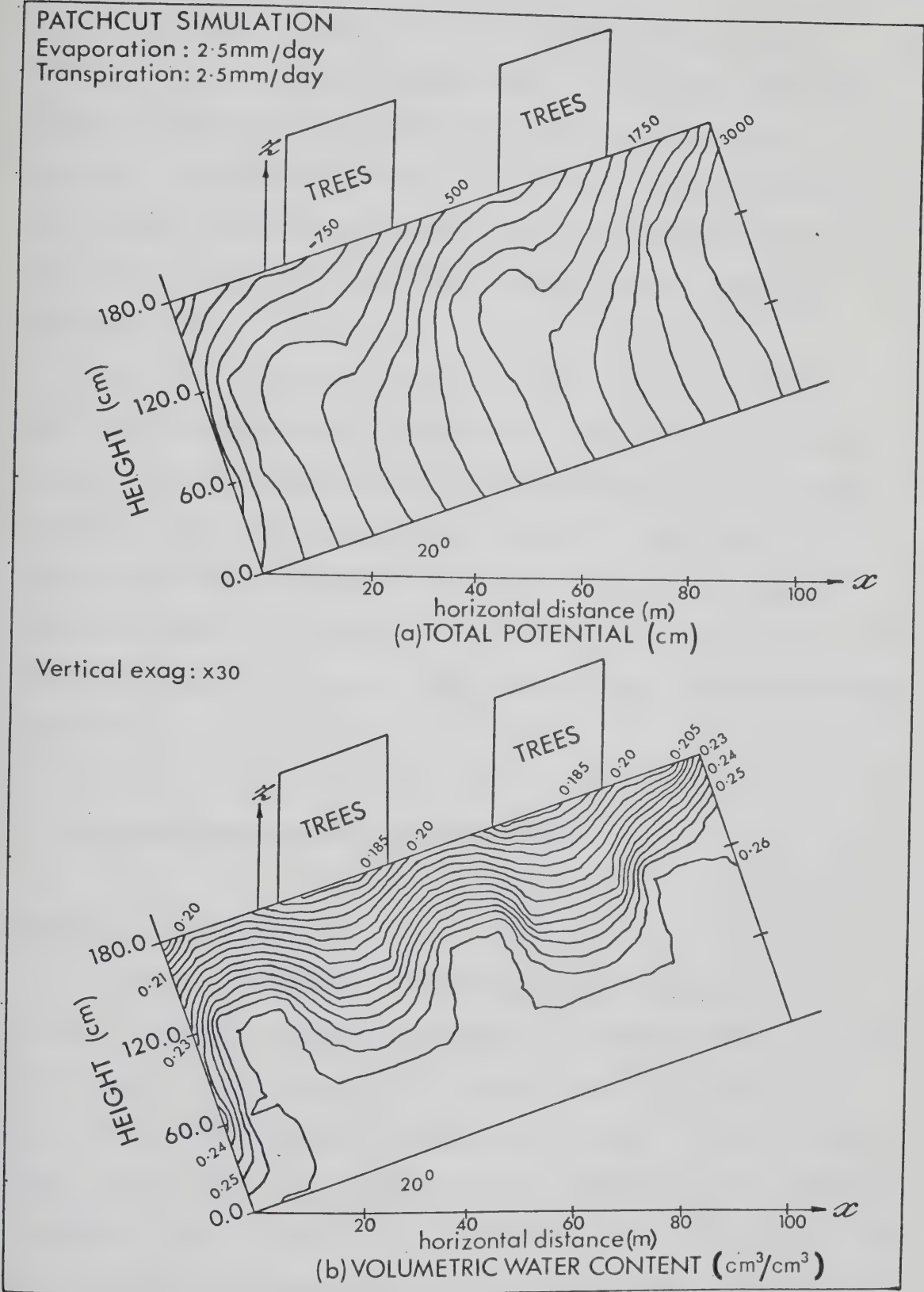


Figure 33. Patchcut simulation (three cut strips and two forested strips) - total potential (a) and water content (b) after 240 hr.



slope. The same holds true for the open strips. The similarity of effects is particularly striking when water content fields are compared (Figs. 32b and 33b). The isolines, indicating points of equal soil water content, show identical patterns under the trees, where they are concave up, and under the open strips, where they are concave down.

The flow systems examined so far are essentially isotropic, homogeneous, unsaturated systems. During these simulations, problems relating to convergence or numerical stability were not encountered. Usually, less than 10 iterations were necessary to obtain convergence. The greatest number of iterations were realized during the first few time steps; for later time steps, fewer iterations were required.

## **B. Combined Saturated-Unsaturated Flow**

### **Rainfall simulation**

The next simulation involves seepage resulting from rainfall, and introduces the effects of saturated flow into the formerly unsaturated flow system. The Yolo Light Clay soil and the 64-node, 90-element mesh (Fig. 20) of earlier slope simulations are used. No-flow boundaries are the same as before, and a positive flux equivalent to a rainfall rate of one cm/day is applied to each boundary node, with the exception of the corner nodes, along the upper surface. This



rate is slightly less than the saturated hydraulic conductivity, or drainage rate of the soil - a situation which implies that overland flow will not occur. The initial pressure potential for this problem is set everywhere equal to -100 cm ( $\theta=0.428$ ). A time step of 6 hr is used to simulate a 10-day period of rainfall.

The initial simulation is for rainfall into a horizontal box of soil from which there is no outlet. This experiment allows us to determine the change in soil water storage, and to compare it with the total volume of water added.

The simulation output (Fig. 34a) indicates that, after 10 days, total potential is highest at the surface, and lowest at the bottom, of the profile. Flow throughout most of the section is vertically downward. Near the lateral boundaries, flow is directed toward these boundaries as well.

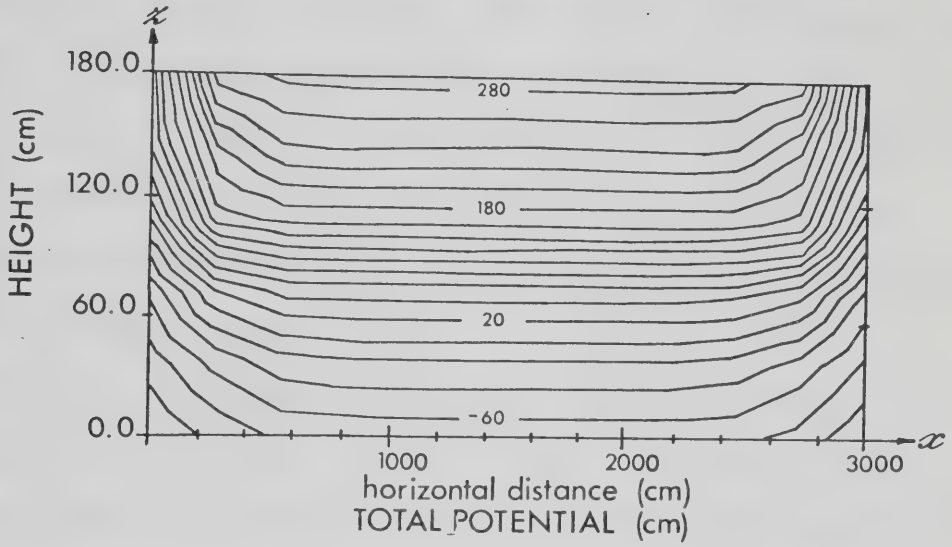
After 10 days, 10 cm of rain has fallen onto the profile. The entire upper 120 cm of soil, with the exception of the regions near the lateral boundaries, is saturated ( $\theta=0.496$ ) (Fig. 34b). This represents an increase in soil water content of about 7 percent, or an addition of 8.4 cm ( $0.07 \times 120$  cm) of water to the top 120 cm of soil over 10 days. The balance, or 1.6 cm of added water, is contained in the bottom 60 cm of soil. These results are consistent with conditions that one might encounter in the field, following a 10-day rainfall.





# CLEARCUT SIMULATION

Rainfall : 10mm/day



Vertical exag: x8

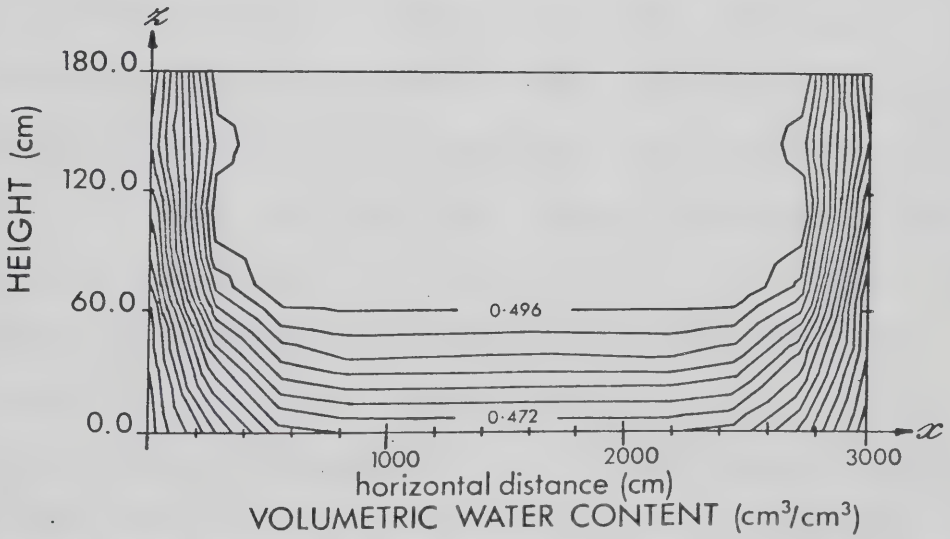


Figure 34. Rainfall on a flat profile - total potential (a) and water content (b) after 240 hr.



The 64-node, 90-element mesh for a sloping section is employed to simulate outflow from the seepage face. In this simple problem, nodes numbered two and three, located along the downslope lateral boundary, are seepage face nodes. The only other difference between this simulation and the preceding one is that, in this problem, rainfall is applied to the corner node (#4) at the intersection between the lower lateral boundary and the upper surface, in addition to the other surface nodes.

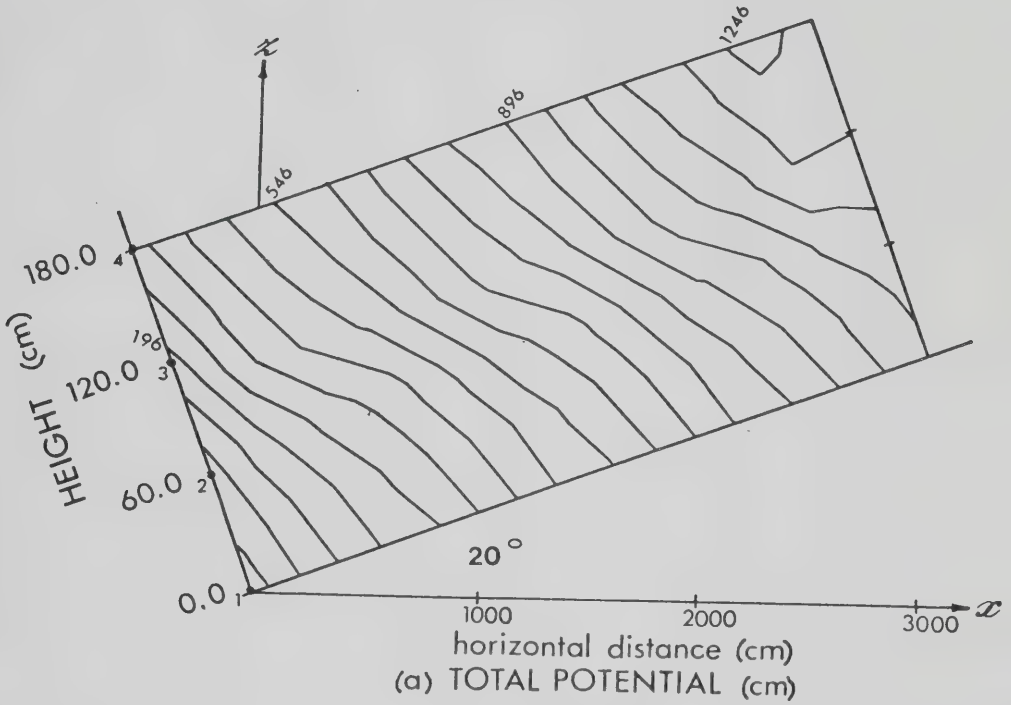
The total potential field that exists at the end of the 10-day period (Fig. 35a) indicates that flow is directed downslope toward the lower lateral boundary. The top 120 cm of soil is saturated ( $\theta=0.496$ ) except near the lateral boundaries (Fig. 35b). It is not clear why there is a pocket of unsaturated soil below seepage face node #3 at the 60 cm depth. One would expect the "saturated" isoline to continue along its path parallel with the slope, and terminate at a depth of about 120 cm on the lower lateral boundary. This assumption is supported by evidence from Fig. 35a, where the isopotential lines show that flow is directed toward the basal portion of the lower lateral boundary.

Outflow did not commence until 4.5 days after the rain started (Fig. 36a). The hydrograph shows an abrupt rise during the first two time steps after flow started, followed by a somewhat erratic, but generally steady, increase over the rest of the simulation period.



# CLEARCUT SIMULATION

Rainfall : 10mm/day



Vertical exag: x9

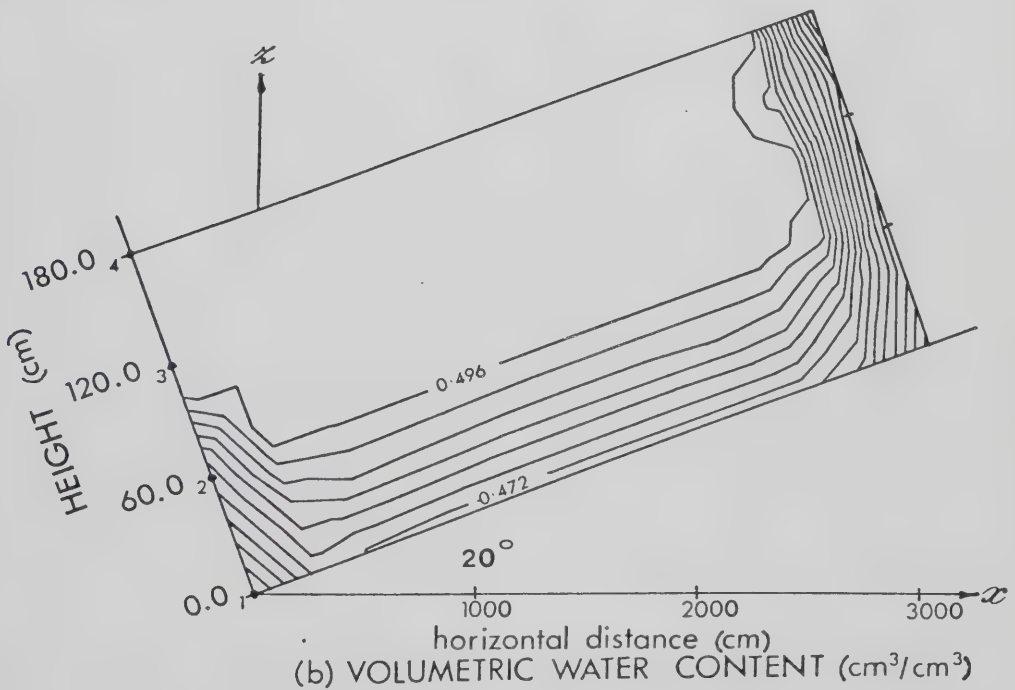


Figure 35. Rainfall on a sloping profile - total potential (a) and water content (b) after 240 hr.



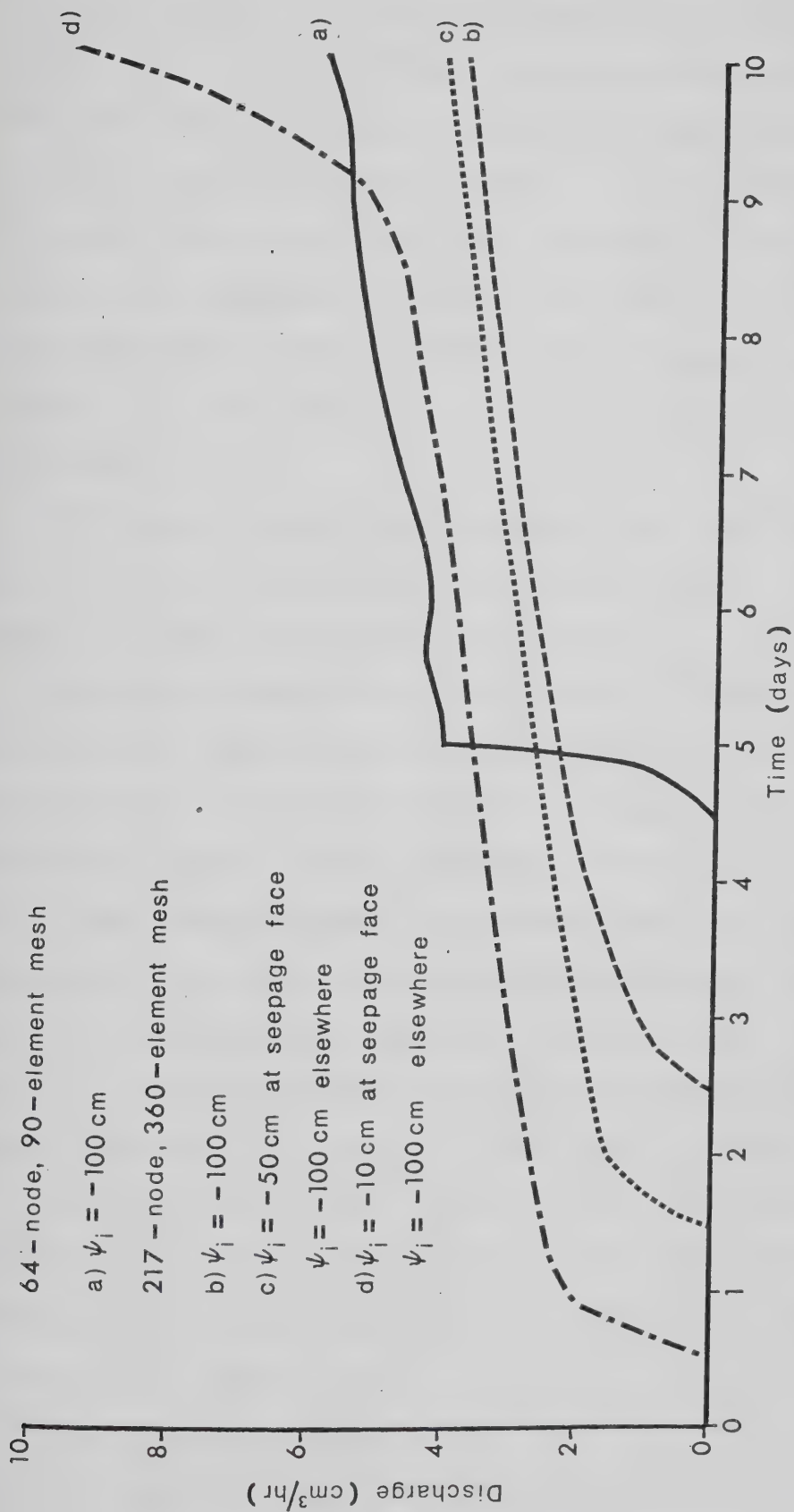


Figure 36. Hydrographs for a 10-day rainfall (10 mm/day), for two mesh sizes, and different initial conditions.





Since there is no physical explanation for the apparent anomaly of an unsaturated pocket below the saturated zone at the lower lateral boundary, additional simulations were run to investigate the problem further. It was hypothesized that the anomaly was related to the coarseness of the mesh and to insufficient seepage face nodes. Accordingly, the problem was rerun using a mesh consisting of 217 nodes and 360 elements. In this case, the number of seepage face nodes was increased to five.

The results show (Figs. 35a and 37a) that changing the mesh size has little effect on flow patterns - the total potential fields are almost identical.

The change does affect the volumetric water content of the profile. Saturation extends to slightly below the 120 cm depth for the fine mesh (Fig. 37b) compared with saturation to slightly above the 120 cm depth for the coarse mesh (Fig. 35b). Noticeable changes are apparent near the lateral boundaries. At the upslope boundary in the fine mesh simulation, saturation reaches a depth of about 100 cm (Fig. 37b). In the coarse mesh simulation, saturation does not occur anywhere within 250 cm of the upper lateral boundary.

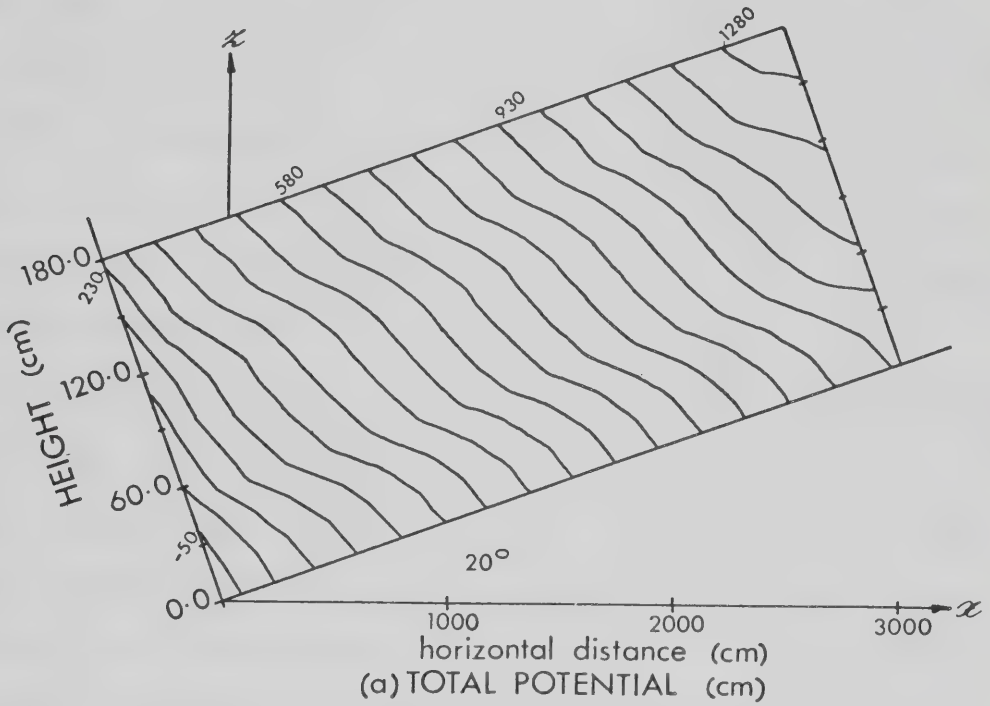
At the lower lateral boundary, for the fine mesh, the unsaturated pocket is more prominent than before, and the seepage face extends to a depth of only 40 cm, compared with 70 cm for the coarse mesh.

When the hydrograph for the fine mesh simulation (Fig. 36b) is compared with that of the coarse mesh simulation



## CLEARCUT SIMULATION

Rainfall : 10mm/day



Vertical exag: x9

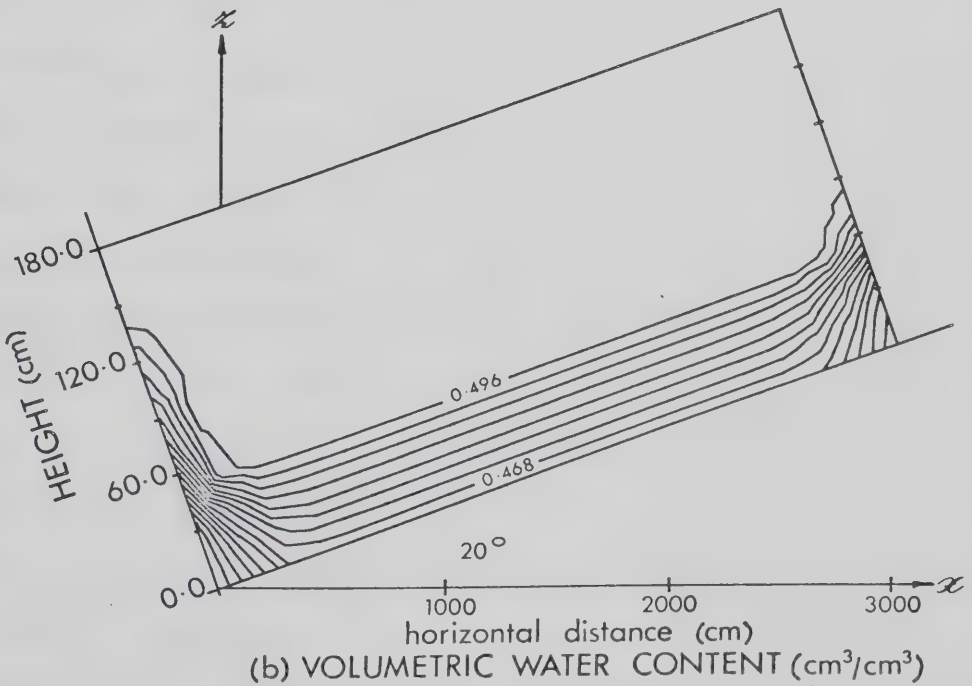


Figure 37. Rainfall on a sloping profile - total potential (a) and volumetric water content (b) after 240 hr. Obtained using a 217-node, 360-element mesh.



(Fig. 36a), it is clear that the hydrograph is influenced by mesh size. Outflow from the seepage face begins two days earlier when the fine mesh is used. It does so because the first seepage face node is located at depth 30 cm, compared with 60 cm in the coarse mesh. The hydrograph for the fine mesh is also much smoother - it lacks the abrupt rise and irregularities that characterize the coarse mesh hydrograph.

Maximum flow rate is greater for the coarse mesh simulation ( $5.8 \text{ cm}^3/\text{hr}$ ). It would appear from the foregoing results that more water is assigned to storage and less to seepage when a fine mesh is used. The fine mesh simulation did not provide any clues as to why an unsaturated region persists at the lower seepage face.

Since the hydraulic conductivity of the soil is governed by soil wetness, the volume of outflow and the time at which seepage commences must obviously be controlled by the initial condition of the soil, as well as by the amount of inflow. This is particularly true in the vicinity of the seepage face. The effects of changing the initial conditions at the seepage face were examined in an ensuing fine mesh simulation. Only one change was implemented - the initial pressure potentials at the seepage face, formerly set at -100 cm, were reinitialized to -50 cm.

This change in initial conditions produced only a minor change in the response of the system, a change which was confined to the region near the seepage face. It did not affect the unsaturated pocket. Outflow began a day earlier



(Fig. 36c) than before. The hydrograph is slightly higher than, and parallels that of, the previous simulation (Figs. 36b and 36c).

Another fine mesh simulation, in which wetter initial conditions at the seepage face were assumed, was run. Initial pressure potentials were set to -10 cm at the seepage face, and to -50 cm at the adjacent nodes.

After 10 days, the modification produced only a slight change in the total potential field (Figs. 37a and 38a), but it was sufficient to cause complete saturation at the seepage face (Fig. 38b) and increased outflow (Fig. 36d). Only the total potential (Figs. 37a and 38a) and water content (Figs. 37b and 38b) in the vicinity of the seepage face were changed.

Initially, the hydrograph (Fig. 36d) is similar to those for the other fine mesh simulations (Figs. 36b and 36c). Outflow begins at the one half day mark and, for 34 time steps, takes place through the uppermost portion of the seepage face. After that time, the entire lower lateral boundary rapidly becomes saturated, resulting in a pronounced increase in outflow from the entire seepage face (Fig. 36d). When these wetter conditions prevail, more iterations are required to obtain convergence.

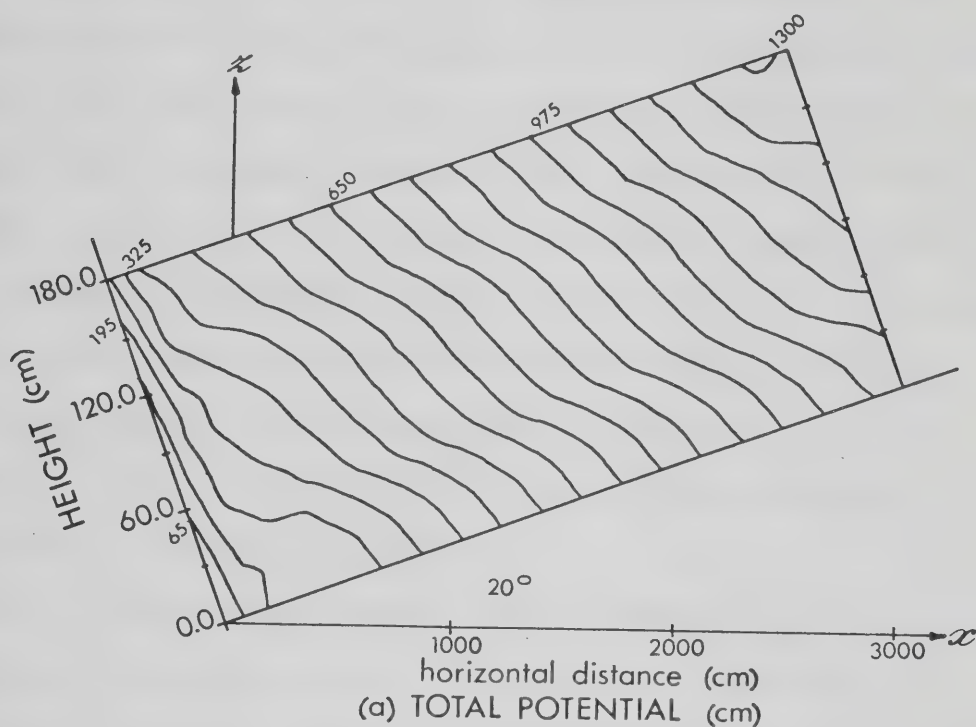
The simulation was extended beyond the 10-day period, but it failed at time step 42 (day 11). Failure was characterized by oscillations which led ultimately to divergence.





## CLEARCUT SIMULATION

Rainfall: 10mm/day



Vertical exag: x9

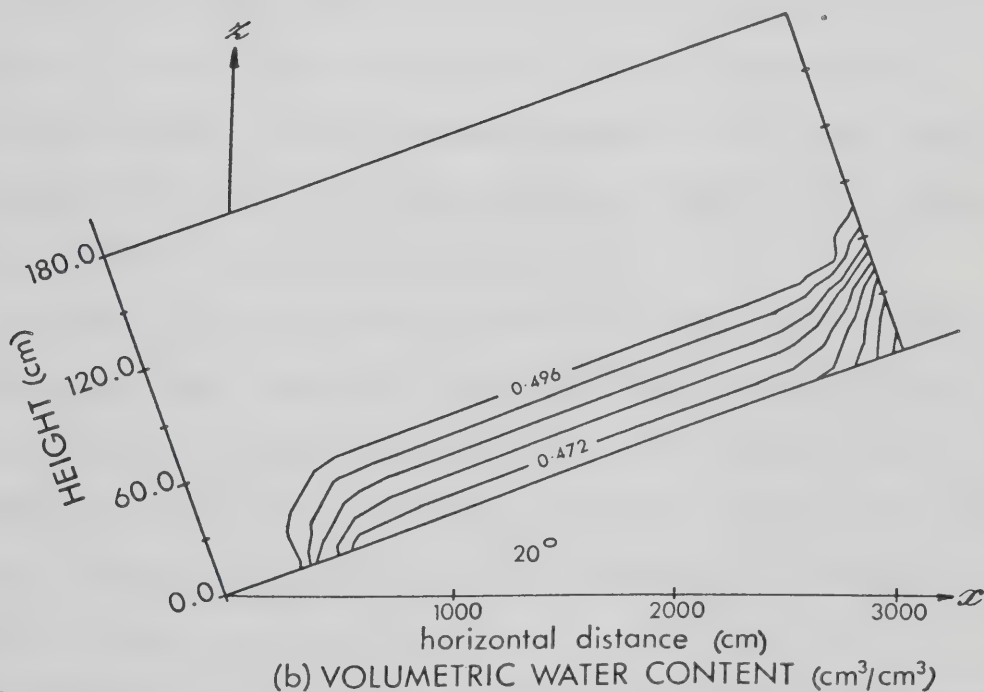


Figure 38. Rainfall on a sloping profile with  $\psi_i = -10, -50$ , and  $-100$  cm - total potential (a) and volumetric water content (b) after 240 hr. Fine mesh simulation.



## Changing boundary conditions

Results from the rainfall simulations suggest that SUBFEM is sensitive to mesh size and to initial conditions. Results from additional, exploratory test simulations suggest that the model is also highly sensitive to changing boundary conditions. Until now, the boundary conditions for each simulation remained unchanged for the entire simulation period. This constraint allowed the behaviour of each hydrologic process to be examined in isolation. In the following simulations the effects of changing boundary conditions are investigated.

The first run involving changing boundary conditions simulated 3 days of rainfall followed by 10 days of evaporation. Initial conditions corresponded to those that existed after 7 days, when the seepage face approached saturation, in the previous simulation. The simulation proceeded smoothly until the new boundary conditions were introduced, at which time the simulation failed. Oscillation occurred and no solution was obtained.

At first, it was assumed that the problem was related to time step size. However, when the time step size was adjusted from 6 hr to 3, 0.5, and 0.1 hr, there was no improvement. It was then hypothesized that either there was an error in the program or that the changes in boundary conditions were too abrupt to allow a solution to be obtained. The program was carefully checked for errors but none were detected. Consequently, it was decided that a



detailed investigation of changing boundary conditions was warranted.

Five simulations were run for each of two changing boundary conditions: the first in which rainfall changed from 10 mm to 2 mm/day, and the second in which rainfall changed from 10 mm to 0 mm/day. Initial conditions were set at the conditions which existed at the end of the 10-day rainfall simulation for the Yolo Light Clay and fine mesh (Figs. 36d and 38). Two time periods were examined - the first hour, and the first day following the time at which the boundary conditions changed. Time step sizes of 6, 3, 1, 0.1, and 0.01 hr were used.

When the rainfall rate was changed from 10 mm to 2 mm/day, there was a marked drop in outflow (Fig. 39) during the first time step ( $\Delta t = 0.01$  hr). There was no appreciable change in the water content field, but there was a significant change in pressure potentials in the saturated zone, particularly at the surface nodes. During the first time step after the boundary conditions were changed, positive pressure potentials at the surface nodes were reduced from about 120 cm to 35 cm. This caused the isolines for total potential to intersect the upper surface at an angle steeper than before.

The effects of time step size on the simulation are shown in Figs. 39 and 40. It is clear that, during the latter part of the simulation, the same solution is obtained regardless of time step size. However, during the early part



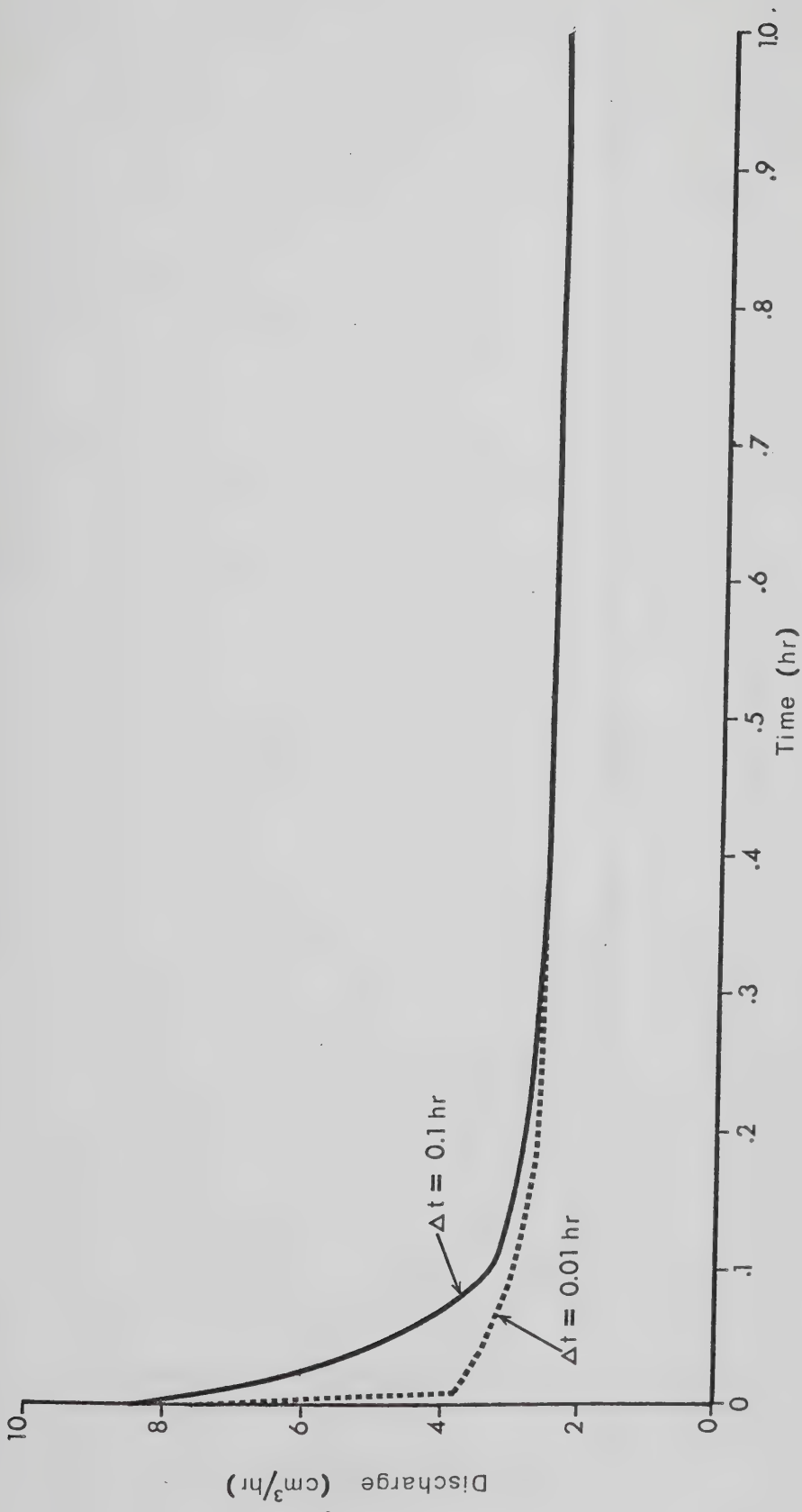


Figure 39. Recession curves - obtained when rainfall rate is changed from 10 to 2 mm/day, and time step sizes are 0.1 and 0.01 hr.





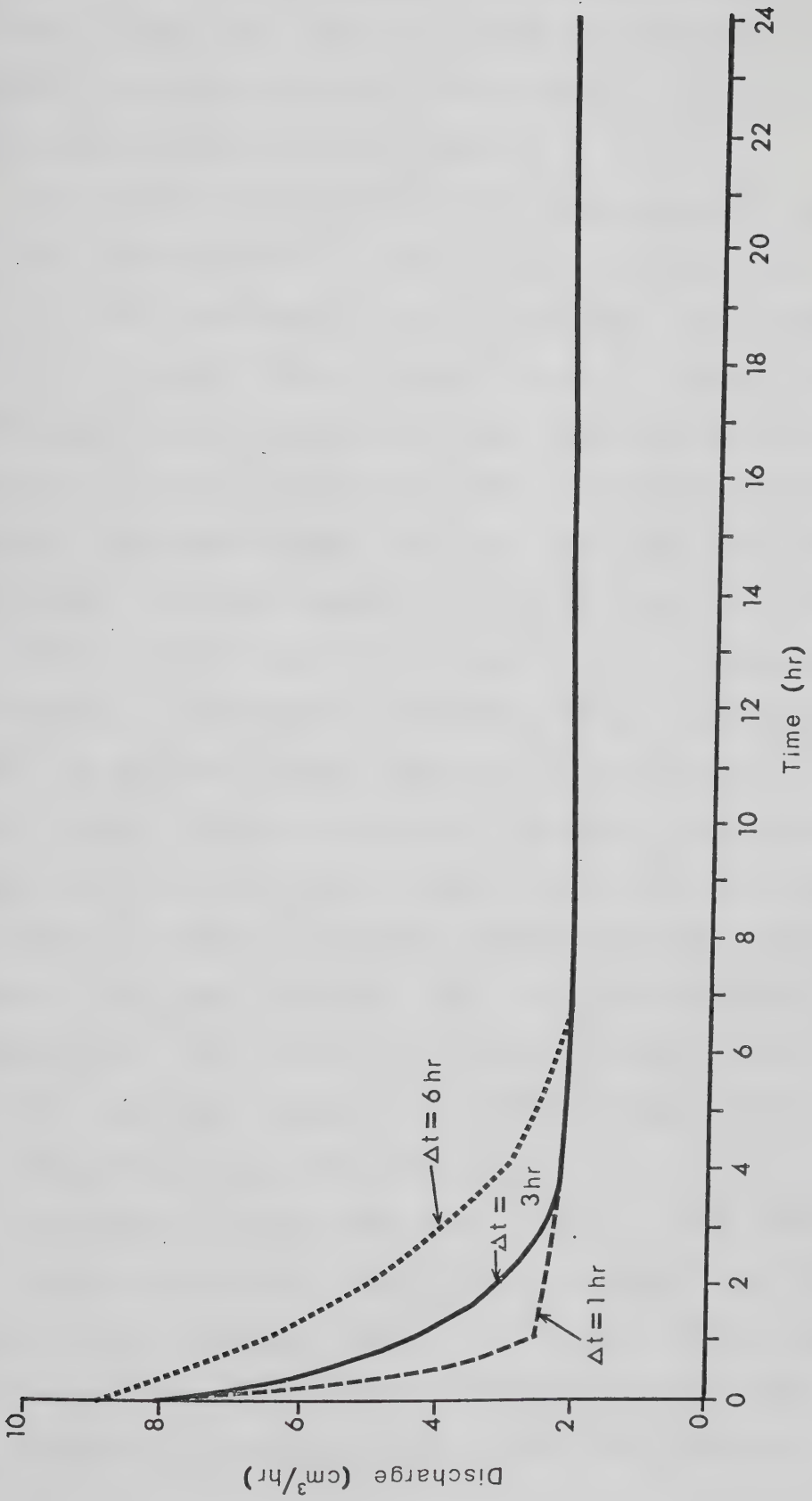


Figure 40. Recession curves - obtained when rainfall rate is changed from 10 to 2 mm/day, and time step sizes are 6, 3, and 1 hr.



of the simulation, immediately following the change in boundary conditions, time step size is important. An improved representation of the recession curve is obtained each time the step size is reduced.

The results obtained for the simulations in which rainfall ceased after 10 days (Figs. 41 and 42) are similar to those for simulations in which rainfall was reduced from 10 mm to 2 mm/day after 10 days (Figs. 39 and 40). Each hydrograph shows a pronounced drop immediately following the change in boundary conditions. Where rainfall persists, outflow continues beyond the first day (Fig. 40). When the rain stops, outflow ceases 13 to 18 hr later (Fig. 42).

At the end of the first time step following cessation of rainfall, the pressure potential in much of the saturated region is uniform, with a value of 14 cm. This is significantly lower than most of the positive pressure potentials which existed at the beginning of the time step. The drop in pressure potential causes the total isopotential lines in the upper 120 cm of soil to bend toward the perpendicular relative to the surface boundary (Figs. 38a and 43). The water content field is not significantly affected during the first time step.

Time step size has the same effect on this simulation as it had on the simulation in which rainfall was reduced from 10 mm to 2 mm/day. Results differ for time steps immediately following changes in boundary conditions, but the differences diminish as the simulation proceeds (Figs.



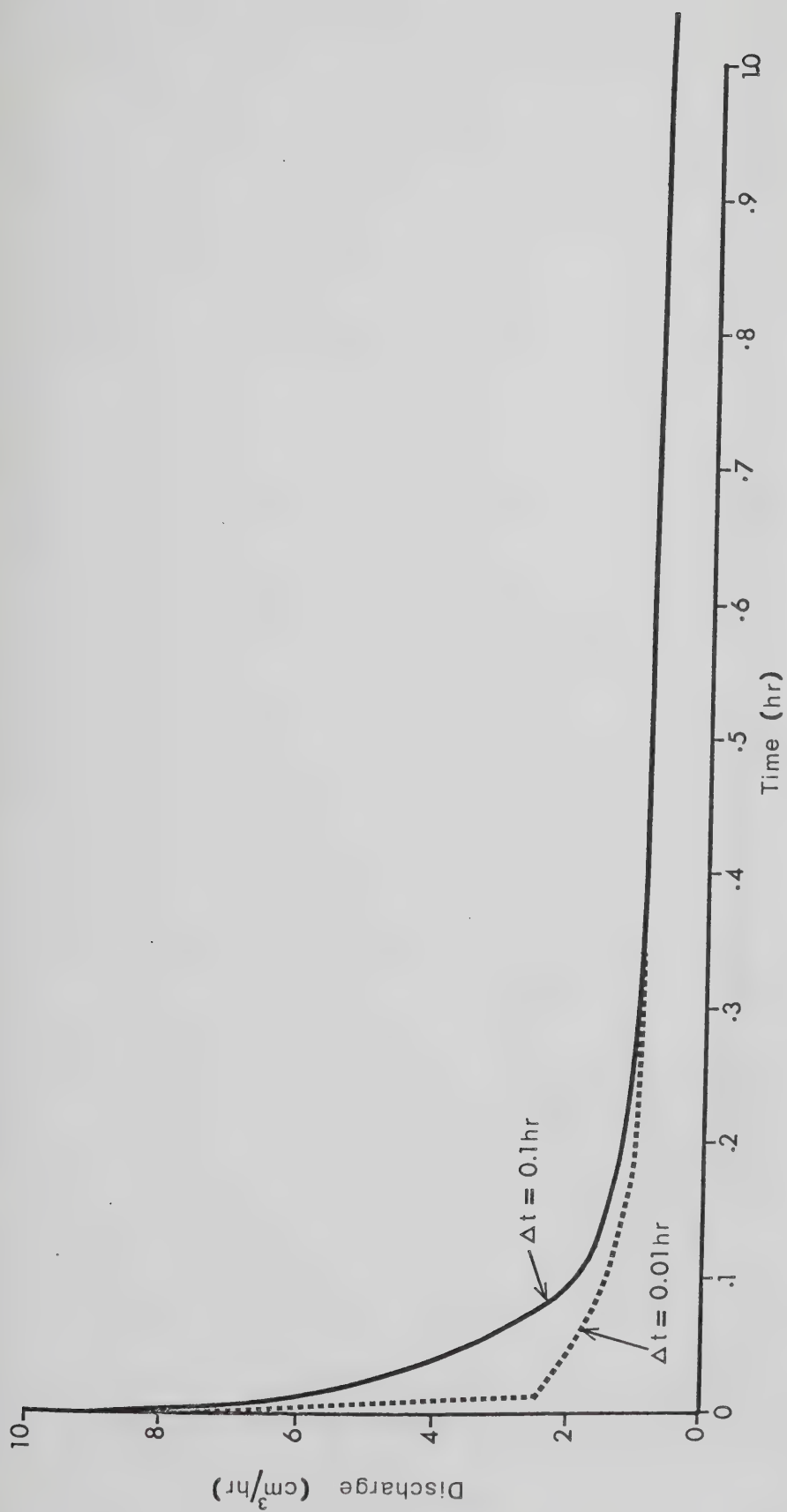


Figure 41. Recession curves - obtained when rainfall rate is changed from 10 to 0 mm/day, and time step sizes are 0.1 and 0.01 hr.



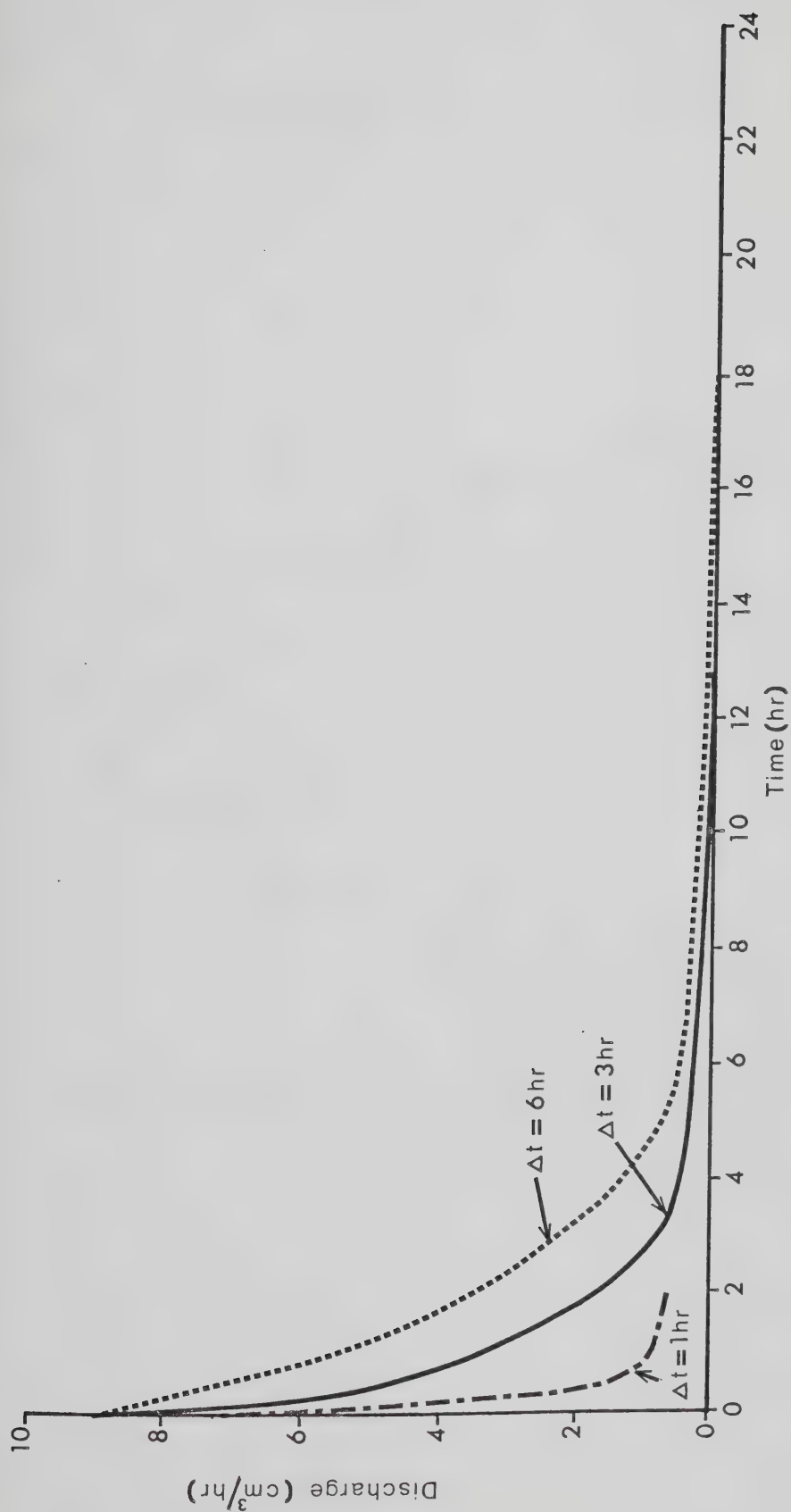


Figure 42. Recession curves - obtained when rainfall rate is changed from 10 to 0 mm/day, and time step sizes are 6, 3, and 1 hr.





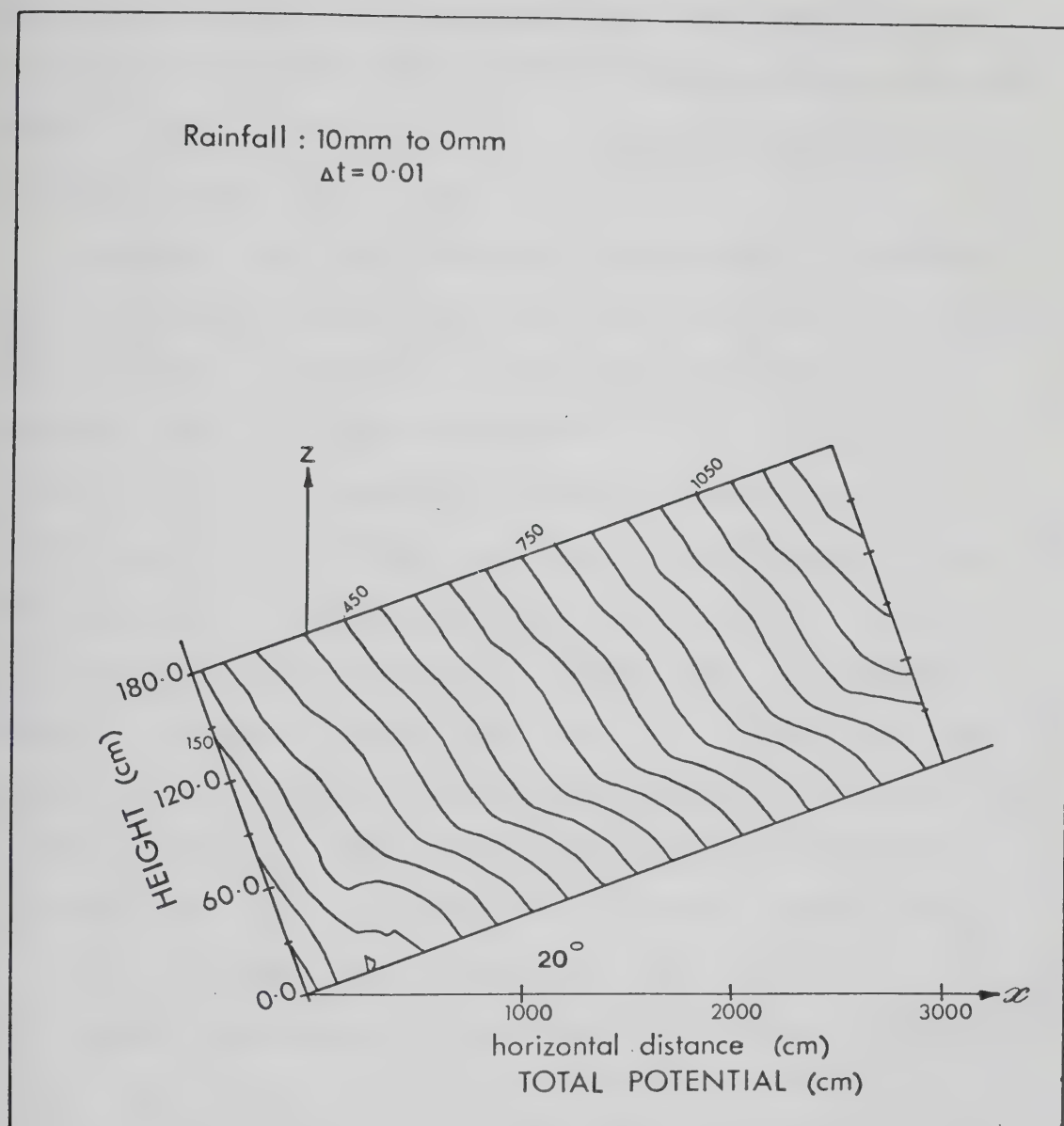


Figure 43. Total potential at end of first time step following cessation of 10 cm rainfall.



41 and 42). Only two time steps were completed for the simulation in which  $\Delta t=1$  hr. The simulation was terminated after 50 iterations during the third time step, when convergence was very slow.

Results from the foregoing simulations for combined saturated-unsaturated flow illustrate the classical concept of interflow. As rainfall continues, a saturated layer develops over an unsaturated zone in the originally unsaturated soil. Eventually, outflow issues from the downslope lateral boundary. Although the situation lacks the conventional prerequisites, such as macropores (root channels and animal burrows), layered soil, and hardpan layer, to produce significant amounts of interflow, there is no question that interflow is occurring. The outflow comes directly from the upper saturated layer, and not from overland, nor via a groundwater system at greater depth.

It is evident from the simulations completed so far for saturated-unsaturated flow that SUBFEM is sensitive to mesh size, time step size, initial conditions, and changing boundary conditions. In the next section, the effects of changing some of these conditions, and the effects of changing saturated hydraulic conductivity will be examined in some detail.



## Sensitivity analyses

### Time step size

The problem selected for sensitivity analyses entails simulation of 5 days of evapotranspiration (3 mm/day) followed by 10 days of rainfall (10 mm/day). The evapotranspiration consists of 1.5 mm/day evaporation and 1.5 mm/day transpiration. In the first set of simulations, the effects of different time steps sizes are investigated. For this purpose, the 64-node, 90-element mesh (Fig. 20) and Yolo Light Clay are used, and the initial pressure potentials are set everywhere equal to -100 cm ( $\theta=0.428$ ). Five time step sizes: 1, 3, 6, 12, and 24 hr, are simulated.

When data for different time step sizes at the end of each day are compared, it is found that, in general, the pressure potential fields (and hence the total potential and water content fields) are very similar. Such differences that occur are usually of the order of about 2 or 3 cm, and appear after the first two or three days of simulation. Larger differences (10 to 15 cm), which occur at some nodes in the vicinity of the seepage face, ordinarily arise as the water content at the seepage face approaches saturation. These differences are sustained for some period following saturation, but subsequently diminish with time. The comparison which showed the greatest differences was that of  $\Delta t=1$  hr and  $\Delta t=24$  hr.

Discharge from the seepage face commenced 10 1/2 days after the start of simulation (Fig. 44). This is true for



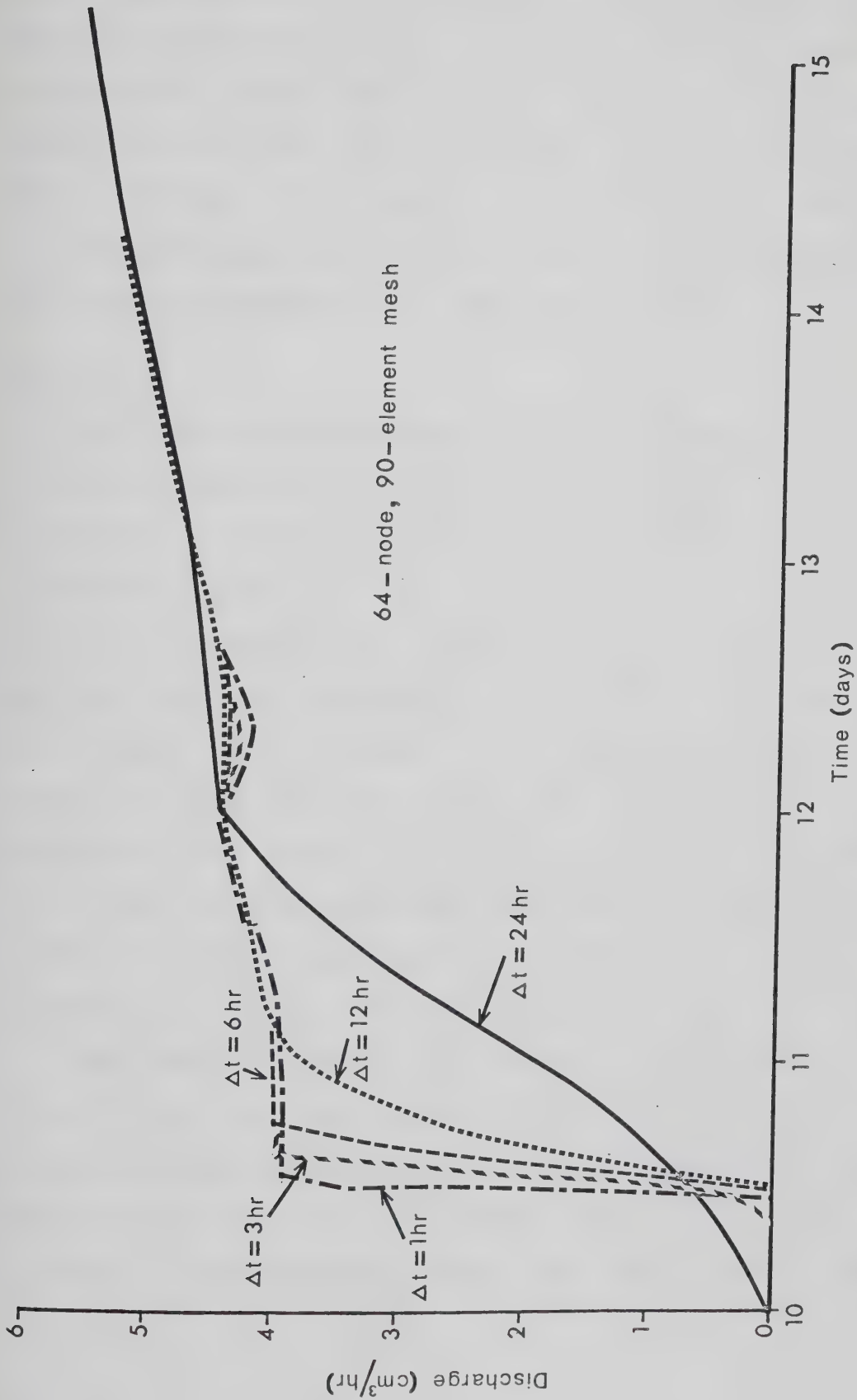


Figure 44. Hydrographs obtained for different time step sizes using a 64-node, 90-element mesh.





simulations of all time step sizes except, perhaps, for the  $\Delta t=24$  hr simulation. It is clear that, with the exception of the  $\Delta t=24$  hr curve, there is very little difference between plots for different time step sizes, beyond the beginning of day 11. However, it is equally evident that the rising limb of the hydrograph is strongly dependent on time step size - its slope increases as the step size decreases.

### Mesh size

Four mesh configurations are used to determine the effects of mesh size on output. Two have already been referred to - the 64-node, 90-element mesh and the 217-node, 360-element mesh. The first has a maximum of two, and the second, five seepage face nodes. Two other, intermediate, mesh patterns are introduced; they consist of 105 nodes on 160 elements, and 114 nodes on 172 elements. These two meshes are identical over much of the region being simulated. They differ only in the vicinity of the seepage face, where the 105-node mesh has 3 seepage face nodes. In contrast, the 114-node mesh has 7 seepage face nodes. The simulations are done for  $\Delta t=3$  hr and  $\Delta t=24$  hr.

The results from this set of simulations indicate that, after 15 days, for each mesh configuration, the total potential field obtained when  $\Delta t=3$  hr is almost identical to that obtained when  $\Delta t=24$  hr. Differences at any given location in the simulated region are rarely greater than 3 or 4 cm.



When results for the same time step size and different mesh sizes are compared, some differences in potential fields are apparent, most noticeably in the proximity of the seepage face. Differences in potential tend to be greater at the bottom of the region than at the top.

A point which is common to all mesh configurations tends to have similar total potential values for different meshes. The isopotential lines are different, however, because each mesh contains a different number of nodes or data points. As this number increases, a greater degree of interpolation within the region is possible. The result is a more accurate representation of the isopotential lines. Consequently, the mesh with the greatest nodal density (the 217-node mesh) should provide the most accurate solution for a given time step size.

The two intermediate-sized meshes give identical results for the region 600 cm from the seepage face and beyond. In the region between the seepage face and the 600 cm horizontal distance mark, differences in total potential between the two meshes tend to increase as the distance from the seepage face diminishes.

The time at which outflow commences from the seepage face is governed by the proximity to the surface of the first seepage face node. The depths to the first seepage face node for the 64-, 105-, 114-, and 217-node systems are 60, 45, 22.5, and 30 cm respectively.



Results from the simulations show (Figs. 45 and 46) that outflow begins soonest when the 114-node simulation is run, and latest when the 64-node system is used. Outflow from each mesh commences in the order in which the first seepage face node is tapped. The hydrographs for  $\Delta t=3$  hr are qualitatively similar to those for  $\Delta t=24$  hr.

The data show (Figs. 45 and 46) that the earlier outflow starts, the more gradual its increase afterwards. In contrast, the longer the delay before discharge begins, the more abrupt is the initial increase in outflow likely to be.

These observations can be related to the fact that if water cannot be discharged from the system, then it must be stored. Thus, in the 64-node system, water will not be discharged until the first seepage face node (at depth 60 cm) reaches saturation. When this condition is attained, some of the water stored in the saturated layer above is released immediately. When the 114-node system is used, the saturated layer has to be only 22.5 cm thick before outflow begins. In this case, less water is discharged than when the saturated layer is 60 cm thick.

### Initial conditions

The 114-node, 172-element mesh with 7 seepage face nodes was chosen to test model sensitivity to changes in initial conditions. In this analysis, a 3-hr time step is used and four initial conditions are compared. At the beginning of the first simulation, the pressure potential is set everywhere equal to  $-100$  cm ( $\theta=0.428$ ).



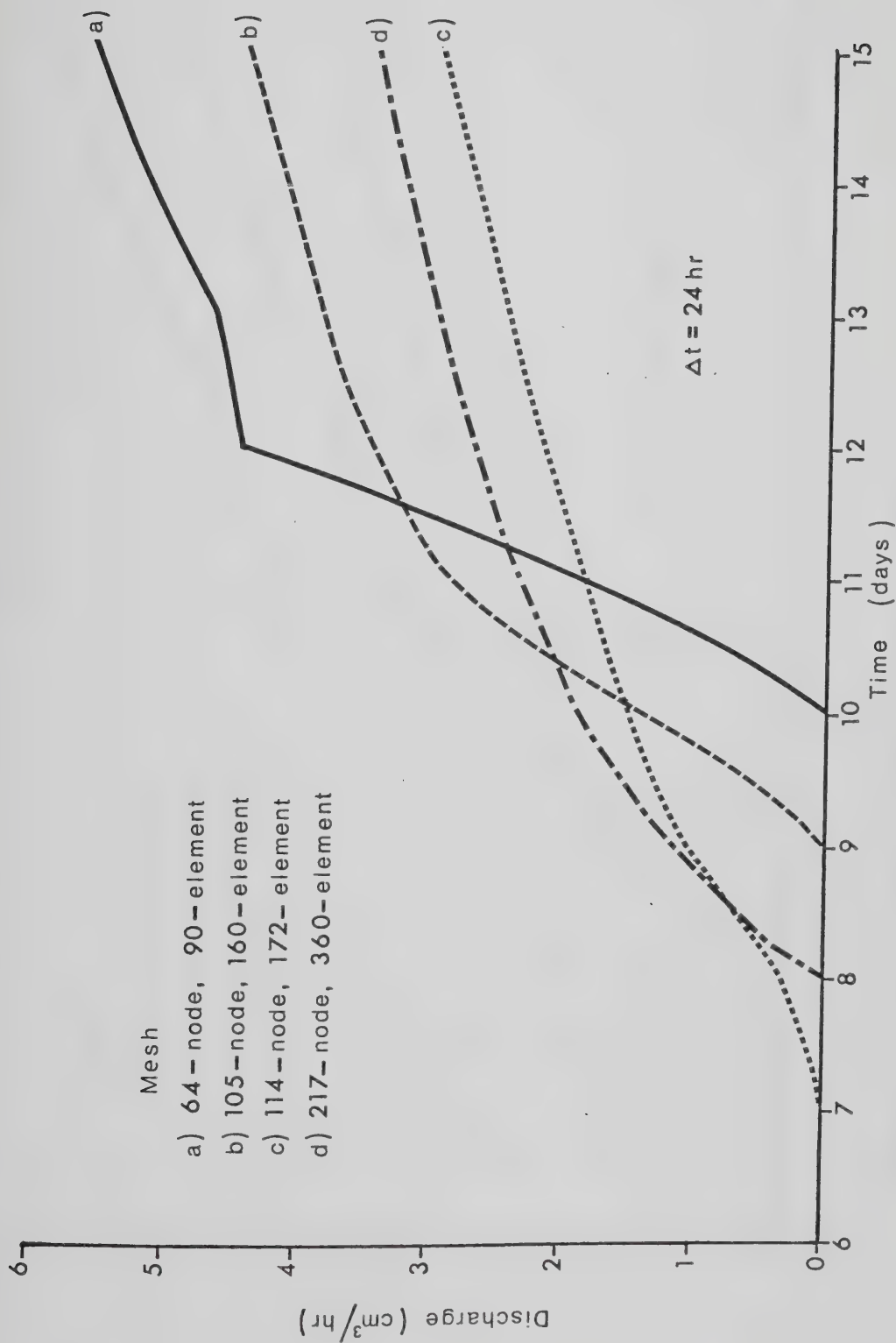


Figure 45. Hydrographs produced by meshes of different coarseness, and a time step size of 24 hr.





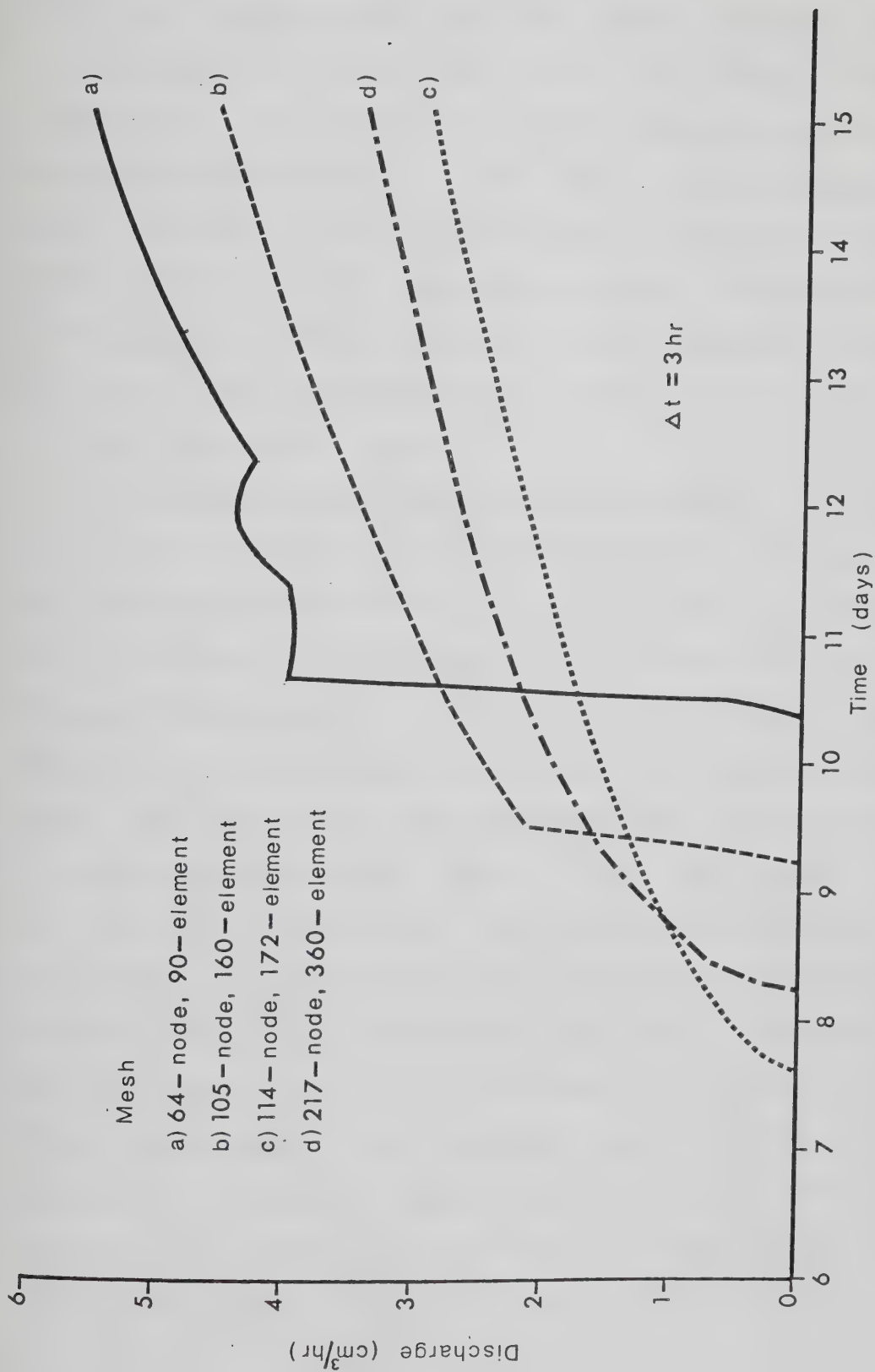


Figure 46. Hydrographs produced by meshes of different coarseness, and a time step size of 3 hr.



In the other simulations, the initial pressure potential fields are not uniform. Instead, each of them corresponds to an upper moist region 45 cm deep overlying a dryer region 135 cm deep. The moist region extends downward along the seepage face, so that there is a uniformly moist band extending 75 cm behind the face. Within both moist and dryer regions initial pressure potential is uniform. For three separate simulations, the initial pressure potential is set at -150 cm in the dryer region, and at -5, -10, and -50 cm in the moist region.

The results from the simulations indicate (Fig. 47) that both the time at which outflow commences and the volume of flow are affected when initial conditions are changed. For a given set of conditions, it is evident that the greater the degree of surface saturation imposed at the beginning of the simulation, the earlier seepage begins. Thus, when the initial pressure potential is set at -5.0 cm in the upper region and -150 cm in the lower region ( $\psi_i = -5 \text{ cm} / -150 \text{ cm}$ ), the discharge from the seepage face begins during day 5 of the simulation. When the initial pressure potential is prescribed uniformly as -100 cm, outflow does not begin until day 7. It also appears that greater initial flows, and greater flows generally, are linked to early initiation of outflow. There is practically no difference between hydrographs obtained when  $\psi_i = -10 \text{ cm} / -150 \text{ cm}$  and  $\psi_i = -5 \text{ cm} / 150 \text{ cm}$  [c) and d) in Fig. 47].



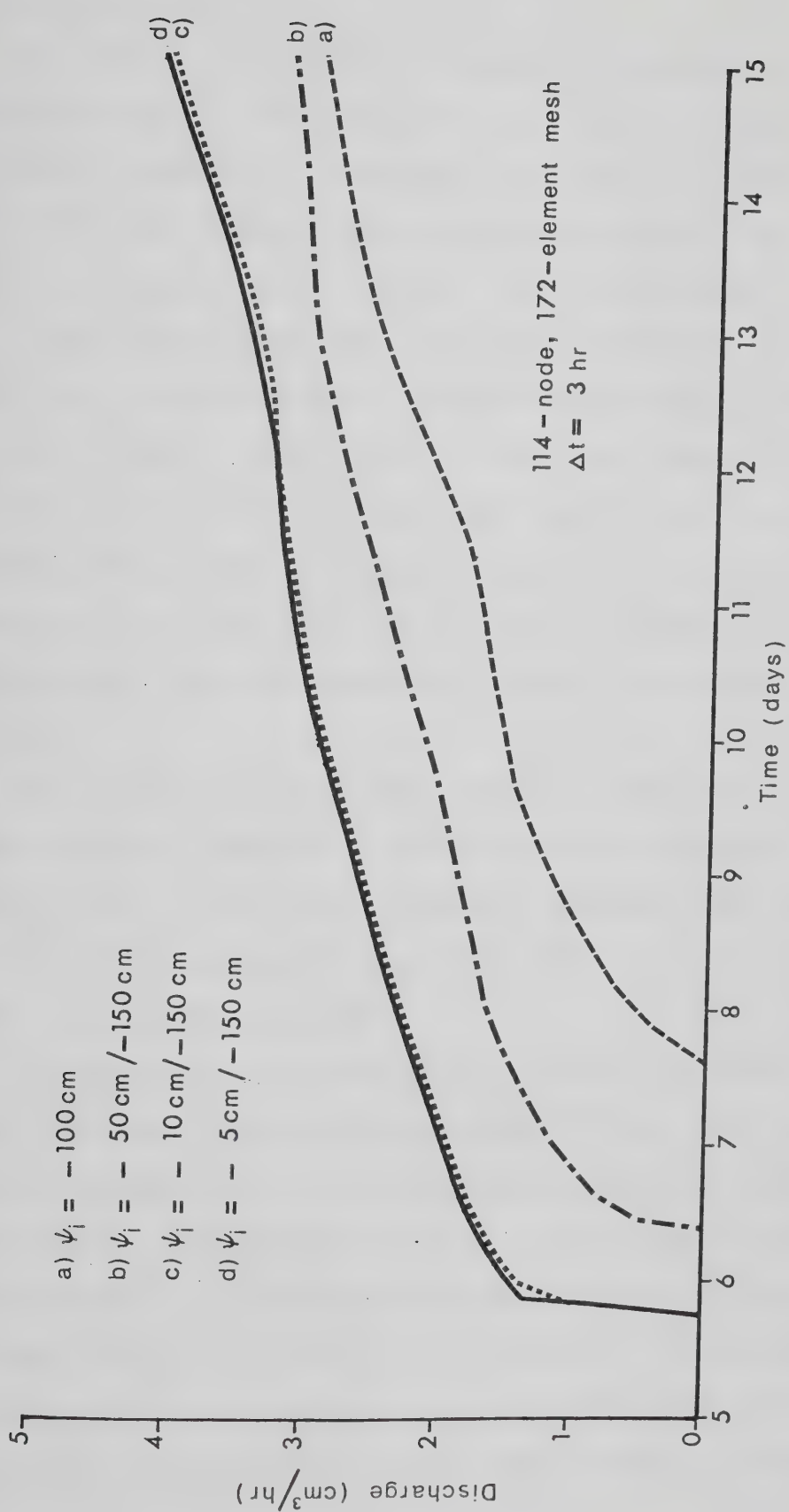


Figure 47. Hydrographs obtained using a 114-node mesh and different initial conditions.



## Hydraulic conductivity

The effects of changing hydraulic conductivity were evaluated using a 3-hr time step, and the 114-node, 172-element mesh with 7 seepage face nodes. Initial pressure potentials were set at -50 cm along the seepage face and upper two rows of nodes, and at -150 cm elsewhere.

Eight simulations were completed. The first concerns Yolo Light Clay which has a saturated hydraulic conductivity of 0.04176 cm/hr (slow). This is the same simulation which was used in the previous experiment for initial conditions analysis (Fig. 47b). It will now serve as the reference simulation for comparing the effects of changes in conductivity. The hydrograph is repeated (Fig. 48a) for this purpose.

In the second simulation, the saturated hydraulic conductivity is reduced by one order of magnitude to 0.004176 cm/hr (very slow). For this problem, the drainage rate is now less than the rainfall rate - a condition which gives rise to overland flow.

The reduction in conductivity causes less water to reach the lower regions of the profile (Fig. 49b) than previously (Fig. 49a), and very little penetrates beyond depth 135 cm. In both simulations, a saturated ( $\theta=0.496$ ) layer together with positive pressure potentials develop in the upper portion of the profile. However, the positive pressure potentials for the simulation with the lower saturated conductivity are much higher. This is a measure of





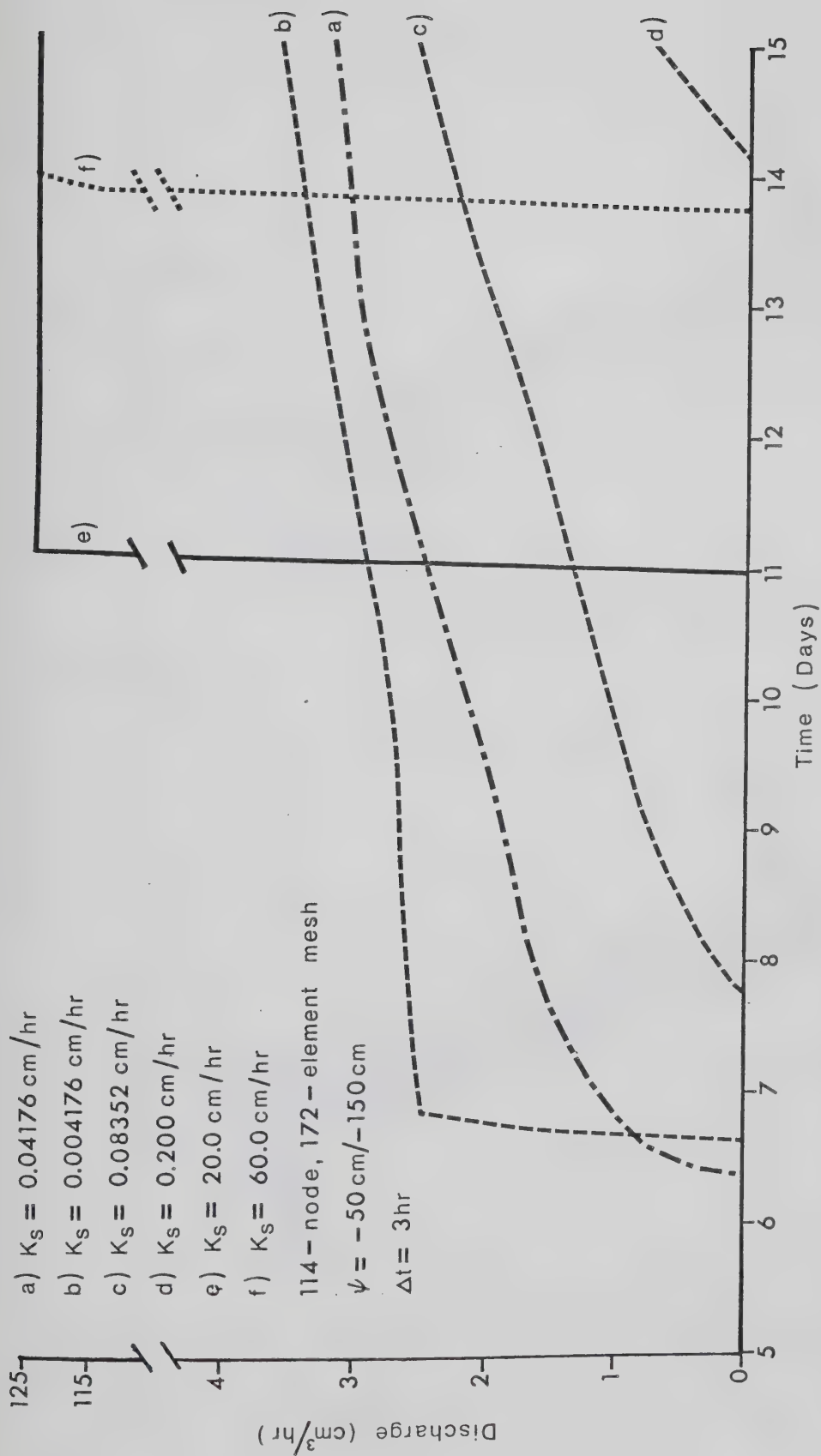
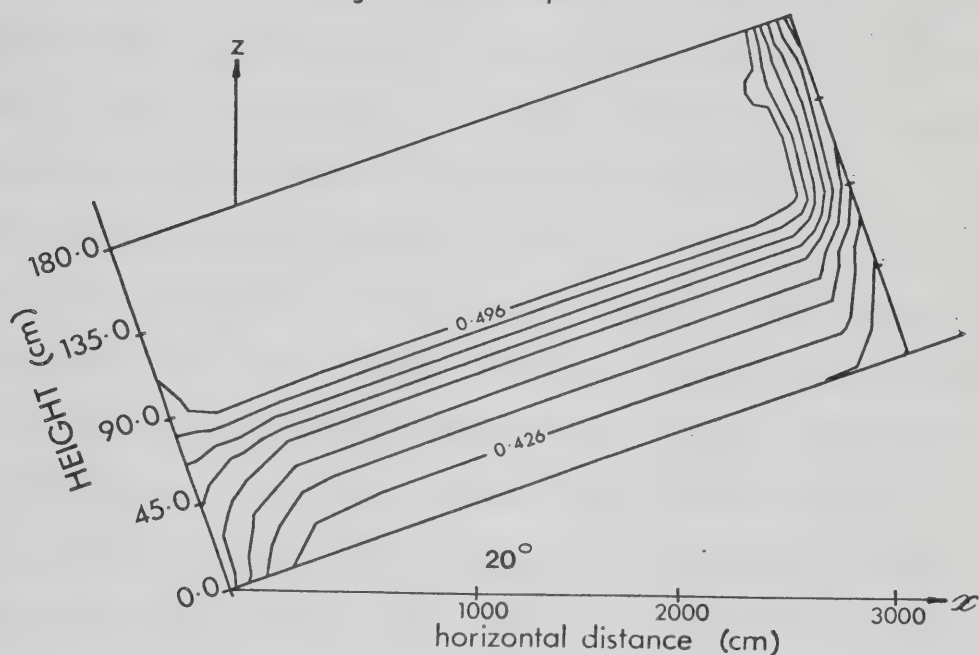


Figure 48. Variation of discharge over time for different values of saturated hydraulic conductivity ( $K_s$ ).



## YOLO LIGHT CLAY

$$K_s = 0.04176 \text{ cm/hr}$$

(a) VOLUMETRIC WATER CONTENT ( $\text{cm}^3/\text{cm}^3$ )

Vertical exag: x9

$$K_s = 0.004176 \text{ cm/hr}$$

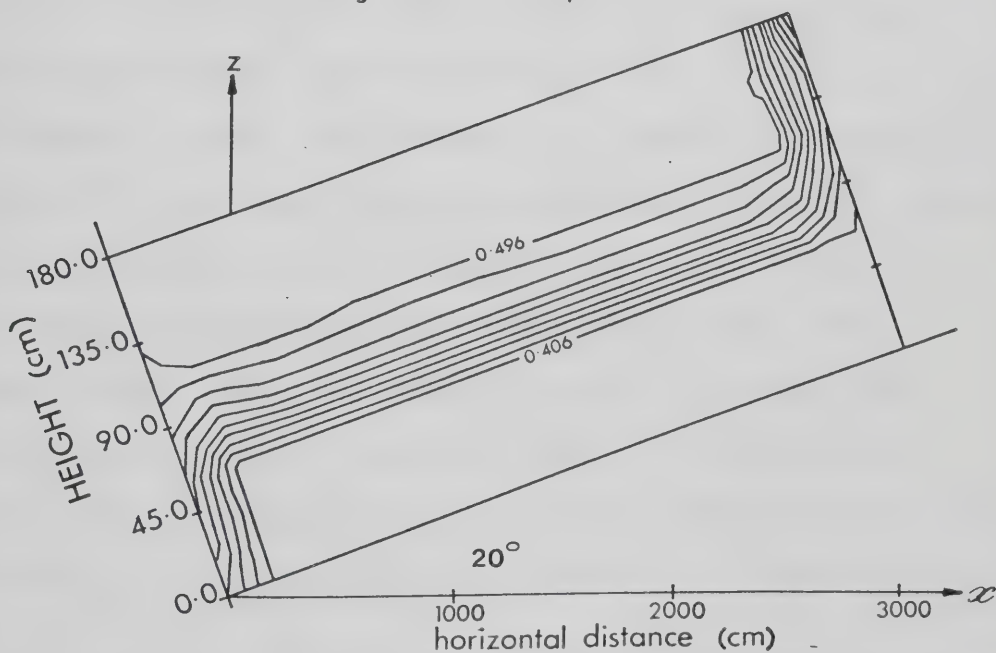
(b) VOLUMETRIC WATER CONTENT ( $\text{cm}^3/\text{cm}^3$ )

Figure 49. Water content in Yolo Light Clay after 10 days of rainfall, for two values of saturated hydraulic conductivity ( $K_s$ ).



the model's response when no provision is made for overland flow. Since rainfall in excess of the drainage rate is not removed through an overland flow routine, the model tries to accommodate the excess water in some other way - evidently by generating high positive pressure potentials.

The results also indicate that, for a given set of conditions, a reduction in saturated conductivity leads to a thinner saturated layer (Figs. 49a and b). Because of this, and since less water is moving downward through the lower regions of the profile, one would expect more water to appear at the seepage face. Inspection of the hydrographs for the two simulations (Figs. 48a and b) shows that this is, indeed, the case.

For the third simulation, the reference conductivity is doubled to 0.08352 cm/hr (slow). When the results are compared with output from the reference simulation, two main trends emerge. First, more water is stored in the profile, especially in the basal portion, and second, outflow from it through the seepage face is reduced (Figs. 48a and c). Because the transmitting capability of the soil has increased, water has more rapid access to the unfilled storage capacity in the lower portion of the profile. Consequently, less water issues from the seepage face. The saturated layer extends from the surface to a depth of about 70 cm.

When the saturated conductivity is increased one order of magnitude above the reference conductivity to 0.4176



cm/hr (moderate), the entire amount of rainfall is used to satisfy available soil water storage. In this case, saturation is not reached anywhere and outflow does not occur.

Similar results are obtained when a simulation is performed on data pertaining to reconstituted Halewood Sandy Loam (Scholl and Hibbert, 1973). The saturated conductivity for this material is about 0.45 cm/hr (moderate).

Some outflow is obtained when the problem is run using a saturated conductivity of 0.20 cm/hr (slow). However, only a small region, in the vicinity of the seepage face, reaches saturation. Consequently, outflow is minimal and does not begin until near the end of the simulation (Fig. 48d).

The remaining two conductivity simulations show that, if inflow is adequate, large saturated conductivity values result in steady, saturated flow. The first of these simulations concerns Calvin Silt Loam (Troendle, 1970) which has a saturated conductivity of 20 cm/hr (rapid). The soil used in the other simulation is Bodine Silt Loam (Huff et al, 1977) which has a saturated conductivity of 60 cm/hr (very rapid).

In both simulations, saturation occurs before they are completed. For the Calvin soil, saturation is attained during day 11 (Fig. 48e), and for the Bodine soil, during day 13 (Fig. 48f). When saturation is reached, all pressure potentials are zero or positive, and total outflow equals total inflow. This condition is maintained for the remainder





of the simulation (Figs. 48e and f).

The time at which outflow from each soil begins is related to the available storage capacity of the soil. This capacity, in turn, depends on the soil's initial water content and its total porosity. Data used in the Bodine soil simulation indicate that, at the start of the simulation, this soil has the capacity to absorb about 6.5 cm of additional water. The corresponding value for the Calvin soil is about 9.5 cm. Because water is being applied and absorbed at a rate of 1 cm/day from day 6 on, one would expect outflow to occur (at the inflow rate) from the Calvin soil 6.5 days later, and from the Bodine soil, 9.5 days later. The simulation results (Figs. 48e and f) are consistent with these expectations.

### C. Model Versus Prototype

Attempts were made to simulate a field experiment which was carried out on the Fernow Experimental Forest, West Virginia, during the late sixties. The field experiment (prototype) lends itself to simulation using SUBFEM because it is two-dimensional and because data from it are quite comprehensive.

The field study was conducted on a fairly uniform north-facing slope with a gradient of about  $19^\circ$ . The soil is predominantly deep Calvin Silt Loam, with inclusions of Dekalb loam, overlying Catskill sandstone and shale. Forest vegetation consists of oaks, sugar maple, yellow poplar,



black cherry, and beech. The plot extends from the ridge to a horizontal distance downslope of 53.3 m. At the lower end of the plot, a collection trench 15.2 m wide and about 1.8 m deep was excavated along the contour perpendicular to the slope, to intercept soil moisture draining downslope (Troendle, 1970).

Backfilling and sealing of the trench was designed so that a wall of pea-sized gravel impinged on the upslope face of the trench, and all water issuing from this face was collected in a trough at the bottom of the trench. The water was then transferred from the trough into an HS flume.

To prevent lateral movement of water out of the plot, its lateral boundaries were trenched to bedrock and backfilled with a mixture of Bentonite clay and soil. Instrumentation was installed to measure soil water content and to monitor perched water tables.

For the purpose of simulation, it was assumed that the basal boundary of the hillside coincided with the bedrock at depth 1.8 m. It was further assumed that this boundary ran parallel with the surface from the ridge to the trench. Another, vertical, impermeable boundary was presumed to exist at the topographic divide, or ridge.

Soil descriptions for the plot indicate a multi-layered profile. For simulation purposes, however, only two layers are considered - the upper, which extends from the surface to a depth of 62.5 cm, and the lower, which lies between depths 62.5 and 175 cm. Since saturated conductivity values



for the upper horizons are not given, a value of 170 cm/hr for the upper layer is assumed. This is an order of magnitude greater than the saturated conductivity for the lower layer. Each layer is considered to be isotropic and homogeneous.

The simulated event concerned a rainstorm which occurred on 8-9 August, 1969. During this storm 7.75 cm of rain fell, in less than 12 hr, onto an originally dry soil. The simulation was accomplished using a 272-node, 462-element mesh.

The distribution of rainfall for the storm is given as: 0.38, 1.02, 1.27, 0.63, 0.51, and 0.13 cm/hr. These rates, which are applied over 2-hr increments for a total of 12 hr, represent the boundary conditions of the problem. On August 6, volumetric soil water content was about 18 percent in the lower layer and between 19 (upslope) and 24 (downslope) percent in the upper layer. The water contents define the initial conditions of the problem. A time period of 12 hr was simulated using a time step of 0.1 hr.

Of the total amount of precipitation that fell during the August storm, only 5.5 percent appeared as outflow from the plot, the rest recharged the soil (Troendle, 1970). In the simulation, no point on the hillslope reached saturation, and no outflow was obtained.

A further simulation of the August storm was carried out. It differed from the preceding one in that initial water contents for the surface soil layer were prescribed as



26 and 28 percent, instead of 19 and 24 percent.

The results from this simulation, also, indicated unsaturated conditions and a complete lack of outflow from the hillslope for the duration of the 12-hr period. Evidently, the entire 7.75 cm of rainfall was absorbed by the soil. Simulated water content data showed that, by the end of the 12-hr period, water content in both layers had increased by about 4.5 percent, or by a total of approximately 8.0 cm - a figure somewhat higher than the original 7.75 cm of rain.

The data for each time step show that, at the bottom of the profile, no appreciable change in water content occurred until after time step 60 (6 hr). During that time, at the surface, the downslope pressure potential increased from -4944 to -371 cm, and the upslope pressure increased from -7210 to about -405 cm. Thus after 6 hr, soil water content at the surface was close to field capacity ( $\psi = -339$  cm).

A fairly steady pattern was evident for the period between 6 and 10 hr. At depth 25 cm, pressure potential did not change very much - remaining at about -616 to -620 cm. Below depth 25 cm, soil water content increased at all depths. Above depth 25 cm, the pressure potential and water content decreased slightly.

After 10 hr, when the rainfall rate was reduced to 0.13 cm/hr, the pressure potential at the surface decreased more rapidly, indicating that the upper soil layer was draining at a rate faster than the supply rate.





It is not clear why there was outflow from the prototype system, yet none from the model system. Some possible explanations are offered below:

1. In the simulation, each soil layer was considered to be homogeneous, thus its spatial variability was not taken into account. If the layers are not homogeneous, then the given point measurements of saturated hydraulic conductivity may not be applicable over the entire hillslope.
2. Each soil layer was assumed to be isotropic for simulation purposes. This may not be the case for the prototype. If the horizontal conductivity exceeds the vertical conductivity, water will tend to move downslope toward the seepage face faster than it will vertically.
3. The model simulates only flow through porous media. It is possible that a different mechanism is operating to produce outflow from the prototype, e.g. turbulent flow through macropores such as root holes and animal burrows.

The simulation just described was the largest attempted during this study. Running the problem using the 272-node, 462-element mesh and 120 time steps entailed 8 minutes of CPU time and 1996 page-minutes of virtual memory. The input data files for this problem are displayed in Appendix D.



## VI. SUMMARY AND CONCLUSIONS

### A. Summary

A physically based, distributed, subsurface flow finite element model (SUBFEM), in which vegetation appears as an integral part, was developed to simulate the effects of different vegetation patterns on soil water distribution and streamflow. Water withdrawal by trees was simulated by means of sinks located at appropriate near-surface nodes within the finite element mesh. Each sink may represent the activity of a single tree or groups of trees. In this study each sink represented water withdrawal by a group of trees.

Data required to drive the model include section geometry and, for each soil or rock layer, saturated hydraulic conductivity and the relation between volumetric water content and pressure potential. Rainfall (or snowmelt), evaporation, and transpiration rates over time are also required. For each time step the program prints out the pressure potential field and boundary fluxes. Boundary fluxes occur at the upper boundary (ground surface) and at the seepage face. The program also prints out the pressure potential, the total potential, and the volumetric water content fields, together with the boundary fluxes, that exist at the end of the simulation.

Initial tests on the model, for one-dimensional and two-dimensional infiltration into originally unsaturated soil, produced results that compared favourably with those



of other investigators who had simulated the same problems. These tests also successfully demonstrated the concepts of advancing wetting front and infiltration capacity.

A series of simulations were completed to determine the effects of transpiration and evaporation, both separately and combined, on water distribution in a large box of soil. The simulations revealed that a smaller volume of soil is affected by evaporation than by transpiration for a fixed evaporation or transpiration demand. Potential gradients, on the other hand, are greater during evaporation.

The next set of experiments concerned evapotranspiration, over 10- and 20-day periods, from sloping profiles. In these simulations, trees were assumed to occupy different positions on the slope: lower slope only, upper slope only, completely forested, clearcut (no trees), and patchcut.

Quite distinct patterns for both total potential and volumetric water content were obtained. They reflected the differential drain on soil water by trees and by evaporation. Soil water content was less, and the volume of soil affected greater, under trees than under open conditions. The isopotential lines indicated that, when evaporation or transpiration occurs, flow is directed up toward the surface in the upper portion of the profile, and downslope at lower depths.

The first simulation in which saturated flow was considered involved rainfall into a horizontal box from



which there was no outlet. The increase in soil water content over the 10-day rainfall period closely approximated the total amount of rainfall.

In a subsequent problem, rainfall over a 10-day period onto a sloping profile was simulated. This time outflow was permitted. Although the simulation involved porous media flow only, results from it illustrated the classical concept of interflow. A saturated layer developed over an unsaturated zone in an originally unsaturated soil, and seepage eventually emerged from the upper portion of the downslope face.

Simulation was used in an attempt to reproduce results from a field experiment conducted on the Fernow Experimental Forest, West Virginia, during the late sixties. A single storm event, in which 7.75 cm of rain fell onto an originally dry soil in less than 12 hr, was simulated.

Field data showed that 5 percent of the precipitation appeared as outflow from the plot. The simulation data indicated that no outflow occurred during or following the storm, and that the entire contribution from the storm was retained in the soil.

## B. Conclusions

The conclusions that follow are based on simulations of flow through isotropic, homogeneous porous media. Results from these simulations suggest that the primary usefulness of SUBFEM rests in its capability to simulate, qualitatively





at least, the processes of infiltration, evaporation, transpiration, and interflow. Because of this, and since it is two-dimensional, it can best be used to study hydrologic processes on vegetated or partially vegetated hillslopes. The simulation of the plot study on Fernow Experimental Forest exemplifies this type of application.

The data requirements of the model are considered to be one of its main limitations. For example, transpiration rates for different tree species under different climatic conditions are difficult to obtain and, generally, are not available. Assigning suitable saturated conductivity values to soil strata is also a problem.

Experience shows that SUBFEM can easily cope with large, unsaturated flow systems. For these simulations, few iterations per time step are required, and only rarely are problems encountered that relate to convergence or numerical instability. Some difficulties arise when saturated-unsaturated flow systems are simulated - notably following certain changes in boundary conditions.

Time step size, under certain conditions, is critical and will determine whether convergence to a solution is possible.

Mesh coarseness can influence the time at which outflow from an originally unsaturated system begins. Sensitivity of response, in this case, is related to the number and position of nodes at the seepage face. For infiltration problems, the more nodes there are at the seepage face, the



earlier outflow begins.

The sensitivity of two model parameters were examined: initial conditions and saturated hydraulic conductivity. Of the two, saturated hydraulic conductivity proved to be the most sensitive.

Both the time at which outflow commences and the volume of flow from an originally unsaturated system are affected by changes in initial conditions. If the region in the vicinity of the seepage face, and the upper portion of soil are wetter than the soil below, then together they serve as a conduit for additional water that enters the system. In general, the wetter the initial conditions, the earlier outflow begins.

SUBFEM is very responsive to changes in saturated hydraulic conductivity. If the value of this parameter is high enough, and the porous material is homogeneous and isotropic, the entire profile may be recharged before outflow occurs - at either the saturated or inflow rate, whichever is lower. Afterwards, if the same inflow rate is maintained, steady state conditions prevail.

Although the model is designed primarily to simulate forest site conditions under which soil absorbs rainfall at most intensities, it was established that, if the rainfall rate exceeds the saturated conductivity, provision must be made in the model to route excess water as overland flow. There are indications that provision should also be made to simulate flow processes other than porous media flow, i.e.



turbulent flow through macropores such as root holes and animal burrows.

### C. Suggestions For Further Research

- a. SUBFEM should be subjected to more rigorous testing by comparing output for a given field situation with observed data from a well-instrumented site.
- b. The subsurface flow model may prove to be a useful tool for determining average saturated hydraulic conductivity values for hillslopes.
- c. It may be worth investigating a number of features, notably the treatment of anisotropy and multi-layered soils, within the model that have not yet been fully tested.
- d. An algorithm which varies the time step size should be incorporated into SUBFEM. It would reduce the time increment during intervals when convergence to a solution is expected to be a problem, such as the period immediately following changes in boundary conditions. The time step size would be increased when the numerical system is stable.
- e. The computing efficiency of SUBFEM could be improved by incorporating the substructure method of analysis (Elwi and Murray, 1977) into the model. In this approach, a hillslope is partitioned into several subunits, each of which is considered to be a large finite element. Each subunit in turn is divided into



still smaller elements. The larger elements are assembled along inter-boundary nodes. Solutions are obtained first for the inter-boundary nodes, and then for nodes contained within the internal structure of the large elements. The procedure is particularly efficient if several large elements are identical.

- f. In many analyses of subsurface flow problems, the investigator is interested not in the internal structure of the system, but in conditions at its boundaries i.e. at the seepage face or at the flux boundaries. For these problems, the Boundary Element Method (Brebbia, 1978) may be a more efficient technique. It has the advantage that much smaller systems of equations are generated, and much less data are required to obtain solutions, when compared to finite element and finite difference methods. The potential application of this method to solving subsurface flow problems should be investigated.
- g. Over the long term, as computer capabilities increase and computing costs diminish, it may be possible to expand the model to the three-dimensional form and, at low cost, use it to simulate problems involving entire watersheds.





## VII. LITERATURE CITED

- Alberta Energy and Natural Resources. 1979. Forests and water. (Brochure).
- American Society of Agricultural Engineers and American Society of Civil Engineers. 1970. Interdisciplinary aspects of watershed management. Proceedings of a Symposium held Aug. 3-6, 1970. Montana State Univ., Bozeman, Montana.
- Amorocho, J. and W.E. Hart. 1964. A critique of current methods in hydrologic systems investigation. Trans., Am. Geophys. Union 45(2): 307-321.
- Anderson, H.W. 1960. Water management forestry - a model approach. Pages 1734-1738 in Proc. Fifth World For. Cong. Univ. of Wash., Seattle, Wash., Aug. 29 - Sept. 10, 1960.
- Anderson, H.W., M.D. Hoover, and K.G. Reinhart. 1976. Forests and water: effects of forest management on floods, sedimentation, and water supply. USDA For. Serv., Pac. Southwest For. Range Exp. Stn., Berkeley, Calif. Gen. Tech. Rep. PSW-18.
- Anderson, M.G. and T.P. Burt. 1978. Toward more detailed field monitoring of variable source areas. Water Resour. Res. 14(6): 1123-1131.
- Bates, C.G. and A.J. Henry. 1928. Forest and streamflow experiment at Wagon Wheel Gap, Colorado. U.S. Mon. Weather Rev. Suppl. 30.
- Beasley, R.S. 1976. Contribution of subsurface flow from the upper slopes of forested watersheds to channel flow. Soil Sci. Soc. Am. Proc. 40(6): 955-957.
- Betson, R.P. 1964. What is watershed runoff? J. Geophys. Res. 69(8): 1541-1552.
- Bettters, D.R. 1975. A timber-water simulation model for lodgepole pine watersheds in the Colorado Rockies. Water Resour. Res. 11(6): 903-908.
- Beven, K.J. 1975. A deterministic, spatially distributed model of catchment hydrology. Unpubl. Ph.D. Thesis. Univ. East Anglia.
- Beven, K. 1978. The hydrological response of headwater and sideslope areas. Hydrol. Sci. Bull. 23(4): 419-437.
- Beven, K.J. and M.J. Kirkby. 1979. A physically based,



variable contributing area model of basin hydrology.  
Hydrol. Sci. Bull. 24(1): 43-70.

- Bochkov, A.P. 1970. Influence of forests and agrosilvicultural-ameliorative activities on the water level of streams and streamlets. Pages 93-100 in Proceedings of the joint FAO/USSR International Symposium on Forest Influences and Watershed Management, held in Moscow, USSR, Aug. 17-Sept. 6. E. Talât and E.G. Dunford (eds).
- Bonell, M. and D.A. Gilmour. 1978. The development of overland flow in a tropical rainforest catchment. J. Hydrol. 39(3-4): 365-382.
- Bouwer, H. and W.C. Little. 1959. A unifying numerical solution for two-dimensional steady flow problems in porous media with an electrical resistance network. Soil Sci. Soc. Am. Proc. 23(2): 91-96.
- Brebbia, A.P. 1978. The boundary element method for engineers. Pentech Press, London.
- Bredehoeft, J.D. and G.F. Pinder. 1970. Digital analysis of areal flow in multiaquifer groundwater systems: a quasi three-dimensional model. Water Resour. Res. 6(3): 883-888.
- Buckingham, E. 1907. Studies on the movement of soil moisture. U.S. Dep. Agric. Bur. Soils Bull. 38. (Original not seen, cited by Philip, 1957).
- Chamberlin, T.W. 1972. Interflow in the mountainous forest soils of coastal British Columbia. Pages 121-127 in Mountain Geomorphology. O. Slaymaker, and H.J. McPherson (eds.) Tantalus Res., Vancouver, B.C.
- Chanasyk, D.S. 1980. A model to evaluate the hydrologic response to land use changes. Unpubl. Ph.D. Thesis. Univ. Alberta.
- Childs, E.C. 1936. The transport of water through heavy clay soils. I. J. Agric. Sci. 26(1): 114-127.
- Childs, E.C. and N. Collis-George. 1950. The permeability of porous materials. Proc. R. Soc. London, Ser. A: 201: 392-405.
- Clarke, R.T. 1973. A review of some mathematical models used in hydrology, with observations on their calibration and use. J. Hydrol. 19(1): 1-20.
- Colman, E.A. 1953. Vegetation and watershed management. (An appraisal of vegetation management in relation to water



supply, flood control, and soil erosion). Ronald Press Co., New York.

- Cooper, H.H. Jr. 1966. The equation of groundwater flow in fixed and deforming coordinates. J. Geophys. Res. 71(20): 4785-4790.
- Crawford, N.H. and Linsley, R.K. 1966. Digital simulation in hydrology: Stanford Watershed Model IV. Dep. Civ. Eng., Stanford Univ. Tech. Rep. 39.
- Csallany, S.C., T.G. McLaughlin, and W.D. Striffler (eds.). 1972. Watersheds in transition. Proceedings of a symposium held at Fort Collins, Colorado, June 19-22.
- Darcy, H. 1856. Les fontaines publiques de la ville de Dijon: Paris, V. Dalmont. (Original not seen, cited by Davis and DeWiest, 1966).
- Davis, S.N. and R.J.M. DeWiest. 1966. Hydrogeology. John Wiley and Sons, Inc., New York.
- Desai, C.S. and J.F. Abel. 1972. Introduction to the finite element method - a numerical method for engineering analysis. Van Nostrand Reinhold Co., New York.
- De Vries, J. and T.L. Chow. 1978. Hydrologic behavior of a forested mountain soil in coastal British Columbia. Water Resour. Res. 14(5): 935-942.
- Dickinson, W.T. and H. Whiteley. 1970. Watershed areas contributing to runoff. Pages 12-26 in Results of Research on Representative and Experimental Basins. Symposium of Wellington, New Zealand, 1-8 Dec. Int. Assoc. Sci. Hydrol. Publ. 96.
- Dunne, T. and R.D. Black. 1970a. An experimental investigation of runoff production in permeable soils. Water Resour. Res. 6(2): 478-490.
- Dunne, T. and R.D. Black. 1970b. Partial area contributions to storm runoff in a small New England watershed. Water Resour. Res. 6(5): 1296-1311.
- Dunne, T., T.R. Moore, and C.H. Taylor. 1975. Recognition and prediction of runoff-producing zones in humid regions. Hydrol. Sci. Bull. 20(3): 305-325.
- Dunne, T., A.G. Price, and S.C. Colbeck. 1976. The generation of runoff from subarctic snowpacks. Water Resour. Res. 12(4): 677-685.
- East Slopes (Alberta) Watershed Research Program. 1966. Fourth Annual Report. Eastern Rockies Forest





Conservation Board, Calgary, Alberta.

- Elwi, A.A. and D.W. Murray. 1977. Substructive analysis of plane frames. Dep. Civ. Eng., Univ. Alberta. Struct. Eng. Rep. 64.
- Environmental Council of Alberta. 1979. The environmental effects of forestry operations in Alberta. Report and recommendations. Environ. Counc. Alberta. Alberta Dep. Lands For.
- Feddes, R.A., P. Kowalik, S.P. Neuman and E.Bresler. 1976. Finite difference and finite element simulation of field water uptake by plants. Hydrol. Sci. Bull. 21(1): 81-98.
- Finnemore, E.J., and B. Perry. 1968. Seepage through an earth dam computed by the relaxation technique. Water Resour. Res. 4(5): 1059-1067.
- Food and Agriculture Organization of the United Nations. 1976a. Hydrological techniques for upstream conservation. FAO, UN, Rome. Food Agric. Organ. Conservation Guide 2.
- Food and Agriculture Organization of the United Nations. 1976b. Conservation in arid and semi-arid zones. FAO, UN, Rome. Food Agric. Organ. Conservation Guide 3.
- Food and Agriculture Organization of the United Nations. 1977. Guidelines for watershed management. FAO, UN, Rome. Food Agric. Organ. Conservation Guide 1.
- Freeze, R.A. 1967. The continuity between groundwater flow systems and flow in the unsaturated zone. Pages 205-240 in Nat. Res. Counc. Can. Soil Moisture. Proc. Hydrol Symp. 6.
- Freeze, R.A. 1969. The mechanism of natural ground-water recharge and discharge. 1. One-dimensional, vertical, unsteady, unsaturated flow above a recharging or discharging ground-water flow system. Water Resour. Res. 5(1): 153-171.
- Freeze, R.A. 1971. Three-dimensional, transient, saturated-unsaturated flow in a ground-water basin. Water Resour. Res. 7(2): 347-366.
- Freeze, R.A. 1972a. Role of subsurface flow in generating surface runoff. 1. Baseflow contributions to channel flow. Water Resour. Res. 8(3): 609-623.
- Freeze, R.A. 1972b. Role of subsurface flow in generating surface runoff. 2. Upstream source areas. Water Resour. Res. 8(5): 1272-1283.





- Freeze, R.A. 1974. Streamflow generation. *Rev. Geophys. Space Phys.* 12(4): 627-647.
- Freeze, R.A. and P.A. Witherspoon. 1966. Theoretical analysis of regional groundwater flow: 1. Analytical and numerical solutions to the mathematical model. *Water Resour. Res.* 2(4): 641-656.
- Geiger, R. 1950. The climate near the ground. Translated from German by M.N. Stewart, C.F. Brooks, F.A. Brooks, W.E. Howell, J.E. McDonald, and H.C.S. Thom. Harvard Univ. Press, Cambridge, Mass.
- Golding, D.L. 1977. Watershed treatment to alter snow accumulation and melt rates. Pages 237-255 in *Alberta Watershed Research Program Symposium Proceedings*. R.H. Swanson and P.A. Logan (eds.). Can. Dep. Fish Environ., Can. For. Serv., North. For. Res. Cent., Edmonton, Alberta. Inf. Rep. NOR-X-176.
- Green, R.E. and J. C. Corey. 1971. Calculation of hydraulic conductivity: a further evaluation of some predictive methods. *Soil Sci. Soc. Am. Proc.* 35(1): 3-8.
- Hanks, R.J. and S.A. Bowers. 1962. Numerical solution of the moisture flow equation for infiltration into layered soils. *Soil Sci. Soc. Am. Proc.* 26(6): 530-534.
- Hanks, R.J., A. Klute, and E. Bresler. 1969. A numeric method for estimating infiltration, redistribution, drainage, and evaporation from soil. *Water Resour. Res.* 5(5): 1064-1069.
- Hanson, W.R. (n.d.). Conserving a watershed. Eastern Rockies Forest Conservation Board, Calgary, Alberta.
- Harr, R.D. 1977. Water flux in soil and subsoil on a steep forested slope. *J. Hydrol.* 33(1-2): 37-58.
- Hewlett, J.D. 1961. Soil moisture as a source of base flow from steep mountain watersheds. U.S. For. Serv., Southeast. For. Exp. Stn. Pap. 132.
- Hewlett, J.D. 1974. Comments on letters relating to 'Role of subsurface flow in generating surface runoff, 2. Upstream source areas' by R. Allan Freeze. *Water Resour. Res.* 10(3): 605-608.
- Hewlett, J.D. and A.R. Hibbert. 1963. Moisture and energy conditions within a sloping soil mass during drainage. *J. Geophys. Res.* 68(4): 1081-1087.
- Hewlett, J.D. and A.R. Hibbert. 1967. Factors affecting the response of small watersheds to precipitation in humid



- areas. Pages 275-290 in Int. Symp. For. Hydrol. Proc., Penn. State Univ. Aug. 29-Sept. 10, 1965. W.E. Sopper and H.W. Lull (eds.). Pergamon Press. Oxford.
- Hewlett, J.D. and W.L. Nutter. 1969. An outline of forest hydrology. Univ. Georgia Press, Athens.
- Hewlett, J.D. and W.L. Nutter. 1970. The varying source area of streamflow from upland basins. Pages 65-83 in Interdisciplinary Aspects of Watershed Management. Proceedings of a symposium held Aug. 3-6. Montana State Univ., Bozeman, Montana. Am. Soc. Agric. Eng. and Am. Soc. Civ. Eng.
- Hibbert, A.R. 1967. Forest treatment effects on water yield. Pages 527-543 in Int. Symp. For. Hydrol. Proc., Penn. State Univ. Aug. 29-Sept. 10, 1965. W.E. Sopper and H.W. Lull (eds.). Pergamon Press, Oxford.
- Holtan, H.N., G.J. Stiltner, W.H. Henson, and N.C. Lopez. 1975. USDAHL-74 revised model of watershed hydrology. U.S. Dep. Agric. Hydrograph Laboratory, Beltsville, Maryland. Agric. Res. Serv. Tech. Bull. 1518.
- Hornberger, G.M., I. Remson, and A.A. Fungaroli. 1969. Numeric studies of a composite soil moisture ground-water system. Water Resour. Res. 5(4): 797-802.
- Horton, J.S. and C.J. Campbell. 1974. Management of phreatophyte and riparian vegetation for maximum multiple use values. USDA For. Serv., Rocky Mount. For. Range Exp. Stn., Fort Collins, Colorado. Res. Pap. RM-117.
- Horton, R.E. 1933. The role of infiltration in the hydrologic cycle. Trans., Am. Geophys. Union. 14: 446-460.
- Horton, R.E. 1936. Hydrologic interrelations of water and soil. Soil Sci. Soc. Am. Proc. 1: 401-429.
- Horton, R.E. 1945. Erosional development of streams and their drainage basins; hydrophysical approach to quantitative morphology. Geol. Soc. Am. Bull. 56(3): 275-370.
- Huff, D.D., R.J. Luxmore, J.B. Mankin, and C.L. Begovitch. 1977. TEHM: A terrestrial ecosystem hydrology model. Oak Ridge Nat. Lab., Environ. Sci. Div., Oak Ridge, Tennessee. Publ. 1019. EDFB/IBP - 76/8. ORNL/NSF/EATC -27.
- International Association of Scientific Hydrology and UNESCO. 1970. Results of research on representative and



- experimental basins. Symposium of Wellington, New Zealand. Dec. 1-8. Int. Assoc. Sci. Hydrol. Publ. 96.
- Jacob, C.E. 1940. On the flow of water in an elastic artesian aquifer. Trans., Am. Geophys. Union. 21: 574-586.
- Jacob, C.E. 1949. Flow of groundwater (Chapter V). Pages 321-386 in Engineering Hydraulics. H. Rouse (ed.). Proc. Fourth Hydraulics Conf., Iowa Institute of Hydraulic Research, June 12-15. John Wiley and Sons, Ltd., New York.
- Jaynes, R.A. 1978. A hydrologic model of aspen-conifer succession in the western United States. USDA For. Serv., Intermt. For. Range Exp. Stn., Ogden, Utah. Res. Pap. INT-213.
- Jeffrey, W.W. 1964. Watershed research in the Saskatchewan River headwaters. Pages 79-130 in Proceedings of the Fourth Hydrology Symposium on Research Watersheds. Ontario Agricultural College, Guelph.
- Jeffrey, W.W. 1965. Experimental watersheds in the Rocky Mountains, Alberta, Canada. Pages 502-521 in Symposium of Budapest, Hungary. Sept. 29-Oct. 5. Int. Assoc. Sci. Hydrol. Publ. 66.
- Jeffrey, W.W. 1969. Forest lands and their management: relevance to water resources. Paper presented at the National Conference on Forest Resource Problems, sponsored by the Science Council, Ottawa, Ontario. June 23-24.
- Kearney, T.H. and R.H. Peebles. 1951. Arizona flora. Calif. Univ. Press, Berkeley and Los Angeles. (Original not seen, cited by Horton and Campbell, 1974).
- Kinney, A. 1900. Forest and Water. The Post Publ. Co., Los Angeles, Calif.
- Kirkby, M.J. (ed.). 1978. Hillslope hydrology. Wiley and Sons, Ltd., New York.
- Kittredge, J. 1948. Forest Influences. McGraw-Hill Book Co., New York.
- Klute, A. 1952. A numerical method for solving the flow equation for water in unsaturated materials. Soil Sci. 73(2): 105-116.
- Kramer, P.J. 1969. Plant and soil water relationships: a modern synthesis. McGraw-Hill, Inc., New York.





- Krygier, J.T. and J.D. Hall (eds.). 1971. Forest land uses and stream environment. Proceedings of a symposium held at Oregon State Univ. Oct. 19-21, 1970.
- Leaf, C.F. 1975. Watershed management in the Rocky Mountain subalpine zone: the status of our knowledge. USDA For. Serv., Rocky Mount. For. Range Exp. Stn., Fort Collins, Colorado. Res. Pap. RM-137.
- Leaf, C.F. and R.R. Alexander. 1975. Simulating timber yields and hydrologic impacts resulting from timber harvest on subalpine watersheds. USDA For. Serv., Rocky Mount. For. Range Exp. Stn., Fort Collins, Colorado. Res. Pap. RM-133.
- Leaf, C.F. and G.E. Brink. 1972. Simulating effects of harvest cutting on snowmelt in Colorado subalpine forest. Pages 191-196 in Proc. Symp. Watersheds in Transition, held at Fort Collins, Colorado, June 19-22. S.C. Csallany, T.G. McLaughlin, and W.D. Striffler (eds.). Am. Water Resour. Assoc., Urbana, Illinois.
- Leaf, C.F. and G.E. Brink. 1973a. Computer simulation of snowmelt within a Colorado subalpine watershed. USDA For. Serv., Rocky Mount. For. Range Exp. Stn., Fort Collins, Colorado. Res. Pap. RM-99.
- Leaf, C.F. and G.E. Brink. 1973b. Hydrologic simulation model of Colorado subalpine forest. USDA For. Serv., Rocky Mount. For. Range Exp. Stn., Fort Collins, Colorado. Res. Pap. RM-107.
- Leaf, C.F. and G.E. Brink. 1975. Land use simulation model of the subalpine coniferous forest zone. USDA For. Serv., Rocky Mount. For. Range Exp. Stn., Fort Collins, Colorado. Res. Pap. RM-135.
- Linsley, R.K. 1976. Representative and experimental basins - where next? Hydrol. Sci. Bull. 21(4): 517-529.
- Linsley, R.K., M.A. Kohler, and J.L.H. Paulhus. 1958. Hydrology for engineers. McGraw-Hill Book Co., New York.
- Love, L.D. 1955. The effect on streamflow of the killing of spruce and pine by the Engelmann spruce beetle. Trans., Am. Geophys. Union 36(1): 113-118.
- Luthin, J.N. and P.R. Day. 1955. Lateral flow above a sloping water table. Soil Sci. Soc. Am. Proc. 19(4): 406-410.
- Martinec, J. 1975. Subsurface flow from snowmelt traced by tritium. Water Resour. Res. 11(3): 496-498.





- Megahan, W.F. 1972. Subsurface flow interception by a logging road in mountains of central Idaho. Pages 350-356 in Proc. Symp. Watersheds in Transition, held at Fort Collins, Colorado, June 19-22. S.C. Csallany, T.G. McLaughlin, and W.D. Striffler (eds.). Am. Water Resour. Assoc., Urbana, Illinois.
- Miller, E.E. and Klute, A. 1967. The dynamics of soil water. Part 1 - Mechanical forces. Pages 209-244 in Irrigation of Agricultural Lands. R.M. Hagan, H. R. Haise, and T.W. Edminster (eds.). Am. Soc. Agron., Wisconsin. Agronomy Monograph 11.
- Molchanov, A.A. 1960. The hydrological role of forests. Translated from Russian by A. Gourevitch, Israel Program for Scientific Translations, Jerusalem, 1963.
- Molz F.J. and I. Remson, 1970. Extraction term models of soil moisture use by transpiring plants. Water Resour. Res. 6(5): 1346-1356.
- Molz, F.J. and I. Remson, 1971. Application of an extraction-term model to the study of moisture flow to plant roots. Agron. J. 63(1): 72-77.
- Molz, F.J., I. Remson, A.A. Fungaroli, and R.L. Drake. 1968. Soil moisture availability for transpiration. Water Resour. Res. 4(6): 1161-1169.
- Moore, R.E. 1939. Water conduction from shallow water tables. Hilgardia 12: 383-401.
- Mosley, M.P. 1979. Streamflow generation in a forested watershed, New Zealand. Water Resour. Res. 15(4): 795-806.
- Neuman, S.P. 1973. Saturated-unsaturated seepage by finite elements. J. Hydraul. Div., Am. Soc. Civ. Eng. Proc. 99(HY12): 2233-2250.
- Niklas, K.J. 1977. Applications of finite element analyses to problems in plant morphology. Ann. Bot. 41(171): 133-153.
- Northwest Hydraulic Consultants Ltd; Hyat Resource Services Ltd., Edmonton, Alberta. 1977. Watershed management for increased water yield. Report submitted to Oldman River Basin Study Management Committee.
- Philip, J.R. 1957. The theory of infiltration: 1 The infiltration equation and its solution. Soil Sci. 83(5): 345-357.
- Pinder, G.F. and J.D. Bredehoeft. 1968. Application of the



digital computer for aquifer evaluation. Water Resour. Res. 4(5): 1069-1093.

Pinder, G.F. and W.G. Gray. 1977. Finite element simulation in surface and subsurface hydrology. Academic Press, New York.

Plamondon, P.A., T.A. Black, and B.C. Goodell. 1972. Hydrologic properties of the forest floor. Pages 341-348 in Proc. Symp. Watersheds in Transition, held at Fort Collins, Colorado, June 19-22. S.C. Csallany, T.G. McLaughlin, and W.D. Striffler (eds.). Am. Water Resour. Assoc., Urbana, Illinois.

Ragan, R.M. 1968. An experimental investigation of partial area contributions. Pages 241-249 in General Assembly of Bern. Int. Assoc. of Sci. Hydrol. Publ. 76.

Rakhmanov, V.V. 1962. Role of forests in water conservation. Translated from Russian by A. Gourevitch and L.M. Hughes, Israel Program for Scientific Translations, Jerusalem, 1966.

Rakhmanov, V.V. 1970a. Dependence of streamflow upon the percentage of forest cover of catchments. Pages 55-64 in Proceedings of the joint FAO/USSR International Symposium on Forest Influences and Watershed Management, held in Moscow, USSR, Aug. 17-Sept. 6. E. Talât and E.G. Dunford (eds.).

Rakhmanov, V.V. 1970b. Effect of forest on runoff in the Upper Volga Basin. Pages 187-204 in Proceedings of the joint FAO/USSR International Symposium on Forest Influences and Watershed Management, held in Moscow, USSR, Aug. 17-Sept. 6. E. Talât and E.G. Dunford (eds.).

Redmond, D.R. 1964. Organization of Inter-Agency watershed research programs for Canada. Pages 299-304 in Proceedings of the Fourth Hydrology Symposium on Research Watersheds. Ontario Agricultural College, Guelph.

Remson, I., C.A. Appel, and R.A. Webster. 1965. Groundwater models solved by digital computer. J. Hydraul. Div., Am. Soc. Civ. Eng. Proc. 91(HY3): 133-147.

Remson, I., G.M. Hornberger, and F.J. Molz. 1971. Numerical methods in subsurface hydrology. Wiley-Interscience, New York.

Richards, L.A. 1931. Capillary conduction of liquids through porous mediums. Physics I: 318-333. (Original not seen, cited by Philip, 1957).



- Rockwood, D.M. 1958. Columbia Basin streamflow routing by computer. J. Waterways Harbors Div., Am. Soc. Civ. Eng. Proc. 84(WW5): 1874-1 to 1874-15.
- Rockwood, D.M. 1961. Columbia Basin streamflow routing by computer. Trans., Am. Soc. Civ. Eng. Pap. 3119: 126(32-56).
- Rockwood, D.M. 1968. Application of Streamflow Synthesis and Reservoir Regulation (SSARR) Program to the Lower Mekong River. In The Use of Analog and Digital Computers in Hydrology. Published jointly by Int. Assoc. Sci. Hydrol., Gentbrugge, Belgium and UNESCO, Paris. (Original not seen, cited by U.S. Army Corps of Engineers, 1971).
- Rodarte, L. 1978. Application of the finite element method to the numerical analysis of a leaky aquifer. Pages 1.3-1.18 in Finite Elements in Water Resources, Proceedings of the Second International Conference on Finite Elements in Water Resources. C.A. Brebbia, W.G. Gray, and G.F. Pinder (eds.). Imperial College, London.
- Rubin, J. 1967. Numerical method for analyzing hysteresis-affected, post-infiltration redistribution of soil moisture. Soil Sci. Soc. Am. Proc. 31(1): 13-20.
- Rubin, J. 1968. Theoretical analysis of two-dimensional, transient flow of water in unsaturated and partly unsaturated soils. Soil Sci. Soc. Am. Proc. 32(5): 607-615.
- Rubin, J. and R. Steinhardt. 1963. Soil water relations during rain infiltration: I. Theory. Soil Sci. Soc. Am. Proc. 27(3): 246-251.
- Satterlund, D.R. 1972. Wildland watershed management. Ronald Press Co., New York.
- Scholl, D. G. and A. R. Hibbert. 1973. Unsaturated flow properties used to predict outflow and evapotranspiration from a sloping lysimeter. Water Resour. Res. 9(6): 1645-1655.
- Sklash, M.G. and R.N. Farvolden. 1979. The role of groundwater in storm runoff. In Contemporary Hydrogeology: The George Burke Maxey Memorial Volume. W. Back and D.A. Stephenson (guest eds.). J. Hydrol. 43(1-4): 45-65.
- Sklash, M.G., R.N. Farvolden, and P. Fritz. 1976. A conceptual model of watershed response to rainfall, developed through the use of oxygen-18 as a natural tracer. Can. J. Earth Sci. 13(2): 271-283.





- Society of American Foresters. 1958. Forestry terminology: A glossary of technical terms used in forestry. Soc. Am. For., Washington, D.C.
- Society of American Foresters and Oregon State University. 1963. Forest watershed management. Symposium held March 25-28 at Oregon State Univ., Corvallis, Oregon.
- Society of American Foresters and Oregon State University. 1966. Practical aspects of watershed management. Proc. Symposium held March 29-30 at Oregon State Univ., Corvallis, Oregon.
- Sopper, W.E. 1971. Watershed management - water supply augmentation by watershed management in wildland areas. Report (NWC71-008) prepared for National Water Commission, Arlington, Virginia.
- Sopper, W.E. and H.W. Lull (eds.). 1967. Forest Hydrology. Proceedings, Symposium held at Penn. State Univ. Pennsylvania, Aug. 29-Sept. 10, 1965. Pergamon Press, Oxford.
- Stephenson, G.R. and R.A. Freeze. 1974. Mathematical simulation of subsurface flow contributions to snowmelt runoff, Reynolds Creek Watershed, Idaho. Water Resour. Res. 10(2): 284-294.
- Swanson, R.H. 1977. The Alberta Watershed Research Program, 1959-1977. Pages 4-20 in Alberta Watershed Research Program Symposium Proceedings. R.H. Swanson and P.A. Logan (eds.). Can. Dep. Fish. Environ., Can. For. Serv., North For. Res. Cent., Edmonton, Alberta. Inf. Rep. NOR-X-176.
- Swanson, R.H. and G.R. Hillman. 1977. Predicted increased water yield after clear-cutting verified in west-central Alberta. Can. Dep. Fish. Environ., Can. For. Serv., North. For. Res. Cent., Edmonton, Alberta. Inf. Rep. NOR-X-198.
- Swift, L.W., W.T. Swank, J.B. Mankin, R.J. Luxmore, and R.A. Goldstein. 1975. Simulation of evapotranspiration and drainage from mature and clearcut deciduous forests and young pine plantation. Water Resour. Res. 11(5): 667-673.
- Talât, E. and E.G. Dunford (eds.). 1970. Forest influences and watershed management. Proceedings of the joint FAO/USSR International Symposium held in Moscow, USSR., Aug. 17-Sept. 6.
- Taylor, G.S. and J.N. Luthin. 1969. Computer methods for transient analysis of water-table aquifers. Water





Resour. Res. 5(1): 144-152.

- Theis, C.V. 1935. The relation between the lowering of the piezometric surface and the rate and duration of discharge of a well using groundwater storage. Trans., Am. Geophys. Union 16: 519-524.
- Thiem, A. 1906. Hydrologische Methoden: Leipzig, Gebhardt. (Original not seen, cited by Davis and DeWiest, 1966).
- Trescott, P.C., G.F. Pinder, and J.F. Jones. 1970. Digital model of alluvial aquifer. J. Hydraul. Div., Am. Soc. Civ. Eng. Proc. 96(HY5): 1115-1128.
- Troendle, C.A. 1970. Subsurface flow on steep-sloped forested soils. Part I: The nature and occurrence of subsurface storm flow. Progress report 4300-FS-NE-1602-19, Northeast Forest Experiment Station, Parsons, West Virginia.
- Troendle, C.A. 1979. A variable source area model for stormflow prediction on first order forested watersheds. Unpubl. Ph.D. Thesis. Univ. Georgia.
- U.S. Army Corps of Engineers. 1971. Runoff evaluation and streamflow simulation by computer. U.S. Army Corps of Engineers, North Pacific Division, Portland, Oregon.
- U.S. Forest Service. 1974. Forest Hydrology, Part II Hydrologic effects of vegetation. U.S. Government Printing Office, Washington, D.C.
- Veihmeyer, F.J. and A.H. Hendrickson. 1938. Soil moisture as an indication of root distribution in deciduous orchards. Plant Physiol. 13(1): 169-177.
- Verma, R.D. and W. Brutsaert. 1970. Unconfined aquifer seepage by capillary flow theory. J. Hydraul. Div., Am. Soc. Civ. Eng. Proc. 96(HY6): 1331-1344.
- Wang, F.C. and V. Lakshminarayana. 1968. Mathematical simulation of water movement through unsaturated nonhomogeneous soils. Soil Sci. Soc. Am. Proc. 32(3): 329-334.
- Weyman, D.R. 1973. Measurements of the downslope flow of water in a soil. J. Hydrol. 20(3): 267-288.
- Whipkey, R.Z. 1965. Subsurface stormflow from forested slopes. Hydrol. Sci. Bull. 10(2): 74-85.



Whisler, E.D. and A. Klute. 1965. The numerical analysis of infiltration, considering hysteresis, into a vertical soil column at equilibrium under gravity. Soil Sci. Soc. Am. Proc. 29(5): 489-494.



## VIII APPENDICES



## VIII. APPENDICES

### A. Appendix A. Development Of Coordinate Functions Using Area Coordinates For Triangular Elements And Integration Of Resulting Expressions

Figure A1 is a triangular finite element of area  $A$ , with nodes at  $i$ ,  $j$ , and  $k$ .

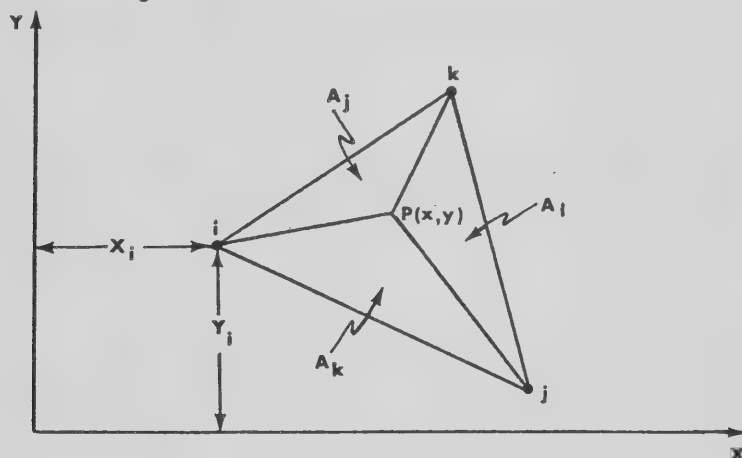


Figure A1. Linear triangular finite element and development of area coordinates.

Point  $P(x, y)$ , which can be any point in the triangle, marks the apices of three subtriangles of areas  $A_i$ ,  $A_j$ , and  $A_k$  such that  $A_i + A_j + A_k = A$ . The triangular area coordinates of  $P(x, y)$  are defined as  $L_i = A_i/A$ ,  $L_j = A_j/A$ ,  $L_k = A_k/A$ , and consequently  $L_i + L_j + L_k = 1$ . Furthermore at node  $i$ ,  $L_i = 1$  and  $L_j = L_k = 0$ . Similar properties hold at nodes  $j$  and  $k$  also and meet the requirements for defining coordinate functions.

The area of a triangle can be defined as half the cross-product of two adjacent sides. Consequently, it can be expressed in terms of the triangular coordinates as a





determinant of a 3x3 matrix

$$2A = \begin{vmatrix} 1 & x_i & y_i \\ 1 & x_j & y_j \\ 1 & x_k & y_k \end{vmatrix} = (x_j y_k - x_k y_j) - (y_k - y_j)x_i + (x_k - x_j)y_i$$

or

$$2A = x_j y_k - x_k y_j + x_i (y_j - y_k) + y_i (x_k - x_j) \quad (A1)$$

Similarly, the areas of the subtriangles may be written (proceeding in a counterclockwise direction) as

$$2A_i = \begin{vmatrix} 1 & x & y \\ 1 & x_j & y_j \\ 1 & x_k & y_k \end{vmatrix}; \quad 2A_j = \begin{vmatrix} 1 & x & y \\ 1 & x_k & y_k \\ 1 & x_i & y_i \end{vmatrix}; \quad 2A_k = \begin{vmatrix} 1 & x & y \\ 1 & x_i & y_i \\ 1 & x_j & y_j \end{vmatrix}$$

or

$$2A_i = (x_j y_k - x_k y_j) + x(y_j - y_k) + y(x_k - x_j) \quad (A2.1)$$

$$2A_j = (x_k y_i - x_i y_k) + x(y_k - y_i) + y(x_i - x_k) \quad (A2.2)$$

$$2A_k = (x_i y_j - x_j y_i) + x(y_i - y_j) + y(x_j - x_i) \quad (A2.3)$$

Since  $L_i = A_i/A$ ,  $L_j = A_j/A$ , and  $L_k = A_k/A$ , the triangular coordinates become

$$L_i = [(x_j y_k - x_k y_j) + x(y_j - y_k) + y(x_k - x_j)]/2A \quad (A3.1)$$

$$L_j = [(x_k y_i - x_i y_k) + x(y_k - y_i) + y(x_i - x_k)]/2A \quad (A3.2)$$

$$L_k = [(x_i y_j - x_j y_i) + x(y_i - y_j) + y(x_j - x_i)]/2A \quad (A3.3)$$



These expressions may also be obtained by generating coordinate functions using global coordinates. One equation which describes a plane over a linear triangular element is

$$\phi_i = a_i + b_i x + c_i y \quad (A4)$$

where  $a_i$ ,  $b_i$ , and  $c_i$  are constants identified with the  $i$ th coordinate function. Given this definition of a coordinate function, together with the prescribed constraints, the following set of equations for the  $i$ th coordinate function is obtained

$$\begin{Bmatrix} \phi_i(x_i, y_i) \\ \phi_j(x_j, y_j) \\ \phi_k(x_k, y_k) \end{Bmatrix} = \begin{Bmatrix} 1 \\ 0 \\ 0 \end{Bmatrix} = \begin{bmatrix} 1 & x_i & y_i \\ 1 & x_j & y_j \\ 1 & x_k & y_k \end{bmatrix} \begin{Bmatrix} a_i \\ b_i \\ c_i \end{Bmatrix}$$

The determinant of the 3x3 matrix is

$$(x_j y_k - x_k y_j) + (y_j - y_k)x_i + (x_k - x_j)y_i$$

which, as stated earlier, is equal to  $2A$ . The solutions  $a_i$ ,  $b_i$ , and  $c_i$  are derived from the expressions

$$2Aa_i = \begin{vmatrix} 1 & x_j & y_j \\ 0 & x_k & y_k \\ 0 & x_i & y_i \end{vmatrix} = (x_j y_k - x_k y_j)$$

$$2Ab_i = \begin{vmatrix} 1 & 1 & y_i \\ 1 & 0 & y_j \\ 1 & 0 & y_k \end{vmatrix} = (y_j - y_k)$$



$$2Ac_i = \begin{vmatrix} 1 & x_i & 1 \\ 1 & x_j & 0 \\ 1 & x_k & 0 \end{vmatrix} = (x_k - x_j)$$

Thus equation A4 becomes

$$\phi_i = [(x_j y_k - x_k y_j) + (y_j - y_k)x + (x_k - x_j)y] / 2A$$

which is identical to equation A3.1. Similar identities hold between  $\phi_j$  and  $L_j$ , and between  $\phi_k$  and  $L_k$ .

Having established the relationship between  $\phi$  and  $L$ , we can proceed to the integration problem

$$\int_A f(\phi_i, \phi_j, \phi_k) dA = \int_A f(L_i, L_j, L_k) dA \quad (A5)$$

The integration on the right hand side is easily performed if  $dA$  is expressed in local coordinates. This can be accomplished by using the relation

$$dL_i dL_j = |J| dA$$

where  $|J|$  is the determinant of the Jacobian matrix

$$[J] = \begin{bmatrix} \partial L_i / \partial x & \partial L_j / \partial x \\ \partial L_i / \partial y & \partial L_j / \partial y \end{bmatrix} = \begin{bmatrix} (y_j - y_k) / 2A & (y_k - y_i) / 2A \\ (x_k - x_j) / 2A & (x_i - x_k) / 2A \end{bmatrix}$$

Therefore  $|J|$  is

$$[(y_j - y_k)(x_i - x_k) - (x_k - x_j)(y_k - y_i)] / 4A^2$$



$$= [(x_j y_k - x_k y_j) + x_i (y_j - y_k) + y_i (x_k - x_j)] / 4A^2 = 1/2A, \text{ and}$$

$$dA = 2AdL_i dL_j$$

Equation A5 can now be written as

$$\begin{aligned} \int_A f(\phi_i, \phi_j) dA &= 2A \int_{L_j} \int_{L_i} f(\phi_i, \phi_j) dL_i dL_j \\ &= 2A \int_{L_j=0}^{L_j=1} \int_{L_i=0}^{L_i=1-L_j} f(L_i, L_j) dL_i dL_j \end{aligned}$$

and it is a relatively simple matter to compute the six types of integrals that appear in the simulation model

$$\int_A L_l^2 dA \quad (l=i, j, k) \quad (A6.1)$$

$$\int_A L_l L_m dA \quad (l=i, j, k; m=i, j, k; l \neq m) \quad (A6.2)$$

$$\int_A \frac{\partial L_i}{\partial x}, \frac{\partial L_j}{\partial x} dA \quad (A6.3)$$

$$\int_A \frac{\partial L_i}{\partial y}, \frac{\partial L_j}{\partial y} dA \quad (A6.4)$$

$$\int_A \frac{\partial L_i}{\partial x}, \frac{\partial L_j}{\partial y} dA \quad (A6.5)$$

$$\int_A \frac{\partial L_j}{\partial x}, \frac{\partial L_i}{\partial y} dA \quad (A6.6)$$





## B. Appendix B. Program SUBFEM - User's Manual

The model developed to meet the objectives of this study is called the Subsurface Flow Finite Element Model (SUBFEM). The computer program, also called SUBFEM, is written in FORTRAN, and is run on the Amdahl 470V/8 computer at the University of Alberta. Metric units are used throughout. The computer code is listed in Appendix C.

The first step toward solving the subsurface flow problem is to define it. Since the model is limited to two-dimensional systems, we are restricted to profiles such as those illustrated in figure 10, and must consider the factors outlined in Chapter III of this treatise.

A triangular, finite element mesh is constructed to fit the profile. It may be regular (with elements of the same size) except near some boundaries, or it may be designed so that smaller elements are located in regions where marked changes in water content and pressure potential are likely to occur, i.e. near the upper boundary and the seepage face. Conversely, large elements can be used where such changes are expected to be minimal, e.g. in the vicinity of the basal, no-flow boundary. Once the mesh has been constructed, the nodes are automatically defined since they are located at the vertices of the triangles.

For computational efficiency, the nodes should be numbered in the direction of shortest side. In most hillslope simulations, this will be in the vertical direction, since the profile being simulated is usually much



longer than it is deep. Several examples of finite element grids are given in Chapter V.

Initial and boundary conditions must also be specified. Initially, some assumed or given pressure potential values are assigned to each node, thereby establishing initial conditions. Three boundary conditions are considered in SUBFEM: no-flow, flux, and seepage face. The no-flow boundary conditions are applicable to the impermeable boundaries, while the flux boundary conditions are usually restricted to the upper boundary. Positive fluxes such as rainfall and snowmelt, and negative fluxes such as evaporation, are treated in the same manner. Flux values are calculated, and assigned to individual flux boundary nodes (Fig. A2).

It is also necessary to specify the maximum extent of the seepage face, even though an unsaturated flow problem is being simulated, or though the extent of the seepage face at the beginning of the simulation is less than maximum.

Water withdrawal through transpiration is computed as a rate, using the same method employed to compute the fluxes. Here, however, the values are assigned to subsurface sink nodes, rather than to boundary nodes.

Information is required on each soil or other material that appears in the simulation. First, the saturated hydraulic conductivity as obtained in the field or in the laboratory; and secondly, the relation between volumetric soil water content and pressure potential. In the latter case, a single-valued, rather than a hysteretic, function is



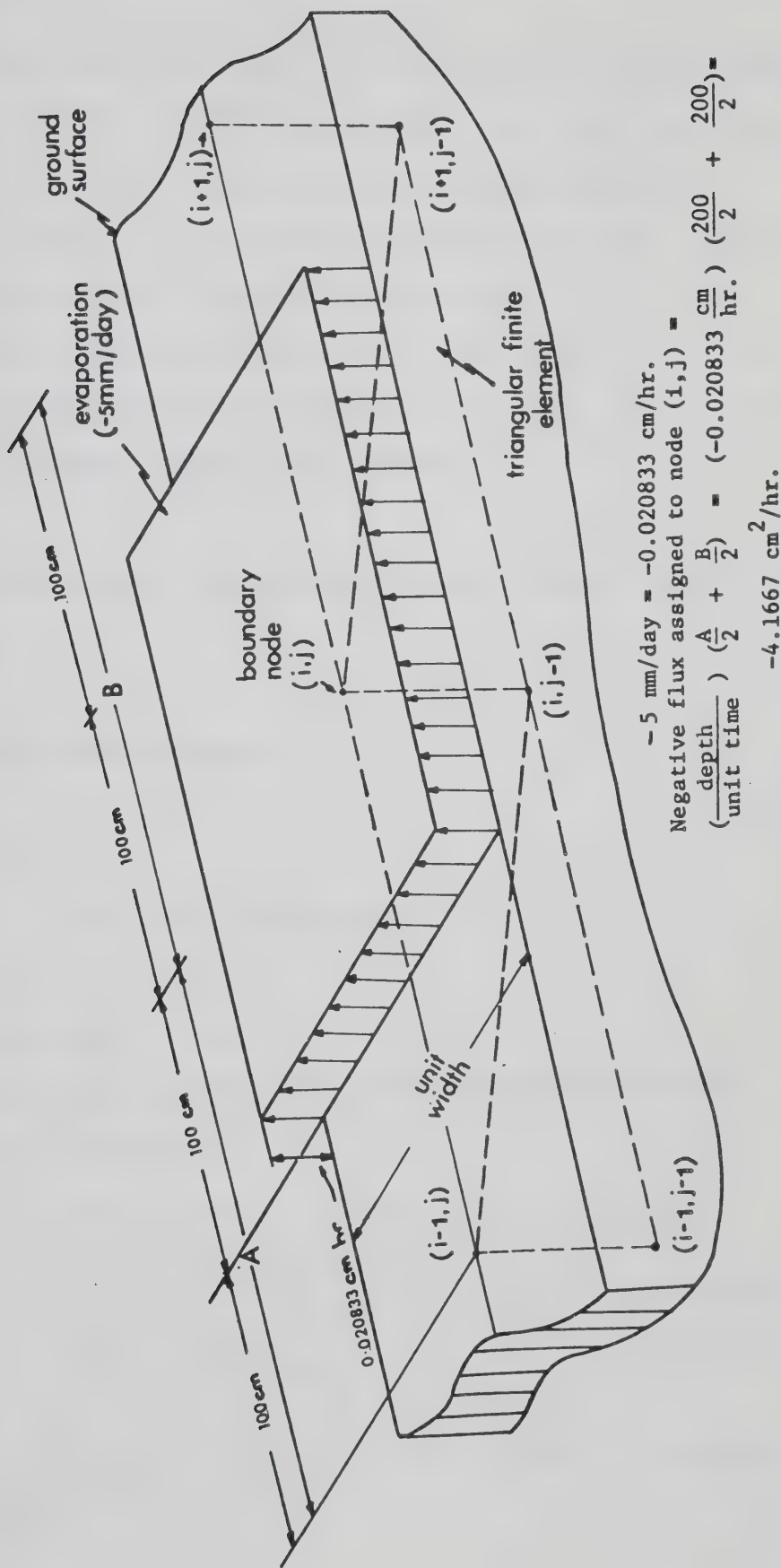


Figure A2. Procedure for computing flux at each boundary node.



assumed.

Input data are read in by five subroutines: INPUT1, HYCOND, INPUT3, INPUT4, and BOUND. The input data required for each of these subroutines, together with the identification of variable and parameter names, and the specified FORMATS, are described below.

Input data for cards A to L are stored in a file assigned to logical unit #5; they are read in subroutines INPUT1, HYCOND, INPUT3, and INPUT4.

Subroutine INPUT1 reads control data (cards A and B) for the system.

#### A. Heading Card(1 card)

HED

FORMAT(20A4)

HED :Title of the problem.

#### B. System Card (1 card)

NSUB,MXND,NUMNST,MASTR,MBEL,IDRY,NS,NC,DELT,NTRANS

FORMAT(8I4,F10.5,I4)

NSUB	:Total number of subsystems. (Insert 1)
MXND <sup>6</sup>	:Maximum number of inter-boundary nodes in any subsystem. (Insert 0)
NUMNST	:Total number of nodes in the master system.
MASTR <sup>6</sup>	:Flag for master matrix. (Insert 1)
MBEL <sup>6</sup>	:Total number of external boundary elements attached to master system. (Insert 0)
IDRY <sup>6</sup>	:If 1, this is a dry run.(Insert 1)
	:If 0, this is a production run.
NS	:Number of materials (soil types, geological

-----  
<sup>6</sup>Redundant





formations, etc.).

NC :Number of incremented pore classes used to compute hydraulic conductivity and specific moisture capacity.

DELT :Time step size.

NTRANS :If 1, this is a transient problem.  
If 0, this is a steady state problem.

Subroutine HYCOND reads in cards C to G.

#### C. Material Description Card (1 card)

ST,ST1,ST2,ST3,ST4,ST5,ST6,ST7,ST8,ST9

FORMAT(10A8)

ST1,ST2,...ST9 :Name of material (soil, rock, or till type).

#### D. Material Properties Card (1 card)

INP,TMAX,SCON,SCONR,RESWAT

FORMAT(I5,F10.4,2E15.5,F5.3)

INP :Number of input data points for the water content/pressure (characteristic) curve - limited to 20 points with present format.

TMAX :Maximum water content (dimensionless)

SCON :Experimentally obtained saturated hydraulic conductivity (cm/unit time)

SCONR :Ratio of saturated horizontal hydraulic conductivity to saturated vertical hydraulic conductivity (dimensionless).

RESWAT :Estimate of residual (immobile) water (dimensionless).

#### E. Water Properties Card (1 card)

SURTEN,DENWAT,VISWAT,TEMP,GRAVITY

FORMAT(F10.6,F10.3,F12.8,2F5.1)

SURTEN :Surface tension of water (dynes/cm).

DENWAT :Density of water ( $\text{g/cm}^3$ ).

VISWAT :Viscosity of water ( $\text{dyne sec/cm}^2$ ).

TEMP :Water temperature (C).



GRAVITY :Gravitational constant ( $\text{cm/sec}^2$ ).

F. Characteristic Curve (Water Content) Card (1 card)

THETA(1),THETA(2),... ...,THETA(INP)

FORMAT(20F4.3)

THETA(1) :Data point with lowest water content  
(dimensionless).

THETA(INP) :Data point with highest water content  
(dimensionless).

G. Characteristic Curve (Pressure) Card(s) (1 to 3 cards)

DP(1),DP(2),... ...,DP(INP)

FORMAT(8F10.2)

DP(1) :Pressure potential that corresponds to THETA(1),  
and which has the highest absolute value (cm).

DP(INP) :Pressure potential that corresponds to  
THETA(INP), and which has the lowest absolute  
value (cm).

A set of cards C to G must be included for each of NS  
materials (soils or geologic strata).

Subroutine INPUT3 reads additional control data for the  
system.

H. Control Data Card (1 card)

IS,NNODE,NEL,NSTEP,IMAX,E,SLOPE,NFIBN,NIBNS,NSEEP

FORMAT(5I4,2E12.5,3I4)

IS :Subsystem number.

NNODE :Number of nodes in the system.

NEL :Number of elements in the system.

NSTEP :Number of time steps.

IMAX :Maximum number of iterations per time step.



E :Specified difference criterion for iterations (cm).  
 SLOPE :Hillside slope (degrees).  
 NFIBN :Local number of first inter-boundary node.  
 NIBNS :Number of inter-boundary nodes.  
 NSEEP :Number of seepage face nodes.

Subroutine INPUT4 reads and writes the nodal and element data, together with initial pressure potential.

#### I. Nodal Geometry Cards (1 card per node)

N,X(N),Z(N)

FORMAT(I6,2F12.2)

N :Node number.  
 X(N) :X coordinate of node.  
 Z(N) :Z coordinate of node.

#### Notes:

- 1)Nodal data cards must be entered in numerical order. If nodes are omitted then the program generates coordinates for intermediate nodal points.
- 2)For constant pressure potential nodes, pressure potential( $\psi$ ) values are known, and the matrices are partitioned so that equations for these nodes are eliminated. Boundary condition information related to these nodes is transferred to the known matrix.

#### J. Initial Pressure Potential Card (1 or more cards)

H(1),H(2),... ...,H(NNODE)

FORMAT(10F8.2)

H(I) :Initial pressure potential at node I

#### K. Material Identity Card (1 or more cards)

MATL(1),MATL(2),... ...,MATL(NNODE)

FORMAT(40I2)



MATL(I) :Code number for material (soil, till, sandstone,  
etc.) at node I.

#### L. Element Data Cards (1 card per element)

M,NP(1,M),NP(2,M),NP(3,M)

FORMAT(4I6)

M :Element number.

NP(I,M) :Nodal point numbers at the three corners of  
the triangular element in counterclockwise order.

#### Note:

Element cards must be in order. If element numbers are omitted, the program generates the intermediate element data.

Data for cards M to V are stored in a file assigned to logical unit #7; they are read in subroutine BOUND.

#### M. New Boundary Conditions Card (1 card)

NEWBC

FORMAT(I3)

NEWBC :Number of times boundary conditions change.

#### N. Boundary Conditions, Time-of-change Card (1 card)

KSTNO(1),KSTNO(2),... ...,KSTNO(NEWBC)

FORMAT(25I3)

KSTNO(1) :Number of time step during which first  
change in boundary conditions occurs.

KSTNO(NEWBC) :Number of time step during which last  
change in boundary conditions occurs.

#### O. Seepage Face Nodes Card (1 card)





NSPF(1),NSPF(2),... ...,NSPF(NSEEP)

FORMAT(25I3)

NSPF(1) :Nodal number of first seepage face node.  
 NSPF(NSEEP) :Nodal number of last seepage face node.

Note:

If there is no outflow at the beginning of a simulation, this card is omitted.

#### P. Specialized Nodes Identification Card (1 card)

NEUM,NFLUX,NSINK,NDIR

FORMAT(4I5)

NEUM :Total number of no-flow boundary nodes.  
 NFLUX :Total number of flux boundary nodes.  
 NSINK :Total number of sinks.  
 NDIR :Total number of Dirichlet (constant pressure potential) boundary nodes.

#### Q. Boundary Conditions and Sinks Card#1 (1 to 3 cards)

BYCD(1),BYCD(2),... ...,BYCD(20)

FORMAT(8E10.3)

BYCD(1),... ...,BYCD(5):Flux values to be assigned to flux boundary nodes<sup>7</sup>  
 BYCD(6),... ...,BYCD(10):Withdrawal rates to be assigned to sink nodes<sup>7</sup>.  
 BYCD(11),... ...,BYCD(20):Pressure potential values to be assigned to constant pressure potential (Dirichlet) nodes<sup>7</sup>.

Note:

One BYCD value may be assigned to several boundary (or sink) nodes.

#### R. Boundary Conditions and Sinks Card#2 (1 card)

NBC(1),NBC(2),... ...,NBC(20)

-----

<sup>7</sup>Identified on cards T through V.



FORMAT(20I4)

NBC(KZ):Cumulative number of nodes to which values BYCD(KZ) must be assigned.

NBC(1),... ...,NBC(5):Flux nodes.

NBC(6),... ...,NBC(10):Sink nodes.

NBC(11),... ...,NBC(20):Constant pressure potential (Dirichlet) nodes.

Example: If BYCD(1)=20.0, BYCD(2)=40.0, BYCD(3)=50.0, and NBC(1)=5, NBC(2)=8, and NBC(3)=18, then the value 20.0 is assigned to the first 5 flux nodes, the value 40.0 to the next 3 (8 minus 5) flux nodes, and the value 50.0 to the next 10 (18 minus 8) flux nodes.

S. No-flow Boundary Nodes - Identification Cards (1 or more cards)

NBOUND(1),NBOUND(2),... ...,NBOUND(NEUM)

FORMAT(20I4)

NBOUND(1) :Number of first no-flow boundary node.

NBOUND(NEUM) :Number of last no-flow boundary node.

T. Flux Nodes - Identification Cards (1 or more cards)

NBOUND(1),NBOUND(2),... ...,NBOUND(NFLUX)

FORMAT(20I4)

NBOUND(1) :Number of first flux boundary node.

NBOUND(NFLUX) :Number of last flux boundary node.

U. Sink nodes - Identification Cards (1 or more cards)

NBOUND(1),NBOUND(2),... ...,NBOUND(NSINK)

FORMAT(20I4)

NBOUND(1) :Number of first sink node.

NBOUND(NSINK) :Number of last sink node.



V. Dirichlet (Constant Pressure Potential) Nodes -  
 Identification Cards (1 or more cards)

NBOUND(1),NBOUND(2),... ...,NBOUND(NDIR)

FORMAT(20I4)

NBOUND(1) :Number of first Dirichlet boundary node.  
 NBOUND(NDIR) :Number of last Dirichlet boundary node.

An example of a complete set of input data for SUBFEM is listed in Appendix D.

Subroutines HYCOND and TABLOK are used to compute hydraulic conductivity and specific moisture capacity, as a function of pressure potential, for each material in the system. The hydraulic conductivity is calculated using a program developed by Green and Corey (1971). This computational procedure is based on knowledge of saturated hydraulic conductivity, and on the relation between unsaturated hydraulic conductivity and pore-size distribution. TABLOK is adapted from the subroutine of the same name used in the TEHM model (Huff et al, 1977).

Subroutine GMATX solves the integral equations and forms the element matrices. It subsequently assembles contributions from each element matrix into the global matrices [A] and [B]/ $\Delta t$ . Finally it produces the terms [A]+[B]/ $\Delta t$  and [B]{P}/ $\Delta t$ .

The boundary conditions are handled by subroutine BOUND. It assigns values to the flux and sink nodes, and partitions from the global matrix the equations for the



constant pressure potential nodes.

Subroutine SKYLIN locates the first non-zero element in each column of the global matrix, and eliminates all the zero elements above that element. This procedure improves storage efficiency. SKYLIN also keeps account of column lengths and the locations of the diagonal elements in the modified matrix array.

Decomposition of the global matrix using Cholesky's method is instituted in subroutine DECOMP. Backsubstitution to obtain the solutions to the specified problem is carried out in subroutine BKSB1.

Fluxes are computed in subroutine FLUX. This subroutine also determines the extent of the seepage face and the outflow from it.

Subroutine ITERAT controls the iteration process and prints out the results at the end of each time step. Results include the fluxes, the pressure potential field, the number of iterations completed during the time step, and a measure of convergence.

Subroutine XPLOT stores into a file (assigned to logical unit #8) for plotting purposes, information pertaining to the final time step. Data stored for each node include: the coordinates, pressure potential, total potential, volumetric water content, and the hydraulic conductivity.

Plotting is done on the AED 512 colour graphics terminal, using the IGPLSD integrated graphics subroutine.





This arrangement permits three-dimensional display of data, and facilitates data manipulation for plotting purposes.

Hardcopy is obtained from the University of Alberta's

CalComp 925/1036 plotter.



## C. Appendix C. Program SUBFEM - Computer Code

```

SUBFEM
1  C SUBSYSTEM ANALYSIS OF FLOW THROUGH POROUS MEDIA,
2  C THE EQUATION SOLVER IS OF SKYLINE IN-CORE TYPE.
3  C*****
4      IMPLICIT REAL*8(A-H,O-Z)
5      REAL*8 NAMES
6  C
7      COMMON /MASTIA/ NNN(1000)
8      COMMON /MASTRA/ BBB(1000)
9      COMMON /SUBIA/  MMM(3500)
10     COMMON /SUBRA/  AAA(85000)
11     COMMON /SUBSR/  CCC(4000)
12     COMMON /DIMCOM/ L1,L2,L3,L4,L5,MXDM,NAMES(5,20),IPT(5,21),
13     *ICOM(5)
14  C
15     ICOM(1)=1000
16     ICOM(2)=1000
17     ICOM(3)=85000
18     ICOM(4)=3500
19     ICOM(5)=4000
20  C
21     CALL MAINMG
22  C
23     END
24  C
25  C
26  C
27  C
28  C
29     SUBROUTINE MAINMG
30  C  THIS SUBROUTINE MANAGES THE READING, THE FORMULATION,
31  C  AND THE SOLUTION OF THE PROBLEM.
32  C
33  C*****
34     IMPLICIT REAL*8(A-H,O-Z)
35     REAL*8 NAMES,NAME,KZZ,KRATIO
36  C
37     COMMON /BORDER/  NEUM,NDIR,KFLAG,NBOUND(60)
38     COMMON /HILL/    SLOPE,COS1,COS2,SIN1,SIN2
39     COMMON /MASTIV/  NSUB,MXND,NUMNST,MASTR,MBEL,IDRY,IN,IO,DELT,NTRANS
40     COMMON /MASTIA/  NNN(1000)
41     COMMON /MASTRA/  BBB(1000)
42     COMMON /SUBIV/   IS,NNODE,NEL,ITTER,NEBEL,NFIBN,NIBNS,NSEEP,NTEMP
43     COMMON /SUBIA/   MMM(3500)
44     COMMON /SUBRA/   AAA(85000)
45     COMMON /SUBSR/   CCC(4000)
46     COMMON/HOOKUP/NS,NC,RESWAT
47     COMMON /DIMCOM/  LA1,LA2,LA3,LA4,LA5,MXDIM,NAMES(5,20),
48     *IPT(5,21),ICOM(5)
49  C
50  C*****
51     IN=5
52     IO=6
53     REWIND 1
54     ND=1
55     NST=1
56     ITTER=0
57     KFLAG=0
58     NEW=0

```



```

59      C
60      C   READ SYSTEM CONTROL VARIABLES
61          CALL INPUT1
62      C
63      C   CALCULATE HYDRAULIC CONDUCTIVITY AND SPECIFIC MOISTURE CAPACITY
64      C   AS A FUNCTION OF PRESSURE HEAD
65          I1=ISPAC(6HWATCON,NS*NC,1)
66          I2=ISPAC(5HSLPOT,NS*NC,1)
67          I3=ISPAC(5HSLCON,NS*NC,1)
68          I4=ISPAC(5HSLCAP,NS*NC,1)
69          I5=ISPAC(6HKRATIO,NS,1)
70          CALL HYCOND(BBB(I1),BBB(I2),BBB(I3),BBB(I4),BBB(I5))
71      C
72      C   READ CONTROL DATA
73      30 CALL INPUT3(NSTEP,IMAX,E)
74      C
75      C   READ SYSTEM GEOMETRY, ELEMENT CONNECTIVITY AND PROPERTIES
76          K1=ISPAC(1HX,NNODE,3)
77          K2=ISPAC(1HZ,NNODE,3)
78          K3=ISPAC(1HH,NNODE,3)
79          K4=ISPAC(3HPSI,NNODE,3)
80          K5=ISPAC(4HPSIP,NNODE,3)
81          K6=ISPAC(5HTHETA,NNODE,3)
82          K7=ISPAC(3HKZZ,NNODE,3)
83          K8=ISPAC(2HCA,NNODE,3)
84          K9=ISPAC(4HGMAT,NNODE*(NNODE+1)/2,3)
85          K10=ISPAC(4HBMAT,NNODE*(NNODE+1)/2,3)
86          K11=ISPAC(3HRHS,NNODE,3)
87          K12=ISPAC(4HQRHS,NNODE,3)
88          K13=ISPAC(4HSINT,NNODE,3)
89          K14=ISPAC(5HSINT2,NNODE,3)
90          K15=ISPAC(4HDIFF,NNODE,3)
91          K16=ISPAC(1HQ,NNODE,3)
92          K17=ISPAC(4HTPOT,NNODE,3)
93          L1=ISPAC(2HNP,NEL*3,4)
94          L2=ISPAC(4HMATL,NNODE,4)
95          L3=ISPAC(2HLD,NNODE,4)
96          L4=ISPAC(3HLDQ,NNODE,4)
97          L5=ISPAC(4HKODE,NNODE,4)
98          L6=ISPAC(4HNSPF,NNODE,4)
99          L7=ISPAC(5HKOLHT,NNODE,4)
100         CALL INPUT4(AAA(K1),AAA(K2),AAA(K3),AAA(K4),
101             *MMM(L1),MMM(L2))
102      C
103      C   READ PRESSURE POTENTIALS, WATER CONTENTS, CONDUCTIVITIES,
104      C   AND CAPACITIES FROM TABLES
105      85 CALL TABLOK(AAA(K3),AAA(K4),AAA(K6),AAA(K7),AAA(K8),
106             *BBB(I1),BBB(I2),BBB(I3),BBB(I4),MMM(L2))
107      C
108      C
109          IF(NST.LE.NSTEP) GO TO 150
110          CALL XPLOT(AAA(K1),AAA(K2),AAA(K3),AAA(K6),AAA(K7),
111             *AAA(K17))
112      C
113      C
114      C   FORM SYSTEM MATRIX FROM ELEMENT MATRICES
115      150 CALL GMATX(AAA(K1),AAA(K2),AAA(K3),AAA(K7),AAA(K8),AAA(K9),
116             *AAA(K10),AAA(K11),AAA(K12),MMM(L1),MMM(L2),MMM(L3),MMM(L4),
117             *BBB(I5))
118      C

```



```

119 C   DEFINE BOUNDARY CONDITIONS
120     CALL BOUND(AAA(K9),AAA(K11),AAA(K12),AAA(K13),
121     *AAA(K14),MMM(L3),MMM(L5),MMM(L6),NSTEP,NST,NEW)
122 C
123 C   FORM DIAGONAL ADDRESSING ARRAY AND
124 C   COMPUTE COLUMN HEIGHTS
125     CALL SKYLIN(AAA(K9),MMM(L3),MMM(L7))
126 C
127 C
128 C   CHOLESKY DECOMPOSITION
129     CALL DECOMP(AAA(K9),AAA(K13),MMM(L7),MMM(L3))
130     CALL BKSBI(AAA(K9),AAA(K13),MMM(L3))
131 C
132 C
133 C
134 C   CARRY OUT ITERATIONS
135     CALL ITERAT(AAA(K1),AAA(K2),AAA(K3),AAA(K4),AAA(K5),AAA(K10),
136     *AAA(K11),AAA(K12),AAA(K13),AAA(K15),AAA(K16),AAA(K17),MMM(L4),
137     *MMM(L5),MMM(L6),IMAX,E,NST,NSTEP)
138     GO TO 85
139 100 RETURN
140     END
141 C
142 C
143 C
144 C
145     SUBROUTINE BKSBI(GMAT,SINT,LD)
146 C
147 C   BACKSUBSTITUTION ALGORITHM: SOLVES THE PROBLEM
148 C   D*L(T)*U=R FOR MASTER SYSTEM (EITHER BOUNDARY
149 C   NODES MATRIX, OR UNSUBSTRUCTURED SYSTEM).
150 C
151 C*****
152     IMPLICIT REAL*8(A-H,O-Z)
153 C
154     COMMON /MASTIV/ NSUB,MXND,NUMNST,MASTR,MBEL,IDRY,IN,IO,DELT,NTRANS
155 C
156     COMMON /SUBIV/ IS,NNODE,NEL,ITTER,NEBEL,NFIBN,NIBNS,NSEEP,NTEMP
157 C
158     DIMENSION GMAT(1),SINT(1),LD(1)
159 C
160     COMPUTE D(-1)*R
161 C
162     IF(MASTR) 250,250,100
163 100 INTNOD=NTEMP
164 C   WRITE(6,500)
165 500 FORMAT(//,10X,'POTENTIAL FIELD AND SURFACE INTEGRALS FOR
166 *MASTER SYSTEM',//)
167     DO 200 JG=1,INTNOD
168     L=LD(JG)
169     SINT(JG)=SINT(JG)/GMAT(L)
170 200 CONTINUE
171     GO TO 50
172 C
173 C   BACKSUBSTITUTION U=L(T)(-1)*R
174 C
175 250 INTNOD=NFIBN-1
176 C   WRITE(6,600)
177 600 FORMAT(//,10X,'GMAT AND PRESSURE HEAD FIELD',//)
178 50 DO 300 JG=2,INTNOD

```





```

179      N=INTNOD-JG+2
180      KL=LD(N-1)+1
181      KU=LD(N)-1
182      IF(KL.GT.KU) GO TO 300
183      K=KL-LD(N)+N
184      DO 350 KK=KL,KU
185      SINT(K)=SINT(K)-GMAT(KK)*SINT(N)
186      350 K=K+1
187      300 CONTINUE
188      IALL=LD(INTNOD)
189      C      WRITE(6,700) (GMAT(I),I=1,IALL)
190      700 FORMAT(10E12.4)
191      C      WRITE(6,700) (SINT(I),I=1,INTNOD)
192      RETURN
193      END
194      C
195      C
196      C
197      C
198      BLOCK DATA
199      C
200      REAL*8 NAME,NAMES
201      C
202      COMMON /DIMCOM/ LAST1, LAST2, LAST3, LAST4, LAST5, MAXDIM,
203      *NAMES(5,20), IPT(5,21), ICOM(5)
204      C
205      DATA LAST1, LAST2, LAST3, LAST4, LAST5, MAXDIM, IPT(1,1), IPT(2,1),
206      *IPT(3,1), IPT(4,1), IPT(5,1)/5*0,20,5*1/
207      C
208      END
209      C
210      C
211      C
212      C
213      SUBROUTINE BOUND(GMAT,RHS,QRHS,SINT,SINT2,LD,KODE,
214      *NSPF,NSTEP,NST,NEW)
215      C
216      C      THIS SUBROUTINE DEFINES THE BOUNDARY CONDITIONS FOR THE
217      C      SYSTEM , ASSIGNS VALUES TO THE SURFACE INTEGRALS, AND
218      C      DELETES EQUATIONS FOR THE CONSTANT HEAD NODES
219      C
220      C      *****
221      IMPLICIT REAL*8(A-H,O-Z)
222      COMMON /BORDER/ NEUM, NDIR, KFLAG, NBOUND(60)
223      C
224      COMMON /MASTIV/ NSUB, MXND, NUMNST, MASTR, MBEL, IDRY, IN, IO, DELT, NTRANS
225      C
226      COMMON /SUBIV/ IS, NNODE, NEL, ITTER, NEBEL, NFIBN, NIBNS, NSEEP, NTEMP
227      C
228      DIMENSION GMAT(1), SINT(1), KODE(1), LD(1), NSPF(1), RHS(1),
229      *SINT2(1), BYCD(20), NBC(20), QRHS(1), KSTNO(50)
230      IALL=NNODE*(NNODE+1)/2
231      NTEMP=NNODE
232      C      WRITE(IO,1300)
233      C      WRITE(IO,200) (GMAT(I),I=1,IALL)
234      1300 FORMAT(/,5X,'THE GLOBAL (G) MATRIX IS: '//)
235      IF(NST.EQ.1.AND.ITTER.EQ.0) GO TO 65
236      C
237      C      IF BOUNDARY CONDITIONS REMAIN UNCHANGED, REASSIGN ORIGINAL VALUES
238      C      TO SURFACE INTEGRAL ARRAY, SINT(I)

```



```

239      C
240      DO 150 KL=1,NNODE
241      150 SINT(KL)=SINT2(KL)
242      IF(ITTER.EQ.0) GO TO 75
243      IF(NDIR.EQ.0) GO TO 700
244      K=4
245      NEND=NDIR
246      GO TO 95
247      C
248      C READ AND WRITE INITIAL CONDITIONS (NUMBER OF NO-FLOW,FLUX,
249      C SINK, CONSTANT-HEAD,SEEPAGE NODES,ETC)
250      C
251      65 NPLUS=1
252      READ(7,750) NEWBC
253      READ(7,22) (KSTNO(KBC),KBC=1,NEWBC)
254      WRITE(10,22) (KSTNO(KBC),KBC=1,NEWBC)
255      IF(NSEEP.EQ.0) GO TO 4000
256      READ(7,22) (NSPF(L),L=1,NSEEP)
257      WRITE(10,22) (NSPF(L),L=1,NSEEP)
258      4000 READ(7,50) NEUM,NFLUX,NSINK,NDIR
259      WRITE(10,50) NEUM,NFLUX,NSINK,NDIR
260      DO 90 I=1,NNODE
261      90 KODE(I)=0
262      K=1
263      NEND=NEUM
264      KA=1
265      KB=6
266      GO TO 85
267      C
268      C DETERMINE IF NEW BOUNDARY VALUES ARE TO BE READ IN
269      C
270      75 NEW=NST-KSTNO(NPLUS)
271      IF(NEW) 220,221,221
272      220 IF(NDIR.EQ.0) GO TO 700
273      K=4
274      NEND=NDIR
275      GO TO 95
276      221 NPLUS=NPLUS+1
277      C
278      C READ AND WRITE INITIAL OR NEW BOUNDARY VALUES
279      C
280      85 DO 905 I=1,NNODE
281      905 SINT(I)=0.0
282      READ(7,33) (BYCD(KY),KY=1,20)
283      WRITE(10,33) (BYCD(KY),KY=1,20)
284      READ(7,100) (NBC(KZ),KZ=1,20)
285      WRITE(10,100) (NBC(KZ),KZ=1,20)
286      IF(NST.EQ.1) GO TO 400
287      GO TO 810
288      400 READ(7,100) (NBOUND(I),I=1,NEND)
289      WRITE(10,100) (NBOUND(I),I=1,NEND)
290      IF (NST.EQ.1) GO TO 95
291      C
292      C ASSIGN NEW BOUNDARY VALUES TO BOUNDARY NODES
293      C
294      810 IA=0
295      IB=5
296      KA=1
297      KB=6
298      DO 3500 J=1,NNODE

```



```

299      IF(KODE(J)-11) 3500,3600,3700
300 3600 IA=IA+1
301      IF(IA-NBC(KA)) 1,1,2
302      2 KA=KA+1
303      1 SINT(J)=BYCD(KA)
304      GO TO 3500
305 3700 IB=IB+1
306      IF(IB-NBC(KB)) 5,5,6
307      6 KB=KB+1
308      5 SINT(J)=BYCD(KB)
309 3500 CONTINUE
310      K=4
311      NEND=NDIR
312 C
313 C   ASSIGN INITIAL VALUES TO BOUNDARY NODES
314 C
315      95 KC=11
316      DO 600 I=1,NEND
317      J=NBOUND(I)
318      GO TO (10,20,30,40),K
319      10 KODE(J)=1
320      IF(I.NE.NEND) GO TO 600
321      NEND=NFLUX
322      K=2
323      IF(NEND) 15,15,650
324      20 IF(I-NBC(KA)) 1900,1900,2000
325 2000 KA=KA+1
326 1900 SINT(J)=BYCD(KA)
327      KODE(J)=11
328      IF(I.NE.NEND) GO TO 600
329      GO TO 15
330      30 IF(I-NBC(KB)) 2100,2100,2200
331 2200 KB=KB+1
332 2100 SINT(J)=BYCD(KB)
333      KODE(J)=12
334      IF(I.NE.NEND) GO TO 600
335      GO TO 80
336      15 NEND=NSINK
337      K=3
338      IF(NEND) 80,80,650
339      80 NEND=NDIR
340      K=4
341      IF(NEND) 140,140,650
342      40 IF(NEW.LT.O) GO TO 2400
343      IF(ITER.GT.O.OR.I.GT.1) GO TO 2400
344      140 DO 1000 MN=1,NTEMP
345 1000 SINT2(MN)=SINT(MN)
346      IF(NDIR.EQ.O) GO TO 700
347 2400 IF(I-NBC(KC)) 1400,1400,1800
348 1800 KC=KC+1
349 1400 KODE(J)=10
350 C
351 C   CONDENSE MATRIX BY ELIMINATING EQUATIONS FOR CONSTANT HEAD NODES
352 C
353      JCUR=J-I+1
354      JJ=JCUR-1
355      IF(JJ) 500,500,800
356 C
357 C   TRANSFER CONSTANT HEAD TERMS TO RIGHT HAND SIDE OF EQUATIONS
358 C   AND DELETE EQUATIONS FOR CONSTANT HEAD NODES

```



```

359      C
360      800 DO 60 KL=1,JJ
361          KK=LD(JCUR)-JCUR+KL
362      60 RHS(KL)=RHS(KL)-BYCD(KC)*GMAT(KK)
363      500 NN=JCUR+1
364          DO 300 LL=NN,NTEMP
365              MM=LD(LL)-LL+JCUR
366              RHS(LL)=RHS(LL)-BYCD(KC)*GMAT(MM)
367              RHS(LL-1)=RHS(LL)
368      300 SINT(LL-1)=SINT(LL)
369              KIN=LD(JCUR)+1
370              IALL=NTEMP*(NTEMP+1)/2
371              DO 70 II=KIN,IALL
372      70 GMAT(II-JCUR)=GMAT(II)
373              NCOLS=NTEMP-JCUR
374              DO 110 KI=1,NCOLS
375                  LIN=LD(JCUR+KI-1)+1
376                  LA=LD(JCUR+KI)-1
377                  DO 120 II=LIN,LA
378      120 GMAT(II-KI)=GMAT(II)
379      110 CONTINUE
380              NTEMP=NTEMP-1
381              IF(I.EQ.NEND) GO TO 700
382      600 CONTINUE
383      650 CONTINUE
384              GO TO 400
385      700 IALL=NTEMP*(NTEMP+1)/2
386      C1100 WRITE(IO,5000)
387      5000 FORMAT(//,5X,'THE SINT TERMS (BO) ARE:',//)
388      C      WRITE(IO,200) (SINT(IA),IA=1,NTEMP)
389      C      WRITE(IO,5500)
390      5500 FORMAT(//,5X,'THE RHS TERMS (BO) ARE:',//)
391      C      WRITE(IO,200) (RHS(IB),IB=1,NTEMP)
392      1100 DO 900 MN=1,NTEMP
393      900 SINT(MN)=SINT(MN)+RHS(MN)
394      C      WRITE(IO,1500)
395      1500 FORMAT(//,5X,'THE CONDENSED GLOBAL (G) MATRIX IS:',//)
396      C      WRITE(IO,200) (GMAT(I),I=1,IALL)
397      C      WRITE(IO,1600)
398      C      WRITE(IO,200) (RHS(I),I=1,NTEMP)
399      1600 FORMAT(//,5X,'THE CONDENSED RIGHT HAND SIDE IS:',//)
400      C      WRITE(IO,200) (SINT(I),I=1,NTEMP)
401      C      WRITE(IO,100) (KODE(I),I=1,NTEMP)
402      C      WRITE(IO,2500)
403      2500 FORMAT(///,'THE BOUNDARY CONDITIONS FOR THE NEXT ITERATION ARE:',/
404      1//)
405      C      WRITE(IO,200) (SINT2(MN),MN=1,NNODE)
406      RETURN
407      C
408      C      FORMAT STATEMENTS
409      C
410      22 FORMAT(25I3)
411      33 FORMAT(8E10.3)
412      50 FORMAT(4I5)
413      100 FORMAT(20I4)
414      200 FORMAT(10E12.4)
415      750 FORMAT(I3)
416      END
417      C
418      C

```





```

419 C
420 C
421 SUBROUTINE DECOMP(GMAT,SINT,KOLHT,LD)
422 C
423 C
424 C CHOLSKY DECOMPOSITION--ALGORITHM, TO COMPUTE G(I,J),L(T),
425 C AND D IN THE L(T) *D DECOMPOSITION,IT ALSO COMPUTES THE
426 C RI* VECTOR AND PROVIDES FOR SKYLINE CONFIGURATION
427 C
428 C
429 C*****
430 IMPLICIT REAL*8(A-H,O-Z)
431 C
432 COMMON /MASTIV/ NSUB,MXND,NUMNST,MASTR,MBEL,IDRY,IN,IO,DELT,NTRANS
433 C
434 COMMON /SUBIV/ IS,NNODE,NEL,ITTER,NEBEL,NFIBN,NIBNS,NSEEP,NTEMP
435 C
436 DIMENSION GMAT(1),SINT(1),KOLHT(1),LD(1)
437 IALL=LD(NTEMP)
438 C WRITE(IO,300) (GMAT(I),I=1,IALL)
439 C WRITE(IO,300) (SINT(I),I=1,NTEMP)
440 IF(KOLHT(2).EQ.1) GO TO 50
441 GMAT(2)=GMAT(2)/GMAT(1)
442 SINT(2)=SINT(2)-GMAT(2)*SINT(1)
443 GMAT(3)=GMAT(3)-(GMAT(1)*GMAT(2)**2)
444 C
445 C FORM ELEMENTS OF GMATRIX
446 C
447 50 IF(MASTR) 100,100,200
448 200 INTNOD=NTEMP
449 C NNODE=NUMNST
450 GO TO 150
451 100 INTNOD=NFIBN-1
452 150 DO 400 JG=3,INTNOD
453 IF(KOLHT(JG).EQ.1) GO TO 400
454 MJ=JG-KOLHT(JG)+1
455 IF(MJ+1.GT.JG-1) GO TO 550
456 MJ1=MJ+1
457 JG1=JG-1
458 DO 500 IG=MJ1,JG1
459 MI=IG-KOLHT(IG)+1
460 IF(MJ-MI) 220,220,230
461 230 MI=MJ
462 220 SUMPR=0.0
463 IG1=IG-1
464 DO 600 IGS=MI,IG1
465 M1=LD(IG)-IG+IGS
466 M2=LD(JG)-JG+IGS
467 SUMPR=SUMPR+GMAT(M1)*GMAT(M2)
468 600 CONTINUE
469 MM=LD(JG)-JG+IG
470 GMAT(MM)=GMAT(MM)-SUMPR
471 500 CONTINUE
472 C
473 C FORM ELEMENTS FOR L(T) MATRIX AND COMPUTE RI* VECTOR
474 C
475 550 SUMPR=0.0
476 JG1=JG-1
477 DO 650 IG=MJ,JG1
478 L=LD(IG)

```



```

479      MM=LD(JG)-JG+IG
480      GMAT(MM)=GMAT(MM)/GMAT(L)
481      650 SUMPR=SUMPR+GMAT(MM)*SINT(IG)
482      SINT(JG)=SINT(JG)-SUMPR
483      C
484      C   FORM DIAGONAL ELEMENTS
485      C
486      SUMPR=0.0
487      JG1=JG-1
488      DO 700 IGS=MJ,JG1
489      LL=LD(IGS)
490      MD=LD(JG)-JG+IGS
491      SUMPR=SUMPR+GMAT(LL)*GMAT(MD)**2
492      700 CONTINUE
493      MD=LD(JG)
494      GMAT(MD)=GMAT(MD)-SUMPR
495      400 CONTINUE
496      C   WRITE(IO,300) (SINT(I),I=1,NTEMP)
497      IALL=LD(NTEMP)
498      C   WRITE(IO,300) (GMAT(I),I=1,IALL)
499      RETURN
500      C
501      C   FORMAT STATEMENTS
502      300 FORMAT(10E12.4)
503      END
504      C
505      C
506      C
507      C
508      SUBROUTINE FLUX(X,Z,PSI,BMAT,QRHS,SINT,Q,TPOT,LDQ,KODE,NSPF)
509      C
510      C   THIS SUBROUTINE COMPUTES FLUXES, DETERMINES THE EXTENT OF THE
511      C   SEEPAGE FACE, AND THE OUTFLOW FROM IT
512      C
513      C*****
514      IMPLICIT REAL*8(A-H,O-Z)
515      COMMON /BORDER/ NEUM,NDIR,KFLAG,NBOUND(60)
516      COMMON /SUBIV/ IS,NNODE,NEL,ITTE,NBEL,NFIBN,NIBNS,NSEEP,NTEMP
517      DIMENSION PSI(1),BMAT(1),SINT(1),Q(1),LDQ(1),KODE(1),
518      *X(1),Z(1),TPOT(1),QRHS(1),NSPF(1)
519      C
520      C   INITIALIZE Q ARRAY AND COMPUTE HYDRAULIC HEAD
521      C
522      KFLAG=0
523      DO 110 I=1,NNODE
524      C   TPOT(I)=Z(I)+PSI(I)
525      110 Q(I)=0.0
526      C   WRITE(8,850) NNODE
527      C   WRITE(6,300)
528      C
529      C   COMPUTE FLUXES
530      C
531      DO 1600 I=1,NNODE
532      KOLT=LDQ(I)-I
533      KDIAG=LDQ(I)
534      DO 500 J=1,NNODE
535      KOUNT=KOLT+J
536      IF(KOUNT.GT.KDIAG) GO TO 650
537      Q(I)=Q(I)+BMAT(KOUNT)*PSI(J)
538      GO TO 500

```



```

539      650 JM=J-1
540      KROW=LDQ(JM)+I
541      Q(I)=Q(I)+BMAT(KROW)*PSI(J)
542      500 CONTINUE
543      Q(I)=Q(I)-QRHS(I)
544      C      WRITE(8,950) I,X(I),Z(I),PSI(I),TPOT(I)
545      1600 CONTINUE
546      C      WRITE(6,100) (PSI(I),I=1,NNODE)
547      C      WRITE(6,200)
548      C      WRITE(6,100) (Q(I),I=1,NNODE)
549      C      WRITE(6,2000)
550      2000 FORMAT(//,5X,'THE QRHS TERMS (FL) ARE:',//)
551      C      WRITE(6,100) (QRHS(I),I=1,NNODE)
552      C      WRITE(6,50)
553      C
554      C
555      C
556      IF(NSEEP.EQ.0) GO TO 1000
557      DO 600 MI=1,NSEEP
558      I=NSPF(MI)
559      IF(KFLAG) 900,900,800
560      C
561      C      IDENTIFY CONSTANT HEAD BOUNDARY NODES
562      C
563      900 IF(KODE(I).EQ.1) GO TO 750
564      IF(Q(I).LE.0.0000001) GO TO 600
565      C
566      C      MAKE NODE A "NO-FLOW" BOUNDARY NODE
567      C
568      800 IF(KODE(I).EQ.1) GO TO 750
569      Q(I)=0.0
570      KODE(I)=1
571      NEUM=NEUM+1
572      NDIR=NDIR-1
573      KFLAG=1
574      WRITE(6,150) I,KODE(I),PSI(I),Q(I),NEUM,NDIR
575      GO TO 600
576      750 IF(PSI(I).LT.0.0) GO TO 600
577      C
578      C      MAKE NODE A CONSTANT HEAD BOUNDARY NODE
579      C
580      700 PSI(I)=0.0
581      KODE(I)=10
582      NDIR=NDIR+1
583      NEUM=NEUM-1
584      WRITE(6,150) I,KODE(I),PSI(I),Q(I),NEUM,NDIR
585      600 CONTINUE
586      C
587      C      REDEFINE SEEPAGE FACE
588      C
589      JJ=0
590      DO 250 J=1,NNODE
591      IF(KODE(J).NE.10) GO TO 250
592      JJ=JJ+1
593      NBOUND(JJ)=J
594      250 CONTINUE
595      1000 CONTINUE
596      RETURN
597      C
598      C      FORMAT STATEMENTS

```



```

599      C
600      50 FORMAT(//,10X,'NODE',10X,'KODE',10X,'PRESSURE',14X,'FLUX',//)
601      100 FORMAT(10E12.4)
602      150 FORMAT(10X,I4,10X,I4,8X,E12.5,8X,E12.5,2I5)
603      200 FORMAT(//,5X,'THE COMPUTED FLUXES ARE',//)
604      300 FORMAT(//,5X,'THE PRESSURE HEAD FIELD IS:',//)
605      850 FORMAT(I4)
606      950 FORMAT(I4,4F12.1)
607      END
608      C
609      C
610      C
611      SUBROUTINE GMATX(X,Z,H,KZZ,CA,GMAT,BMAT,RHS,QRHS,NP,MATL,
612      *LD,LDQ,KRATIO)
613      C
614      C      THIS ROUTINE FORMS THE ELEMENT MATRICES FOR EACH TRIANGULAR ELEMENT,
615      C      SOLVES THE INTEGRAL EQUATIONS,AND ASSEMBLES THE CONTRIBUTIONS
616      C      FROM EACH ELEMENT COEFFICIENT MATRIX TO FORM THE GLOBAL MATRICES.
617      C
618      C      *****
619      C      IMPLICIT REAL*8 (A-H,O-Z)
620      C      REAL*8 KRATIO,KZZ
621      C      COMMON /SUBIV/ IS,NNODE,NEL,ITTE,NBEL,NFIBN,NIBNS,NSEEP,NTEMP
622      C      COMMON /MASTIV/ NSUB,MXND,NUMNST,MASTR,MBEL,IDRY,IN,IO,DELT,NTRANS
623      C      COMMON /HILL/ SLOPE,COS1,COS2,SIN1,SIN2
624      C      DIMENSION ELMAT(3,3),A(3),B(3),XL(5),ZL(5),AL(3),BL(3),GMAT(1),
625      C      *KZZ(1),CA(1),X(1),Z(1),H(1),NP(3,1),KRATIO(1),
626      C      *MATL(1),LD(1),CELMAT(3,3),BMAT(1),RHS(1),LDQ(1),QRHS(1)
627      C      WRITE(6,2153)
628      2153 FORMAT(//,13X,'ELEM          AVK (VERT.)          AVCA',//)
629      C
630      C
631      C      INITIALIZE GLOBAL MATRICES
632      C
633      C
634      C      MUP=NNODE*(NNODE+1)/2
635      C      DO 3 IG=1,MUP
636      C      GMAT(IG)=0.0
637      C      3 BMAT(IG)=0.0
638      C
639      C
640      C      FORM DIAGONAL ADDRESSING ARRAY
641      C
642      C
643      C      L=0
644      C      DO 410 N=1,NNODE
645      C      L=L+N
646      410 LD(N)=L
647      C      DO 300 M=1,NEL
648      C
649      C      FORM UPPER TRIANGULAR ELEMENT MATRIX
650      C
651      C      DO 200 I=1,3
652      C      DO 200 J=1,3
653      C      ELMAT(I,J)=0.0
654      200 CELMAT(I,J)=0.0
655      C      I=NP(1,M)
656      C      J=NP(2,M)
657      C      K=NP(3,M)
658      C      COMPUTE AVERAGE CONDUCTIVITY COMPONENTS FOR EACH ELEMENT

```





```

659      AVKXX=0.0
660      AVKZZ=0.0
661      AVKXZ=0.0
662      NKOUNT=1
663      40 IF(NKOUNT-2) 10,20,30
664      10 IA=MATL(I)
665      RQ=KRATIO(IA)
666      NUM=I
667      GO TO 50
668      20 IA=MATL(J)
669      RQ=KRATIO(IA)
670      NUM=J
671      GO TO 50
672      30 IA=MATL(K)
673      RQ=KRATIO(IA)
674      NUM=K
675      50 AVKXX=AVKXX+(COS2*RQ+SIN2)*KZZ(NUM)
676      AVKZZ=AVKZZ+(SIN2*RQ+COS2)*KZZ(NUM)
677      AVKXZ=AVKXZ+COS1*SIN1*KZZ(NUM)*(RQ-1)
678      AVCA=2*CA(I)+CA(J)+CA(K)
679      AVC2=CA(I)+2*CA(J)+CA(K)
680      AVC3=CA(I)+CA(J)+2*CA(K)
681      NKOUNT=NKOUNT+1
682      IF(NKOUNT.LE.3) GO TO 40
683      AVKXX=AVKXX/3.0
684      AVKZZ=AVKZZ/3.0
685      AVKXZ=AVKXZ/3.0
686      C
687      C      FORM ELEMENT DIMENSIONS
688      C
689      C      A(1)=X(K)-X(J)
690      C      A(2)=X(I)-X(K)
691      C      A(3)=X(J)-X(I)
692      C      B(1)=Z(J)-Z(K)
693      C      B(2)=Z(K)-Z(I)
694      C      B(3)=Z(I)-Z(J)
695      C      AREA2=A(3)*B(2)-A(2)*B(3)
696      C
697      C      CARRY OUT INTEGRATIONS
698      C
699      C      WRITE(6,2152) M,AVKXX,AVKZZ,AVKXZ
700      2152 FORMAT(10X,I6,3E20.4)
701      DEN=2.*AREA2
702      C      WRITE(6,1000) M
703      1000 FORMAT(/,10X,20HTHE DEN. FOR ELEMENT,13,3HIS:,//)
704      C      WRITE(6,1001) DEN
705      1001 FORMAT(10X,E15.6)
706      XL(1)=X(I)
707      XL(2)=X(J)
708      XL(3)=X(K)
709      ZL(1)=Z(I)
710      ZL(2)=Z(J)
711      ZL(3)=Z(K)
712      C
713      DO 245 I=1,3
714      DO 246 J=1,3
715      IF(I-J) 226,225,246
716      226 K=(6-I-J)
717      AL(1)=XL(K)-XL(J)
718      AL(2)=XL(I)-XL(K)

```



```

719      BL(1)=ZL(J)-ZL(K)
720      BL(2)=ZL(K)-ZL(I)
721      ELMAT(I,J)=(AVKZZ*AL(1)*AL(2)+AVKXX*BL(1)*BL(2))/DEN
722      IF (SLOPE.EQ.O.O) GO TO 60
723      ELMAT(I,J)=ELMAT(I,J)+(AVKXZ*(AL(2)*BL(1)+BL(2)*AL(1)))/DEN
724      60 CONTINUE
725      GO TO 255
726      225 IF (I-2) 230,235,240
727      235 XL(I+2)=XL(1)
728      ZL(I+2)=ZL(1)
729      AVCA=AVC2
730      GO TO 230
731      240 XL(I+2)=XL(2)
732      ZL(I+2)=ZL(2)
733      AVCA=AVC3
734      230 ELMAT(I,J)=(AVKZZ*((XL(I+1)-XL(I+2))**2)+AVKXX*((ZL(I+1)-ZL(I+2))*
735      1*2))/DEN
736      IF(SLOPE.EQ.O.O) GO TO 70
737      ELMAT(I,J)=ELMAT(I,J)+(2.O*AVKXZ*BL(1)*AL(1))/DEN
738      70 CONTINUE
739      IF(NTRANS) 260,255,260
740      260 CELMAT(I,J)=AVCA*AREA2/24.O
741      C
742      C   FORM UPPER TRIANGULAR GLOBAL MATRICES,(A) AND (B)
743      C
744      255 IF(I-2) 305,310,315
745      305 IG=NP(1,M)
746      GO TO 320
747      310 IG=NP(2,M)
748      GO TO 320
749      315 IG=NP(3,M)
750      320 IF(J-2) 325,330,335
751      325 JG=NP(1,M)
752      GO TO 340
753      330 JG=NP(2,M)
754      GO TO 340
755      335 JG=NP(3,M)
756      340 IF(IG-JG) 405,415,425
757      425 IIG=IG
758      IIJ=JG
759      JG=IIG
760      IG=IIJ
761      405 MM=LD(JG)-JG+IG
762      GMAT(MM)=GMAT(MM)+ELMAT(I,J)
763      GO TO 246
764      415 MM=LD(JG)-JG+IG
765      GMAT(MM)=GMAT(MM)+ELMAT(I,J)
766      BMAT(MM)=BMAT(MM)+CELMAT(I,J)
767      246 CONTINUE
768      245 CONTINUE
769      C   WRITE(6,110) M
770      C   WRITE(6,250) ((ELMAT(I,J),J=1,3),I=1,3)
771      C   WRITE(6,250) ((CELMAT(I,J),J=1,3),I=1,3)
772      300 CONTINUE
773      C   WRITE(6,345)
774      C   WRITE(6,354) (GMAT(MM),MM=1,MUP)
775      C   WRITE(6,355)
776      C   WRITE(6,354) (BMAT(MM),MM=1,MUP)
777      C
778      C

```



```

779      C   FORM (G) MATRIX AND RHS
780      C
781      C
782          IF(NTRANS) 2100,2000,2100
783      2100 DO 450 N=1,NNODE
784          MM=LD(N)
785          GMAT(MM)=GMAT(MM)+BMAT(MM)/DELT
786      450 RHS(N)=0.0
787      C
788      C
789          DO 600 I=1,NNODE
790          KOLT=LD(I)-1
791          KDIAG=LD(I)
792          DO 500 J=1,NNODE
793          KOUNT=KOLT+J
794          IF(KOUNT.GT.KDIAG) GO TO 650
795          RHS(I)=RHS(I)+BMAT(KOUNT)*H(J)/DELT
796          GO TO 500
797      650 JM=J-1
798          KROW=LD(JM)+1
799          RHS(I)=RHS(I)+BMAT(KROW)*H(J)/DELT
800      500 CONTINUE
801      600 CONTINUE
802          GO TO 555
803      2000 DO 455 KS=1,NNODE
804          455 RHS(KS)=0.0
805          555 DO 900 L=1,MUP
806          900 BMAT(L)=GMAT(L)
807          DO 950 M=1,NNODE
808          QRHS(M)=RHS(M)
809      950 LDQ(M)=LD(M)
810      C
811      C   PRINT OUT GLOBAL MATRICES
812      C
813      C   WRITE(6,348)
814      C   WRITE(6,354) (GMAT(MM),MM=1,MUP)
815      C   WRITE(6,352)
816      C   WRITE(6,354) (H(I),I=1,NNODE)
817      C   WRITE(6,360)
818      C   WRITE(6,354) (RHS(I),I=1,NNODE)
819      C   RETURN
820      110 FORMAT(//,10X,22HMATRIX FOR ELEMENT NO.,I2,/)
821      250 FORMAT(20X,3E25.8)
822      345 FORMAT(//,10X,17HGLOBAL (A) MATRIX,/)
823      348 FORMAT(//,10X,17HGLOBAL (G) MATRIX,/)
824      352 FORMAT(//,10X,31HTHE INITIAL SOLUTION VECTOR IS:,/)
825      354 FORMAT(10E12.4)
826      355 FORMAT(//,10X,17HGLOBAL (B) MATRIX,/)
827      360 FORMAT(//,10X,34HTHE RHS VECTOR (1/DELT*(B)*(H) IS:,/)
828      C   END
829      C
830      C
831      C
832      C
833      C   SUBROUTINE HYCOND(WATCON,SLPOT,SLCON,SLCAP,KRATIO)
834      C
835      C   THIS SUBROUTINE CALCULATES HYDRAULIC CONDUCTIVITY AND SPECIFIC
836      C   MOISTURE CAPACITY AS A FUNCTION OF PRESSURE POTENTIAL.IT IS
837      C   ADAPTED FROM THE WORK OF GREEN AND COREY (1971) AT THE SAVANNAH
838      C   RIVER LABORATORY. CALCULATIONS ARE BASED ON PAPERS BY MARSHALL

```



```

839 C AND MILLINGTON-QUIRK. THIS IS A VARIATION OF A PROGRAM DEVELOPED BY
840 C DR. RAY KUNZE TO CALCULATE HYDRAULIC CONDUCTIVITY OF POROUS SOLIDS
841 C FROM WATER RETENTION DATA.
842 C SEE:
843 C GREEN, R. E. AND J. C. COREY. 1971. SOIL SCI. SOC. AM.
844 C PROC. 35(1):3-8.
845 C
846 C *****
847 C INPUT VARIABLES
848 C
849 C THETA=WATER CONTENT FOR EACH INPUT POINT (CM**3/CM**3)
850 C INP=NUMBER OF INPUT DATA POINTS (IN IS LIMITED TO 20 WITH
851 C PRESENT FORMAT)
852 C NC=NUMBER OF INCREMENTED PORE CLASSES CHOSEN FOR CALCULATING
853 C DATA (NC IS LIMITED TO 25)
854 C TMAX=MAXIMUM WATER CONTENT (CM**3/CM**3)
855 C SCON=EXPERIMENTALLY OBTAINED SATURATED CONDUCTIVITY (CM/UNIT TIME)
856 C SCONR=KRATIO:RATIO OF HORIZONTAL TO VERTICAL HYDRAULIC
857 C CONDUCTIVITY (PRINCIPAL DIRECTIONS OF PERMEABILITY)
858 C DP=DESORPTION PRESSURE (CM OF WATER)
859 C RESWAT=ESTIMATE OF RESIDUAL(IMMOBILE) WATER
860 C
861 C INTERMEDIATE CALCULATED VARIABLES
862 C
863 C STDINC=STANDARD WATER CONTENT INCREMENT FOR CALCULATED
864 C VALUES(CM**3/CM**3)
865 C TINC=INCREMENTED THETA (CM**3/CM**3)
866 C DPI=INCREMENTED DP FOR RESPECTIVE TINC (CM OF WATER)
867 C CLS=SQUARED RECIPROCAL OF NUMBER OF WATER CONTENT CLASSES
868 C (KL)
869 C PCH=INTERMEDIATE SUM OF PRODUCTS OF COEFFICIENTS AND
870 C HEADS IN CONDUCTIVITY EQUATION
871 C SPCH=FINAL SUM OF PRODUCTS
872 C ACF=CONVERSION FACTOR THAT TAKES INTO ACCOUNT TEMPERATURE
873 C AND GRAVITY INFLUENCES
874 C =4*1440*60*(SURFACE TENSION)**2/(8*DYN. VISCOSITY*
875 C DENSITY*GRAVITY)
876 C UNITS FOR VARIABLES IN ACF
877 C 1440=MIN/DAY
878 C 60=SEC/MIN
879 C SURTEN=NEWTON/M
880 C VISWAT=PASCAL*SEC
881 C DENWAT=G/CM**3
882 C ^GRAVITY=CM/SEC**2
883 C
884 C OUTPUT VARIABLES
885 C
886 C CCAL=CALCULATED CONDUCTIVITY (CM/UNIT TIME), CALLED 'CALCULATED K '
887 C MATF=CONDUCTIVITY (CM/UNIT TIME) MATCHED WITH SATURATION VALUE,
888 C CALLED 'SAT MATCH'
889 C FACTOR=EXPERIMENTALLY MEASURED SATURATED CONDUCTIVITY
890 C DIVIDED BY CALCULATED SATURATED CONDUCTIVITY
891 C THETA=WATER CONTENT AT UPPER END OF
892 C INCREMENT (CM**3/CM**3) .
893 C PRESSURE=DESORPTION PRESSURE (CM OF WATER)
894 C IMPLICIT REAL*8 (A-H,O-Z)
895 C REAL*8 MATF,KRATIO
896 C COMMON/HOOKUP/NS,NC,RESWAT
897 C DIMENSION WATCON(NS,1),SLPOT(NS,1),SLCON(NS,1),SLCAP(NS,1),
898 C *TINC(51),CCAL(51),THETA(51),DP(51),SPCH(51),DPI(51),MATF(51),

```





```

899      *KRATIO(NS)
900      LS=1
901      C      READ INPUT PARAMATERS AND VARIABLES
902      1086 READ(5,1114) ST,ST1,ST2,ST3,ST4,ST5,ST6,ST7,ST8,ST9
903      1114 FORMAT(10A8)
904      READ(5,1116) INP,TMAX,SCON,SCONR,RESWAT
905      1116 FORMAT(I5,F10.4,2E15.5,F5.3)
906      READ(5,1120) SURTEN,DENWAT,VISWAT,TEMP,GRAVTY
907      1120 FORMAT(F10.6,F10.3,F12.8,2F5.1)
908      C      NOTE ORDER OF INPUT DATA=
909      C      THETA(1)=LOWEST WATER CONTENT
910      C      DP(1)=HIGHEST PRESSURE (ABSOLUTE VALUE)
911      READ(5,1117) (THETA(J),J=1,INP)
912      1117 FORMAT(20F4.3)
913      READ(5,1119) (DP(J),J=1,INP)
914      1119 FORMAT(8F10.2)
915      KRATIO(LS)=SCONR
916      C      CALCULATE CONVERSION FACTOR
917      ACF=30.*SURTEN**2/(VISWAT*DENWAT*GRAVTY)
918      ACF=ACF*1440.
919      C      CALCULATE INCREMENT SIZE
920      RNC=NC
921      STDINC=(TMAX-THETA(1))/RNC
922      C      INITIALIZE TINC AND DPI ARRAYS
923      TINC(1)=THETA(1)
924      DPI(1)=DP(1)
925      NCP1=NC+1
926      C      INDEX I REFERS TO INCREMENTED VARIABLES
927      C      INDEX J REFERS TO INPUT DATA
928      C      CALCULATE THETA INCREMENT LIMITS
929      DO 1003 I=2,NCP1
930      TINC(I)=TINC(I-1)+STDINC
931      C      CALCULATE PRESSURE INCREMENT LIMITS
932      DO 1004 J=1,INP
933      JO=J
934      IF(THETA(J).GE.TINC(I))GO TO 1005
935      1004 CONTINUE
936      1005 DPI(I)=((TINC(I)-THETA(JO-1))/(THETA(JO)-THETA(JO-1)))*(DP(JO)
937      1-DP(JO-1))+DP(JO-1)
938      1003 CONTINUE
939      C      ADJUST DPI TO GIVE VALUES AT MIDPOINT OF INCREMENT
940      DPI(NCP1)=0.0
941      DO 1178 I=1,NC
942      DPI(I)=(DPI(I)+DPI(I+1))*0.5
943      1178 CONTINUE
944      C      CALCULATE ADJUSTED NUMBER OF CLASSES (ANC) CORRESPONDING TO TOTAL
945      C      WATER CONTENT
946      ANC=(TMAX-0.0)/STDINC
947      C      CALCULATE SQUARED RECIPROCAL OF 'ANC'
948      CLS=(1.0/ANC)**2
949      C      CALCULATE PRODUCT OF COEFFICIENT AND 'HEAD' TERMS FOR
950      C      EACH PORE CLASS
951      KL=NC
952      DO 1176 J=1,NC
953      NL=NCP1-J
954      PCH=0.0
955      DO 1175 I=J,NC
956      PCH=PCH+(2*I+1-2*J)*(1./DPI(NL))**2
957      1175 NL=NL-1
958      SPCH(KL)=PCH

```



```

959 C CORRECT POROSITY TERM WITH COTINC FUNCTION (CORRECTION
960 C NEEDED ONLY WHEN LIMITED THETA RANGE IS USED)
961 COTINC=TINC(NCP1)-RESWAT
962 C CALCULATE K FOR A GIVEN WATER CONTENT AND PRESSURE
963 CCAL(KL)=SPCH(KL)*ACF*COTINC**2*CLS
964 KL=KL-1
965 1176 CONTINUE
966 C CALCULATE MATCHING FACTOR
967 FACTOR=SCON/CCAL(NC)
968 C ADJUST TINC AND DPI VALUES AT UPPER LIMIT OF INCREMENTS
969 C FOR PLOTTING AND CALCULATE MATCHED CONDUCTIVITY AT
970 C EACH WATER CONTENT
971 DO 1179 I=1,NC
972 TINC(I)=TINC(I+1)
973 DPI(I)=(DPI(I)+DPI(I+1))*0.5
974 1179 MATF(I)=FACTOR*CCAL(I)
975 DPI(NC)=0.0
976 C PRINT OUTPUT
977 1400 PRINT 1090,ST,ST1,ST2,ST3,ST4,ST5,ST6,ST7,ST8,ST9
978 1090 FORMAT(1H1,20X,10A8/)
979 PRINT 1180,INP,TMAX,SCON,FACTOR,SCONR
980 1180 FORMAT(T1,'OINP= ',I3,T15,'TMAX= ',F5.4,T30,'SCON= ',1PE10.3,T50,
981 + 'FACTOR= ',1PE10.3,T70,'SCONR= ',1PE10.3)
982 PRINT 1121,SURTEN,DENWAT,VISWAT,RESWAT,TEMP
983 1121 FORMAT(1X,'SURTEN=',F10.6,' DENWAT=',F10.2,' VISWAT=',F12.8,'
984 + RESWAT=',F5.3,2X,' TEMP= ',F4.1,' C'//)
985 PRINT 1406,GRAVITY,ACF
986 1406 FORMAT(' GRAVITY= ',F5.1,' ACF= ',1PE10.3)
987 PRINT 1403
988 1403 FORMAT('OCLASS',3X,'PRESSURE',6X,'THETA',7X,'CALCULATED K',6X,'SAT
989 + MATCH'/2X,'(I)',3X,'(CM WATER)',4X,'(BY VOL)',7X,'(CM/TIME)',8X,'
990 + (GM/TIME)')
991 PRINT 1404,(I,DPI(I),TINC(I),CCAL(I),MATF(I),I=1,NC)
992 1404 FORMAT(' ',I3,3X,OPF10.2,6X,OPF5.3,7X,1PE10.3,7X,1PE10.3)
993 PRINT 1125,(J,THETA(J),DP(J),J=1,INP)
994 1125 FORMAT('O',T2,'INPUT DATA FOR THE ABOVE OUTPUT'//1X,T4,'J',T10,
995 1'THETA',T20,'PRESSURE'//((1X,T2,I3,T10,F4.3,T19,F10.2)))
996 C SET UP STORED DATA ARRAYS
997 DO 1185 I=1,NC
998 WATCON(LS,I)=TINC(I)
999 SLPOT(LS,I)=DPI(I)
1000 SLCON(LS,I)=MATF(I)
1001 1185 CONTINUE
1002 LS=LS+1
1003 IF(LS.GT.NS) GO TO 2
1004 GO TO 1086
1005 2 CONTINUE
1006 C COMPUTE SPECIFIC MOISTURE CAPACITY
1007 DO 800 I=1,NS
1008 DO 800 J=1,NC
1009 IF(J.NE.1) GO TO 900
1010 950 SLCAP(I,J)=0.0
1011 GO TO 800
1012 900 IF (J.EQ. NC) GO TO 950
1013 SLCAP(I,J)=(WATCON(I,J+1)-WATCON(I,J))/(SLPOT(I,J)-SLPOT(I,J+1))
1014 800 CONTINUE
1015 PRINT 1500
1016 1500 FORMAT ('OCLASS',3X,'PRESSURE',6X,'CAPACITY'/2X,'(I)',3X,
1017 *'(CM WATER)',5X,'(1/CM)')
1018 DO 2000 K=1,NS

```



```

1019      WRITE(6,2050) K
1020      2050 FORMAT (//,3X,'SOIL NO.',I2,/)
1021      DO 2000 L=1,NC
1022      WRITE (6,2075) L,SLPOT(K,L),SLCAP(K,L)
1023      2075 FORMAT(2X,I3,3X,E10.3,4X,E10.3)
1024      2000 CONTINUE
1025      RETURN
1026      END
1027      C
1028      C
1029      C
1030      SUBROUTINE INPUT1
1031      C
1032      C   THIS SUBROUTINE READS CONTROL DATA OF MASTER SYSTEM
1033      C
1034      C*****
1035      IMPLICIT REAL*8(A-H,O-Z)
1036      C
1037      COMMON /MASTIV/ NSUB,MXND,NUMNST,MASTR,MBEL,IDRY,IN,IO,DELT,NTRANS
1038      COMMON/HOOKUP/NS,NC,RESWAT
1039      C
1040      DIMENSION HED(20)
1041      C
1042      READ(IN,1000) HED
1043      WRITE(IO,2000) HED
1044      READ(IN,1100) NSUB,MXND,NUMNST,MASTR,MBEL,IDRY,NS,NC,DELT,NTRANS
1045      WRITE(IO,2100) NSUB,MXND,NUMNST,MASTR,MBEL,IDRY,NS,NC,DELT,NTRANS
1046      C
1047      RETURN
1048      C
1049      C   FORMAT STATEMENTS
1050      C
1051      1000 FORMAT(20A4)
1052      1100 FORMAT(8I4,F10.5,I4)
1053      2000 FORMAT(20X,20A4///)
1054      2100 FORMAT('MASTER SYSTEM CONTROL VARIABLES'//,
1055      *'NUMBER OF SUBSYSTEMS                                =' ,I4//,
1056      *'MAXIMUM NUMBER OF INTER-BOUNDARY NODES'//          =' ,I4//,
1057      *'NODES IN ANY SUBSYSTEM                               =' ,I4//,
1058      *'NUMBER OF NODES IN MASTER SYSTEM                    =' ,I4//,
1059      *'FLAG FOR MASTER MATRIX                               =' ,I4//,
1060      *'NUMBER OF GLOBAL EXTERNAL BOUNDARY CONDITIONS       =' ,I4//,
1061      *'DRY RUN FLAG                                          =' ,I4//,
1062      *'NUMBER OF MATERIALS                                  =' ,I4//,
1063      *'NUMBER OF PORE CLASSES                               =' ,I4//,
1064      *'TIME STEP SIZE                                        =' ,F10.5//,
1065      *'PROBLEM TYPE (STEADY=0,TRANSIENT=1)                  =' ,I4//)
1066      C
1067      END
1068      C
1069      C
1070      C
1071      C
1072      C
1073      C
1074      C
1075      C
1076      C
1077      C
1078      SUBROUTINE INPUT3(NSTEP,IMAX,E)

```



```

1079 C
1080 C   THIS SUBROUTINE READS CONTROL DATA FOR EACH SUBSYSTEM
1081 C
1082 C*****
1083 IMPLICIT REAL*8(A-H,O-Z)
1084 C
1085 COMMON /MASTIV/ NSUB,MXND,NUMNST,MASTR,MBEL,IDRY,IN,IO,DELT,NTRANS
1086 COMMON /HILL/ SLOPE,COS1,COS2,SIN1,SIN2
1087 C
1088 COMMON /SUBIV/ IS,NNODE,NEL,ITTER,NEBEL,NFIBN,NIBNS,NSEEP,NTEMP
1089 C
1090 READ(IN,1000) IS,NNODE,NEL,NSTEP,IMAX,E,SLOPE,NFIBN,
1091 *NIBNS,NSEEP
1092 WRITE(IO,2000) IS,NNODE,NEL,NSTEP,IMAX,E,SLOPE,NFIBN,
1093 *NIBNS,NSEEP
1094 PI=3.141592653589793DO
1095 ANGLE=PI*SLOPE/180.0
1096 COS1=DCOS(ANGLE)
1097 COS2=COS1**2
1098 SIN1=DSIN(ANGLE)
1099 SIN2=SIN1**2
1100 RETURN
1101 C
1102 C
1103 C   FORMAT STATEMENTS
1104 C
1105 1000 FORMAT(5I4,2E12.5,3I4)
1106 2000 FORMAT('1',T30,'SUBSYSTEM NUMBER ',I5
1107 *//,'NUMBER OF NODES',I5
1108 *//,'NUMBER OF ELEMENTS',I5
1109 *//,'NUMBER OF TIME STEPS',I5
1110 *//,'MAXIMUM NUMBER OF ITERATIONS PER TIME STEP',I5
1111 *//,'SPECIFIED DIFFERENCE CRITERION FOR ITERATIONS',E10.5
1112 *//,'HILLSIDE SLOPE (DEGREES)',F10.5
1113 *//,'LOCAL NUMBER OF FIRST INTER-BOUNDARY NODE',I5
1114 *//,'NUMBER OF INTER-BOUNDARY NODES',I5
1115 *//,'NUMBER OF SEEPAGE FACE NODES',I5//)
1116 C
1117 END
1118 C
1119 C
1120 C
1121 C
1122 SUBROUTINE INPUT4(X,Z,H,PSI,NP,MATL)
1123 C
1124 C   THIS SEGMENT READS AND WRITES THE NODAL AND ELEMENT DATA,
1125 C   TOGETHER WITH INITIAL PRESSURE POTENTIAL
1126 C
1127 C*****
1128 IMPLICIT REAL*8(A-H,O-Z)
1129 C
1130 COMMON /MASTIV/ NSUB,MXND,NUMNST,MASTR,MBEL,IDRY,IN,IO,DELT,NTRANS
1131 C
1132 COMMON /SUBIV/ IS,NNODE,NEL,ITTER,NEBEL,NFIBN,NIBNS,NSEEP,NTEMP
1133 C
1134 DIMENSION X(1),Z(1),H(1),PSI(1),
1135 *NP(3,1),MATL(1)
1136 C   READ PRELIMINARY INFORMATION
1137 WRITE(IO,101)
1138 WRITE(IO,115)

```





```

1139      L=1
1140      READ(IN, 104) N,X(N),Z(N)
1141      GO TO 4
1142      30 READ(IN, 104) N,X(N),Z(N)
1143      DN=N-L
1144      DX=(X(N)-X(L))/DN
1145      DZ=(Z(N)-Z(L))/DN
1146      15 L=L+1
1147      IF(N-L) 10,4,50
1148      50 X(L)=X(L-1)+DX
1149      Z(L)=Z(L-1)+DZ
1150      MATL(L)=MATL(L-1)
1151      GO TO 15
1152      4 WRITE(IO, 104) N,X(N),Z(N)
1153      IF(NNODE-N) 10,20,30
1154      10 WRITE(IO, 105) N
1155      CALL EXIT
1156      20 READ(IN, 120) (H(N),N=1,NNODE)
1157      READ(IN, 130) (MATL(N),N=1,NNODE)
1158      DO 150 N=1,NNODE
1159      150 PSI(N)=H(N)
1160      WRITE(IO, 106)
1161      WRITE(IO, 102)
1162      WRITE(IO, 180) (N,X(N),Z(N),H(N),MATL(N),N=1,NNODE)
1163      C
1164      C READ AND WRITE ELEMENT DATA
1165      C
1166      WRITE(IO, 107)
1167      WRITE(IO, 108)
1168      ML=0
1169      39 IF(ML.GE.NEL) GO TO 40
1170      READ(IN, 113) M,NP(1,M),NP(2,M),NP(3,M)
1171      WRITE(IO, 113) M,NP(1,M),NP(2,M),NP(3,M)
1172      MM=ML+1
1173      IF(MM.EQ.M) GO TO 25
1174      60 ML1=ML+1
1175      IF(ML1.EQ.M) GO TO 25
1176      ML2=ML+2
1177      MLM1=ML-1
1178      IF(MLM1.LE.0) GO TO 45
1179      DO 55 I=1,3
1180      55 NP(I,ML1)=NP(I,MLM1)+1
1181      IF(ML2.EQ.M) GO TO 25
1182      DO 56 I=1,3
1183      56 NP(I,ML2)=NP(I,ML)+1
1184      ML=ML2
1185      GO TO 60
1186      25 ML=M
1187      GO TO 39
1188      40 CONTINUE
1189      WRITE(IO, 110)
1190      WRITE(IO, 113) (M,(NP(J,M),J=1,3),M=1,NEL)
1191      45 WRITE(IO, 111)
1192      RETURN
1193      C
1194      C FORMAT STATEMENTS
1195      C
1196      33 FORMAT(2F10.4)
1197      100 FORMAT(3I3)
1198      101 FORMAT('1',5X,'OUTPUT OF INPUT NODAL DATA')

```



```

1199      102 FORMAT(///,10X,19H NODAL POINT OUTPUT,///53H      NODE      X COORD
1200      1 Z COORD      INIT. HEAD      MATL,///)
1201      104 FORMAT(I6,2F12.2)
1202      105 FORMAT(1H0,28HERROR IN NODAL DATA,NODE=,I4)
1203      106 FORMAT('1',5X,'OUTPUT OF COMPLETE NODAL DATA ')
1204      107 FORMAT('1',5X,'OUTPUT OF INPUT ELEMENT DATA ')
1205      108 FORMAT(///,10X,13H ELEMENT DATA///,
1206      124H      ELEM      I      J      K)
1207      110 FORMAT('1',5X,'OUTPUT OF COMPLETE ELEMENT DATA',//)
1208      111 FORMAT('MLM1 IS LESS THAN OR EQUAL TO ZERO ')
1209      420 FORMAT(F8.2,4F8.4,3I3)
1210      113 FORMAT(4I6)
1211      115 FORMAT(///,10X,19H NODAL POINT OUTPUT,///'      NODE      X COORD
1212      1 Z COORD,      MATL',///)
1213      120 FORMAT(10F8.2)
1214      130 FORMAT(40I2)
1215      180 FORMAT(I6,2F12.2,F14.2,4X,I3)
1216      END
1217      C
1218      C
1219      C
1220      C
1221      FUNCTION ISPAC(NAME,LENGTH,K)
1222      C
1223      C      A SIMPLE MANAGER WHICH WORKS WITH 5 FIXED LENGTH COMMON BLOCKS,
1224      C      A 5-COLUMN NAME DIRECTORY AND POINTER DIRECTORY.
1225      C
1226      C*****
1227      REAL*8 NAMES,NAME
1228      C
1229      COMMON /DIMCOM/ LAST1,LAST2,LAST3,LAST4,LAST5,MAXDIM,
1230      *NAMES(5,20),IPT(5,21),ICOM(5)
1231      C
1232      C      CHECK IF NAME ALREADY EXISTS.
1233      C
1234      ISPACE=LOCOM(NAME,K)
1235      IF(ISPACE.EQ.0) GO TO 10
1236      GO TO 100
1237      C
1238      C      ENTER NEW NAME IN DIRECTORY.
1239      C
1240      10 GO TO (20,30,40,50,60),K
1241      20 LAST1=LAST1+1
1242      LAST=LAST1
1243      GO TO 70
1244      30 LAST2=LAST2+1
1245      LAST=LAST2
1246      GO TO 70
1247      40 LAST3=LAST3+1
1248      LAST=LAST3
1249      GO TO 70
1250      50 LAST4=LAST4+1
1251      LAST=LAST4
1252      GO TO 70
1253      60 LAST5=LAST5+1
1254      LAST=LAST5
1255      C
1256      70 IF(LAST.GT.MAXDIM) GO TO 200
1257      NAMES(K,LAST)=NAME
1258      ISPACE=IPT(K,LAST)

```



```

1259      IPT(K, LAST+1)=ISPACE+LENGTH
1260      IF((IPT(K, LAST+1)-1).GT.ICOM(K)) GO TO 300
1261      ISPAC=ISPACE
1262  C
1263      RETURN
1264  C
1265  C   EXITS RESULTING FROM DIAGNOSED ERRORS
1266  C
1267      100 WRITE(6, 1000) NAME
1268      1000 FORMAT(22H***NAME ALREADY EXISTS, 10X, A8)
1269      GO TO 400
1270      200 WRITE(6, 2000) NAME, K
1271      2000 FORMAT(17H***TABLE OVERFLOW, 10X, A8, I4)
1272      GO TO 400
1273      300 WRITE(6, 3000) NAME, K, IPT(K, LAST), LENGTH
1274      3000 FORMAT(23H***COMMON AREA OVERFLOW, A8, I4)
1275      400 CALL EXIT
1276  C
1277      END
1278  C
1279  C
1280  C
1281  C
1282      SUBROUTINE ITERAT(X, Z, H, PSI, PSIP, BMAT, RHS, QRHS, SINT, DIFF, Q, TPOT,
1283      *LDQ, KODE, NSPF, IMAX, E, NST, NSTEP)
1284  C
1285  C   THIS SUBROUTINE CONTROLS THE ITERATION CYCLE.
1286  C
1287  C*****
1288  C
1289  C
1290      IMPLICIT REAL*8(A-H, O-Z)
1291      COMMON /BORDER/ NEUM, NDIR, KFLAG, NBOUND(60)
1292      COMMON /SUBIV/ IS, NNODE, NEL, ITTER, NEBEL, NFIBN, NIBNS, NSEEP, NTEMP
1293  C
1294  C
1295      DIMENSION H(1), PSI(1), PSIP(1), SINT(1), DIFF(1), KODE(1), BMAT(1),
1296      *QRHS(1), LDQ(1), Q(1), NSPF(1), X(1), Z(1), TPOT(1), RHS(1)
1297      IF(ITTER) 90, 95, 90
1298      95 DO 110 I=1, NNODE
1299          PSI(I)=0.0
1300      110 PSIP(I)=0.0
1301          J=0
1302          DO 600 I=1, NNODE
1303              IF(KODE(I).EQ.10) GO TO 600
1304              J=J+1
1305              PSIP(I)=SINT(J)
1306              PSI(I)=(H(I)+SINT(J))/2.0
1307      600 CONTINUE
1308  C   WRITE(6, 1000)
1309  C   WRITE(6, 105) (PSIP(I), I=1, NNODE)
1310  C   WRITE(6, 100)
1311  C   WRITE(6, 101)
1312  C   WRITE(6, 105) (PSI(I), I=1, NNODE)
1313  C   WRITE(6, 1230)
1314      1230 FORMAT(/, 5X, 'THE RHS TERMS ARE (IT.):', //)
1315  C   WRITE(6, 105) (RHS(I), I=1, NNODE)
1316      ITTER=1
1317      GO TO 85
1318      100 FORMAT(/, 'FIRST ESTIMATE OF P(K+1/2:', //)

```



```

1319      105 FORMAT(10E12.4)
1320      90 TEST=0.0
1321      DO 350 I=1,NNODE
1322      350 PSI(I)=0.0
1323      J=0
1324      DO 650 I=1,NNODE
1325      IF(KODE(I).EQ.10) GO TO 650
1326      J=J+1
1327      PSI(I)=SINT(J)
1328      650 CONTINUE
1329      C
1330      C   COMPUTE FLUXES
1331      C
1332      CALL FLUX(X,Z,PSI,BMAT,QRHS,SINT,Q,TPOT,LDQ,KODE,NSPF)
1333      C
1334      DO 140 I=1,NNODE
1335      DIFF(I)=PSI(I)-PSIP(I)
1336      TEST=DMAX1(TEST,DABS(DIFF(I)))
1337      140 CONTINUE
1338      IF(ITTER.EQ.1) GO TO 1700
1339      CHGE=TEST-CHEK
1340      C   IF(CHGE) 1500,2000,2000
1341      C1500 IF(CHGE.GE.-0.001) GO TO 2000
1342      1700 CHEK=TEST
1343      WRITE(6,700) ITTER,TEST
1344      700 FORMAT('ITTER=',I3,5X,'TEST=',E12.5)
1345      C   WRITE(6,800)
1346      800 FORMAT('/',5X,' DIFF PSI',/)
1347      C   DO 750 I=1,NNODE
1348      C 750 WRITE(6,850) DIFF(I),PSI(I)
1349      850 FORMAT(5X,2E12.5)
1350      IF(TEST.LT.E) GO TO 50
1351      ITTER=ITTER+1
1352      IF(ITTER.GE.IMAX) GO TO 190
1353      DO 150 I=1,NNODE
1354      PSIP(I)=PSI(I)
1355      150 PSI(I)=(H(I)+PSI(I))/2.0
1356      GO TO 85
1357      50 CONTINUE
1358      C   WRITE(6,120)
1359      C   WRITE(6,105) (PSI(I),I=1,NNODE)
1360      WRITE(6,3000)
1361      WRITE(6,105) (Q(I),I=1,NNODE)
1362      2100 ITTER=0
1363      DO 60 I=1,NNODE
1364      PSIP(I)=H(I)
1365      H(I)=PSI(I)
1366      60 PSI(I)=PSI(I)+(PSI(I)-PSIP(I))/2.0
1367      WRITE(6,500) NST
1368      500 FORMAT(/,10X,'END OF: TIME STEP',I5,/)
1369      70 WRITE(6,300)
1370      300 FORMAT('/',,'INITIAL PRESSURE POTENTIAL - NEXT TIME STEP',/)
1371      WRITE(6,400) (H(I),I=1,NNODE)
1372      C   WRITE(6,1400)
1373      1400 FORMAT('/',,'TOTAL HYDRAULIC POTENTIAL',/)
1374      C   WRITE(6,400) (TPOT(I),I=1,NNODE)
1375      400 FORMAT(10F12.1)
1376      C   WRITE(6,3000)
1377      C   WRITE(6,105) (Q(I),I=1,NNODE)
1378      C   IF(NST.NE.NSTEP) GO TO 2200

```





```

1379      C      WRITE(8,960) NNODE
1380      960 FORMAT(I4)
1381      C      DO 950 I=1,NNODE
1382      C      TPOT(I)=H(I)+Z(I)
1383      C 950 WRITE(8,900) I,X(I),Z(I),H(I),TPOT(I)
1384      900 FORMAT(I4,4F12.1)
1385      2200 ITTER=0
1386      NST=NST+1
1387      C      IF(NST.GT.NSTEP) GO TO 1600
1388      GO TO 85
1389      2000 WRITE(6,2050) CHGE
1390      GO TO 1600
1391      190 WRITE(6,200)
1392      200 FORMAT(//,'IMAX EXCEEDED',//)
1393      1600 CALL EXIT
1394      85 CONTINUE
1395      RETURN
1396      1000 FORMAT(//,'FIRST ESTIMATE OF P(K+1):',//)
1397      101 FORMAT(//,10X,'P(K+1/2)=',//)
1398      120 FORMAT(//,5X,'LATEST ESTIMATE OF P(K+1):',//)
1399      2050 FORMAT(//,5X,'THE SOLUTION FOR THIS PROBLEM DOES NOT CONVERGE',//,
1400      *5X,'THE LATEST CHANGE IS:',F10.3,//)
1401      3000 FORMAT(//,5X,'THE COMPUTED FLUXES ARE',//)
1402      END
1403      C
1404      C
1405      C
1406      C
1407      FUNCTION LOCOM(NAME,K)
1408      C
1409      C      LOCATES INDEX OF A GIVEN NAME IN NAMES DIRECTORY.
1410      C
1411      C*****
1412      REAL*8 NAME,NAMES
1413      C
1414      COMMON /DIMCOM/ LAST1,LAST2,LAST3,LAST4,LAST5,MAXDIM,
1415      *NAMES(5,20),IPT(5,21),ICOM(5)
1416      C
1417      GO TO (10,20,30,40,50),K
1418      10 LAST=LAST1
1419      GO TO 60
1420      20 LAST=LAST2
1421      GO TO 60
1422      30 LAST=LAST3
1423      GO TO 60
1424      40 LAST=LAST4
1425      GO TO 60
1426      50 LAST=LAST5
1427      C
1428      60 IF(LAST.EQ.0) GO TO 200
1429      DO 100 M=1,LAST
1430      IF(NAMES(K,M).NE.NAME) GO TO 100
1431      LOCOM=M
1432      RETURN
1433      100 CONTINUE
1434      200 LOCOM=0
1435      C
1436      RETURN
1437      C
1438      END

```



```

1439 C
1440 C
1441 SUBROUTINE XPLOT(X,Z,H,THETA,KZZ,TPOT)
1442 C
1443 C THIS SUBROUTINE ENTERS APPROPRIATE DATA INTO A FILE
1444 C FOR SUBSEQUENT PLOTTING ON THE AED512 INTEGRATED GRAPHICS
1445 C FACILITY
1446 C
1447 C*****
1448 IMPLICIT REAL*8(A-H,O-Z)
1449 REAL*8 KZZ
1450 COMMON /SUBIV/ IS,NNODE,NEL,ITTER,NEBEL,NFIBN,NIBNS,NSEEP,NTEMP
1451 DIMENSION X(1),Z(1),H(1),THETA(1),KZZ(1),TPOT(1)
1452 C
1453 WRITE(8,960) NNODE
1454 DO 950 I=1,NNODE
1455 TPOT(I)=H(I)+Z(I)
1456 950 WRITE(8,900) I,X(I),Z(I),H(I),TPOT(I),THETA(I),KZZ(I)
1457 900 FORMAT(I4,4F12.1,F12.4,E15.5)
1458 960 FORMAT(I4)
1459 CALL EXIT
1460 RETURN
1461 END
1462 C
1463 SUBROUTINE SKYLIN(GMAT,LD,KOLHT)
1464 C
1465 C THIS SUBROUTINE FORMS AND STORES GLOBAL MATRIX IN ONE-
1466 C DIMENSIONAL ARRAY, COMPUTES COLUMN LENGTHS AND ADJUSTS FOR
1467 C SKYLINE, IT ALSO IDENTIFIES NEW LOCATIONS OF DIAGONAL ELEMENTS
1468 C
1469 C*****
1470 IMPLICIT REAL*8(A-H,O-Z)
1471 C
1472 COMMON /MASTIV/ NSUB,MXND,NUMNST,MASTR,MBEL,IDRY,IN,IO,DELT,NTRANS
1473 C
1474 C
1475 COMMON /SUBIV/ IS,NNODE,NEL,ITTER,NEBEL,NFIBN,NIBNS,NSEEP,NTEMP
1476 DIMENSION GMAT(1),LD(1),KOLHT(1)
1477 C
1478 C COMPUTE COLUMN LENGTHS AND ADJUST FOR SKYLINE
1479 C
1480 KK=1
1481 MUM=1
1482 MSUM=0
1483 320 IF(GMAT(MUM).EQ.O) GO TO 315
1484 KOLHT(KK)=LD(KK)-MUM+1
1485 LENG=KOLHT(KK)
1486 KL=LD(KK)-KOLHT(KK)
1487 DO 325 II=1,LENG
1488 325 GMAT(MSUM+II)=GMAT(KL+II)
1489 MUM=LD(KK)+1
1490 MSUM=MSUM+KOLHT(KK)
1491 LD(KK)=MSUM
1492 KK=KK+1
1493 IF(NNODE-KK) 330,320,320
1494 315 MUM=MUM+1
1495 GO TO 320
1496 330 CONTINUE
1497 C WRITE(IO,500)
1498 C WRITE(IO,354) (LD(I),I=1,NNODE)

```



```

1499 C      WRITE(IO,600)
1500 C      WRITE(IO,354) (KOLHT(I),I=1,NNODE)
1501 C      IALL=LD(NNODE)
1502 C      WRITE(IO,355) (GMAT(I),I=1,IALL)
1503 C      355 FORMAT(10X,10E10.4)
1504 C      RETURN
1505 C
1506 C      FORMAT STATEMENTS
1507 C
1508 C      500 FORMAT(10X,25HDIAGONAL ADDRESSING ARRAY,/)
1509 C      600 FORMAT(10X,20HCOLUMN HEIGHTS ARRAY,/)
1510 C      354 FORMAT(10X,10I5)
1511 C      END
1512 C
1513 C
1514 C
1515 C
1516 C      SUBROUTINE TABLOK(H,PSI,THETA,KZZ,CA,WATCON,SLPOT,SLCON,
1517 C      *SLCAP,MATL)
1518 C
1519 C
1520 C      TABLOK IS ADAPTED FROM THE SUBROUTINE OF THE SAME NAME USED IN
1521 C      THE "TEHM" MODEL.
1522 C      SEE:
1523 C      HUFF, D. D., R. J. LUXMORE, J. B. MANKIN, AND C. L. BEGOVITCH.
1524 C      1977. TEHM: A TERRESTRIAL ECOSYSTEM HYDROLOGY MODEL. OAK RIDGE
1525 C      NAT. LAB. ENVIRON. SCI. DIV., OAK RIDGE, TENNESSEE. PUBL.
1526 C      1019. EDFB/IBP-76/8. ORNL/NSF/EATC-27.
1527 C
1528 C
1529 C      WATCON IS THE TABLE OF WATER CONTENTS
1530 C      SLPOT IS THE TABLE OF PRESSURE POTENTIALS
1531 C      SLCON IS THE TABLE OF CONDUCTIVITIES
1532 C      SLCAP IS THE TABLE OF SPECIFIC MOISTURE CAPACITIES
1533 C
1534 C
1535 C*****
1536 C
1537 C
1538 C      IMPLICIT REAL*8(A-H,O-Z)
1539 C      REAL*8 KZZ
1540 C      COMMON/HOOKUP/NS,NC,RESWAT
1541 C      COMMON /SUBIV/ IS,NNODE,NEL,ITTER,NEBEL,NFIBN,NIBNS,NSEEP,NTEMP
1542 C      DIMENSION H(1),THETA(1),PSI(1),KZZ(1),CA(1),MATL(1),
1543 C      *WATCON(NS,1),SLPOT(NS,1),SLCON(NS,1),SLCAP(NS,1)
1544 C
1545 C      WRITE(6,100) ((WATCON(IL,KL),SLPOT(IL,KL),SLCON(IL,KL),
1546 C      *SLCAP(IL,KL),KL=1,NC),IL=1,NS)
1547 C      100 FORMAT(/,F5.3,F10.2,E10.3,3X,E10.3)
1548 C      WRITE(6,200) NS,NC,NNODE,RESWAT
1549 C      200 FORMAT(/,'NS=',I4,'NC=',I4,'NNODE=',I4,'RESWAT=',F5.3)
1550 C      WRITE(6,300) (PSI(IM),IM=1,NNODE)
1551 C      300 FORMAT(/,F14.2)
1552 C      WRITE(6,63)
1553 C      DO 60 N=1,NNODE
1554 C      J=MATL(N)
1555 C      IF(PSI(N).GE.0.0) GO TO 72
1556 C      DO 61 K=1,NC
1557 C      I=K
1558 C      IF(DABS(PSI(N)).GE.SLPOT(J,I)) GO TO 70

```



```

1559      61 CONTINUE
1560      GO TO 60
1561      70 IF(I.LT.2) GO TO 71
1562      C    VALUES WITHIN TABLE RANGE
1563      PROPTN=(DABS(PHI(N))-SLPOT(J,I))/(SLPOT(J,I-1)-SLPOT(J,I))
1564      THETA(N)=WATCON(J,I)-(WATCON(J,I)-WATCON(J,I-1))*PROPTN
1565      KZZ(N)=SLCON(J,I)-(SLCON(J,I)-SLCON(J,I-1))*PROPTN
1566      CA(N)=SLCAP(J,I)-(SLCAP(J,I)-SLCAP(J,I-1))*PROPTN
1567      GO TO 60
1568      C    VALUES AT DRY END OUTSIDE TABLE RANGE
1569      71 PROPTN=(DABS(PHI(N))-SLPOT(J,I))/(15000-SLPOT(J,I))
1570      THETA(N)=WATCON(J,I)-(WATCON(J,I)-RESWAT)*PROPTN
1571      KZZ(N)=SLCON(J,I)-(SLCON(J,I)*PROPTN)
1572      CA(N)=0.0
1573      GO TO 60
1574      C    VALUES AT SATURATION
1575      72 THETA(N)=WATCON(J,NC)
1576      KZZ(N)=SLCON(J,NC)
1577      CA(N)=0.0
1578      60 CONTINUE
1579      C    60 WRITE(6,65) N,MATL(N),PSI(N),THETA(N),KZZ(N),CA(N)
1580      RETURN
1581      C
1582      63 FORMAT(//,11X,'N MATL      PSI              THETA              KZZ',
1583      *'              CAP',//)
1584      65 FORMAT(10X,2I3,4E15.5)
1585      END

```





## D. Appendix D. Example Of Input Data Set Required To Run

## SUBFEM

FERNOW

```

1  PROTOTYPE SIMULATION: FERNOW EXPT. FOREST, W. VIRGINIA
2      1  0 272  1  0  1  2 25  0.1  1
3  CALVIN SILT LOAM - UPPER HORIZONS (TO 60 cm)
4      3  0.455  1.70E+02  1.000E+00  0.0
5      73.49  0.999  0.011380  15.0980.0
6      .235.318.455
7      10300.00  339.0  0.0
8  CALVIN SILT LOAM - LOWER HORIZONS (BELOW 60 cm)
9      3  0.280  1.70E+01  1.000E+00  0.0
10     73.49  0.999  0.011380  15.0980.0
11     .175.240.280
12     7210.00  339.0  0.0
13     1 272 462 120 75  5.0E-02  19.0E+00  0  0  6
14     1  0.0  0.0
15     8  0.0  175.
16     9  150.  60.6
17     16  150.  235.6
18     17  300.  121.2
19     24  300.  296.2
20     25  450.  181.8
21     32  450.  356.8
22     33  600.  242.4
23     40  600.  417.4
24     41  750.  303.0
25     48  750.  478.0
26     49  900.  363.6
27     56  900.  538.6
28     57  1050.  424.2
29     64  1050.  599.2
30     65  1200.  484.8
31     72  1200.  659.8
32     73  1350.  545.4
33     80  1350.  720.4
34     81  1500.  606.0
35     88  1500.  781.0
36     89  1650.  666.6
37     96  1650.  841.6
38     97  1800.  727.2
39     104  1800.  902.2
40     105  1950.  787.9
41     112  1950.  962.9
42     113  2100.  848.5
43     120  2100.  1023.5
44     121  2250.  909.1
45     128  2250.  1084.1
46     129  2400.  969.7
47     136  2400.  1144.7
48     137  2550.  1030.3
49     144  2550.  1205.3
50     145  2700.  1090.9
51     152  2700.  1265.9
52     153  2850.  1151.5
53     160  2850.  1326.5
54     161  3000.  1212.1
55     168  3000.  1387.1
56     169  3150.  1272.7
57     176  3150.  1447.7
58     177  3300.  1333.3

```







119	14	8	15	16
120	15	9	17	10
121	16	10	17	18
122	28	16	23	24
123	29	17	25	18
124	30	18	25	26
125	42	24	31	32
126	43	25	33	26
127	44	26	33	34
128	56	32	39	40
129	57	33	41	34
130	58	34	41	42
131	70	40	47	48
132	71	41	49	42
133	72	42	49	50
134	84	48	55	56
135	85	49	57	50
136	86	50	57	58
137	98	56	63	64
138	99	57	65	58
139	100	58	65	66
140	112	64	71	72
141	113	65	73	66
142	114	66	73	74
143	126	72	79	80
144	127	73	81	74
145	128	74	81	82
146	140	80	87	88
147	141	81	89	82
148	142	82	89	90
149	153	87	95	88
150	154	88	95	96
151	155	89	97	90
152	156	90	97	98
153	168	96	103	104
154	169	97	105	98
155	170	98	105	106
156	182	104	111	112
157	183	105	113	106
158	184	106	113	114
159	196	112	119	120
160	197	113	121	114
161	198	114	121	122
162	210	120	127	128
163	211	121	129	122
164	212	122	129	130
165	224	128	135	136
166	225	129	137	130
167	226	130	137	138
168	238	136	143	144
169	239	137	145	138
170	240	138	145	146
171	252	144	151	152
172	253	145	153	146
173	254	146	153	154
174	266	152	159	160
175	267	153	161	154
176	268	154	161	162
177	280	160	167	168
178	281	161	169	162



179	282	162	169	170
180	294	168	175	176
181	295	169	177	170
182	296	170	177	178
183	308	176	183	184
184	309	177	185	178
185	310	178	185	186
186	322	184	191	192
187	323	185	193	186
188	324	186	193	194
189	336	192	199	200
190	337	193	201	194
191	338	194	201	202
192	350	200	207	208
193	351	201	209	202
194	352	202	209	210
195	364	208	215	216
196	365	209	217	210
197	366	210	217	218
198	378	216	223	224
199	379	217	225	218
200	380	218	225	226
201	392	224	231	232
202	393	225	233	226
203	394	226	233	234
204	406	232	239	240
205	407	233	241	234
206	408	234	241	242
207	420	240	247	248
208	421	241	249	242
209	422	242	249	250
210	434	248	255	256
211	435	249	257	250
212	436	250	257	258
213	448	256	263	264
214	449	257	265	258
215	450	258	265	266
216	462	264	271	272





## BDFERN

```

1      5
2      21 41 61 81101121
3      7 6 5 4 3 2
4      47 33 0 0
5      2.858E+01 5.715E+01
6
7
8      1 33 0 0 0 0 0 0
9      1 2 3 4 5 6 7 9 17 25 33 41 49 57 65 73 81 89 97 105
10     113 121 129 137 145 153 161 169 177 185 193 201 209 217 225 233 241 249 257 265
11     266 267 268 269 270 271 272
12     8 16 24 32 40 48 56 64 72 80 88 96 104 112 120 128 136 144 152 160
13     168 176 184 192 200 208 216 224 232 240 248 256 264
14     7.614E+01 1.523E+02
15
16
17     1 33
18     9.527E+01 1.906E+02
19
20
21     1 33 0 0 0 0 0
22     4.761E+01 9.522E+01
23
24
25     1 33
26     3.825E+01 7.650E+01
27
28
29     1 33
30     9.375E+00 1.875E+01
31
32
33     1 33

```











**B30372**